

Section 11

Transportation

BY

JOHN T. BENEDICT *Retired Standards Engineer and Consultant, Society of Automotive Engineers*
V. TERREY HAWTHORNE *Vice President, Engineering and Technical Services, American Steel Foundries*
KEITH L. HAWTHORNE *Senior Assistant Vice President, Transportation Technology Center, Association of American Railroads*
MICHAEL C. TRACY *Captain, U.S. Navy*
MICHAEL W. M. JENKINS *Professor, Aerospace Design, Georgia Institute of Technology*
SANFORD FLEETER *Professor of Mechanical Engineering and Director, Thermal Sciences and Propulsion Center, School of Mechanical Engineering, Purdue University*
AARON COHEN *Retired Center Director, Lyndon B. Johnson Space Center, NASA and Zachry Professor, Texas A&M University*
G. DAVID BOUNDS *Senior Engineer, PanEnergy Corp.*

11.1 AUTOMOTIVE ENGINEERING by John T. Benedict

General	11-3
Traction Required	11-3
Fuel Consumption	11-5
Transmission Mechanisms	11-6
Automatic Transmissions	11-9
Final Drive	11-10
Suspensions	11-11
Wheel Alignment	11-12
Steering	11-12
Brakes	11-13
Tires	11-16
Air Conditioning and Heating	11-16
Body Structure	11-17
Materials	11-18
Trucks	11-18
Motor Vehicle Engines	11-20

11.2 RAILWAY ENGINEERING by V. Terrey Hawthorne and Keith L. Hawthorne (in collaboration with David G. Blaine, E. Thomas Harley, Charles M. Smith, John A. Elkins, and A. John Peters)

Diesel-Electric Locomotives	11-20
Electric Locomotives	11-25
Freight Cars	11-27
Passenger Equipment	11-33
Track	11-37
Vehicle-Track Interaction	11-38

11.3 MARINE ENGINEERING by Michael C. Tracy

The Marine Environment	11-40
Marine Vehicles	11-41

Seaworthiness	11-41
Engineering Constraints	11-47
Propulsion Systems	11-48
Main Propulsion Plants	11-48
Propulsors	11-52
Propulsion Transmission	11-55
High-Performance Ship Systems	11-57
Cargo Ships	11-59

11.4 AERONAUTICS by M. W. M. Jenkins

Definitions	11-59
Standard Atmosphere	11-59
Upper Atmosphere	11-59
Subsonic Aerodynamic Forces	11-60
Airfoils	11-61
Stability and Control	11-70
Helicopters	11-71
Ground-Effect Machines (GEM)	11-72
Supersonic and Hypersonic Aerodynamics	11-72
Linearized Small-Disturbance Theory	11-77

11.5 JET PROPULSION AND AIRCRAFT PROPELLERS by Sanford Fleeter

Essential Features of Airbreathing or Thermal-Jet Engines	11-82
Essential Features of Rocket Engines	11-84
Notation	11-87
Thrust Equations for Jet-Propulsion Engines	11-89
Power and Efficiency Relationships	11-89
Performance Characteristics of Airbreathing Jet Engines	11-90
Criteria of Rocket-Motor Performance	11-93
Aircraft Propellers	11-95

11-2 TRANSPORTATION

11.6 ASTRONAUTICS

by Aaron Cohen

Space Flight	11-100
Astronomical Constants of the Solar System (BY MICHAEL B. DUKE) ..	11-101
Dynamic Environments (BY MICHAEL B. DUKE)	11-103
Space-Vehicle Trajectories, Flight Mechanics, and Performance (BY O. ELNAN, W. R. PERRY, J. W. RUSSELL, A. G. KROMIS, AND D. W. FELLEENZ)	11-104
Orbital Mechanics (BY O. ELNAN AND W. R. PERRY)	11-105
Lunar- and Interplanetary-Flight Mechanics (BY J. W. RUSSELL)	11-106
Atmospheric Entry (BY D. W. FELLEENZ)	11-107
Attitude Dynamics, Stabilization, and Control of Spacecraft (BY M. R. M. CRESPO DA SILVA)	11-109
Metallic Materials for Aerospace Applications (BY ROBERT L. JOHNSTON)	11-111
Structural Composites (BY IVAN K. SPIKER)	11-112
Stress Corrosion Cracking (BY SAMUEL V. GLORIOSO)	11-113
Materials for Use in High-Pressure Oxygen Systems (BY ROBERT L. JOHNSTON)	11-113
Space Environment (BY L. J. LEGER AND MICHAEL B. DUKE)	11-114
Space-Vehicle Structures (BY THOMAS L. MOSER AND ORVIS E. PIGG)	11-116

Vibration of Structures (BY LAWRENCE H. SOBEL)	11-117
Space Propulsion (BY HENRY O. POHL)	11-118
Spacecraft Life Support and Thermal Management (BY WALTER W. GUY)	11-120
Docking of Two Free-Flying Spacecraft (BY SIAMAK GHOFRANIAN AND MATTHEW S. SCHMIDT)	11-125

11.7 PIPELINE TRANSMISSION

by G. David Bounds

Natural Gas	11-126
Crude Oil and Oil Products	11-129
Solids	11-131

11.8 CONTAINERIZATION

(Staff Contribution)

Container Specifications	11-134
Road Weight Limits	11-135
Container Fleets	11-135
Container Terminals	11-135

11.1 AUTOMOTIVE ENGINEERING

by John T. Benedict

REFERENCES: "Motor Vehicle Facts and Figures, 1995," American Automobile Manufacturers Association. "Fundamentals of Automatic Transmissions and Transaxles," Chrysler Corp. "Year Book," The Tire and Rim Association, Inc. "Automobile Tires," The Goodyear Tire and Rubber Co. "Fundamentals of Vehicle Dynamics," GMI Engineering and Management Institute. "Vehicle Performance and Economy Prediction," GMI Engineering and Management Institute. Various publications of the Society of Automotive Engineers, Inc. (SAE) including: "Tire Rolling Losses," Proceedings P-74; "Automotive Aerodynamics," PT-78; "Driveshaft Design Manual," AE-7; "Design for Fuel Economy," SP-452; Bosch, "Automotive Handbook"; Limpert, "Brake Design and Safety"; Fitch, "Motor Truck Engineering Handbook"; "Truck Systems Design Handbook," PT-41; "Antilock Systems for Air-Braked Vehicles," SP-789; "Vehicle Dynamics, Braking and Steering," SP-801; "Heavy-Duty Drivetrains," SP-868; "Transmission and Driveline Developments for Trucks," SP-893; "Design and Performance of Climate Control Systems," SP-916; "Vehicle Suspension and Steering Systems," SP-952; "ABS/TCS and Brake Technology," SP-953; "Automotive Transmissions and Drivelines," SP-965; "Automotive Body Panel and Bumper System Materials and Design," SP-902; "Light Truck Design and Process Innovation," SP-1005.

GENERAL

(See also Sec. 9.6, "Internal Combustion Engines.")

In the United States the **automobile** is the **dominant mode** of personal transportation. Approximately nine of every ten people commute to work in a private motor vehicle. Public transportation is the means of transportation to work for 5 percent of the work force. More than 90 percent of households have a motor vehicle. Nearly two-thirds have two or more vehicles.

U.S. Federal Highway Administration data, illustrated in Fig. 11.1.1, shows that cars, vans, station wagons, or pickup trucks were used for more than **90 percent** of all trips. In 1993, **1.72 trillion passenger-miles** were traveled by car and truck. Automobile and truck usage accounted for 80.8 percent of intercity passenger-miles, and, when bus usage is added, the figure increases to 82 percent. Intercity motor carriers of freight handled 29 percent of the freight ton-miles; while 37 percent was carried by railroad. Pipelines and inland waterways, respectively, accounted for 19 percent and 15 percent of the freight shipments.

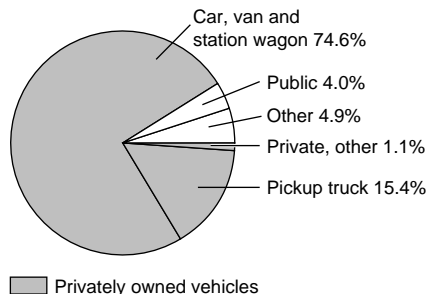


Fig. 11.1.1 Personal trips grouped by mode of transportation. ("Motor Vehicle Facts & Figures.")

In 1994, **147 million cars**, **48 million trucks**, and **676,000 buses** were registered in the United States. Included were 9 million new cars, of which 1.7 million were imported. The average age of cars was 8.4 years. More than 15 million cars were at least 15 years old.

Sales statistics for the 1994 model year reflect continued popularity of small and midsize cars, which accounted for the five top-selling makes. However, the most notable 1994 sales trend was seen in the continued rapid rise of **truck sales**. Total sales of the top five pickup trucks, sport-

utility vehicles, and minivans (which are classified as trucks) surpassed total sales of the top five automobiles.

In 1994, 9 million passenger cars were sold in the United States. **Truck** sales rose to 6.4 million, constituting 42 percent of the 15.4 million total vehicle sales in the United States. The two top-selling nameplates were Ford and Chevrolet pickup trucks, whose sales exceeded any of the passenger car nameplates.

Average **dimensions** of the three top-selling 1994 passenger cars produced by the "big three" U.S. manufacturers were: wheelbase, 107 in (2,718 mm); length, 190 in (4,826 mm); width, 71 in (1,803 mm); tread, 58 in (1,473 mm); height, 54.5 in (1,384 mm); and turning diameter, 38 ft (11.6 m). Weight (mass) of a typical compact size car was 3,145 lb (1,427 kg).

Characteristics of cars purchased in 1994 are further described by their **optional equipment** and accessories: engine, four-cylinder, 46 percent; six-cylinder, 39 percent; eight-cylinder, 14 percent. Additional percentages include: automatic transmission, 88; power steering, 93; antilock brakes, 56; and air conditioning, 94. **Front-wheel drive (FWD)** accounted for nearly 90 percent of the vehicle totals.

TRACTION REQUIRED

The total resistance, which determines the traction force and power (road load horsepower) required for steady motion of a vehicle on a level road, is the sum of: (1) air resistance and (2) friction resistance. **Road load horsepower**, therefore, can be divided into two general parts; aerodynamic horsepower, which includes all aerodynamic losses (both internal and external to the vehicle), and mechanical horsepower or rolling resistance horsepower, which includes drivetrain power losses from the engine to the driving wheels, the wheel bearing losses of front and rear wheels, and the power losses in the four tires. The **rolling resistance** and power consumption of the tires is such a dominant factor that, for a first-order approximation, the frictional loss and the power consumed by the vehicle's equipment and accessories may be disregarded.

Tire rolling resistance, as reported by Hunt, Walter, and Hall (Conference Proceedings, P-74, SAE) was about 1 percent of the load carried at low speeds and increased to about 1.5 percent at 60 mi/h (96.6 km/h). For modern radial-ply passenger car tires, these values are about 1.2 to 1.4 percent at 30 mi/h (48.3 km/h), increasing to 1.6 to 1.8 percent at 70 mi/h (112.7 km/h).

Greater tire deflection, caused by deviation from recommended loads and air pressures (see Table 11.1.1) increases tire resistance. Low temperatures do likewise. Figure 11.1.2 shows the dependence of rolling resistance on inflation pressure for an FR78-14 tire tested at 1,280 lb

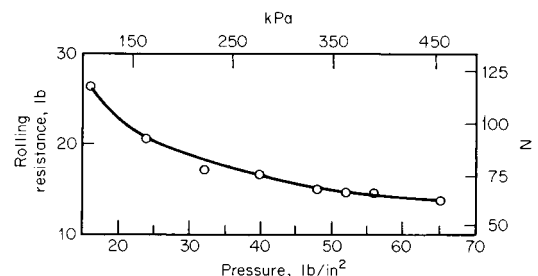


Fig. 11.1.2 Dependence of rolling resistance on inflation pressure for FR78-14 tire, 1,280-lb load and 60-mi/h speed. ("Tire Rolling Losses.")

11-4 AUTOMOTIVE ENGINEERING

Table 11.1.1 Passenger-Car Tire Inflation Pressures and Load Limits

Tire size designation	Cold inflation pressure, lb/in ² (kPa)							Diam., in (mm)	r/ mi
	17 (120)	20 (140)	23 (160)	26 (180)	29 (200)	32 (220)	35 (240)		
13-in nominal wheel diameter—80 series									
P135/80*13	540 (245)	584 (265)	628 (285)	661 (300)	694 (315)	728 (330)	761 (345)	21.4 (544)	965
P145/80*13	606 (275)	661 (300)	705 (320)	750 (340)	783 (355)	827 (375)	860 (390)	22.1 (561)	948
P155/80*13	683 (310)	739 (335)	783 (355)	838 (380)	882 (400)	926 (420)	959 (435)	22.7 (577)	922
P165/80*13	761 (345)	816 (370)	871 (395)	926 (420)	981 (445)	1025 (465)	1069 (485)	23.3 (592)	897
P175/80*13	838 (380)	904 (410)	970 (440)	1025 (465)	1080 (490)	1135 (515)	1179 (535)	23.9 (607)	873
P185/80*13	915 (415)	992 (450)	1058 (480)	1124 (510)	1190 (540)	1246 (565)	1301 (590)	24.6 (625)	851
13-in nominal wheel diameter—70 series									
P175/70*13	739 (335)	794 (360)	849 (385)	893 (405)	948 (430)	992 (450)	1036 (470)	22.6 (574)	925
P185/70*13	805 (365)	871 (395)	926 (420)	992 (450)	1036 (470)	1091 (495)	1135 (515)	23.2 (589)	903
P195/70*13	882 (400)	948 (430)	1014 (460)	1080 (490)	1135 (515)	1190 (540)	1246 (565)	23.8 (605)	878
P205/70*13	959 (435)	1036 (470)	1113 (505)	1179 (535)	1235 (560)	1301 (590)	1356 (615)	24.3 (617)	862

* Space for R, B, or D tire-type designation.
SOURCE: The Tire and Rim Association, Inc.

(581 kg) load and 60 mi/h (96.6 km/h) speed. A tire's rolling resistance is fairly constant from 25 to 60 mi/h (40 to 97 km/h), hence power consumption is a direct function of vehicle speed and load carried by the tire.

There is general agreement that, at 45 mi/h (72.4 km/h), in 70°F (21°C) air, a run of approximately 20 min is necessary to reach **temperature equilibrium** in the tires. This is a significant factor, since tire rolling resistance typically decreases by about 25 percent during the first 10 min of operation.

Aerodynamic drag force is a function of a car's shape, size, and speed. Air resistance varies closely with the square of car speed and has a value in the range of 50 to 85 lbf (223 to 378 N) at 50 mi/h (80 km/h). The total car air drag and mechanical (friction) resistance at 50 mi/h varies from 90 to 200 lbf (400 to 890 N), and a road load power requirement of 15 to 20 hp (11 to 15 kW) at 50 mi/h is typical.

Drag force is defined by the equation $D = C_D (\frac{1}{2} \rho V^2)A$, where A is the car's frontal cross-sectional area, ρ is the air density, V is car speed, and C_D is a nondimensional drag coefficient determined by the vehicle's shape. Frontal area of automobiles varies from about 18 to 23 ft² (1.7 to 2.1 m²). Contemporary cars have drag coefficients ranging from 0.27 to 0.55. For comparison, the **drag coefficients** and **power requirements** for various automobile body shapes are shown in Fig. 11.1.3. Typically, drag coefficients for heavy-duty trucks and truck/trailers (not shown) range from about 0.6 to more than 1. Other drag coefficients include: motorcycles, 0.5 to 0.7; buses, 0.6 to 0.7; streamlined buses, 0.3 to 0.4.

The aerodynamic portion of road load power increases as a function of the cube of car speed. The mechanical portion increases at a slower rate and, from about 25 to 60 mi/h (40 to 97 km/h), is almost a direct function of car weight.

The term "aero horsepower" is used in the automotive industry to denote the power required to overcome the air drag on a vehicle at 50 mi/h on a level highway. Aero horsepower is equal to 0.81 times drag coefficient times the vehicle frontal area. The **aero horsepower** of midsize cars is about 7.7 hp (5.7 kW). A typical subcompact car is 30 percent lower, at 5.3 hp (4 kW). By contrast, a **heavy-duty truck** has an aero horsepower as high as 100 hp (75 kW) at 50 mi/h.






	Drag coefficient	Drag power in kW, average values for A = 2m ² at various speeds		
		40 km/h	120 km/h	160 km/h
 Open convertible	0.5 ... 0.7	1	27	63
 Station wagon (2-box)	0.5 ... 0.6	0.91	24	58
 Conventional form (3-box)	0.4 ... 0.55	0.78	21	50
 Wedge shape, headlights & bumpers integrated in body	0.3 ... 0.4	0.58	16	37
 Optimum streamlining	0.15 ... 0.20	0.29	7.8	18

Fig. 11.1.3 Drag coefficient and aerodynamic power requirements for various body shapes. (Bosch, "Automotive Handbook," SAE.)

A reduction of 1 aero horsepower is the **fuel-efficiency equivalent** of taking 300 lb (135 kg) of weight out of a car. Figure 11.1.4 shows a typical relationship between aerodynamic and mechanical horsepower for vehicle constant-speed operation (Kelly and Holcombe: "Automotive Aerodynamics," PT-16, SAE). Variations in the body, drivetrain, and tires alter the shapes of the curves—but equal road load power for aerodynamic and mechanical requirements at 50 to 55 mi/h is typical. At 55 mi/h (88 km/h), a car expends about half of its power overcoming air drag. For speeds above 55 mi/h, there is a 2 to 3 mi/gal (0.9 to 1.3 km/L) decrease in fuel economy for each 10 mi/h (16 km/h) increase in speed, depending on power plant, driveline components, and drag coefficient. At about 55 mi/h and up, any percentage reduction of the vehicle's aerodynamic drag makes a decrease in fuel consumption

of one-half or more of that same percentage. For example, for a typical automobile, a 10 percent reduction in aerodynamic drag yields a 5 percent reduction in fuel consumption at 55 mi/h.

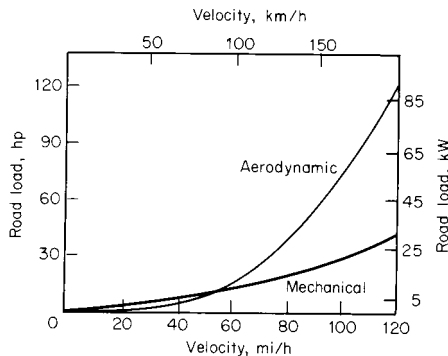


Fig. 11.1.4 Vehicle road load horsepower requirements. (Four-door sedan: frontal area 22 ft²; weight 3,675 lb; $C_D = 0.45$.) (“Automotive Aerodynamics,” PT-78.)

Average values of **traction requirements** for several large cars with average weight (including two passengers and luggage) of 4,000 lb (1,814 kg) are shown in Fig. 11.1.5. Curves A, R, and T represent the air, rolling, and total resistance, respectively, on a level road, with no wind. Curves T', parallel to curve T, represent the displacement of the latter for gravity effects on the grades indicated, the additional traction being equal to the car weight (4,000 lb) times the percent grade. Curve E shows the traction available in high gear in this average car. The intersection of the “traction available” curve with any of the constant-gradient curves indicates the top speed that may be attained on a given grade. For example, this hypothetical large car should negotiate a 12.5 percent grade in high gear at 60 mi/h (97 km/h). Top speed on a level grade would be about 100 mi/h (161 km/h).

Effects of Transmission Gear Ratios Constant-horsepower parabolas, which apply to any vehicle, are shown as light curves in Fig. 11.1.5.

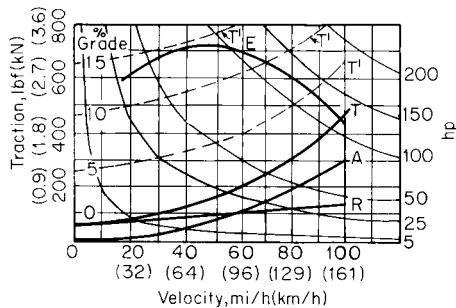


Fig. 11.1.5 Traction available and traction required for a typical large automobile.

Except for small effects of friction losses, changes in gear ratio move points of a curve for traction available from an engine along these constant-power parabolas to traction values multiplied by the change in gear reduction. Such shifting of the traction values available from engines follows gear changes in the axle as well as in the gear box.

Acceleration The difference between traction force available from power generated by an engine and the force required for constant speed on a given grade may be used for acceleration [acceleration = $21.9(100) \times (\text{surplus traction force}/\text{total effective car mass})$], where acceleration is in mi/h · s, force is in lbf, and mass is in lbm.

Car weight must include a factor for the rotating parts of the engine, which may be of considerable magnitude when a high gear ratio is used. It is common for about one-third or more of the torque developed at the

engine crankshaft to be absorbed in accelerating the engine, drivetrain and its rotating masses, and the road wheels. For this instance, this means that the “effective mass” equals $1.33 \times$ actual mass.

The **effective mass** of engine rotating parts increases as the square of the engine revolutions per mile and, for a typical example, may equal or approach the car mass at a gear ratio giving about 12,000 engine rev/min. Since the effective mass of engine rotating parts increases with the square of the gear reduction, and the traction force increases directly, there is an optimum gear reduction for maximum acceleration.

The maximum acceleration rate possible is limited by the friction between the driving tires and the road surface. The coefficient of friction is dependent on vehicle speed, tire condition, and road conditions. At 50 mi/h (80 km/h) on a dry roadway, the coefficient of friction is about 1.0; but, when the roadway is wet, this drops to 0.4 or lower, depending on the amount of water and the polish of the surface (“Bosch Automotive Handbook,” 3d English ed., SAE, 1993).

For a car with 2,000 lb (907 kg) weight on the driving wheels, the limiting traction force would be about 2,000 lbf (8,900 N) on a dry pavement and less than half this value on a wet pavement. From the equation given previously, the theoretical **maximum accelerations** possible under these two conditions for a car of 4,000 lb (1,814 kg) would be equivalent to a speed change of from 0 to 60 mi/h (97 km/h) in about 5.5 and 11 s, respectively. For 0 to 60 mi/h acceleration, a rough approximation of the time also is given by the empirical equation (Campbell, “The Sports Car,” Robert Bentley, Inc., 1978): $t = (2W/T)^{0.6}$, where t = time, s; W = weight, lb; T = maximum engine torque, lb · ft.

FUEL CONSUMPTION

Because motor vehicles consume more than 25 percent of the nation’s gasoline fuel and it is in the national interest to conserve energy supplies, the corporate average fuel economy (CAFE) of cars and trucks was regulated in 1975. Calculated according to production and sales level of a company’s various models, the CAFE for cars was mandated to rise from 18 mi/gal in 1978 to 27 mi/gal in 1985 and thereafter. For light trucks, from 17.2 mi/gal in 1979 to 20.6 in 1995, and 20.7 in 1996. The upward trend in fuel economy is shown graphically in Figs. 11.1.6 (cars) and 11.1.7 (light trucks and vans).

Vehicle **design-related factors** that affect fuel economy are: the vehicle’s purpose; performance goals; size; weight; aerodynamic drag; engine type, size, output, and brake specific fuel consumption; transmis-

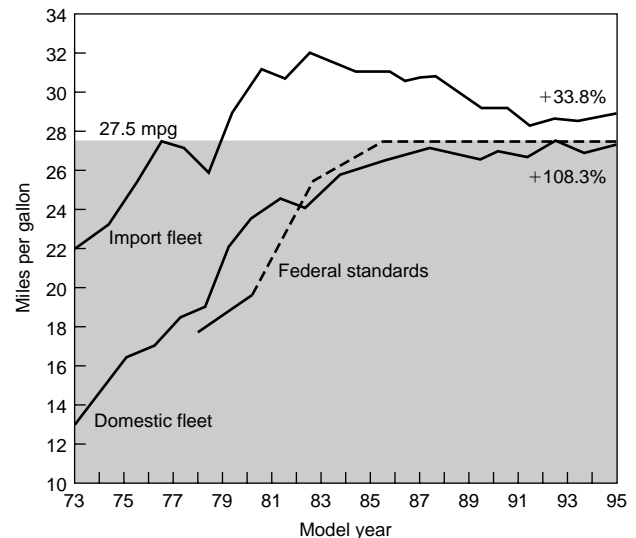


Fig. 11.1.6 Passenger car corporate average fuel economy. (“Motor Vehicle Facts & Figures.”)

11-6 AUTOMOTIVE ENGINEERING

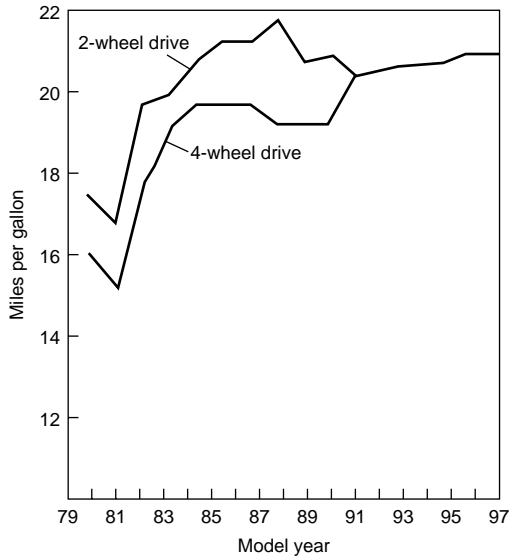


Fig. 11.1.7 U.S. federal light truck fuel economy standards. ("Motor Vehicle Facts & Figures.")

sion type; axle ratio; tire construction; and federal standards for fuel economy, emissions, and safety.

The principal customer- or owner-related factors include: driving pattern; trip length and number of stops; driving technique, especially acceleration, speed, and braking; vehicle maintenance; accessory operation; vehicle loading; terrain; and weather. Several popular accessories affect fuel economy as follows: automatic transmission, 2 to 3 mi/gal; air conditioning, 1 to 3 mi/gal; power steering, about 1/2 mi/gal; and power brakes, negligible.

Figure 11.1.8 illustrates how fuel economy is affected by design changes such as axle ratio, engine displacement, and vehicle weight. **Weight** is a key determinant of fuel economy. For a rough rule-of-thumb, it may be estimated that the addition of 300 lb weight increases fuel consumption about 1 percent (approximately 1/3 mi/gal for a typical compact car) at highway speed, and about 0.8 mi/gal in city driving. In terms of metric units, a rough estimate that evolved from European engineering practice indicates that, for every 100 kg vehicle weight, 1 L of fuel is consumed for every 100 km traveled.

The examples plotted in Fig. 11.1.9 for subcompact and intermediate-size cars show **fuel economy range** for the urban driving cycle for engine warm and cold (short-trip). Also plotted in this graph is the road load fuel economy variation with speed from 30 to 70 mi/h. This graph also illustrates the general point that specific fuel consumption is the greatest when the engine is subjected to low loads, since this is where the ratio between idling losses (due to friction, leaks, and nonuniform fuel distribution) and the brake horsepower is most unfavorable.

TRANSMISSION MECHANISMS

Friction clutches are either (1) the single-disk type (Fig. 11.1.10), connecting the engine to a manual transmission, or (2) the hydraulically operated multiple-disk type (Fig. 11.1.11, schematic), for control of the various planetary-gear changes in automatic transmissions. In (1), the area of the friction facing is usually based on a pressure of 30 lb/in² (206.9 kPa), and the torque rating on a friction coefficient of 0.25. The clutch is held in engagement by several coiled springs or a diaphragm spring and is disengaged by means of a pedal with such leverage that 30 to 40 lb (133 to 178 N) will overcome the clutch springs.

Fluid couplings between the engine and transmission formerly were used to provide a smooth drive by the flow of oil between the flat radial blades in two adjacent toroidal casings (Fig. 11.1.12a, schematic). The difference in centrifugal force between the mass of oil contained in each toroid, when either is running at a speed higher than the other, causes a flow of oil from the periphery of the faster one to the slower one. Since this mass of oil is also rotating around the shaft at the speed of the

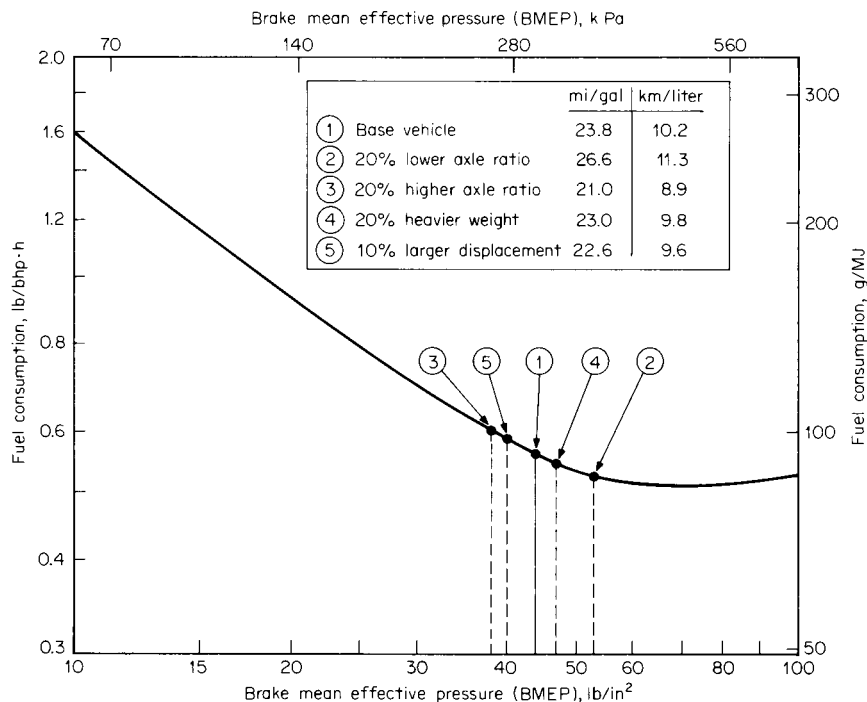


Fig. 11.1.8 Effect of vehicle design changes on road load 55-mi/h fuel consumption. (Chrysler Corp.)

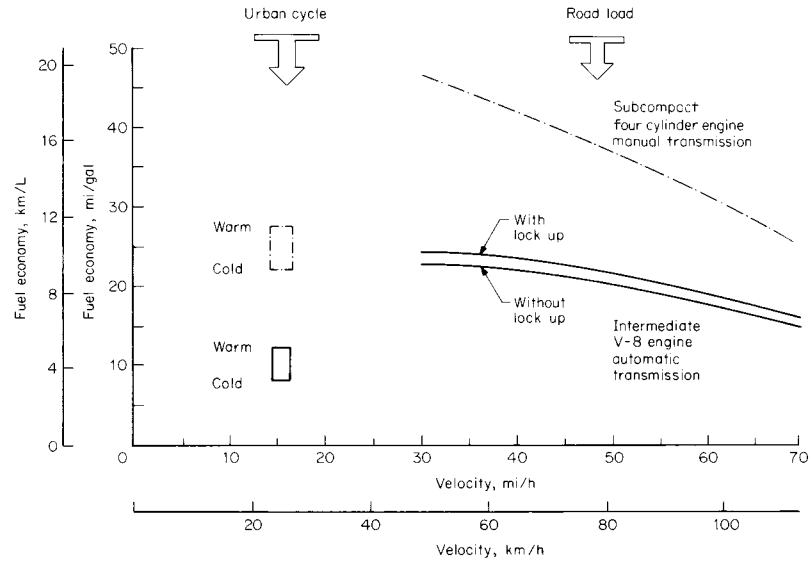


Fig. 11.1.9 Vehicle fuel consumption increases with speed, for subcompact and midsize cars. (Chrysler Corp.)

driving torus, its impact on the blades of the slower torus develops a torque on the latter. The developed torque is equal to, and cannot exceed, the torque of the driving torus. In this respect it is similar to a slipping friction clutch. The driven member must always run at a lower speed, though at high rotative speeds, and when the torque demand is small, the slip may be only 2 or 3 percent. The stalled torque increases with the square of the engine speed, so that very little is developed when idling. Since torque may be transmitted in either direction, depending only on which member is rotating at the higher speed, the engine may be used as a brake as with friction clutches, and the car may be started by pushing.

Torque-converter couplings (Fig. 11.1.13a) have largely replaced fluid couplings because the torque transmitted can be increased at high slippage. The circulation of oil between the driving, or higher-speed, torus (the pump) and the driven or lower-speed, torus (the turbine) results from the difference in centrifugal force developed in these two units, just as in the fluid coupling. With the torque converter, however, the turbine blades are given a curvature so that an additional torque is developed by the reaction of a backward-spinning mass of oil as it leaves the turbine. Stationary, or stator, blades are interposed between the turbine and the pump to change the direction of the oil spin. The entrance angle of the stator blades required for tangential flow varies

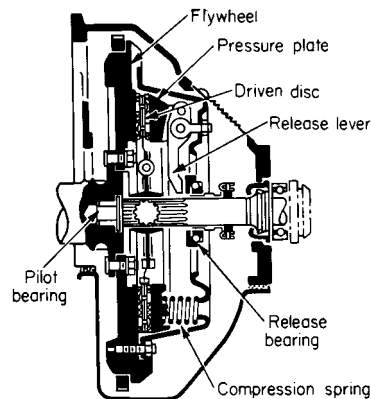


Fig. 11.1.10 Single-plate dry-disk friction clutch.

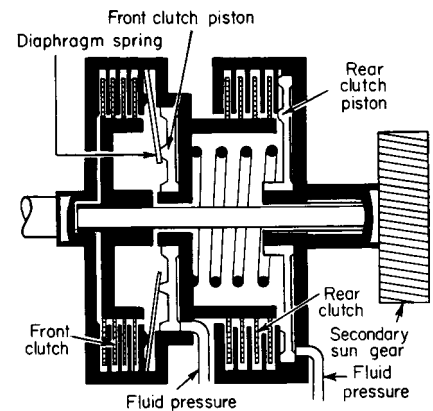


Fig. 11.1.11 Schematic of two hydraulically operated multiple-disk clutches in an automatic transmission. (Ford Motor Co.)

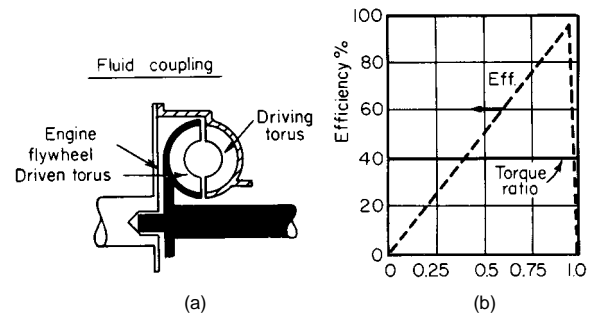


Fig. 11.1.12 Fluid coupling: (a) section; (b) characteristics.

widely with the slip ratio. For a given blade angle there is a hydraulic shock loss at any slip ratio greater or less than that which provides tangential flow. This is reflected in the rapid fall of the efficiency curve in Fig. 11.1.14b on each side of the maximum. The essential parts of a torque converter with its stationary stator are shown in Fig. 11.1.14a. A stalled-torque multiplication of 2.0 to 2.7 is used in various designs.

11-8 AUTOMOTIVE ENGINEERING

When the torque ratio is almost unity, the slip is such that oil from the turbine starts to impinge on the back of the stator blades. By mounting the stator assembly on a **sprag**, or one-way clutch (Fig. 11.1.13a), it remains stationary while subject to the reversing action of the

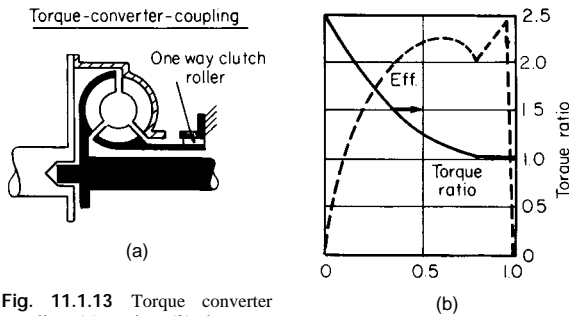


Fig. 11.1.13 Torque converter coupling: (a) section; (b) characteristics.

backward-spinning oil mass as it leaves the turbine. When the slip reaches the point where the oil flow from the turbine begins to spin forward, the stator is free to turn with it. When the slip is further reduced, the unit acts as a fluid coupling with improved efficiency (Fig. 11.1.13b). Such a unit is a **fluid torque-converter coupling**. Some designs

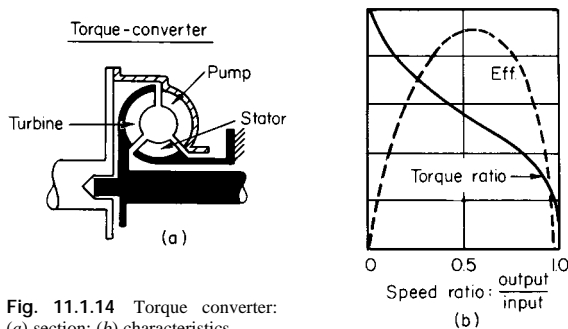


Fig. 11.1.14 Torque converter: (a) section; (b) characteristics.

eliminate slippage by the inclusion of a friction clutch which carries the load when a predetermined car speed is reached. These clutches are hydraulically operated, the engagement being controlled automatically by accelerator position and car speed.

Figure 11.1.15 compares a torque-converter coupling to a friction clutch on **car performance** in direct drive. The increase in traction available for acceleration from a standing start substantiates its public acceptance. An axle gear is generally used which gives a propeller shaft speed about 90 percent as great as with a manual transmission at the same car speed. The gain in engine efficiency compensates for the losses of the automatic transmissions under steady cruising speeds.

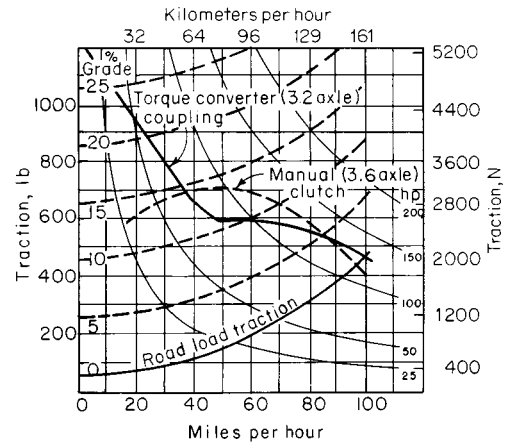


Fig. 11.1.15 Comparative traction available in the performance of a fluid torque-converter coupling and a friction clutch.

However, there may be a considerable **loss of power during acceleration** unless supplemented by such modifications as one or more auxiliary gear ratios or variable-angle stator vanes. Various design modifications of torque-converter couplings have been introduced by different manufacturers, such as two or more stators, each independently mounted on one way clutches, and variable pitch angles for the stator blades. These provide compromises in blade angles for the development of rapid acceleration without sacrifice of high efficiency while cruising.

Manual transmissions installed as standard equipment on American cars have three, four, or five forward speeds, including direct drive, and one reverse. These speeds are obtained by sliding either one of two gears along a splined shaft to bring it into mesh with a corresponding gear on a countershaft which is, in turn, driven by a pair of gears in constant mesh. Helical gears are used to minimize noise. A “**synchron-mesh**” device (Fig. 11.1.16), acting as a friction clutch, brings the gears to be meshed approximately to the correct speed just before meshing and minimizes “**clashing**,” even with inexperienced drivers. Gear

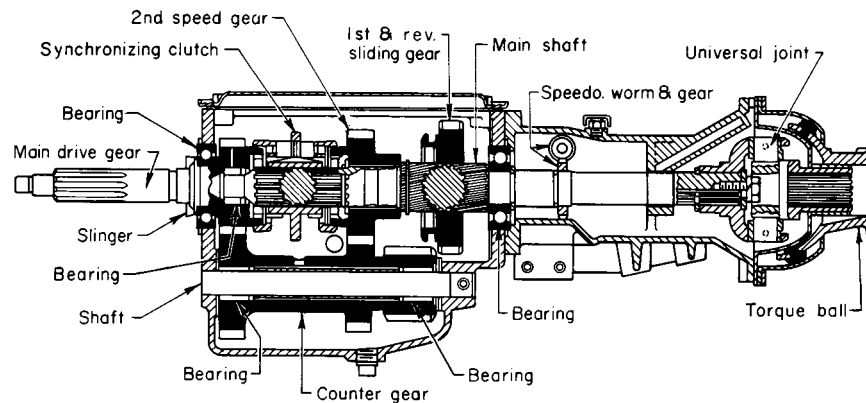


Fig. 11.1.16 Three-speed synchronmesh transmission. (Buick.)

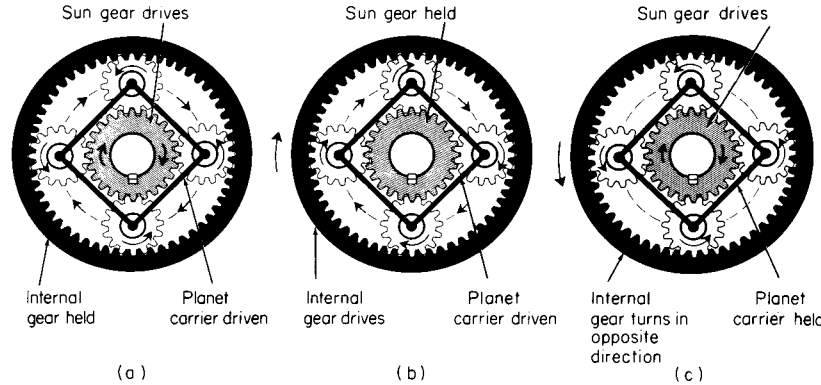


Fig. 11.1.17 Planetary gear action: (a) Large speed reduction: ratio = $1 + (\text{internal gear diam.})/(\text{sun gear diam.}) = 3.33$ for example shown. (b) Small speed reduction: ratio = $1 + (\text{sun gear diam.})/(\text{internal gear diam.}) = 1.428$. (c) Reverse gear ratio = $(\text{internal gear diam.})/(\text{sun gear diam.}) = -2.33$.

changes are generally in geometric ratios. Transmission ratios average about 2.76 in first gear, 1.64 in second, 1.0 in third or direct drive, and 3.24 in reverse. The shift lever is generally located on the steering column. Four-speed transmissions usually have the shift lever on the floor. Average gear ratios are about 2.67 in first, 1.93 in second, 1.45 in third, and 1.0 in fourth or direct drive.

Overdrives have been available for some cars equipped with manual transmissions. These are supplemental planetary gear units with three planetary pinions driven around a stationary sun gear. The surrounding internal gear is coupled to the propeller shaft, which thus turns faster than the engine. The gear ratio is selected to permit the engine to slow down to about 70 percent of the propeller-shaft speed and operate with less noise and friction. These units automatically come into action when the driver momentarily releases the accelerator pedal at a car speed above 25 to 28 mi/h (40 to 45 km/h).

AUTOMATIC TRANSMISSIONS

Automatic transmissions commonly use torque-converter couplings with planetary-gear units that can supply one or two gear reductions and reverse, depending on the design, by simultaneously engaging or locking various elements of planetary systems (Fig. 11.1.17). Automatic control is provided by disk clutches or brake bands which lock the various elements, operated by oil pressure as regulated by governors at car speeds where shifts are made from one speed to another.

A schematic of a representative automatic transmission, combining a three-element torque converter and a compound planetary gear is shown in Fig. 11.1.18. The speed reductions and reverse are provided by a compound planetary system consisting of two simple systems in series. The two sun gears are an integral unit with the same number of teeth,

and the forward internal gear carries the planets of the rear unit. The internal gears of both systems are all of the same size, and consequently all planets are of equal size. This arrangement, together with three clutches, two brake bands, and suitable one-way sprags, makes possible three forward gear or torque ratios, plus direct drive and reverse.

Many automatic transmissions use a **lockup clutch** to improve performance and fuel economy. The torque converter is used for power and smoothness while accelerating in first and second gears until road speed reaches about 40 mi/h (64 km/h). Then, after the transmission upshifts from second to third gear, the clutch automatically locks up the torque converter so there is a direct mechanical drive through the transmission. Normal slippage in the converter is eliminated, engine speed is reduced, and fuel economy is improved. The lockup clutch disengages automatically during part-throttle or full-throttle downshifts and, when the vehicle is slowed, to a speed slightly below the lockup speed.

Approximately two-thirds of 1995 cars have **electronically controlled** automatic transmissions. Combined electronic-hydraulic units for control of automatic transmissions are, increasingly, superseding systems that rely solely on hydraulic control. Hydraulic actuation is retained for the clutches, while **electronic modules** assume control functions for gear selection and for modulating pressure in accordance with torque flow. **Sensors** monitor load, selector-lever position, program, and kick-down switch positions, along with rotational speed at both the engine and transmission shafts. The control unit processes these data to produce control signals for the transmission. **Advantages** include: diverse shift programs, smooth shifts, flexibility for various vehicles, simplified hydraulics, and elimination of one-way clutches.

Worldwide, automatic transmission engineering practice includes some evolving design development and growing production acceptance of **continuously variable transmissions (CVT)**. The CVT can convert the

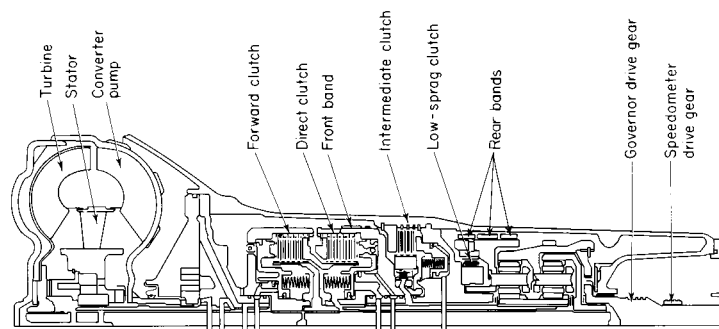


Fig. 11.1.18 Three-element torque converter and planetary gear. (General Motors Corp.)

11-10 AUTOMOTIVE ENGINEERING

engine's continuously varying operating curve to an operating curve of its own, and every engine operating curve into an operating range within the field of potential driving conditions. The **theoretical advantage** (over fixed-ratio transmissions) lies in a potential for enhancing vehicle performance and fuel economy while reducing exhaust emissions. This is done by maintaining the engine in a performance range for best fuel economy. There are, however, **practical limitations** and considerations that constrain the full exploitation of the CVT's theoretical capabilities.

The CVT can operate mechanically (belt or friction roller), hydraulically, or electrically. Currently, the highest level of development has been attained with **mechanical continuously variable** designs using steel belts. A general feature of CVT is manipulation of engine speed, with the objective of maintaining constant engine speed; or optimizing engine speed changes in response to changing driving conditions. CVT **developmental activity** includes: high-torque and high-speed belts, electronic control for line pressure and engine speed, torque converters with electronically controlled lockup clutch, and roller vane pumps with electronically operated flow control valve.

FINAL DRIVE

The **differential** is a unit attached to the ring gear (Figs. 11.1.19 and 11.1.20) which equalizes the traction of both wheels and permits one wheel to turn faster than the other, as needed on curves. Each axle is driven by a bevel gear meshing with pinions on a cross-shaft pinion pin

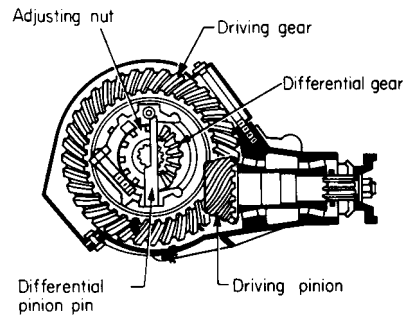


Fig. 11.1.19 Rear-axle hypoid gearing.

secured to the differential case. The case also carries the ring gear. An undesirable feature of the conventional differential is that no more traction may be developed on one wheel than on the other. If one wheel slips on ice, there is no traction to move the car. **Limited-slip differentials**

are offered as optional equipment on most cars. One design has four pinions which are carried on two separate cross shafts at right angles to each other, each being driven by V-shaped notches in the carrier. As torque is developed to drive either axle, one pinion cross shaft or the other moves axially and locks the corresponding disk-clutch plates between that axle drive gear and the differential housing. In another design, similar disk clutches are locked by spring pressure, which prevents differential action until a differential torque greater than the limit established by the springs is developed.

The **semifloating rear axle** (Fig. 11.1.20) used on many rear-wheel drive cars has a bearing for each drive axle at the outer end of the housing as well as near the differential carrier, with the full load on each wheel taken by the drive axles in combined bending and shear. The **full-floating axle**, generally used on commercial vehicles, supports each wheel on two bearings carried by the axle housing or an extension to it. Each wheel is bolted to a flange on one of the axle shafts. The axle shafts carry none of the vehicle weight and may be withdrawn without jacking up the wheel.

The **front-wheel drive (FWD)** cars commonly use a **transaxle** that combines a torque converter, automatic three-speed or four-speed transmission, final drive gearing, and differential into a compact drive system, such as illustrated in the cutaway view shown in Fig. 11.1.21. Typically, the torque converter, transaxle unit, and differential are housed in an integral aluminum die casting. The differential oil sump is separate from the transaxle sump. The torque converter is attached to the crankshaft through a flexible driving plate. The converter is cooled by circulating the transaxle fluid through an oil-to-water type cooler, located in the radiator side tank.

Engine torque is transmitted to the torque converter through the input shaft to multiple disk clutches in the transaxle. The power flow depends on the application of the clutches and bands. As illustrated in Fig. 11.1.22, the transaxle consists of two multiple-disk clutches, an overrunning clutch, two servos, a hydraulic accumulator, two bands, and two planetary gear sets, to provide three or four forward ratios and a reverse ratio.

The common sun gear of the planetary gear sets is connected to the front clutch by a driving shell that is splined to the sun gear and to the front clutch retainer. The hydraulic system consists of an oil pump and a single valve body that contains all of the valves except the governor valves.

Output torque from the main centerline is delivered through helical gears to the transfer shaft. This gear set is a factor in the final drive (axle) ratio. The shaft also carries the governor and the parking sprag. An integral helical gear on the transfer shaft drives the differential ring gear. In a representative FWD vehicle, the final drive gearing is completed with either of two gear sets to produce overall ratios of 3.48, 3.22, and 2.78.

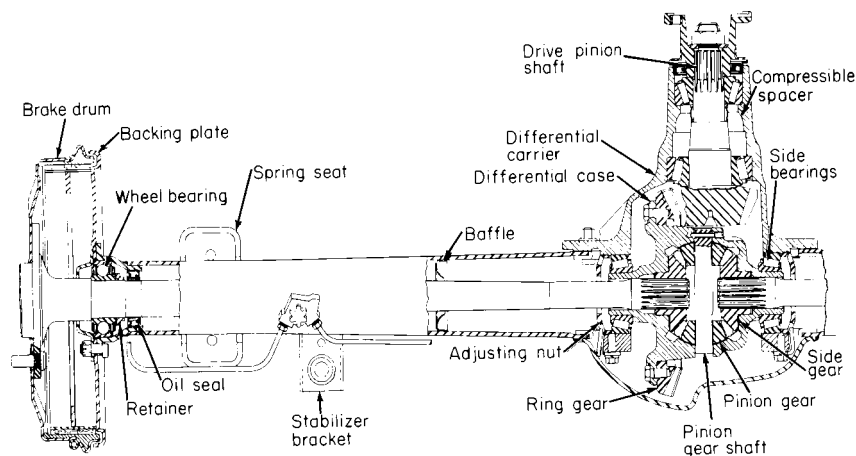


Fig. 11.1.20 Rear axle. (Oldsmobile.)

Advances introduced in 1995 include an **electronically controlled four-speed automatic transaxle with nonsynchronous shifting** that allows independent movement of two gear sets at one time and smooths torque demand and coasting down-shifts.

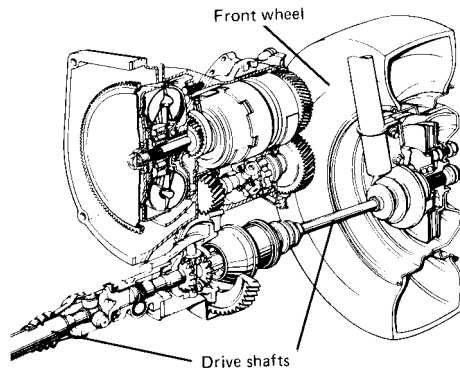


Fig. 11.1.21 Automatic transaxle used on front-wheel-drive car. (Chrysler Corp.)

Various types of **four-wheel drive (4WD)** systems have been developed to improve driving performance and vehicle stability on roads with a low friction coefficient surface. Most systems distribute driving force evenly (50:50) to the front and rear wheels. Driving performance, stability, and control near the limits of tire adhesion are improved, especially on low-friction surfaces. However, because of the improved levels of stability and control, the driver may be unaware that the vehicle is approaching a critical limit. The **advanced technology** in the 4WD field now extends to the "intelligent" four-wheel drive system. This system is designed to distribute driving force to front and rear wheels at varying, optimal ratios (instead of equal front/rear sharing of driving force) according to driving conditions and the critical limit of vehicle dynamics. The result is improved balancing of stability considerations along with cornering performance and critical limit predictability.

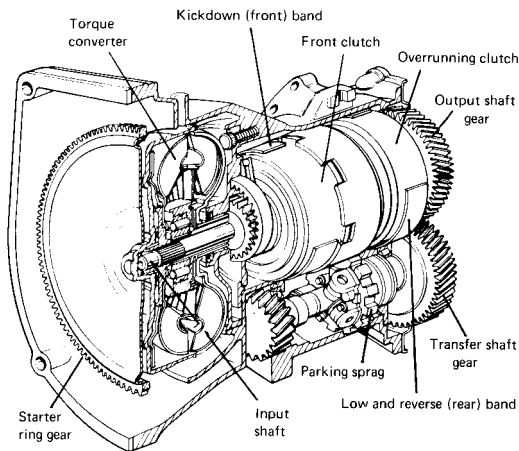


Fig. 11.1.22 Cross-section view of typical transaxle. (Chrysler Corp.)

SUSPENSIONS

Rear Suspensions Torque reactions may be taken through longitudinal leaf springs, as in the **Hotchkiss drive**, or through radius rods when coil springs are used. Some designs in the past used a torque tube around the propeller shaft, bolted to the axle housing, with universal joints for both at the forward ends. Most contemporary rear suspension designs

use either coil springs (Fig. 11.1.23) or leaf springs. Spring stiffness at the rear wheels ranges from 85 lb/in (15 N/mm) to about 160 lb/in (28 N/mm). Shock absorbers, to dampen road shock and vibration, are used on all cars.

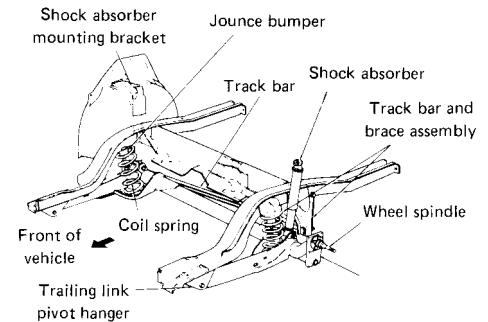


Fig. 11.1.23 Trailing-arm type rear suspension with coil springs, used on some front-wheel-drive cars. (Chrysler Corp.)

Front-Wheel Suspensions Independent front-wheel suspensions are used on all cars. Rear-wheel drive cars typically use the short-and-long-arm (SLA) design, with the steering knuckle held directly between the wishbones by spherical joints (Fig. 11.1.24). The upper wishbone is shorter than the lower, to allow the springs to deflect without lateral movement of the tire at the point of ground contact.

A modification of the conventional suspension consists of sloping the upper wishbones down toward the rear, so that the steering spindle is given more "caster" when the front springs are compressed. This geometry causes the torque produced from braking at the front wheels to develop a couple on the inclined wishbones, which tends to raise the front of the car frame. By suitable proportioning of the parts it is possible by this means to reduce "nose diving" of the car when the brakes are applied. The load on these wishbones is generally taken by coil springs acting on the lower wishbone or by torsion-bar springs mounted longitudinally.

Figure 11.1.25 shows a representative application of the **spring strut (McPherson)** system for the front suspension of front-wheel drive cars. The lower end of the telescoping shock absorber (strut) is mounted within a coil spring and connected to the steering knuckle. The upper end is anchored to the car body structure.

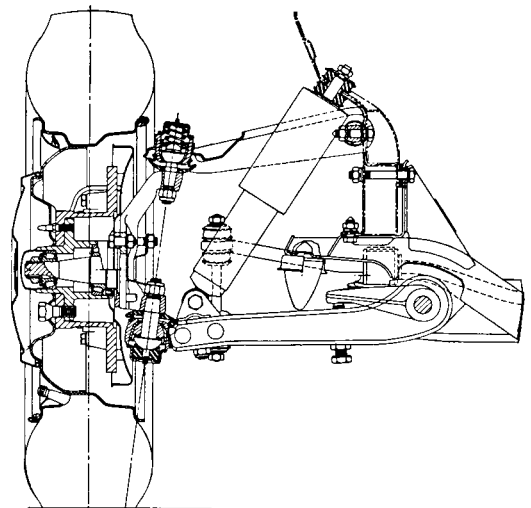


Fig. 11.1.24 Front-wheel suspension for rear-wheel-drive car.

11-12 AUTOMOTIVE ENGINEERING

Suspension system state of the art, with electronic control modules, includes user-selected dynamic tailoring of suspension characteristics and a continuously variable road-sensing suspension that senses wheel motion and other parameters.

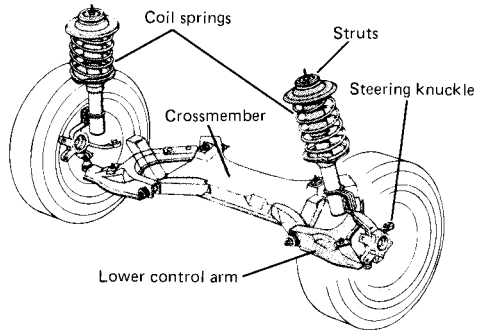


Fig. 11.1.25 Typical McPherson strut, coil spring front suspension for front-wheel-drive car. (Chrysler Corp.)

WHEEL ALIGNMENT

Caster is the angle, in side elevation, between the steering axis and the vertical. It is considered positive when the upper end of the steering axis is inclined rearward. Manufacturer's specifications vary considerably, with the range from $1\frac{1}{2}$ to $-2\frac{1}{4}$ °. **Camber**, the inclination of the wheel plane from the vertical, is positive when the wheel leans outward, and varies from 1 to $-\frac{1}{2}$ ° with many preferring 0°. **Toe-in** of a pair of wheels is the difference in transverse distance between the wheel planes taken at the extreme rear and front points of the tire treads. It is limited to $\frac{1}{4}$ in (6.4 mm), with $\frac{1}{8}$ in (3.2 mm) or less generally preferred.

STEERING

The force applied to the steering wheel is generally multiplied through a **worm-and-roller**, a **recirculating-ball**, or a **rack-and-pinion** type of steering gear. The overall ratios are such that 20° to 33° rotation of the steering wheel results in 1° turn of the front wheels for manual steering and 17.6° to 25.0° for power steering. The **responsiveness** of rack-and-pinion steering (Fig. 11.1.26a) results from the basic design, in which one pinion is attached directly to the steering shaft. This gear meshes with the rack, which directly extends the linkage to turn the front wheels. By comparison, a recirculating-ball steering shaft (Fig. 11.1.26b) includes a wormshaft turned by the steering shaft. The wormshaft rolls inside a set of ball bearings. Movement of the bearings causes a ball nut to move. The ball nut contains gear teeth that mesh to a sector of gear teeth. As the steering wheel turns, the sector rotates and moves a connection of

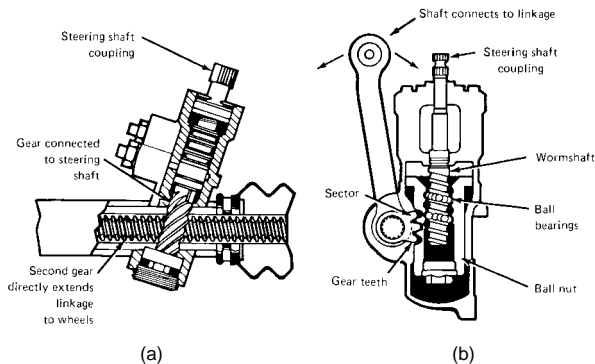


Fig. 11.1.26 Two commonly used types of steering gears. (a) Rack-and-pinion; (b) recirculating ball.

parallel links to turn the wheels of the car. Both steering gear systems operate satisfactorily. The rack-and-pinion is more direct.

Figure 11.1.27 illustrates the geometry of the prevalent **Ackermann steering gear** layout. To avoid slippage of the wheels when turning a curve of radius r , the point of intersection M for the projected front-wheel axes must fall in a vertical plane through the center of the rear axle. The torque, in foot-pounds, required to turn the wheels of a vehicle standing on smooth concrete varies with the angle of turn, from about 6 percent of the weight on the front axle, in pounds, to start a turn, to 17 percent for a 30° turn.

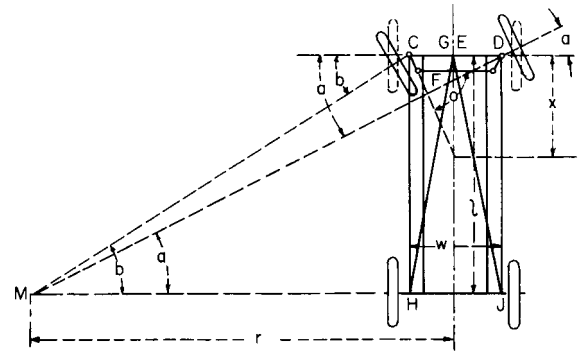


Fig. 11.1.27 Geometry of the Ackermann steering gear.

Power-Assisted Steering

Power steering is a steering control system in which an auxiliary power source assists the driver by providing the major force required to direct the road wheels of the car. The **principal components** of the power steering system (Fig. 11.1.28) are: power steering gear, with servo valve; oil pump, with flow control and relief valves; reserve tank; hydraulic tubing; and oil cooler. These components operate in conjunction with the car's steering wheel, linkage system, and steered wheels. The physical

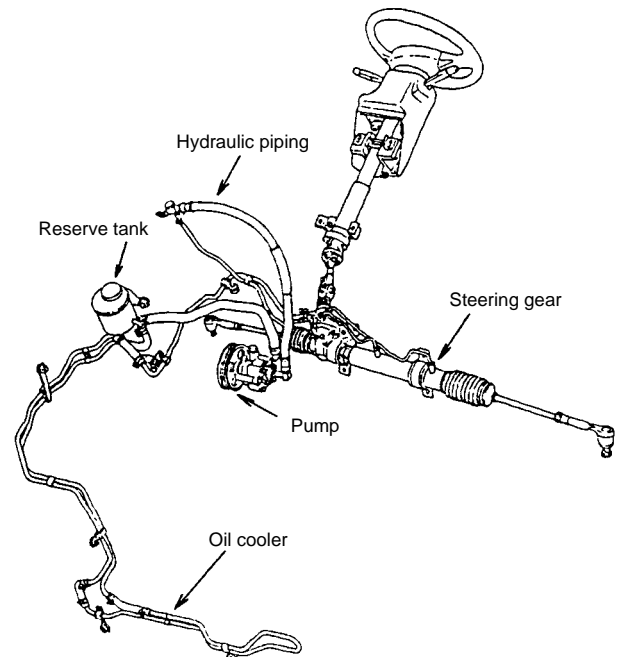


Fig. 11.1.28 Principal components of power steering systems with variable displacement pump. (Reprinted with permission from SAE, SP-952, ©1993, Society of Automotive Engineers, Inc.)

effort required to steer an automobile, especially when parking, is appreciably lessened by the power-assisted steering device. This permits reduction in the gear ratio between the steering wheel and the car wheels from some 30 to 15, with consequent reduction in the number of turns of the steering wheel for the complete movement of the front wheels from extreme right to left from 5.5 to 3. Power-assisted steering has been offered for many years on U.S. cars as standard or optional equipment. Public acceptance is such that 88 percent of the cars sold in 1993 were so equipped.

All systems provide (1) steering control in case of failure of the hydraulic-power assistance, and (2) a “feel of the road,” by which the driver’s effort on the steering wheel is proportional to the force needed to turn the front wheels and by which the tendency of a car to straighten out from a turn or the drag of a soft front tire may be felt at the steering wheel.

Power assistance is effected by hydraulic pressure from an engine-drive pump, acting on a piston in the steering linkage. The piston and its cylinder are incorporated in the steering-gear housing. Oil pressure on the piston is controlled by a valve, such as the balanced spool valve of Fig. 11.1.29.

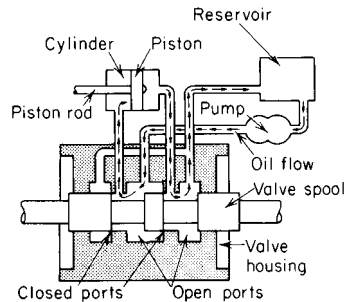


Fig. 11.1.29 Control valve positioned for full-turn power steering assistance using maximum pump pressure.

When the spool is moved slightly to the right, lands on the spool restrict the return of oil from the pump through both return circuits, thus building up delivery pressure. Since the pump delivery is still open to the left end of the power cylinder while the right end is open to the pump suction, a force is developed to move the piston to the right. The greater the restriction imposed on the return of oil to the pump, the greater will be the pressure and the resulting force on the piston.

The spool is centered to the neutral position by suitable centering springs. These provide an increasing effort on the steering wheel for increasing steering angle. Although they aid in straightening out from a turn, they do not give the driver a feel of the force required to provide the steering direction. Hydraulic reaction against the spool, which is felt at the steering wheel and is proportional to the force developed by the steering gear, is developed by subjecting the ends of the spool to the oil pressure on either side of the power piston.

The valve is held in its neutral position by preloading the centering springs. Steering effort at the wheel overcomes this preload. During normal, straight-highway driving, the steering effort is less than the preload and there is no hydraulic assistance; the steering gear is freely reversible, and the driver can “feel the road” and correct for elements such as road camber and crosswinds. The caster action of the front wheels straightens the path of the car when it is coming out of a turn. Any steering effort greater than the preload of the centering springs allows the spool movement to develop a steering assistance proportional to the steering effort and to correspondingly reduce, but not eliminate, the road reactions and shocks felt by the driver.

Oil pumps for power-assisted steering gears are generally driven from the engine by belts, though in some instances they have been driven at higher speeds directly from the electric generator. A typical unit delivers 1.75 gal/min (6.62 L/min) at engine idling speed, at any pressure up to 1,200 lb/in² (8.3 MPa) as may be required while parking.

Three types of rotary pumps for the high pressures required are shown in Fig. 11.1.30 (see also Sec. 14.1). Centrifugal force holds the sliding elements against a cam-shaped or eccentric case at high speeds. At low speeds, the sliding elements are held against the case—in design *a* by springs and in design *c* by oil pressure admitted to the base of the vanes. The double cam of design *c*, in addition to doubling the normal volumetric displacement, provides for balancing the oil pressure on each side of the rotor and on the bearings. The cam is contoured for uniform acceleration.

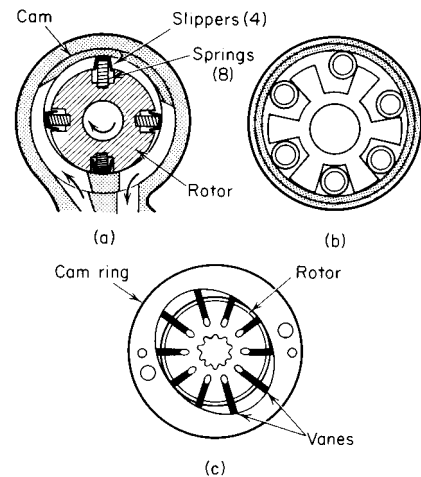


Fig. 11.1.30 Rotary pump types: (a) Chrysler; (b) Ford (Eaton); (c) General Motors (Saginaw).

Variable displacement vane pumps (instead of fixed displacement) are used to raise the efficiency of power steering systems. The variable displacement design reduces power consumption by curtailing the surplus oil flow at the middle and high revolution speeds of the steering apparatus. The amount of oil that is pumped is matched to the requirements of the system in its various operating stages.

BRAKES

Stopping distance—the distance traveled by a vehicle after an obstacle has been spotted until the vehicle is brought to a halt—is the sum of the distances traveled during the reaction time and the braking time.

The braking ratio z , usually expressed as a percentage, is the ratio between braking deceleration and the acceleration due to gravity ($g = 32.2 \text{ ft/s}^2$ or 9.8 m/s^2). The upper and lower braking ratio values are limited by static friction between tire and road surface and the legally prescribed values for stopping distances.

The reaction time is the time that elapses between the driver’s perception of an object and commencement of action to apply the brakes. This time is not constant; it varies from 0.3 to 1.7 s, depending on personal and external factors. For a reaction time of 1 s, Table 11.1.2 gives stopping distances for various speeds and values of braking ratio (deceleration rates).

The maximum retarding force that can be applied to a vehicle through its wheels is limited by the friction between the tires and the road, equal to the coefficient of friction times the vehicle weight. With a coefficient of 1.0, which is about the maximum for dry pavement, this force can equal the car weight and can develop a retardation of 1.0 g . In this instance, stopping distance $S = V^2/29.9$, where V is in mi/h and S is expressed in feet. For metric units, where S is meters and V is km/h, the equation is $S = V^2/254$.

For typical vehicle, tire, and road conditions, with a 0.4 coefficient of friction, 0.4 g deceleration rate, and a reaction time of 1 s, the following is a rule-of-thumb equation for stopping distance; $S \approx (V/10)^2 + (3V/10)$, where S is stopping distance in meters and V is the speed in km/h.

11-14 AUTOMOTIVE ENGINEERING

Table 11.1.2 Stopping Distances (Calculated)

Braking ratio z , %	Driving speed before applying brakes, mi/h (km/h)									
	12 (20)	25 (40)	31 (50)	37 (60)	43 (70)	50 (80)	56 (90)	62 (100)	69 (110)	75 (120)
	Reaction distance traveled in 1 s (no braking), ft (m)									
	18 (5.6)	36 (11)	46 (14)	56 (17)	62 (19)	72 (22)	82 (25)	92 (28)	102 (31)	108 (33)
	Stopping distance (reaction + braking), ft (m)									
30	36 (11)	105 (32)	151 (46)	207 (63)	269 (82)	344 (105)	427 (130)	509 (155)	607 (185)	705 (215)
50	29 (8.7)	75 (23)	108 (33)	148 (45)	187 (57)	233 (71)	285 (87)	344 (105)	410 (125)	476 (145)
70	26 (7.8)	66 (20)	92 (28)	121 (37)	151 (46)	187 (57)	230 (70)	272 (83)	318 (97)	360 (110)
90	24 (7.3)	53 (18)	82 (25)	105 (32)	131 (40)	164 (50)	197 (60)	233 (71)	272 (83)	312 (95)

SOURCE: Bosch, "Automotive Handbook," SAE.

The automobile's brake system is based on the principles of hydraulics. Hydraulic action begins when force is applied to the brake pedal. This force creates pressure in the master cylinder, either directly or through a power booster. It serves to displace hydraulic fluid stored in the master cylinder. The displaced fluid transmits the pressure through the fluid-filled brake lines to the wheel cylinders that actuate the brake shoe (or pad) mechanisms. Actuation of these mechanisms forces the brake pads and linings against the rotors (front wheels) or drums (rear wheels) to stop the wheels.

All automobiles have two independent systems of brakes for safety. One is generally a **parking brake** and is rarely used to stop a car from speed, though it should be able to. The brake manually operates on the rear wheels through cables or mechanical linkage from an auxiliary foot lever (or a hand pull); it is held on by a ratchet until released by some means such as a push button or a lever.

The main system, or **service brakes**, on all U.S. cars is hydraulically operated, with equalized pressure to all four wheels, except with disk brakes on front wheels, where a proportioning valve is used to permit increased pressure to the disk calipers. Rubber seals preclude the use of petroleum products; hydraulic fluids are generally mixtures of glycols with inhibitors. Figure 11.1.31 shows the **split system**, for improved

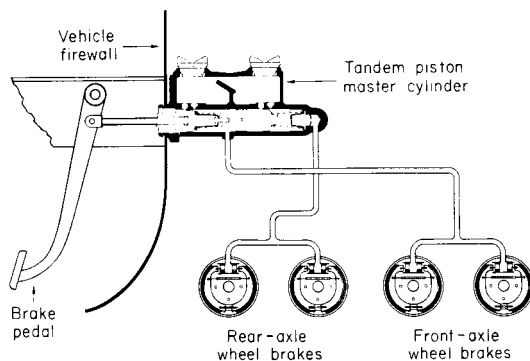


Fig. 11.1.31 "Split" hydraulic brake system.

safety, with two independent master cylinders in tandem, each actuating half the brakes, either front or rear or one front and the opposite rear. Failure of either hydraulic section allows stopping of the car by brakes on two wheels.

Figure 11.1.32 shows the customary design of a **brake dual master cylinder** by which the brake shoes are applied in the conventional internal-expanding brakes (Fig. 11.1.33). When the brakes are released, a spring in the master cylinder returns the pistons to their

original positions. This uncovers the compensating ports, permitting brake fluid to enter from the reservoir or to escape from the wheel cylinders after brake application. The check valve facilitates the maintenance of 8 to 16 lb/in² (55 to 110 kPa) line pressure to prevent the entrance of air into the system.

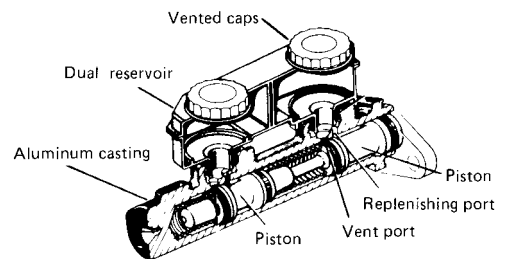


Fig. 11.1.32 Typical design of a dual master cylinder for a split brake system.

Three types of **internal-expanding brakes** (Fig. 11.1.33) have been accepted in service. All are **self-energizing**, where the drum rotation increases the applying force supplied by the wheel cylinder.

With the **trailing shoe** (Fig. 11.1.33a), friction is opposed to the actuating force. The resulting deenergizing of this shoe causes it to do about one-third the work of the leading shoe. Its tendency to lock or squeal is less, and the length and position of the lining are not so critical. The type of brake shown in Fig. 11.1.33a, with one leading and one trailing shoe, formerly was used for the rear wheels. The braking work and wear of the two shoes can be equalized by use of a larger bore for that half of the wheel cylinder which operates the trailing shoe.

The design shown in Fig. 11.1.33b has two leading shoes, each actuated by a single-piston wheel cylinder and each self-energizing. This design has been used for the front wheels where the Fig. 11.1.33a design was used for the rear wheels.

Figure 11.1.33c shows the **Bendix Duo-Servo design**, used on many cars, in which the self-energizing action of **two leading shoes** is much increased by turning them "**in series**"; the braking force developed by the primary shoe becomes the actuating force for the secondary shoe. The action reverses with rotation.

Adjustment for lining wear is effected automatically on most cars. If sufficient wear has developed, a linkage may turn the notched wheel on the adjusting screw (Fig. 11.1.33c) by movement of the primary shoe relative to the anchor pin when the brake is applied with the car moving in reverse. On other designs, adjustment is by linkage between the hand brake and the adjusting wheel.

Brake drums are designed to be as large as practicable in order to develop the necessary torque with the minimum application effort and

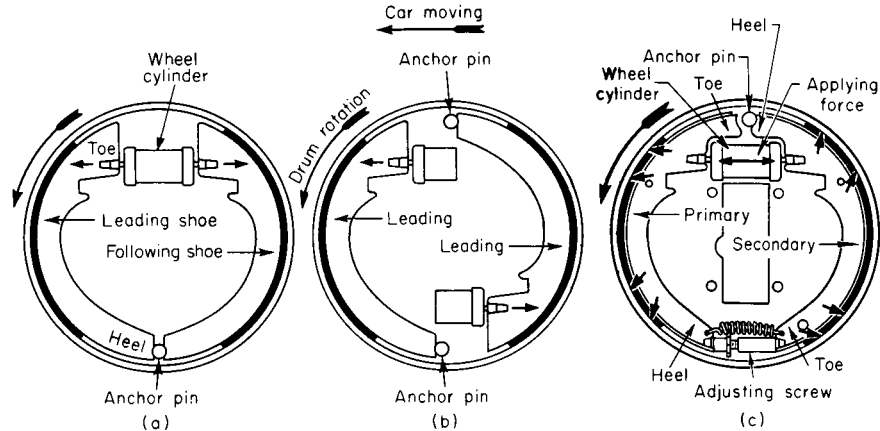


Fig. 11.1.33 Three types of internal-expanding brakes.

to limit the temperature developed in dissipating the heat of friction. The 14- and 15-in (36- and 38-cm) wheel-rim diameters limit the drum diameters to 10 to 12 in (25 to 30 cm), and the 13-in (33-cm) rims limit the diameters to 8 to 9½ in (20 to 24 cm). Drum widths limit unit pressures between the linings and the drums to 16 to 23 lb (7.2 to 10.4 kg) of car weight per in². Drum friction surfaces are usually cast iron or iron alloy. Drum brake shoes and disk brake caliper pads are lined with compounds of resin, metal powder, solid lubricant, abrasives, organic and inorganic fillers, and fibers. Environmental concerns led to the development of asbestos-free brake system friction materials. These materials take into account the full range of brake performance requirements, including the mechanism of brake noise and the causes for brake judder (abnormal vibration), and squeal. Current nonasbestos, nonsteel friction materials for brake linings and pads include those with main fibers of carbon and aramid plastic. Secondary fibers are copper and ceramic. Friction coefficients range from 0.3 to 0.4.

Where identical brakes are used on front and rear wheels, the rear-wheel cylinders are smaller, so that about 40 to 45 percent of total braking force is developed at the rear wheels. With the split system (Fig. 11.1.31), a smaller master cylinder for the rear brakes gives a similar division. Master cylinders are about 1 in (25.4 mm) in diameter, and other parts of the brake system are so proportioned that a 100-lb (445-N) brake-pedal force develops 600- to 1,200-lb/in² (4.1- to 8.3-MPa) fluid pressure. Air in a hydraulic system makes the brakes feel spongy, and it must be bled wherever it accumulates, as at each wheel cylinder.

Caliper disk brakes (Fig. 11.1.34) offer better heat dissipation by direct contact with moving air; they are not self-energizing, so that there is

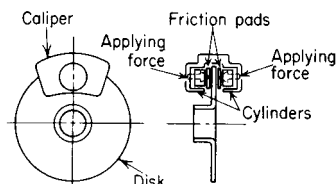


Fig. 11.1.34 Caliper disk brake (schematic).

less drop in the friction coefficient with temperature rise of the brake pads. Contrarily, the absence of self-energization requires higher hydraulic-system pressures and consequent power boosters on heavier cars. Wear of the friction pads is normally greater because of the smaller area of contact and the greater exposure to road dirt. The pads are consequently made thicker than the linings of drum brakes, and automatic retraction is incorporated in the hydraulic cylinders.

Power-assisted brakes relieve the driver of much physical effort in retarding or stopping a car. They are either standard or optional equip-

ment on virtually all car models. The supplemental force is developed on a diaphragm by vacuum from the engine intake manifold, either mechanically to the master cylinder or hydraulically, to boost (1) the force between the pedal and the master cylinder, or (2) the hydraulic pressure between the master cylinder and the brakes. Common characteristics are (1) a braking force which is related to pedal pressure so that the driver can feel a pedal reaction proportional to the force applied, and (2) ability to apply the brakes in the absence of the supplemental power.

Figure 11.1.35 illustrates a passenger-car vacuum-suspended type of power brake, where vacuum exists on both sides of the main power element when the brakes are released. In the released position, there is contact between the valve plunger and the poppet; thus the port is closed between the power cylinder and the atmosphere.

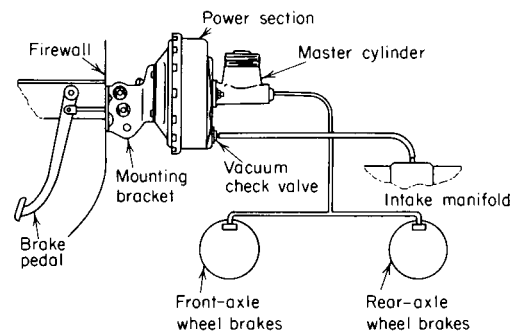


Fig. 11.1.35 Power-assisted brake installation.

Physical effort applied to the brake pedal moves the valve operating rod toward the master-cylinder section. Initial movement of this rod closes the port between the poppet and the power piston. This closes the vacuum passage and brings the valve plunger into contact with the resilient reaction disk. Additional movement of the valve rod then separates the valve plunger from the poppet, thus opening the atmospheric port and admitting air to the control chamber. Air pressure in this chamber depends upon the amount of physical effort applied to the pedal. The pressure differences between the two sides of the power piston cause it to move toward the master cylinder, closing the vacuum port and transferring its force through the reaction disk to the hydraulic piston of the master cylinder. This force tends to extrude the reaction disk against the valve plunger and react against the valve operating rod, thus reducing the pedal effort required. An inherent feature of the vacuum-suspended type of power brake is the existence of vacuum, without an additional reservoir, for at least one brake stop after the engine is stopped. Figure 11.1.36 shows the relationship between pedal effort and hydraulic line pressure.

11-16 AUTOMOTIVE ENGINEERING

Antilock brakes were installed on 56 percent of 1994 cars. On eight percent of these cars, the additional feature of **traction control** was included. Antilock brake systems (ABS) prevent wheel lockup during braking. Under normal braking conditions, the driver operates the brakes as usual. On slippery roads, or during severe braking, as the driver pushes on the brake pedal and causes the wheels to approach lockup, the ABS takes over and **modulates brake line pressure**. Thus, braking force is applied independently of pedal force.

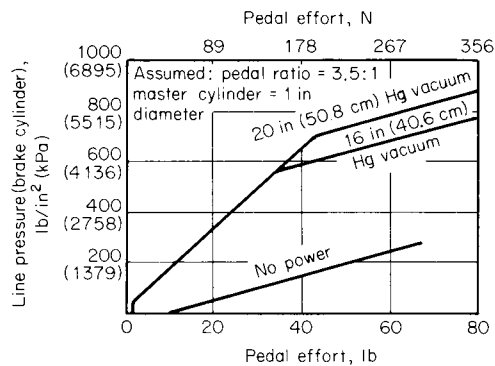


Fig. 11.1.36 Performance chart of a typical power-assisted brake.

Traction control functions as an extension of antilock brake systems, with which it shares numerous components. Traction control helps maintain directional stability along with good traction. An ABS system with traction control uses brake applications to **control slip**. The amount of force transferred when starting off or during deceleration or acceleration is a function of the amount of slip between the tire and the road. The combined antilock and traction control systems make extensive use of automotive **electronics** including elements such as sensors (to measure wheel angular velocity), microprocessors, and brake force distribution controllers.

TIRES

The automotive pneumatic tire performs four **main functions**: supporting a moving load; generating steering forces; transmitting vehicle driving and braking forces; and providing isolation from road irregularities by acting as a spring in the total suspension system. A tire is made up of two basic parts: the tread, or road-contacting part, which must provide traction and resist wear and abrasion; and the body, consisting of rubberized fabric that gives the tire strength and flexibility.

Pneumatic tires are in an engineering classification called “**tensile structures**.” Other examples of tensile structures are bicycle wheels (spokes in tension, rim in compression); sailboat sails (fabric in tension, air in compression); and prestressed concrete (tendons in tension, concrete in compression).

Tensile structures contain a compression member to provide a tensile preload in the tensile member. In tires, the **cords** are the tensile members and the **compressed air** is the compression member. The common **misunderstanding** is that the tire uses air pressure beneath the rigid wheel to lift it from the flattened tire. Actually, this is invalid; load support must come through the tire casing structure and enter the rim through the tire bead.

The three **principal types** of automobile and truck tires are the cross-ply or bias-ply, the radial-ply, and the bias-belted (Fig. 11.1.37). In the **bias-ply** tire design, the cords in each layer of fabric run at an angle from one bead (rim edge) to the opposite bead. To balance the tire strength symmetrically across the tread center, another layer is added at an opposing angle of 30 to 38°, producing a two-ply tire. The addition of two more criss-crossed plies make a four-ply tire.

In the **radial tire** (used on most automobiles), cords run straight across from bead to bead. The second layer of cords runs the same way;

the plies do not cross one another. Reinforcing belts of two or more layers are laid circumferentially around the tire between the radial body plies and the tread. The **bias-belted** tire construction is similar to the conventional bias-ply tire, but it has circumferential belts like those in the radial tire.

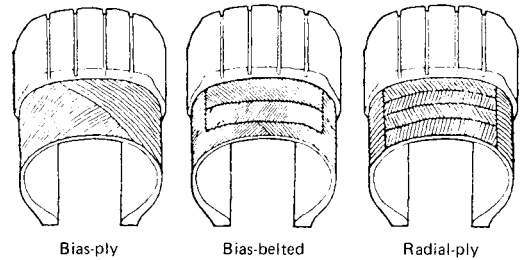


Fig. 11.1.37 Three types of tire construction.

Of the three types, the radial-ply offers the longest tread life, the best traction, the coolest running, the highest gasoline mileage, and the greatest resistance to road hazards. The bias-ply tire provides a softer, quieter ride and is the least expensive. The bias-belted tire design is intermediate between the good-quality bias-ply and the radial tire. It has a longer tread life and is cooler running than the bias-ply, and it gives a smoother low-speed ride than the radial tire. Figure 11.1.38 explains the coding system used for **metric tire size** designation. See Table 11.1.1 for **inflation pressures** and **load limits** for 13-in tires.

Various means for continuous measurement and remote display of car and truck **tire pressures** are well established in vehicle engineering practice. The new designs for tire pressure monitoring systems (on 1996 model vehicles) use **wheel-mounted sensors**. The module containing the sensor, a 6-V lithium battery, and a radio transmitter, is mounted on the wheel rim inside the tire. Once a minute, the tire pressure signal is transmitted to a dash-mounted receiver. The encoded signal is translated and displayed for each wheel. In one U.S. car application, the monitor is installed when optional **run-flat** tires are ordered. Such tires typically allow driving to continue for up to 200 miles at 55 mi/h with zero air pressure. The tires perform so well that there is a possibility that the driver will not be aware of the tire pressure loss, hence the need for monitoring.

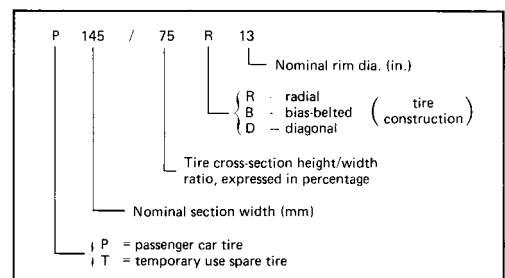


Fig. 11.1.38 Explanation of the international coding system for metric tire size (P series) designations.

AIR CONDITIONING AND HEATING

(See also Sec. 12.4.)

Automobiles are generally **ventilated** through an opening near the windshield with a plenum chamber to separate rain from air. Airflow developed by car motion is augmented, especially at low speed, by a variable-speed, electrically driven blower. When **heat** is required, this air is passed through a finned core served by the engine-jacket water. Core design typically calls for delivery of 20,000 Btu/h (6 kW) and 125 ft³/min (0.1 m³/s) airflow at 130°F (55°C) with 0°F (−18°C) ambient. Car **temperature** is controlled by (1) mixing ambient with heated

air, (2) mixing heated with recirculated air, or (3) variation of blower speed. Provision is always made to direct heated air against the interior of the windshield to prevent formation of ice or fog. Figure 11.1.39 illustrates schematically a three-speed blower that drives fresh air through (1) a radiator core or (2) a bypass. The degree and direction of air heating are further regulated by the doors.

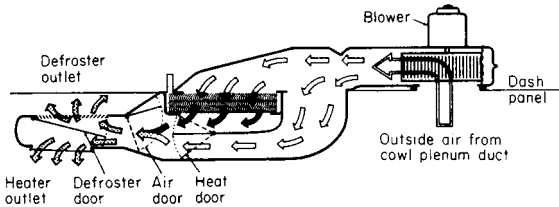


Fig. 11.1.39 Heater airflow diagram.

In 1994, approximately 94 percent of cars built in the United States were equipped with air-conditioning systems. The refrigeration capacity of a typical system is 18,000 Btu/h, or 1.5 tons, at 25 mi/h. Cooling capacity increases with car speed. In a “cool-down” test, beginning at a test point with 110°F ambient temperature and bright sunshine, the car is “soaked” until its interior temperature has leveled off (at about 140°F). The car is then started and run at 25 mi/h, with interior car temperature checked at up to 48 locations throughout the passenger compartment.

After 10 min of operation, the average car temperature has dropped to the range of 80 to 90°F (27 to 32°C). However, in terms of passenger comfort, at 2 min after starting, the air discharged from the outlets is at about 70°F—and, at 10 minutes, the discharge air is at 55°F. And, by adjusting the outlets, the cool air is directed onto the front seat occupants as desired.

Figure 11.1.40 shows schematically a combined air-heating and air-cooling system; various dampers control the proportions of fresh and recirculated air to the heater or evaporator core; air temperature is controlled by a thermostat, which switches the compressor on and off through a magnetic clutch. Electronic control systems eliminate manual changeover and thermostatically actuate the heating and cooling functions.

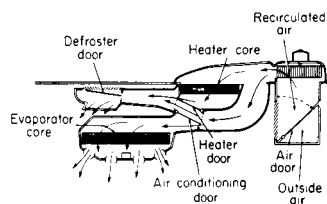


Fig. 11.1.40 Combined heater and air conditioner. (Chevrolet.)

General acceptance of ozone depletion attributable, in part, to chlorinated refrigerants in vehicular air-conditioning systems, led to legislation and regulations that brought about significant changes in air conditioning system design. These systems must be safe and environmentally acceptable, while performing the full range of vehicle cooling and heating requirements.

Regulations banning the use of chlorofluorocarbons (CFSs) have been adopted to protect the planet’s ozone layer from these chemicals. In the mid-1990s, automotive air conditioning systems commonly use HFC-134a refrigerant, which has thermodynamic properties similar to the formerly used CFC-12. Extensive developmental activity and engineering performance testing shows that cooling capacity and compressor power consumption for the two refrigerants are closely comparable. Figure 11.1.41 presents a schematic drawing of a representative air conditioning system using HFC-134a refrigerant and a variable displacement compressor.

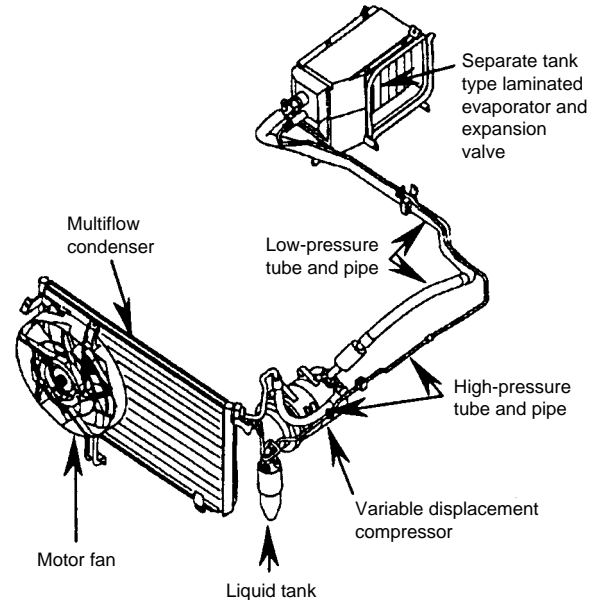


Fig. 11.1.41 Schematic of air conditioning system using HFC-134a refrigerant. (Reprinted with permission from SAE, SP-916, ©1992, Society of Automotive Engineers, Inc.)

BODY STRUCTURE

Vehicle design layout can be characterized generally as front-engine, rear-wheel drive (large cars); front-engine, front-wheel drive (small and midsize cars); four-wheel drive (utility vehicles); and midengine, rear-wheel drive (sports cars). The two most commonly used basic body constructions are the unit construction and the body-and-frame. As illustrated in Figs. 11.1.42 and 11.1.43, a car of the body-and-frame design has a body that is bolted to a separate frame. Most of the suspension,

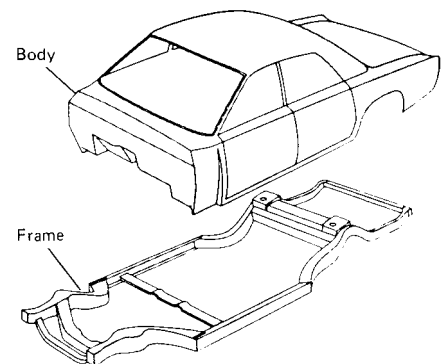


Fig. 11.1.42 Separate body and frame design.

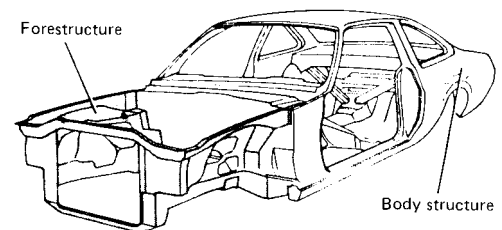


Fig. 11.1.43 Unit construction design for automobiles.

11-18 AUTOMOTIVE ENGINEERING

Table 11.1.3 Pounds of Material in a Typical Family Vehicle, 1978–1995

Material	1978		1985		1990		1995	
	lb	%	lb	%	lb	%	lb	%
Regular steel, sheet, strip, bar, and rod	1,915.0	53.6	1,481.5	46.5	1,405.0	44.7	1,398.0	43.6
High- and medium-strength steel	133.0	3.7	217.5	6.8	238.0	7.6	279.5	8.7
Stainless steel	26.0	0.7	29.0	0.9	34.0	1.1	46.0	1.4
Other steels	55.0	1.5	54.5	1.7	39.5	1.3	43.5	1.4
Iron	512.0	14.3	468.0	14.7	454.0	14.5	398.5	12.4
Plastics and plastic composites	180.0	5.0	211.5	6.6	229.0	7.3	246.5	7.7
Aluminum	112.5	3.2	138.0	4.3	158.5	5.0	187.5	5.8
Copper and brass	37.0	1.0	44.0	1.4	48.5	1.5	43.5	1.4
Powder metal parts	15.5	0.4	19.0	0.6	24.0	0.8	28.0	0.9
Zinc die castings	31.0	0.9	18.0	0.6	18.5	0.6	16.0	0.5
Magnesium castings	1.0	0.0	2.5	0.0	3.0	0.0	5.0	0.2
Fluids and lubricants	198.0	5.5	184.0	5.8	182.0	5.8	190.0	5.9
Rubber	146.5	4.1	136.0	4.3	136.5	4.3	136.0	4.2
Glass	86.5	2.4	85.0	2.7	86.5	2.8	91.5	2.9
Other materials	120.5	3.4	99.0	3.1	83.5	2.7	98.5	3.1
Total	3,569.5	100.0	3,187.5	100.0	3,140.5	100.0	3,208.0	100.0

SOURCE: "American Metal Market," copyright 1995 Capital Cities/ABC Inc. and "Motor Vehicle Facts & Figures," AAMA.
NOTE: 1 lb = 0.45 kg.

bumper, and brake loads are transmitted to the car's frame. A car of the **unit construction** or unitized design, commonly used for small and mid-size cars, utilizes the body structure to react to stresses and loads. Unit bodies are complex structures consisting of stamped sheet metal sections that are welded together, forming a framework to which an outer skin is attached.

MATERIALS

(See also Sec. 6.)

In the 1990s, the trend toward smaller, lighter, more fuel-efficient, more corrosion-resistant cars has led to growth in the use of such materials as high-strength steel, galvanized steel, aluminum, and a variety of plastics materials. Table 11.1.3 provides a **breakdown of materials usage** beginning with 1978 and including a 1995 projection. In this table, the "other" material category includes sound deadeners and sealers, paint and corrosion-protective dip, ceramics, cotton, cardboard, and miscellaneous other materials.

Motor vehicle design and materials specification are greatly influenced by life-cycle requirements that extend to **recycling** the material from scrapped vehicles. In the mid 1990s, 94 percent of scrapped vehi-

cles are processed for recycling. Approximately 75 percent of an automobile's material content is recycled. Figure 11.1.44 shows a general breakdown for materials disposition from **recycled vehicles**.

TRUCKS

Since the beginning of the motor vehicle industry at the turn of the century, **trucks** have been an important segment of the industry. Many of the first motor vehicles were trucks, and closely paralleled automobile design technology. In the United States, in 1992, a total of nearly **60 million trucks** were in use. More than 50 million (of the total) were **light trucks** weighing 6,000 lb or less; about 5 million were light trucks weighing between 6,000 and 10,000 lb; and 700,000 were light trucks between 10,000 and 14,000 lb. The remaining approximately 3.3 million ranged in **medium** and **heavy** sizes from 14,001 to 60,000 lb and larger. In 1994 the average age of trucks in use was 8.4 years. About 29 percent of U.S. intercity ton-miles of goods and freight are transported by truck.

The breakdown of 6.4 million **truck sales** in 1994 was: 6.1 million light trucks, 167,000 medium-duty, and 186,000 heavy-duty. In 1994, light trucks were bought with the following percentages of optional equipment: automatic transmission, 78; four-wheel antilock brakes, 32; rear antilock brakes, 54; power steering, 97; four-wheel drive, 34; diesel engine, 4; and air conditioning, 86.

Trucks, generally, are grouped by **gross vehicle weight (GVW)** rating into light-duty (0 to 14,000 lb), medium-duty (14,001, to 33,000 lb), and heavy-duty (over 33,000 lb) categories. To determine GVW classification, truck capacities are further broken down into **classes 1 to 8**, as listed in Table 11.1.4.

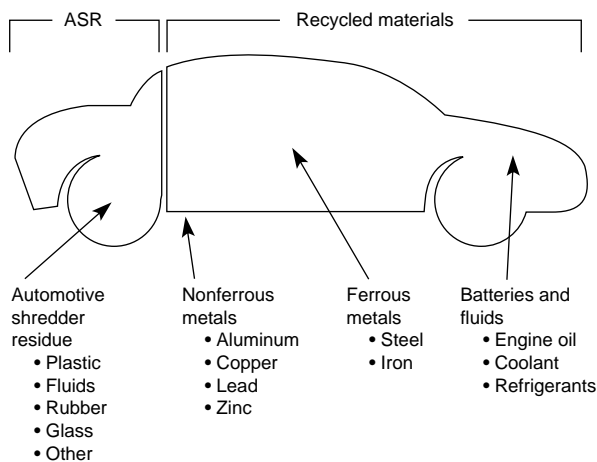


Fig. 11.1.44 Materials disposition from recycled vehicles. ("Motor Vehicle Facts & Figures," AAMA.)

Table 11.1.4 Gross Vehicle Weight Classification

GVW group	Class	Weight, kg (max)
6000 lb or less	1	2722
6001–10,000 lb	2	4536
10,001–14,000 lb	3	6350
14,001–16,000 lb	4	7258
16,001–19,500 lb	5	8845
19,501–26,000 lb	6	11,794
26,001–33,000 lb	7	14,469
33,001 lb and over	8	14,970

Truck Service Operations

Truck usage, purpose, or "vocation" is categorized by type of **service operation** as follows:

Class A Service: operation of motor vehicles on smooth, hard-surfaced highways in **level** country, where transmission gears are used only to accelerate the vehicle and payload from rest. Fast axle gear ratios are used.

Class B Service: operation of motor vehicles on smooth, hard-surfaced highways in **hilly** country where numerous grades are encountered. Requires intermittent use of transmission for short periods to surmount grades. The intermediate range of axle gear ratios is used in this class of service.

Class C Service: operation of motor vehicles for dump truck service, where the vehicle operates on loose **dirt, sand, or muddy roads** that offer high rolling resistance. This class of service also covers operation under conditions where the transmission is used for long periods in overcoming bad road conditions on long mountain grades. Vehicle design for this class of service usually calls for the slow range of axle gear ratios.

Class D Service: operation of motor vehicles in connection with **semi-trailers or trailers**. This type of service is confined to smooth, hard-surfaced highways. In this service, the gross vehicle weight is the gross train weight, that is, the total weight of truck, trailer, and load.

Truck weight classifications are used to differentiate truck sizes. To fully define the vehicle, engine type and truck mission or purpose need to be known. Figure 11.1.45 illustrates medium- and heavy-duty **truck classifications** by gross weight and vocation. Figure 11.1.46 shows life expectancy within the weight classes.

Class 8 (33,001 lb or over)



Class 7 (26,001 to 33,000 lbs.)



Class 6 (19,500 to 26,000 lbs.)



Fig. 11.1.45 Medium- and heavy-duty truck classification by gross weight and vehicle usage. (Reprinted with permission from SAE, SP-868, ©1991, Society of Automotive Engineers, Inc.)

Truck Engineering

A heavy-duty **truck drivetrain** is treated as an engineered, integral system that starts at the engine flywheel housing, transmission mounting surface, and flywheel pilot bearing and ends at the rear axle suspension mounting points. The most important information needed is the end-user description, including a customer/fleet profile. The following items provide a framework for starting and focusing the **truck engineering process**:

- Current vehicle specifications
- Gross cargo weight and percent of time at gross cargo weight
- What is hauled, where it is hauled
- Competition, including driveline
- Future trends and changes

- Past experience
- Trade-in cycle

System characteristics that dictate design include:

1. Basic vehicle performance: startability, gradeability, acceleration, fuel economy, trip time
2. Reliability and expected system life
3. Noise emission—pass-by
4. Ergonomics—controls, in-cab noise, vibration
5. Dynamics—vibration related to noise, safety, or early component failure
6. Mechanical mounting and attachment of system components
7. Maintenance and serviceability

Performance is a basic requirement in designing a truck or truck-trailer. Broadly, performance relates to a truck's ability to move a load economically under varying conditions of operation. The ability of a truck to move a load depends on the engine, transmission, axle ratio, and tire matched to the expected gross weight, road conditions, and road speed. The **engine** must provide adequate power to maintain the desired road speed with the specified load; the **transmission** must embody a range of speed selection to permit the engine to operate in the optimum range; **axle ratio** must be compatible with required road speed.

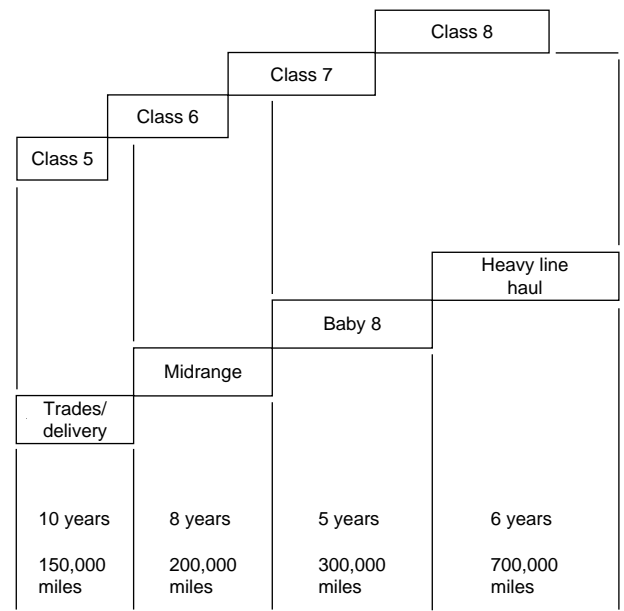


Fig. 11.1.46 Truck life expectancy in medium- and heavy-duty service. (Reprinted with permission from SAE, SP-868, ©1991, Society of Automotive Engineers, Inc.)

Power requirements for a given vehicle must be known before an engine and driveline can be selected. **Power required** is the sum of air, rolling, and grade resistances. Assuming the road surface remains constant, the grade resistance may be considered as increased rolling resistance. The **total resistance** and the power required can be determined when the following factors are known:

- Gross vehicle weight
- Maximum frontal cross-section area
- Drag coefficient
- Vehicle speed
- Road surface and grade

Truck **top speed** is design-controlled using one or more of three approaches:

1. **Gear limited:** the engine provides adequate reserve power to reach governed maximum rotational speed while driving the fully laden

11-20 RAILWAY ENGINEERING

vehicle over level ground. In this case, maximum truck speed is proportional to the maximum governed engine speed, cruise gear ratios, and tire rolling radius. Reserve power is provided to permit the truck to maintain the desired **geared speed** when slight grades or head winds are encountered.

2. **Road speed governed:** applied and installed as a means to limit vehicle top speed, without sacrificing performance when the truck is operating at speeds below maximum. Safety is a principal purpose of a road speed governor. Governing also contributes to engine life and fuel economy through reduced engine speed while cruising at the maximum **governed truck speed**. Electronic fuel systems provide increased engine-driver/train-vehicle control.

3. **Horsepower limited:** the horsepower to propel the truck over level ground must overcome rolling resistance and air resistance. Rolling resistance increases linearly with vehicle speed. Air resistance increases as the cube of vehicle speed.

Because the power required to overcome air resistance increases as the **cube of vehicle speed**, aerodynamic drag or wind resistance is a

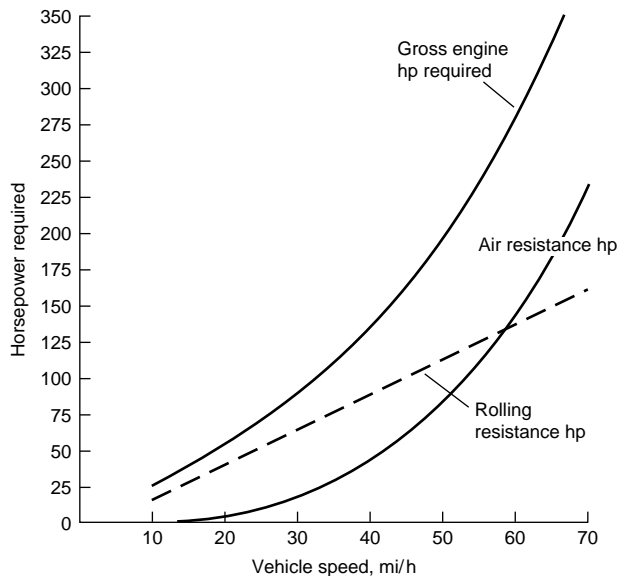


Fig. 11.1.47 Aerodynamic drag effect on truck power requirement to overcome air resistance. (Reprinted with permission from SAE, "Motor Truck Engineering Handbook," ©1994, Society of Automotive Engineers, Inc.)

significant consideration in truck engineering and truck operations. For heavy-duty trucks, including truck-trailer combinations, frontal area ranges from 50 to 102 ft² (4.6 to 9.5 m²). Drag coefficients range from about 0.6 to 1.0. The **drag coefficient** for a representative Class 8 truck-trailer is about 0.7.

Published data and testing indicate that **fuel savings** from aerodynamic improvements are equivalent to fuel savings attained by chassis weight reduction and require fewer services to maintain. Approximately half the driving force reaching the powered wheels is needed to overcome air resistance at cruising speed, as shown in Fig. 11.1.47. This is similar, in order of magnitude, to the aerodynamic effects discussed earlier for automobiles. For trucks, a reduction of approximately 10 percent in drag results in a fuel savings of about 5 percent, or nearly 1000 gallons per year.

Truck Noise Emissions

Commercial vehicle manufacturers are required to comply with a U.S. federal law restricting the **pass-by noise** emitted from a new production vehicle. A maximum sound pressure level of 80 dBA is allowed when subjecting a vehicle to the pass-by test described in SAE J366, "Exterior Sound Level for Heavy Trucks and Buses." This procedure measures the maximum **exterior sound level** the vehicle produces under a prescribed condition where the vehicle does not exceed 35 mi/h. Tire noise becomes a significant factor at higher speeds, so the test is designed specifically to include all noise except tires. Another procedure, SAE J57, "Truck Noise Control," is used to measure tire noise.

Truck Design Constraints and Prospects

Historically, **commercial trucks** replaced the horse and wagon. Dirt roads evolved into a paved national highway system. Early truck developments focused on increased load-carrying capacity, higher highway speeds, and improved component life. Currently, component life improvements continue while loads are limited to conserve the highway structure. Truck speeds are limited to conserve fuel and improve safety.

Conservation of natural resources and the highway system are important considerations that will extend into the future. Concerns over the air we breathe and vehicle traffic densities are **important factors** that significantly influence truck design engineering and operational performance.

It is expected that **environmental, energy conservation**, and public safety concerns will continue to influence and direct the focus of future driver/train and overall truck vehicle engineering.

MOTOR VEHICLE ENGINES

For details on engines, see Sec. 9. For antifreeze-protection data, see Sec. 6.

11.2 RAILWAY ENGINEERING

by V. Terrey Hawthorne and Keith L. Hawthorne

(in collaboration with David G. Blaine, E. Thomas Harley, Charles M. Smith, John A. Elkins, and A. John Peters)

REFERENCES: *Proceedings*, Association of American Railroads (AAR), Mechanical Division. *Proceedings*, American Railway Engineering Association (AREA). *Proceedings*, American Society of Mechanical Engineers (ASME). "The Car and Locomotive Cyclopedic," Simmons-Boardman. J. K. Tuthill, "High Speed Freight Train Resistance," *University of Illinois Engr. Bull.*, **376**, 1948. A. I. Totten, "Resistance of Light Weight Passenger Trains," *Railway Age*, **103**, Jul. 17, 1937. J. H. Armstrong, "The Railroad—What It Is, What It Does," Simmons-Boardman, 1978. Publications of the International Government-Industry Research Program on Track Train Dynamics, Chicago. Publications of AAR Research and Test Department, Chicago. Max Ephraim, Jr., "The AEM-7—A New High Speed, Light Weight Electric Passenger Locomotive," ASME RT Division, 82-RT-7, 1982. W. J. Davis, Jr., *General Electric Review*, October 1926. R. A. Allen, Conference on the Economics and Performance of Freight Car

Trucks, October 1983. "Engineering and Design of Railway Brake Systems," The Air Brake Association, Sept. 1975. Code of Federal Regulations, Title 40, Protection of Environment. Code of Federal Regulations, Title 49, Transportation.

DIESEL-ELECTRIC LOCOMOTIVES

Diesel-electric locomotives and electric locomotives are classified by wheel arrangement; letters represent the number of adjacent driving axles in a rigid truck (A for one axle, B for two axles, C for three axles, etc.). Idler axles between drivers are designated by numerals. A plus sign indicates articulated trucks or motive power units. A minus sign indicates separate swivel trucks not articulated. This nomenclature is

fully explained in Standard S-523 issued by the Association of American Railroads (AAR). Virtually all modern locomotives are of either B-B or C-C configuration.

The high efficiency of the diesel engine is an important factor in its selection as a prime mover for traction. This efficiency at full or part load makes it ideally suited to the variable service requirements found in daily railroad operations. The diesel engine is a constant-torque machine that cannot be started under load and hence requires a variably coupled transmission arrangement. The electric transmission system allows it to make use of its full rated power output at low track speeds for starting and efficient hauling of heavy trains. Examples of the various diesel-electric locomotive types in service are shown in Table 11.2.1. A typical diesel-electric locomotive is shown in Fig. 11.2.1.

Most of the diesel-electric locomotives have a dc generator or rectified alternator coupled directly to the diesel engine crankshaft. The generator/alternator is electrically connected to dc series traction motors having nose suspension mountings. Some recent locomotives utilize gate turn-off (GTO) inverters and ac traction motors to obtain the benefits of increased adhesion and increased horsepower per axle. The tooth ratio of the axle-mounted gears to the motor pinion gears which they engage is determined by the speed range and is related to the type of service. A high ratio is used for freight where high tractive efforts and low speeds are required, whereas high-speed passenger locomotives have a lower ratio.

Diesel Engines Most new diesel-electric locomotives are equipped with either a V-type, two strokes per cycle, or V-type, four strokes per cycle, engine. Engines range from 8 to 20 cylinders each. Output power ranges from 1,000 hp to over 4,400 hp for a single engine application.

Two-cycle engines are aspirated with either a gear-driven blower or a turbocharger. Because these engines lack an intake stroke for natural aspiration, the turbocharger is gear driven at lower engine speeds. At higher engine speeds, when the exhaust gases contain enough energy to drive the turbocharger, an overriding clutch disengages the gear train. Free-running turbochargers are used on four-cycle engines, as at lower

speeds the engines are aspirated by the intake stroke. Two-cycle engines utilize a unit fuel injector which pumps, meters, and atomizes the fuel. The four-cycle engines use separate metering pumps and atomizing injectors.

The engine control governor is an electrohydraulic device used to regulate the speed and horsepower output of the diesel engine. It is a self-contained unit mounted on the engine and driven from one of the engine camshafts. It is equipped with its own oil supply and pressure pump.

The governor contains four solenoids which are actuated individually or in combination from the 74-V auxiliary generator/battery supply by a series of switches actuated by the engineer's throttle. There are eight power positions of the throttle, each corresponding to a specific value of engine rpm and horsepower. The governor maintains the predetermined value of engine rpm through a mechanical linkage to the engine fuel racks which control the amount of fuel metered to the cylinders.

One or more centrifugal pumps, gear-driven from the engine crankshaft, force water through passages in the cylinder heads and liners. The water temperature is automatically controlled by regulating shutter and fan operation, which in turn controls the passage of air through the cooling radiators, or by bypassing the water around the radiators. The fans (one to four per engine) may be motor driven or mechanically driven by the engine crankshaft. If mechanical drive is used, current practice is to drive the fans through a clutch, since it is wasteful of energy to operate the fans when cooling is not required.

The lubricating oil system supplies clean oil at the proper temperature and pressure to the various bearing surfaces of the engine, such as crankshaft, camshaft, wrist pins, and cylinder walls, and supplies oil to the heads of the pistons to remove excess heat. One or more gear-type pumps driven from the crankshaft are used to move the oil from the crankcase through strainers to the bearings and to the piston cooling passages, after which the oil runs by gravity to the crankcase. A heat exchanger is located in the system to permit all the oil to pass through it at some time during a complete cycle. The oil is cooled by passing engine cooling water through the other side of the exchanger. Paper

Table 11.2.1 Locomotives in Service in North America

Locomotive*		Service	Arrangement	Weight min./max. (1,000 lb)	Tractive effort		Number of cylinders	Horsepower rating (r/min)
Builder	Model				Starting† for min./max. weight (1,000 lb)	At continuous‡ speed (mi/h)		
Bombardier	HR-412	General purpose	B-B	240/280	60/70	60,400 (10.5)	12	2,700 (1,050)
Bombardier	HR-616	General purpose	C-C	380/420	95/105	90,600 (10.0)	16	3,450 (1,000)
Bombardier	LRC	Passenger	B-B	252 nominal	63	19,200 (42.5)	16	3,725 (1,050)
EMD	SW-1001	Switching	B-B	230/240	58/60	41,700 (6.7)	8	1,000 (900)
EMD	MP15	Multipurpose	B-B	248/278	62/69	46,822 (9.3)	12	1,500 (900)
EMD	GP40-2	General purpose	B-B	256/278	64/69	54,700 (11.1)	16	3,000 (900)
EMD	SD40-2	General purpose	C-C	368/420	92/105	82,100 (11.0)	16	3,000 (900)
EMD	GP50	General purpose	B-B	260/278	65/69	64,200 (9.8)	16	3,500 (950)
EMD	SD50	General purpose	C-C	368/420	92/105	96,300 (9.8)	16	3,500 (950)
EMD	F40PH-2	Passenger	B-B	260 nominal	65	38,240 (16.1)	16	3,000 (900)
GE	B18-7	General purpose	B-B	231/268	58/67	61,000 (8.4)	8	1,800 (1,050)
GE	B30-7A	General purpose	B-B	253/280	63/70	64,600 (12.0)	12	3,000 (1,050)
GE	C30-7A	General purpose	C-C	359/420	90/105	96,900 (8.8)	12	3,000 (1,050)
GE	B36-7	General purpose	B-B	260/280	65/70	64,600 (12.0)	16	3,600 (1,050)
GE	C36-7	General purpose	C-C	367/420	92/105	96,900 (11.0)	16	3,600 (1,050)
EMD	AEM-7	Passenger	B-B	201 nominal	50	33,500 (10.0)	NA§	7,000 §
EMD	GM6C	Freight	C-C	365 nominal	91	88,000 (11.0)	NA	6,000 §
EMD	GM10B	Freight	B-B-B	390 nominal	97	100,000 (5.0)	NA	10,000 §
GE	E60C	General purpose	C-C	364 nominal	91	82,000 (22.0)	NA	6,000 §
GE	E60CP	Passenger	C-C	366 nominal	91	34,000 (55.0)	NA	6,000 §
GE	E25B	Freight	B-B	280 nominal	70	55,000 (15.0)	NA	2,500 §

* Engines: Bombardier—model 251, 4-cycle, V-type, 9 × 10½ in cylinders.

EMD—model 645E, 2-cycle, V-type, 9½ × 10 in cylinders.

GE—model 7FDL, 4-cycle, V-type, 9 × 10½ in cylinders.

† Starting tractive effort at 25% adhesion.

‡ Continuous tractive effort for smallest pinion (maximum).

§ Electric locomotive horsepower expressed as diesel-electric equivalent (input to generator).

¶ Not applicable.

11-22 RAILWAY ENGINEERING

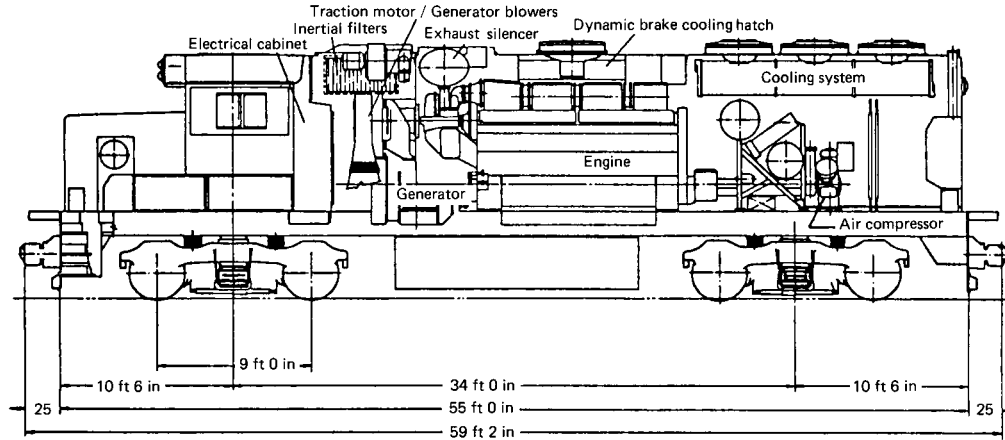


Fig. 11.2.1 Locomotive general arrangement. (Courtesy of M. Ephraim, ASME, Rail Transportation Division.)

element cartridge filters in series with the oil flow are used to remove any fine impurities in the oil before it enters the engine.

Electric Transmission Equipment A main generator or three-phase ac alternator is directly coupled to the diesel engine crankshaft. Alternator output is rectified through a full-wave bridge to minimize ripple to a level acceptable for operation of series field dc motors or for input to the solid-state inverter system for ac motors.

Generator power output is controlled by (1) varying engine speed through movement of the engineer's controller and (2) controlling the flow of current in its battery field or in the field of a separate exciter generator. The shunt and differential fields (if used) are designed to maintain a constant generator power output for a given engine speed as the propulsion system and voltage vary. They do not completely accomplish this, thus the battery field or separately excited field must be controlled by the load regulator to provide the final adjustment in excitation to load the engine properly. This field is also automatically deenergized to reduce or remove the load, when certain undesirable conditions occur, to prevent damage to the power plant or other traction equipment.

The engine main generator or alternator power plant functions at any throttle setting as a constant-horsepower source of energy. Therefore, the main generator voltage must be controlled to provide constant power output for each specific throttle position under varying conditions of locomotive speed, train resistance, atmospheric pressure, and quality of fuel. The load regulator, which is an integral part of the governor, accomplishes this within the maximum safe values of main-generator voltage and current. For example, when the locomotive experiences an increase in track gradient with a consequent reduction in speed, traction-motor counter-emf decreases, causing a change in traction-motor and main-generator current. Because this alters the load demand on the engine, the speed of the engine tends to change to compensate. As the speed changes, the governor begins to reposition the fuel racks, but at the same time a pilot valve in the governor directs hydraulic pressure into a load regulator vane motor which changes the resistance value of the load regulator rheostat in series with the main-generator excitation circuit. This alters the main-generator excitation current and consequently, main-generator voltage and returns the value of main-generator power output to normal. Engine fuel racks return to normal, consistent with constant values of engine speed.

The load regulator is effective within maximum and minimum limit values of the rheostat. Beyond these limits the power output of the engine is reduced. However, protective devices in the main generator excitation circuit limit the voltage output to ensure that values of current and voltage in the traction motor circuits are within safe limits.

Auxiliary Generating Apparatus Dc power for battery charging, lighting, control, and cab heaters is furnished by a separate generator, geared to the main engine. Voltage output is regulated within 1 percent

of 74 V over the full range of engine speeds. Auxiliary alternators with full-wave bridge rectifiers are also utilized for this application.

Traction motor blowers are mounted above the locomotive underframe. Air from the centrifugal blower housings is carried through the underframe and into the motor housings through flexible ducts. Other designs are being developed to vary the air output with cooling requirements to conserve parasitic energy demands.

Traction motors are nose-suspended from the truck frame and bearing-suspended from the axle (Fig. 11.2.2). The traction motors employ

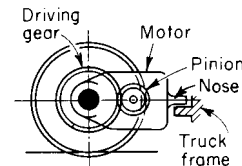


Fig. 11.2.2 Axle-hung traction motor for diesel-electric and electric locomotives.

series-exciting (main) and commutating field poles. The current in the series field is reversed to change locomotive direction and may be partially shunted through resistors to reduce counter-emf as locomotive speed is increased. Newer locomotives dispense with field shunting to improve commutation. Early locomotive designs also required motor connection changes (series, series/parallel, parallel) referred to as transition, to maintain motor current as speed increased.

AC traction motors employ a variable-frequency supply derived from a computer-controlled solid-state inverter system, fed from the rectified alternator output. Locomotive direction is controlled by reversing the sequence of the three-phase supply.

The development of the modern traction alternator with its high output current has resulted in a trend toward traction motors that are permanently connected in parallel. DC motor armature shafts are equipped with grease-lubricated roller bearings, while ac traction-motor shafts are supplied with a grease-lubricated roller bearing at the free end and an oil-lubricated bearing at the pinion drive end. Traction-motor support bearings are usually of the plain sleeve type with lubricant wells and spring-loaded felt wicks which maintain constant contact with the axle surface.

Electrical Controls In the conventional dc propulsion system, electropneumatic or electromagnetic contactors are used to make and break the circuits between traction motors and the main generator. They are equipped with interlocks for various control-circuit functions. Similar contactors are used for other power and excitation circuits of lower power (amperage). An electropneumatic or electric-motor-operated cam switch, consisting of a two-position drum with copper segments

moving between spring-loaded fingers, is generally used to reverse traction-motor field current ("reverser") or to set up the circuits for dynamic braking. This switch is not designed to operate under load. On some dc locomotives these functions have been accomplished with a system of contactors. In the ac propulsion systems, the power-control contactors are totally eliminated since their function is performed by the solid-state switching devices in the inverters.

Cabs In order to promote uniformity and safety, the AAR has issued standards for many locomotive cab features, such as cab seats, water cooler and toilet installation, and flooring. Locomotive cab noise levels are prescribed by CFR 49§229.121.

Propulsion control circuits transmit the engineer's movements of the throttle lever, reverse lever, and transition or dynamic-brake control lever in the controlling unit to the power-producing equipment of each unit operating in multiple in the locomotive consist. Before power is applied, all reversers must move to provide proper motor connections for the directional movement desired, taking into account the direction in which each locomotive unit is headed. Power contactors complete the circuits between generators and motors. For dc propulsion systems excitation circuits then function to provide the proper main-generator field current while the engine speed increases to correspond to the engineer's throttle position. In ac propulsion systems, all power circuits are controlled by computerized switching of the inverter. To provide for multiple-unit operation, the control circuits are connected between locomotive units by jumper cables. The AAR has issued Standard S-512 covering standard dimensions and contact identification for 27-point control jumpers used between diesel-electric locomotive units.

Wheel slip is detected by some form of sensing equipment connected electrically to the motor circuits or mechanically to the axles. When slipping occurs on some units, relays automatically reduce main generator excitation until slipping ceases, whereupon power is gradually reapplied. On newer units, an electronic system senses small changes in motor current and reduces motor current before a slip occurs. An advanced system recently introduced adjusts wheel creep to maximize wheel-to-rail adhesion. Wheel speed is compared to ground speed, which is accurately measured by radar. A warning light and/or buzzer in the operating cab informs the engineer, who, if the slip condition persists, must then notch back on the throttle.

Batteries Lead-acid storage batteries of 280 or 420 A·h capacity are usually used for starting the diesel engine. Thirty-two cells on each locomotive unit are used to provide 64 V to the system. (See also Sec. 15.) The batteries are charged from the 74-V power supply.

Air Brake System The "independent" brake valve handle at the engineer's position controls air pressure supplied from the locomotive reservoirs to the brake cylinders on the locomotive itself. The "automatic" brake valve handle (Fig. 11.2.3) controls the air pressure in the

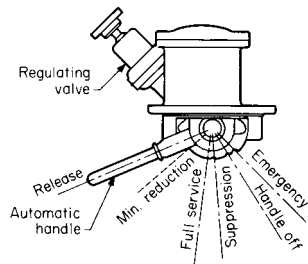


Fig. 11.2.3 Automatic-brake valve-handle positions for 26-L brake equipment.

brake pipe to the train. The AAR has issued Standard S-529, "Specifications for New Locomotive Standard Air Brake Equipment."

Compressed air for braking and for various pneumatic controls on the locomotive is supplied by a two-stage three-cylinder compressor, usually connected directly or through a clutch to the engine crankshaft. An unloader or the clutch is activated to maintain a pressure of approximately 130 to 140 lb/in² (896 to 965 kPa) in the main reservoirs. When

charging an empty trainline with the locomotive at standstill (maximum compressor demand), the engineer may increase engine (and compressor) speed without feeding power to the traction motors.

Dynamic Braking On most locomotives, dynamic brakes supplement the air brake system. The traction motors are used as generators to convert the kinetic energy of the locomotive and train into electrical energy, which is dissipated through resistance grids located near the locomotive roof. Motor-driven blowers, designed to utilize some of this braking energy, force cooler outside air over the grids and out through roof hatches. By directing a generous and evenly distributed airstream over the grids, their physical size is reduced in keeping with the relatively small space available in the locomotive. On some locomotives, resistor-grid cooling is accomplished by an engine-driven radiator/braking fan, but energy conservation is causing this arrangement to be replaced by motor-driven fans which can be powered in response to need using the parasitic power generated by dynamic braking itself.

By means of a cam-switch reverser, the traction motors are connected to the resistance grids; the motor fields are usually connected in series across the main generator to supply the necessary high excitation current. The magnitude of the braking force is set by controlling the traction motor excitation and the resistance of the grids. Conventional dynamic braking is not usually effective below 10 mi/h (16 km/h), but it is very useful at 20 to 30 mi/h (32 to 48 km/h). Some locomotives are equipped with "extended range" dynamic braking which enables dynamic braking to be used at speeds as low as 3 mi/h (5 km/h) by shunting out grid resistance (both conventional and extended range shown on Fig. 11.2.4). Dynamic braking is now controlled according to the "ta-

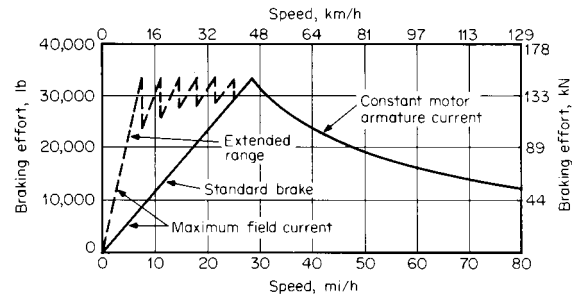


Fig. 11.2.4 Dynamic-braking effort versus speed. (Electro-Motive Division, General Motors Corp.)

pered" system, although the "flat" system has been used in the past. Dynamic braking control requirements are specified by AAR Standard S-518. Dynamic braking is especially advantageous on long grades where accelerated brake shoe wear and potential thermal damage to wheels could otherwise be problems. Other advantages are relieving crews from setting up air brake retainers on freight cars and smoother control of train speed. Dynamic brake grids can also be used for a self-contained load-test feature which permits a standing locomotive to be tested for power output. On locomotives equipped with ac traction motors a constant dynamic braking (flat-top) force can be achieved from the horsepower limit down to 2 mi/h (3 km/h).

Performance

Engine Indicated Horsepower The horsepower delivered at the diesel locomotive drawbar is the end result of a series of subtractions from the original indicated horsepower of the engine, made to take into account efficiency of transmission equipment and losses due to the power requirements of various auxiliaries. The formula for the engine's indicated horsepower is

$$ihp = PLAN/33,000 \tag{11.2.1}$$

where P = mean effective pressure in the cylinder, lb/in²; L = length of piston stroke, ft; A = piston area, in²; and N = total number of cycles completed per min. Factor P is governed by the overall condition of the

11-24 RAILWAY ENGINEERING

engine, quality of fuel, rate of fuel injection, completeness of combustion, compression ratio, etc. Factors L and A are fixed with design of engine. Factor N is a function of engine speed, number of working chambers, and strokes needed to complete a cycle. (See also Secs. 4 and 9.)

Engine Brake Horsepower In order to calculate the horsepower delivered to the crankshaft coupling (main-generator connection), frictional losses in bearings and gears must be subtracted from the **indicated horsepower** (ihp). Some power is also used to drive lubricating-oil pumps, governor, water pump, scavenging blower, and other auxiliary devices. The resultant horsepower at the coupling is **brake horsepower** (bhp).

Rail Horsepower A portion of the engine bhp is transmitted mechanically via couplings or gears to operate the traction motor blowers, air brake compressor, auxiliary generator, and radiator cooling fan generator or alternator. Part of the auxiliary generator electric output is used to run some of the auxiliaries. The remainder of the engine bhp transmitted to the main generator or main alternator for traction purposes must be multiplied by generator efficiency (usually about 91 percent), and the result again multiplied by the efficiency of the traction motors (including power circuits) and gearing to develop rail horsepower. Power output of the main generator for traction may be expressed as

$$\text{Watts}_{\text{traction}} = E_g \times I_m \quad (11.2.2)$$

where E_g is the main-generator voltage and I_m is the traction motor current in amperes, multiplied by the number of parallel paths or the dc link current in the case of an ac traction system.

Rail horsepower may be expressed as

$$\text{hp}_{\text{rail}} = V \times \text{TE}/375 \quad (11.2.3)$$

where V is the velocity, mi/h, and TE is tractive effort at the rail, lb.

Thermal Efficiency The thermal efficiency of the diesel engine at the crankshaft, or the ratio of bhp output to the rate at which energy of the fuel is delivered to the engine, is about 33 percent. Thermal efficiency at the rail is about 26 percent.

Drawbar Horsepower The drawbar horsepower represents power available at the rear of the locomotive to move the cars and may be expressed as

$$\text{hp}_{\text{drawbar}} = \text{hp}_{\text{rail}} - \text{locomotive running resistance} \times V/375 \quad (11.2.4)$$

where V is the speed in mi/h. Running resistance calculations are discussed later under Vehicle/Track Interaction. Theoretically, therefore, drawbar horsepower available is power output of the diesel engine less parasitic losses described above.

Speed-Tractive Effort At full throttle the losses vary somewhat at different values of speed and tractive efforts, but a curve of tractive effort plotted against speed is nearly hyperbolic. Figure 11.2.5 is a typical speed-tractive effort curve for a 3,500 hp (2,600 kW) freight locomotive. The diesel-electric locomotive has full horsepower available over the entire speed range (within limits of adhesion described below). The reduction in power as continuous speed is approached is referred to as "power matching." This allows the mixing of units with varied power per axle at the same continuous speed.

Adhesion In Figure 11.2.6 the maximum value of tractive effort represents the usually achievable level just before the wheels slip under average rail conditions. Adhesion is usually expressed as a percentage with the nominal level being 25 percent. This means that a force equal to 25 percent of the total locomotive weight on drivers is available as tractive effort. Actually, at the point of wheel slip, adhesion will vary widely with rail conditions, from as low as 5 percent to as high as 35 percent or more. Adhesion is severely reduced by lubricants which spread as thin films in the presence of moisture on running surfaces. Adhesion can be increased with sand applied to the rails from the locomotive sanding system. More recent wheel slip systems permit wheel creep (very slow controlled slip) to achieve greater levels of tractive effort. Higher adhesion levels are available from ac traction motors; for

example, 45 percent at start-up and low speed with a nominal value of 35 percent.

Traction Motor Characteristics Motor torque is a function of armature current and field flux (which is a function of field current). Since

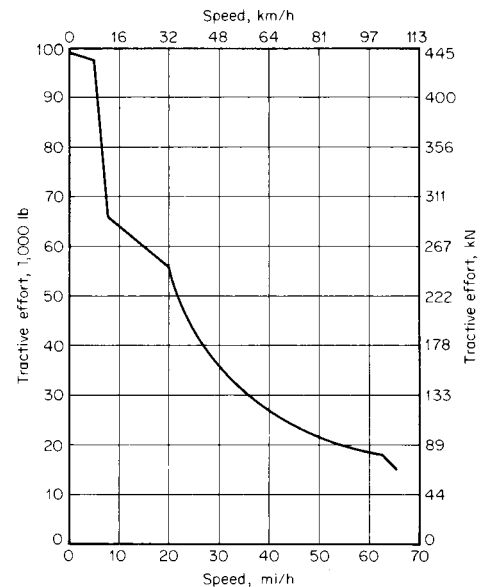


Fig. 11.2.5 Tractive effort versus speed.

traction motors are series connected, armature and field current are the same (except when field shunting circuits are introduced), and therefore tractive effort is a function solely of motor current. Figure 11.2.7 presents a group of traction motor characteristic curves with tractive effort, speed and efficiency plotted against motor current for full field (FF) and at 35 (FS1) and 55 (FS2) percent field shunting. Wheel diameter and gear ratio must be specified when plotting torque in terms of tractive effort. (See also Sec. 15.)

Traction motors are usually rated in terms of maximum continuous current. This represents the current at which the heating effect due to electrical losses in the armature and field windings is sufficient to raise the temperature of the motor to its maximum safe limit when cooling air

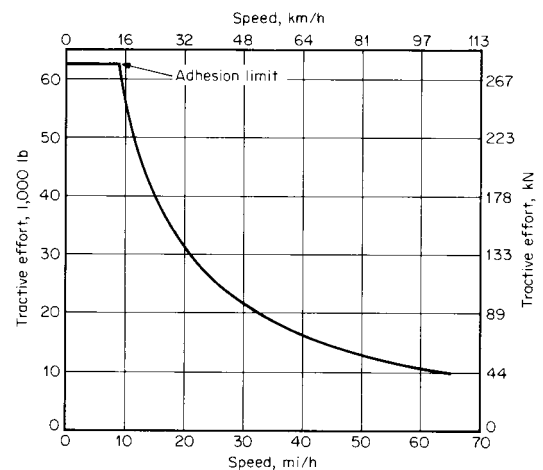


Fig. 11.2.6 Typical tractive-effort versus speed characteristics. (Electro-Motive Division, General Motors Corp.)

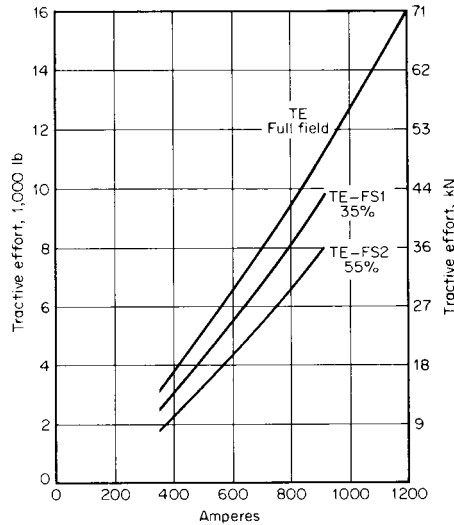


Fig. 11.2.7 Traction-motor characteristics. (Electro-Motive Division, General Motors Corp.)

at maximum expected ambient temperature is forced through it at the prescribed rate by the blowers. Continuous operation at this current level ideally allows the motor to operate at its maximum safe power level, with waste heat generated equal to heat dissipated. The tractive effort corresponding to this current is usually somewhat lower than that allowed by adhesion at very low speeds. Higher current values may be permitted for short periods of time (as when starting). These ratings are specified in time intervals and are posted on or near the load meter (ammeter) dial in the cab.

Maximum Speed Traction motors are also rated in terms of their maximum safe speed in r/min, which in turn limits locomotive speed. The gear ratio and wheel diameter are directly related to speed as well as the maximum tractive effort and the minimum speed at which full horsepower can be developed at the continuous rating of the motors. Maximum locomotive speed may be expressed as follows:

$$(mi/h)_{max} = \frac{\text{wheel diameter (in)} \times \text{maximum motor r/min}}{\text{gear ratio} \times 336} \quad (11.2.5)$$

where the gear ratio is the number of teeth on the motor gear mounted on the axle divided by the number of teeth on the pinion mounted on the armature shaft.

Locomotive Compatibility The AAR has developed two standards in an effort to improve compatibility between locomotives of different model, manufacture, and ownership: a standard 27-point control system (Standard S-512, Table 11.2.2) and a standard control stand (Standard S-523, Fig. 11.2.8). These features allow locomotives to be combined in multiple-unit service on all railroads irrespective of model or manufacturer.

Energy Conservation Efforts to improve efficiency and fuel economy have resulted in major changes in the prime movers, including more efficient turbocharging, fuel injection, and combustion. The auxiliary (parasitic) power demands have also been reduced with improvements which include fans and blowers which only move the air required by the immediate demand, air compressors that declutch when unloaded, and a selective low-speed idle. Fuel-saver switches permit dropping trailing locomotive units off the line when less than maximum power is required, and allow the remaining units to operate at maximum efficiency.

ELECTRIC LOCOMOTIVES

Electric locomotives are presently in limited use in North America. Freight locomotives are in dedicated service primarily for coal or min-

Table 11.2.2 Standard Dimensions and Contact Identification of 27-Point Control Plug and Receptacle for Diesel-Electric Locomotives

Receptacle point	Function	Code	Wire size, AWG
1	Power reduction setup, if used	(PRS)	14
2	Alarm signal	SG	14
3	Engine speed	DV	14
4*	Negative	N	14 or 10
5	Emergency sanding	ES	14
6	Generator field	GF	12
7	Engine speed	CV	14
8	Forward	FO	12
9	Reverse	RE	12
10	Wheel slip	WS	14
11	Spare		14
12	Engine speed	BV	14
13	Positive control	PC	12
14	Spare		14
15	Engine speed	AV	14
16	Engine run	ER	14
17	Dynamic brake	B	14
18	Unit selector circuit	US	12
19	2d negative, if used	(NN)	12
20	Brake warning light	BW	14
21	Dynamic brake	BG	14
22	Compressor	CC	14
23	Sanding	SA	14
24	Brake control/power reduction control	BC/PRC	14
25	Headlight	HL	12
26	Separator blowdown/remote reset	SV/RR	14
27	Boiler shutdown	BS	14

* Receptacle point 4—AWG wire size 12 is "standard" and AWG wire size 10 is "Alternate standard" at customer's request. A dab of white paint in the cover latch cavity must be added for ready identification of a no. 10 wire present in a no. 4 cavity.

eral hauling. Electric passenger locomotives are used in high-density service in the northeastern United States and a combination electric passenger and freight locomotive has been produced for use in Mexico.

Electric locomotives draw power from overhead catenary systems. While earlier systems used either direct current up to 3,000 V or single-phase alternating current at 11,000 V, 25 Hz, the newer systems use 25,000 or 50,000 V at 60 Hz. The higher voltage levels can only be used where clearances permit. Three-phase supply was tried briefly in this country and overseas about 50 years ago, but was abandoned because of the complexity of the required double catenary.

While the older dc locomotives used resistance control, ac locomotives have used a variety of systems including Scott-connected transformers; series ac motors; motor generators and dc motors; ignitrons and dc motors; silicon thyristors and dc motors; and, more recently, chopper control in experimental locomotives. Examples of the various electric locomotives in service are shown in Table 11.2.1.

An electric locomotive used in high-speed passenger service is shown in Fig. 11.2.9. High short-time ratings (Figs. 11.2.10 and 11.2.11) render electric locomotives suitable for passenger service where high acceleration rates and high speeds are combined to meet demanding schedules.

The modern electric locomotive in Fig. 11.2.9 obtains power for the main circuit and motor control from the catenary through a pantograph. A motor-operated switch provides for the transformer change from series to parallel connection of the primary windings to give a constant secondary voltage with either 25 kV or 12.5 kV primary supply. The converters for armature current consist of two asymmetric type bridges for one motor. The traction-motor fields are each separately fed from a one-way connected-field converter.

Identical control modules separate the control of motors on each truck. Motor sets are therefore connected to the same transformer wind-

11-26 RAILWAY ENGINEERING

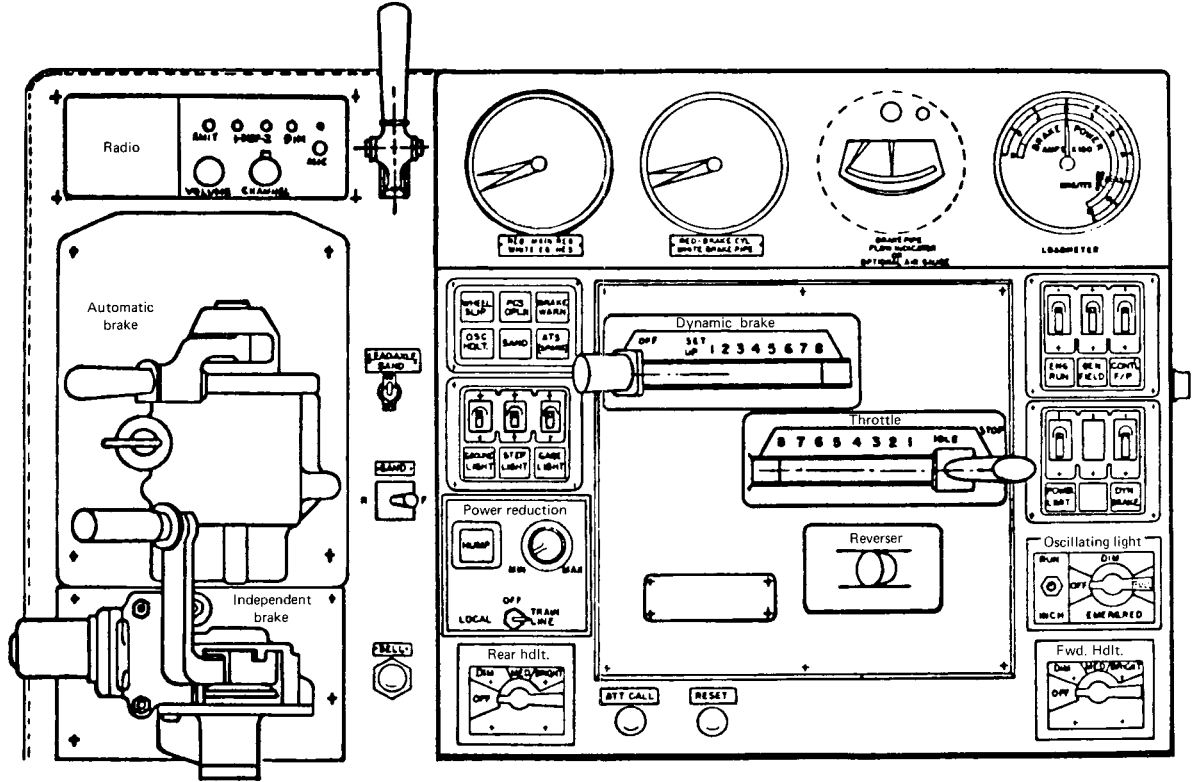


Fig. 11.2.8 AAR standard control stand.

ing. Wheel slip correction is also modularized, utilizing one module for each two-motor truck set. This correction is made with a complementary wheel-slip detection and correction system. A magnetic pickup speed signal is used for the basic wheel slip. Correction is enhanced by a magnetoelastic transducer used to measure force swings in the traction-motor reaction rods. This system provides the final limit correction.

To optimize the utilization of available adhesion, the wheel-slip control modules operate independently to allow the motor modules to receive different current references depending on their respective adhesion conditions.

All auxiliary machines, air compressor, traction motor blower, cooling fans, etc., are driven by three-phase 400-V, 60-Hz induction motors powered by a static inverter which has a rating of 175 kVA at a 0.8 power factor. When cooling requirements are reduced, the control system automatically reduces the voltage and frequency supplied to the blower motors to the required level. As a backup, the system can be powered by the static converter used for the head-end power requirements of the passenger cars. This converter has a 500-kW, 480-V, three-phase, 60-Hz output capacity and has a built-in overload capacity of 10 percent for half of any 1-h period.

Dynamic brake resistors are roof-mounted and are cooled by ambient

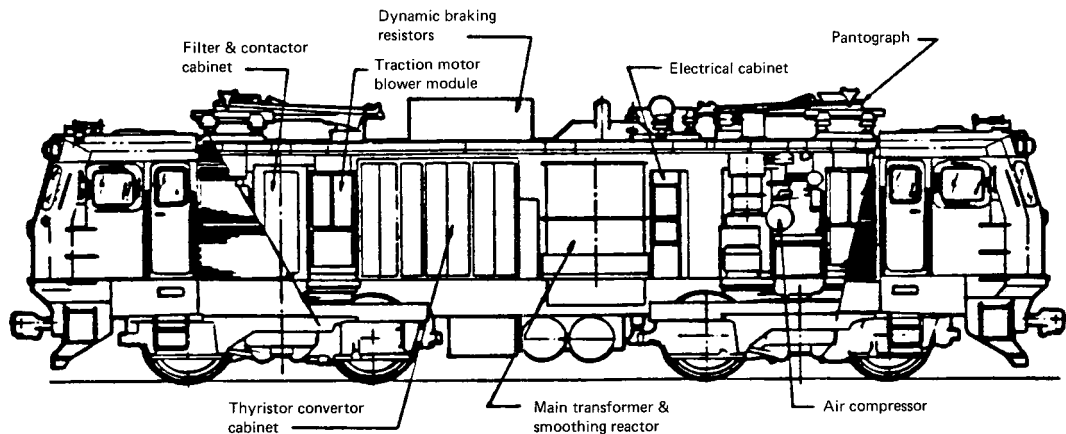


Fig. 11.2.9 Locomotive general arrangement. (Courtesy of M. Ephraim, ASME, Rail Transportation Division.)

airflow induced by locomotive motion. The dynamic brake capacity relative to train speed is shown in Fig. 11.2.12.

Many electric locomotives utilize traction motors identical to those used on diesel-electric locomotives. Some, however, use frame sus-

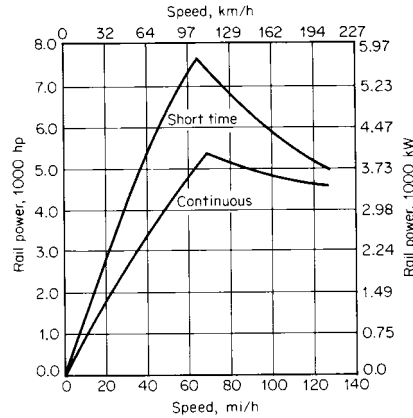


Fig. 11.2.10 Speed-horsepower characteristics (half-worm wheels). [Gear ratio = 85/36; wheel diameter = 50 in (1,270 mm); ambient temperature = 60°F (15.5°C).] (Courtesy of M. Ephraim, ASME, Rail Transportation Division.)

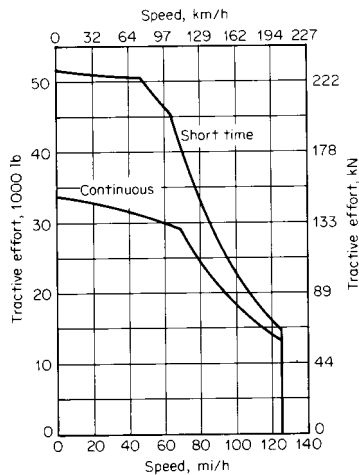


Fig. 11.2.11 Tractive effort versus speed (half-worm wheels). [Voltage = 11.0 kV at 25 Hz; gear ratio = 85/36; wheel diameter = 50 in (1,270 mm).] (Courtesy of M. Ephraim, ASME, Rail Transportation Division.)

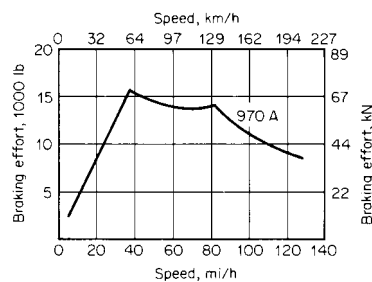


Fig. 11.2.12 Dynamic-brake performance. (Courtesy of M. Ephraim, ASME, Rail Transportation Division.)

ended motors with quill-drive systems (Fig. 11.2.13). In these systems, torque is transmitted from the traction motor by a splined coupling to a quill shaft and rubber coupling to the gear unit. This transmission allows for greater relative movement between the traction motor (truck frame) and gear (wheel axle) and reduces unsprung weight.

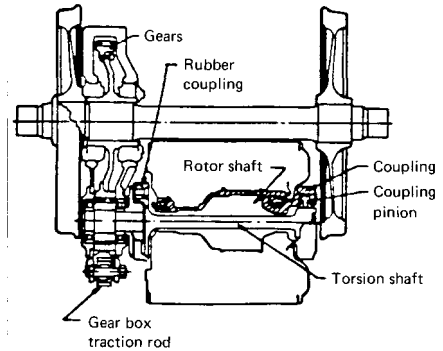


Fig. 11.2.13 Frame-suspended locomotive transmission. (Courtesy of M. Ephraim, ASME, Rail Transportation Division.)

FREIGHT CARS

Freight Car Types

Freight cars are designed and constructed for either general service or specific loadings. The Association of American Railroads (AAR) has established design and maintenance criteria to assure the interchangeability of freight cars on all North American railroads. Freight cars which do not conform to AAR standards have been placed in service by special agreement of the railroads over which the cars operate. The AAR "Manual of Standards and Recommended Practices" specifies dimensional limits, weights, and other design criteria for cars which may be freely interchanged between North American railroads. This manual is revised annually by the AAR. Many of the standards are reproduced in the "Car and Locomotive Cyclopedia," which is revised about every 4 years. Safety appliances (such as end ladders, sill steps, and uncoupling levers), braking equipment, and certain car design features and maintenance practices must comply with the Safety Appliances Act, the Power Brake Law, and the Freight Car Safety Standards covered by the Federal Railroad Administration's (FRA) Code of Federal Regulations (CFR Title 49). Maintenance practices are discussed in the Field Manual of the AAR Interchange Rules and pricing information is provided in the companion Office Manual.

The AAR identifies most cars by nominal capacity, type, and in some cases there are restrictions as to type of load (i.e., food, automobile parts, coil steel, etc.). Most modern cars have nominal capacities of either 70 or 100 tons.* A 100-ton car is limited to a maximum gross rail load of 263,000 lb (119.3 t*) with 6½ by 12 in (165 by 305 mm) axle journals, four pairs of 36-in (915-mm) wheels and a 70-in (1,778 mm) rigid wheel base. Some 100-ton cars are rated at 286,000 lb and are handled by individual railroads on specific routes or by mutual agreement between the handling railroads. A 70-ton car is limited to a maximum gross rail load of 220,000 lb (99.8 t) with 6 by 11 in (152 by 280 mm) axle journals, four pairs of 33-in (838-mm) wheels with trucks having a 66-in (1,676-mm) rigid wheel base.

On some special cars where height limitations are critical, 28-in (711-mm) wheels are used with 70-ton axles and bearings. In these cases wheel loads are restricted to 22,400 lb (10.2 t). Some special cars are equipped with 38-in (965-mm) wheels in four wheel trucks having 7 by 14 in (178 by 356 mm) axle journals and 72-in (1,829-mm) wheel base. This application is prevalent in articulated double-stack (two-high) container cars. Interchange of these very heavy cars is by mutual agreement between the operating railroads involved.

* 1 ton = 1 short ton = 2,000 lb; 1 t = 1 metric ton = 1,000 kg = 2205 lb.

11-28 RAILWAY ENGINEERING

The following are the most common car types in service in North America. Dimensions given are for typical cars; actual measurements may vary.

Box Cars (Fig. 11.2.14a) There are six popular box-car types.

1. Unequipped box cars may have sliding doors or plug doors. Plug doors provide a tight seal from weather and a smooth interior. Unequipped box cars are usually of 70-ton capacity. These cars have tongue-and-groove or plywood lining on the interior sides and ends with nailable floors (either wood or steel with special grooves for locking nails). The cars carry typical general merchandise lading: packaged, canned, or bottled foodstuffs; finished lumber; bagged or boxed bulk commodities; or, when equipped with temporary door fillers, bulk commodities such as grain. [70 ton: $L = 50$ ft 6 in (15.4 m), $H = 11$ ft 0 in (3.4 m), $W = 9$ ft 6 in (2.9 m), truck centers = 40 ft 10 in (12.4 m).]

2. Specially equipped box cars usually have the same dimensions as unequipped cars but include special equipment to restrain lading from impacts and over-the-road vibrations. Equipped cars may have hydraulic-cushion units to dampen longitudinal shock at the couplers.

3. Insulated box cars have plug doors and special insulation. These cars carry foodstuffs such as unpasteurized beer, produce, and dairy products. These cars may be precooled by the shipper and maintain a heat loss rate equivalent to 1°F (0.55°C) per day.

4. Refrigerated box cars are used where transit times are longer. These cars are equipped with diesel-powered refrigeration units and are primarily used to carry produce. These are often 100-ton cars [$L = 52$ ft 6 in (16.0 m), $H = 10$ ft 6 in (3.2 m), truck centers = 42 ft 11 in (13.1 m)].

5. "All door" box cars have doors which open the full length of the car for loading package lumber products such as plywood and gypsum board.

6. High-cubic-capacity box cars with an inside volume of 10,000 ft³ (283 m³) have been designed for light-density lading.

Box-car door widths vary from 6 to 10 ft for single-door cars and 16 to 20 ft (4.9 to 6.1 m) for double-door cars. "All door" cars have clear doorway openings in excess of 25 ft (7.6 m). The floor height above rail for an empty uninsulated box car is approximately 44 in (1,120 mm) and for an empty insulated box car approximately 48 in (1,220 mm). The floor height of a loaded car can be as much as 3 in (76 mm) lower than the empty car.

Covered hopper cars (Fig. 11.2.14b) are used to haul bulk commodities which must be protected from the environment. Modern covered hopper cars are typically 100-ton cars with roof hatches for loading and from two to six bottom outlets for discharge. Cars used for dense commodities, such as fertilizer or cement, have two bottom outlets, round roof hatches, and volumes of 3,000 to 4,000 ft³ (84.9 to 113.2 m³). [100 ton: $L = 39$ ft 3 in (12.0 m), $H = 14$ ft 10 in (4.5 m), truck centers = 26 ft 2 in (8.0 m).] Cars used for grain service (corn, wheat, rye, etc.) have three or four bottom outlets, longitudinal trough roof hatches, and volumes of from 4,000 to 5,000 ft³ (113 to 142 m³). Cars used for hauling plastic pellets have four to six bottom outlets (for pneumatic unloading with a vacuum system), round roof hatches, and volumes of from 5,000 to 6,000 ft³ (142 to 170 m³). [100 ton: $L = 65$ ft 7 in (20.0 m), $H = 15$ ft 5 in (4.7 m), truck centers = 54 ft 0 in (16.5 m).]

Open-top hopper cars (Fig. 11.2.14c) are used for hauling bulk commodities such as coal, ore, or wood chips. A typical 100-ton coal hopper car will vary in volume depending on the light weight of the car and density of the coal to be hauled. Volumes range from 3,900 to 4,800 ft³ (110 to 136 m³). Cars may have three or four manually operated or 12 to 16 automatically operated bottom hoppers. Some cars are equipped with rotating couplers on one end to allow rotary dumping without uncoupling. [100 ton: $L = 53$ ft ½ in (16.2 m), $H = 12$ ft 8½ in (3.9 m), truck centers = 40 ft 6 in (12.3 m).] Cars intended for aggregate or ore service have smaller volumes for the more dense commodity. These cars typically have two manual bottom outlets. [100 ton: $L = 40$ ft 8 in (12.4 m), $H = 11$ ft 10½ in (3.6 m), truck centers = 29 ft 9 in (9.1 m).] Hopper cars used for chip services are configured for low-density loads. Volumes range from 6,500 to 7,500 ft³ (184 to 212 m³).

High-side gondola cars (Fig. 11.2.14d) are open-top cars typically used to haul coal or wood chips. These cars are similar to open-top hopper cars in volume but require a rotary coupler on one end for rotary dumping to discharge lading since they do not have bottom outlets. Rotary-dump coal gondolas are usually used in dedicated, unit-train service between a coal mine and an electric power plant. The length over coupler pulling faces is approximately 53 ft 1 in (16.2 m) to suit the standard coal dumper. [100 ton: $L = 50$ ft 5½ in (15.4 m), $H = 11$ ft 9 in (3.6 m), $W = 10$ ft 5¾ in (3.2 m), truck centers = 50 ft 4 in (15.3 m).] Wood chip cars are used to haul chips from sawmills to paper mills or particle-board manufacturers. These high-volume cars are either rotary-dumped or, when equipped with end doors, end-dumped. [100 ton: $L = 62$ ft 3 in (19.0 m), $H = 12$ ft 7 in (3.8 m), $W = 10$ ft 5¾ in (3.2 m), truck centers = 50 ft 4 in (15.3 m).] Rotary-dump aggregate or ore cars, called "ore jennies," have smaller volumes for the high-density load.

Bulkhead flat cars (Fig. 11.2.14e) are used for hauling such commodities as packaged finished lumber, pipe, or with special inward canted floors, pulpwood. Both 70- and 100-ton bulkhead flats are used. Typical deck heights are approximately 50 in (1,270 mm). [100 ton: $L = 61$ ft ¾ in (18.6 m), $W = 10$ ft 1 in (3.1 m), $H = 11$ ft 0 in (3.4 m), truck centers = 55 ft 0 in (16.8 m).] A few special bulkhead flat cars designed for pulpwood and lumber service have a full-height, longitudinal divider from bulkhead to bulkhead.

Tank cars (Fig. 11.2.14f) are used for liquids, compressed gases, and other ladings, such as sulfur, which can be loaded and unloaded in a molten state. Nonhazardous liquids such as corn syrup, crude oil, and mineral spring water are carried in nonpressure cars. Cars used to haul hazardous substances such as liquefied petroleum gas (LPG), vinyl chloride, and anhydrous ammonia are regulated by the U.S. Department of Transportation. Newer and earlier-built retrofitted cars equipped for hazardous commodities have safety features including safety valves, specially designed top and bottom "shelf" couplers which increase the interlocking effect between couplers and decrease the danger of disengagement due to derailment, head shields on the ends of the tank to prevent puncturing, bottom-outlet protection if bottom outlets are used, and thermal insulation to reduce the risk of rupturing in a fire. These features resulted from industry-government studies in the RPI-AAR Tank Car Safety Research and Test Program.

Cars for sulfur and other viscous-liquid service have heating coils on the shell so that steam may be used to liquefy the lading for discharge. [Pressure cars, 100 ton: volume = 20,000 gal (75.7 m³), $L = 59$ ft 11¾ in (18.3 m), truck centers = 49 ft 0¼ in (14.9 m).] [Nonpressure, 100 ton, volume = 21,000 gal (79.5 m³), $L = 51$ ft 3¼ in (15.6 m), truck centers = 38 ft 11¼ in (11.9 m).]

Intermodal Cars Conventional 89-ft (27.1-m) intermodal flat cars are equipped to haul one 45-ft (13.7 m) and one 40-ft (12.2 m) trailer with or without nose-mounted refrigeration units, two 45-ft (13.7 m) trailers (dry vans), or combinations of containers from 20 to 40 ft (6.1 to 12.2 m) in length. Hitches to support trailer fifth wheels may be fixed for trailer-only cars or retractable for conversion to haul containers or for driving trailers onto the cars where circus loading is required. Trailer hauling service (Fig. 11.2.14g) is called TOFC (trailer on flat car). Container service (Fig. 11.2.14h) is called COFC (container on flat car). [70 ton: $L = 89$ ft 4 in (27.1 m), $W = 10$ ft 3 in (3.1 m), truck centers = 64 ft 0 in (19.5 m).]

Introduction of larger trailers in highway service has led to the development of alternative TOFC and COFC cars. One technique involves articulation of skeletonized or well-type units into multiunit cars for lift-on loading and lift-off unloading (stand-alone well car, Fig. 11.2.14i and articulated well car, Fig. 11.2.14o). These cars are typically composed of from three to ten units. Well cars consist of a center well for double-stacked containers. [10-unit, skeletonized car; $L = 46$ ft 6¾ in (14.2 m) per end unit, $L = 465$ ft 3½ in (141.8 m).]

Another approach to hauling larger trailers is the two-axle skeletonized car. These cars, used either singly or in multiple combinations, can haul a single trailer from 40 to 48 ft long (12.2 to 14.6 m) with nose-

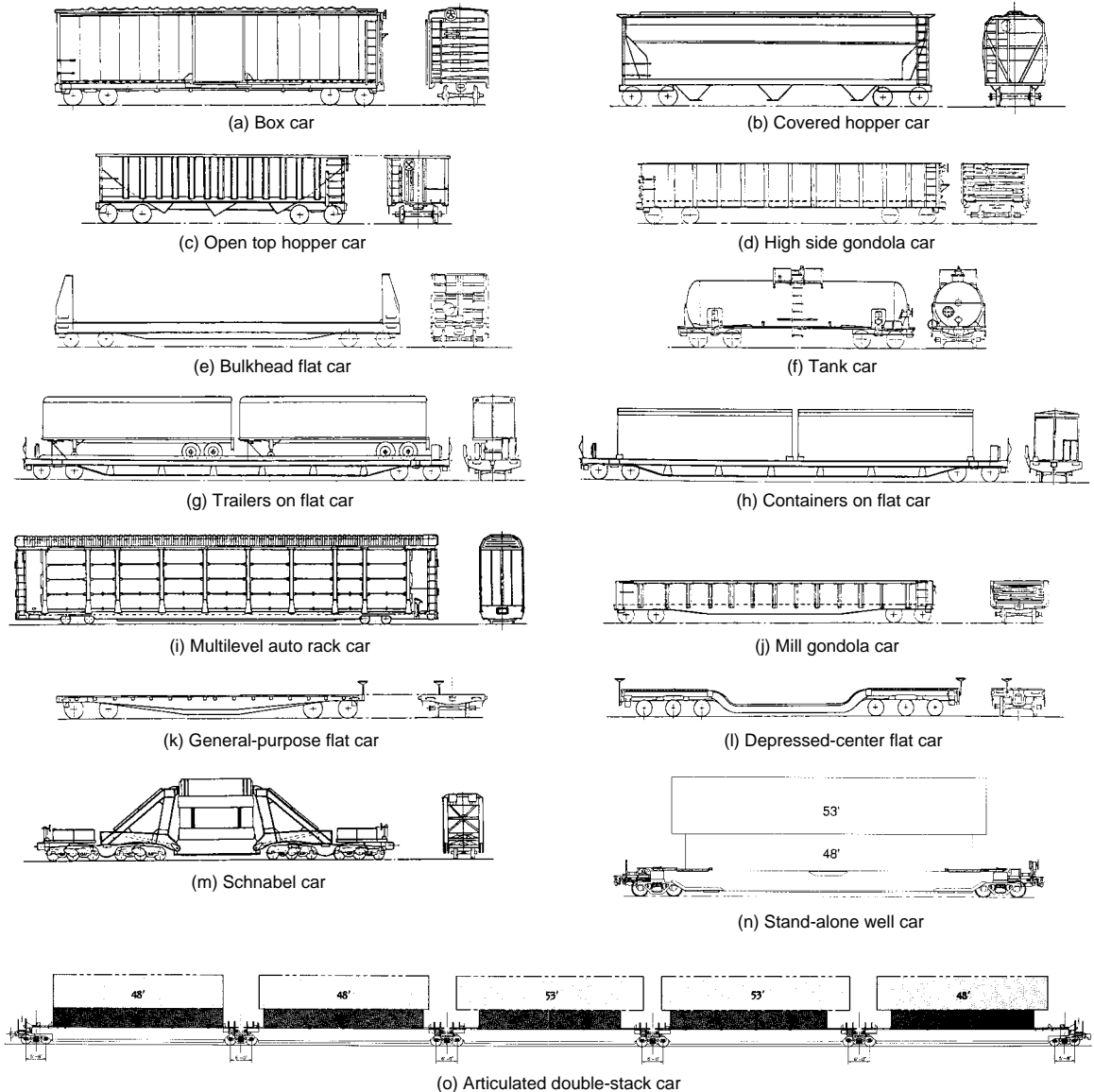


Fig. 11.2.14 Typical freight cars.

mounted refrigeration unit and 36- or 42-in (914- to 1070-mm) spacing between the kingpin and the front of the trailer.

Bilevel and trilevel **auto rack cars** (Fig. 11.2.14*i*) are used to haul finished automobiles and other vehicles. Most recent designs of these cars feature fully enclosed racks to provide security against theft and vandalism. [70 ton: $L = 89$ ft 4 in (27.2 m), $H = 18$ ft 11 in (5.8 m), $W = 10$ ft 7 in (3.2 m), truck centers = 64 ft 0 in (19.5 m).]

Mill gondolas (Fig. 11.2.14*j*) are 70-ton or 100-ton open-top cars principally used to haul pipe, structural steel, scrap metal, and when specially equipped, coils of aluminum or tinplate and other steel materials. [100 ton: $L = 52$ ft 6 in (16.0 m), $W = 9$ ft 6 in (2.9 m), $H = 4$ ft 6 in (1.4 m), truck centers = 43 ft 6 in (13.3 m).]

General-purpose or machinery flat cars (Fig. 11.2.14*k*) are 70-ton or 100-ton cars used to haul machinery such as farm equipment and highway tractors. These cars usually have wood decks for nailing lading-

restraint dunnage. Some heavy-duty six-axle cars are used for hauling off-highway vehicles such as army tanks and mining machinery. [100 ton, four axle: $L = 60$ ft 0 in (18.3 m), $H = 3$ ft 9 in (1.1 m), truck centers = 42 ft 6 in (13.0 m).] [200 ton, 8 axle: $L = 44$ ft 4 in (13.5 m), $H = 4$ ft 0 in (1.2 m), truck centers = 33 ft 9 in (10.3 m).]

Depressed-center flat cars (Fig. 11.2.14*l*) are used for hauling transformers and other heavy, large materials which require special clearance considerations. Depressed-center flat cars may have four-, six-, or dual four-axle trucks with span bolsters, depending on weight requirements.

Schnabel cars (Fig. 11.2.14*m*) are special cars for transformers and nuclear components. With these cars the load itself provides the center section of the car structure during shipment. Some Schnabel cars are equipped with hydraulic controls to lower the load for height restrictions and shift the load laterally for wayside restrictions. [472 ton: $L =$

11-30 RAILWAY ENGINEERING

22 ft 10 in to 37 ft 10 in (7.0 to 11.5 m), truck centers = 55 ft 6 in to 70 ft 6 in (16.9 to 21.5 m).] Schnabel cars must be operated in special trains.

Freight Car Design

The AAR provides specifications to cover minimum requirements for design and construction of new freight cars. Experience has demonstrated that the AAR Specifications alone do not ensure an adequate car design for all service conditions. The designer must be familiar with the intended service and increase the design criteria for the particular car above the minimum criteria provided by the AAR. The AAR requirements include stress calculations for the load-carrying members of the car and physical tests which may be required at the option of the AAR committee approving the car design. In some cases, it is advisable to operate an instrumented prototype car in service to detect problems which might result from unexpected track or train-handling input forces. The car design must comply with width and height restrictions shown in AAR clearance plates furnished in the specifications, Fig. 11.2.15. In addition, there are limitations on the height of the center of

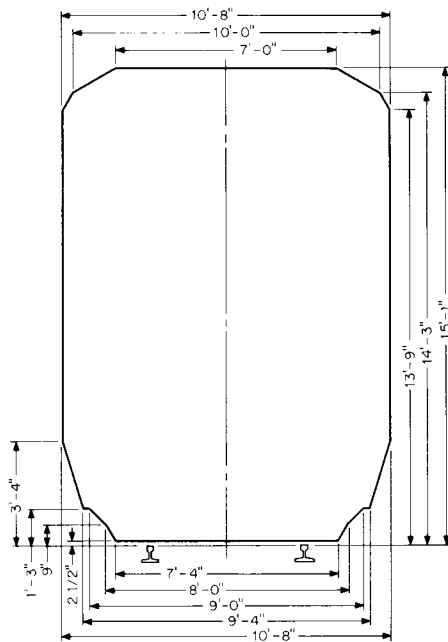


Fig. 11.2.15 AAR plate B equipment-clearance diagram.

gravity of the loaded car and on the vertical and horizontal curving capability allowed by the clearance provided at the coupler. The AAR provides a method of calculating the minimum radius curve which the car design can negotiate when coupled to another car of the same type or to a standard AAR "base" car. In the case of horizontal curves, the requirements are based on the length over the pulling faces of the car.

In the application for approval of a new or untried type of car, the Car Construction Committee of the AAR may require either additional calculations or tests to assess the design's ability to meet the AAR minimum requirements. These tests might consist of a static compression test of 1,000,000 lb (4.4 MN), a static vertical test applied at the coupler, and impact tests simulating yard impact conditions.

Freight cars are designed to withstand single-ended impact or coupling loads based upon the type of cushioning provided in the car design. Conventional friction, elastomer, or combination draft gears or short-travel hydraulic cushion units which provide less than 6 in (152 mm) of travel require a structure capable of withstanding a 1,250,000-lb (5.56-MN) impact load. For cars with hydraulic units that provide greater than 14 in (356 mm) of travel, the required design im-

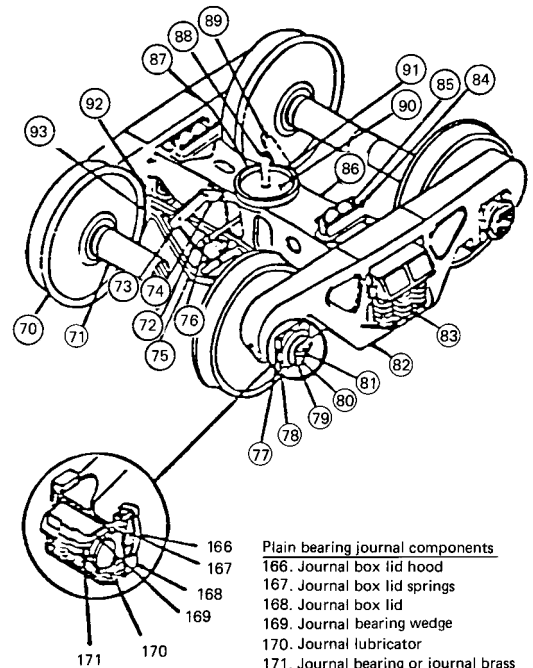
pact load is 600,000 lb (2.7 MN). In all cases, the structural connections to the car must be capable of withstanding a static compressive (squeeze) end load of 1,000,000 lb (4.44 MN) or a dynamic (impact) compressive load of 1,250,000 lb (5.56 MN).

The AAR has recently adopted requirements for unit trains of high-utilization cars to be designed for 3,000,000 mi (4.8 Gm) of service based upon fatigue life estimates. General-interchange cars which accumulate less mileage in their life should be designed for 1,000,000 mi (1.6 Gm) of service. Road environment spectra for various locations within the car are being developed for different car designs for use in this analysis. The fatigue strengths of various welded connections are provided in the AAR "Manual of Standards and Recommended Practices," Sec. C, Part II.

Many of the design equations and procedures are available from the AAR. Important information on car design and approval testing is contained in the AAR "Manual of Standards and Recommended Practice," Sec. C-II M-1001, Chap. XI.

Freight-Car Suspension

Most freight cars are equipped with standard three-piece trucks (Fig. 11.2.16) consisting of two side-frame castings and one bolster casting. Side-frame and bolster designs are subjected to both static and fatigue test requirements specified by the AAR. The bolster casting is equipped with a female centerplate bowl upon which the car body rests and side bearings located [generally 25 in (635 mm)] each side of the centerline.



- | | |
|-----|---------------------------------------|
| 166 | Plain bearing journal components |
| 167 | 166. Journal box lid hood |
| 168 | 167. Journal box lid springs |
| 169 | 168. Journal bearing wedge |
| 170 | 169. Journal lubricator |
| 171 | 170. Journal bearing or journal brass |

- | | |
|--|-----------------------------|
| <u>Unit beam roller bearing truck components</u> | |
| 70. Wheel | 82. Truck side frame |
| 71. Axle | 83. Truck springs |
| 72. Truck dead lever | 84. Truck side bearing |
| 73. Dead lever fulcrum | 85. Side bearing roller |
| 74. Dead lever fulcrum bracket | 86. Truck bolster |
| 75. Brake beam | 87. Truck center plate cast |
| 76. Bottom rod | 88. Truck live lever |
| 77. Roller bearing adapter | 89. Center pin |
| 78. Roller bearing assembly | 90. Horizontal wear plate |
| 79. End cap | 91. Vertical wear plate |
| 80. End cap retaining bolt | 92. Brake shoe key |
| 81. Locking plate | 93. Brake shoe |

Fig. 11.2.16 Unit-beam roller-bearing truck with inset showing plain-bearing journal. (AAR Research and Test Department.)

In most cases, the side bearings have clearance to the car body and are equipped with either flat sliding plates or rollers. In some cases, constant-contact side bearings or centerplate extension pads provide a resilient material between the car body and the truck bolster.

The centerplate arrangement consists of various styles of wear plates or friction materials and a vertical loose or locked pin between the truck centerplate and the car body.

Truck springs nested into the bottom of the side-frame opening support the end of the truck bolster. Requirements for spring designs and the grouping of springs are generally specified by the AAR. Historically, the damping provided within the spring group has utilized a combination of springs and friction wedges. In addition to friction wedges, in more recent years, some cars have been equipped with hydraulic damping devices which parallel the spring group.

A few trucks with a "steering" feature which includes an interconnection between axles to increase the lateral interaxle stiffness and decrease the interaxle yaw stiffness. Increased lateral stiffness improves the lateral stability and decreased yaw stiffness improves the curving characteristics.

Freight-Car Wheel-Set Design

A freight-car wheel set consists of wheels, axle, and bearings. Cast- and wrought-steel wheels are used on freight cars in North America (AAR "Manual of Standards and Recommended Practice," Sec. G). Freight-car wheels are subjected to thermal loads from braking, as well as mechanical loads at the wheel-rail interface. Experience with thermal damage to wheels has led to the introduction of "low stress" or curved plate wheels (Fig. 11.2.17). These wheels are less susceptible to the

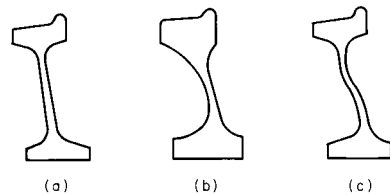


Fig. 11.2.17 Wheel-plate designs. (a) Flat plate; (b) parabolic plate; (c) S-curved plate.

development of circumferential tensile residual stresses which render the wheel vulnerable to sudden failure if a flange or rim crack occurs. New wheel designs introduced for interchange service must be evaluated using a finite-element technique employing both thermal and mechanical loads (AAR S-660).

Freight-car wheels range in diameter from 28 to 38 in (711 to 965 mm) depending on car weight, Table 11.2.3. The old AAR standard tread profile (Fig. 11.2.18a) has been replaced with the AAR-1B (Fig. 11.2.18c) profile which represents a worn profile to minimize early tread loss due to wear and provides a stable profile over the life of the tread. Several variant wheel tread profiles, including the AAR-1B, were developed from the basic Heumann design, Fig. 11.2.18b. One of these was for application in Canada and provided increasing concavity into the

Table 11.2.3 Wheel and Journal Sizes of Eight-Wheel Cars

Nominal car capacity, ton	Maximum gross weight, lb	Journal (bearing) size, in	Wheel diameter, in
50	177,000	5½ × 10	33
*	179,200	6 × 11	28
70	220,000	6 × 11	33
100	263,000‡	6½ × 12	36
125†	315,000	7 × 12	38

* Limited by wheel rating.
 † Not approved for free interchange.
 ‡ 286,000 in special cases.

throat of the flange, a design feature of the Heumann profile. This reduces curving resistance and increases wheel wear life.

Wheels are also specified by chemistry and heat treatment. Low-stress wheel designs of Classes B and C are required for freight cars. Class B wheels have a carbon content of 0.57 to 0.67 percent and are rim-quenched. Class C wheels have a carbon content of 0.67 to 0.77 percent and are also rim-quenched. Rim quenching provides a hardened running surface for a long wear life. Lower carbon levels than those in Class B may be used where thermal cracking is experienced but freight-car equipment generally does not require their use.

Axles used in interchange service are solid steel forgings with raised wheel seats. Axles are specified by journal size for different car capacities, Table 11.2.3.

Most freight car bearings are grease-lubricated, tapered-roller bearings (see Sec. 8). The latest bearing designs eliminate the need for periodic field lubrication.

Wheels are mounted and secured on axles with an interference fit. Bearings are mounted with an interference fit and retained by an end cap bolted to the end of the axle. Wheels and bearings for cars in interchange service must be mounted by an AAR-inspected and -approved facility.

Special Features

Many components are available to enhance the usefulness of freight cars. In most cases, the design or performance of the component is specified by the AAR.

Coupler Cushioning Switching of cars in a classification yard can result in relatively high coupler forces at the time of the impact between the moving and standing cars. Nominal coupling speeds of 4 mi/h (6.4 km/h) or less are sometimes exceeded, with lading damage a possible result. Conventional cars are equipped with an AAR-approved draft gear, usually a friction-spring energy-absorbing device, mounted between the coupler and the car body. The rated capacity of draft gears ranges between 20,000 ft·lb (27.1 kJ) for earlier units to over 65,000 ft·lb (88.1 kJ) for later designs. Impact forces of 1,250,000 lb (5.56 MN) can be expected when a moving 100-ton car strikes a string of standing cars at 8 to 10 mi/h (12.8 to 16 km/h). Hydraulic cushioning devices are available which will reduce the impact force to 500,000 lb (2.22 MN) at impact speeds of 12 to 14 mi/h (19 to 22 km/h). These

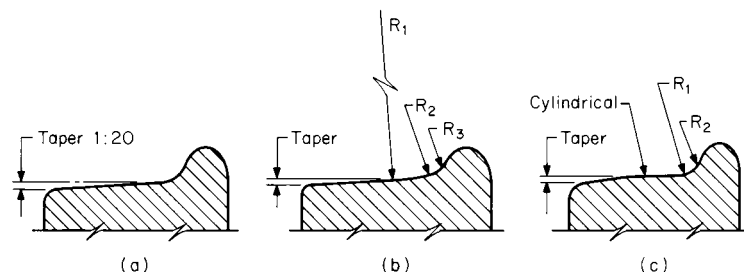


Fig. 11.2.18 Wheel-tread designs. (a) Obsolete standard AAR; (b) Heumann, (c) new AAR-1B.

11-32 RAILWAY ENGINEERING

devices may be either mounted at each end of the car (end-of-car devices) or mounted in a long beam which extends from coupler to coupler (sliding centersill devices).

Lading Restraint Many forms of lading restraint are available, from tie-down chains for automobiles on rack cars to movable bulkheads for boxcars. Most load-restraining devices are specified by the AAR "Manual of Standards and Recommended Practices" and approved car loading arrangements are specified in AAR "Loading Rules," a multi-volume publication for enclosed, open-top, and TOFC and COFC cars.

Covered Hopper Car Discharge Gates The majority of covered hopper cars are equipped with rack-and-pinion slide gates which allow the lading to discharge by gravity onto conveyor equipment located between the rails. These gates can be operated manually with a simple bar or a torque-multiplying wrench or mechanically with an impact or hydraulic wrench. Many special covered hopper cars are equipped with discharge gates with nozzles and metering devices for vacuum or pneumatic unloading.

Coupling Systems A majority of freight cars are connected with AAR standard couplers. A specification has been developed to permit the use of alternative coupling systems such as articulated connectors, drawbars, and rotary-dump couplers.

Freight-Train Braking

The retarding forces acting on a railway train are rolling and mechanical resistance, aerodynamic drag, curvature and grade, plus that force resulting from the friction of the brake shoes rubbing on the wheel treads. On locomotives so equipped, the dynamic or rheostatic brake using the traction motors as generators can provide all or a portion of the retarding force to control train speed on down grades and sometimes during retardation and service stops.

Quick-action automatic air brakes of the type specified by the AAR are the common standard in North America. With the automatic air brake, the brake pipe extends through every vehicle in the train, connected by hoses between each locomotive unit and car. The front and rear brake pipe angle cocks are closed.

Air pressure is provided by compressors on the locomotive units to the main reservoirs, usually at 130 to 150 lb/in² (900 to 965 kPa). (Pressure values are gage pressures.) The engineer's automatic brake valve in release position provides air to the brake pipe on freight trains at reduced pressure, usually at 75, 80, 85, or 90 lb/in² (520, 550, 585, or 620 kPa) depending on the type of service, train weight, descending grades, and speeds that a train will operate. In passenger service, brake pipe pressure is usually 90 or 100 lb/in² (620 or 760 kPa).

When brake pipe pressure is increased, the control valve allows the reservoir capacity on each car and locomotive to be charged and at the

same time connects the brake cylinders to exhaust. Brake pipe pressure is reduced when the engineer's brake valve is placed in a service position, and the control valve cuts off the charging function and allows the reservoir air on each car to flow into the brake cylinder. This moves the piston and, through a system of levers and rods, pushes the brake shoes against the wheel treads.

When the engineer's automatic brake valve is placed in the emergency position the brake pipe pressure (BP) is reduced very rapidly. The control valves on each car move to the emergency-application position and rapidly open a large vent valve, exhausting brake pipe pressure to atmosphere. This will serially propagate the emergency application through the train at from 900 to 950 ft/s (280 to 290 m/s). With the control valve in the emergency position both auxiliary- and emergency-reservoir volumes (pressures) equalize with the brake cylinder, and higher brake cylinder pressure (BCP) results, building up at a faster rate than in service applications.

The foregoing briefly describes the functions of the fundamental automatic air brake based on the functions of the control valve. AAR-approved brake equipment is required on all freight cars used in interchange service. The functions of the control valve have been refined to permit the handling of longer trains by more uniform brake performance. Important improvements in this design have been (1) reduction of the time required to apply the brakes on the last car of a train, (2) more uniform and faster release of the brakes, and (3) availability of emergency application with brake pipe pressure greater than 40 lb/in² (275 kPa).

The braking ratio of a car is defined as the ratio of brake shoe (normal) force to the car's rated gross weight. Two types of brake shoes, high-friction composition and high-phosphorus cast iron, are in use in interchange service. As these shoes have very different friction characteristics, different braking ratios are required to assure uniform train braking performance (Table 11.2.4). Actual or net shoe forces are measured with calibrated devices. The calculated braking ratio *R* (nominal) is determined from the equation

$$R = PLANE \times 100/W \quad (11.2.6)$$

where *P* = brake cylinder pressure, 50 lb/in² gage; *L* = mechanical ratio of brake levers; *A* = brake cylinder area, in²; *N* = number of brake cylinders; *E* = brake rigging efficiency = *E_r* × *E_b* × *E_c*; and *W* = car weight (lb).

To estimate rigging efficiency consider each pinned joint and horizontal sliding joint as a 0.01 loss of efficiency; i.e., in a system with 20 pinned and horizontal sliding joints, *E_r* = 0.80. For unit-type (hangerless) brake beams *E_b* = 0.90 and for the brake cylinder *E_c* = 0.95, giving overall efficiency of 0.684 or 68.4 percent.

Table 11.2.4 Braking Ratios, AAR Standard S-401

Type of brake rigging and shoes	With 50 lb/in ² brake cylinder pressure			Hand brake* Minimum percent of gross rail load
	Percent of gross rail load		Maximum percent of light weight	
	Min.	Max.		
Conventional body-mounted brake rigging or truck-mounted brake rigging using levers to transmit brake cylinder force to the brake shoes				
Cars equipped with cast iron brake shoes	13	20	53	13
Cars equipped with high-friction composition brake shoes	6.5	10	30	11
Direct-acting brake cylinders not using levers to transmit brake cylinder force to the brake shoes				
Cars equipped with cast iron brake shoes				
Cars equipped with high-friction composition brake shoes	6.5	10	33	11
Cabooses†				
Cabooses equipped with cast iron brake shoes			35–45	
Cabooses equipped with high-friction composition brake shoes			18–23	

* Hand brake force applied at the horizontal hand brake chain with AAR certified or AAR approved hand brake.

† Effective for cabooses ordered new after July 1, 1982, hand brake ratios for cabooses to the same as lightweight ratios for cabooses.

NOTE: Above braking ratios also apply to cars equipped with empty and load brake equipment.

The total retarding force in pounds per ton may be taken as:

$$F = (PLef/W) = F_g G \quad (11.2.7)$$

where P = total brake-cylinder piston force, lbf; L = multiplying ratio of the leverage between cylinder pistons and wheel treads; ef = product of the coefficient of brake shoe friction and brake rigging efficiency; W = loaded weight of vehicle, tons; F_g = gravity force, 20 lb/ton/percent grade; G = ascending grade, percent.

Stopping distance can be found by adding the distance covered during the time the brakes are fully applied to the distance covered during the equivalent instantaneous application time.

$$S = \frac{0.0334 V_2^2}{\left[\frac{W_n B_n (p_a / p_n) ef}{W_a} \right] + \left(\frac{R}{2000} \right) \pm (G)} + 1.467 t_1 \left[V_1 - \left(\frac{R + 2000G}{91.1} \right) \frac{t_1}{2} \right] \quad (11.2.8)$$

where S = stopping distance, ft; V_1 = initial speed when brake applied, mi/h; V_2 = speed, mi/h, at time t_1 ; W_a = actual vehicle or train weight, lb; W_n = weight on which braking ratio B_n is based, lb (see table for values of W_n for freight cars):

Capacity, ton	W_n , 1,000 lb
50	177
70	220
100	263
125	315

(for passenger cars and locomotives: W_n is based on empty or ready-to-run weight); B_n = braking ratio (total brake shoe force at stated brake cylinder, lb/in², divided by W_n); p_n = brake cylinder pressure on which B_n is based, usually 50 lb/in², p_a = full brake cylinder pressure, t_1 to stop; e = overall rigging and cylinder efficiency, decimal; f = typical friction of brake shoes, see below; R = total resistance, mechanical plus aerodynamic and curve resistance, lb/ton; G = grade in decimal, + upgrade, - downgrade; t_1 = equivalent instantaneous application time, s.

Equivalent instantaneous application time is that time on a curve of average brake cylinder buildup versus time for a train or car where the area above the buildup curve is equal to the area below the curve. A straight-line buildup curve starting at zero time would have a t_1 of half the total buildup time.

The friction coefficient f varies with the speed; it is usually lower at high speed. To a lesser extent, it varies with brake shoe force and with the material of the wheel and shoe. For stops below 60 mi/h (97 km/h), a conservative figure for a high-friction composition brake shoe on steel wheels is approximately

$$ef = 0.30 \quad (11.2.9)$$

In the case of high-phosphorus iron shoes, this figure must be reduced by approximately 50 percent.

P_n is based on 50 lb/in² (345 kPa) air pressure in the cylinder; 80 lb/in² is a typical value for the brake pipe pressure of a fully charged freight train. This will give a 50-lb/in² (345 kPa) brake cylinder pressure during a full service application on AB equipment, and a 60 lb/in² (415 kPa) brake cylinder pressure with an emergency application.

To prevent wheel sliding, $F_R \leq \phi W$, where F_R = retarding force at the wheel rims resisting rotation of any pair of connected wheels, lb; ϕ = coefficient of wheel-rail adhesion or friction (a decimal); and W = weight upon a pair of wheels, lb. Actual or adhesive weight on wheels when the vehicle is in motion is affected by weight transfer (force transmitted to the trucks and axles by the inertia of the car body through the truck center plates), center of gravity, and vertical oscillation of body weight upon truck springs. The value of ϕ varies with speed as shown in Fig. 11.2.19.

The relationship between the required coefficient ϕ_1 of wheel-rail adhesion to prevent wheel sliding and rate of retardation A in miles per hour per second may be expressed by $A = 21.95 \phi_1$.

Test Devices Special devices have been developed for testing brake components and cars on a repair track.

End-of-Train Devices To eliminate the requirement for a caboose car crew at the end of the train, special electronic devices have been developed to transmit the end-of-train brake-pipe pressure by telemetry to the locomotive operator.

To eliminate the requirement for a caboose car crew at the end of the train, special electronic devices have been developed to transmit the end-of-train brake-pipe pressure by telemetry to the locomotive operator.

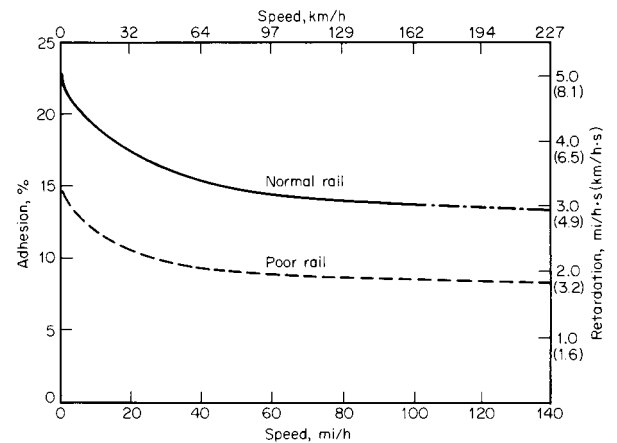


Fig. 11.2.19 Typical wheel-rail adhesion. Track has jointed rails. (Air Brake Association.)

PASSENGER EQUIPMENT

During the past two decades most main-line or long-haul passenger service in North America has become a function of government agencies, i.e., Amtrak in the United States and Via Rail in Canada. Equipment for intraurban service is divided into three major categories: commuter rail, full-scale rapid transit, and light rail transit, depending upon the characteristics of the service. Commuter rail equipment operates on a conventional railroad right-of-way usually intermixed with other long-haul passenger and freight traffic. Full-scale rapid transit operates on a dedicated right-of-way which is commonly in subways or on elevated sections. Light-rail transit (LRT) utilizing light rail vehicles (LRV) is derived from the older trolley or streetcar concepts and may operate in any combination of surface subway or elevated dedicated rights-of-way, semireserved surface rights-of-way with grade crossing, or intermixed with other traffic on surface streets. In a few cases LRT shares the trackage with freight operations which are usually conducted at night on a noninterference basis.

Since main-line and commuter rail equipment operates over a conventional railroad right-of-way, the structural design is heavy to provide the "crashworthiness" of the vehicles in the possible event of a collision with freight equipment or a grade-crossing accident with an automobile or a truck. Although transit vehicles are designed to stringent structural criteria, the requirements are somewhat less severe to compensate for the fact that freight equipment does not usually occupy the same track and there are usually no highway grade crossings. Minimum weight is particularly important for transit vehicles so that demanding schedules over lines with close station spacing can be met with minimum energy consumption.

Main-Line Passenger Equipment In recent years the design of main-line passenger equipment has been controlled by specifications provided by the operating authority. All of the newer cars provided for Amtrak have had stainless steel structural components. These cars have been designed to be locomotive-hauled and to use a locomotive 480-V

11-34 RAILWAY ENGINEERING

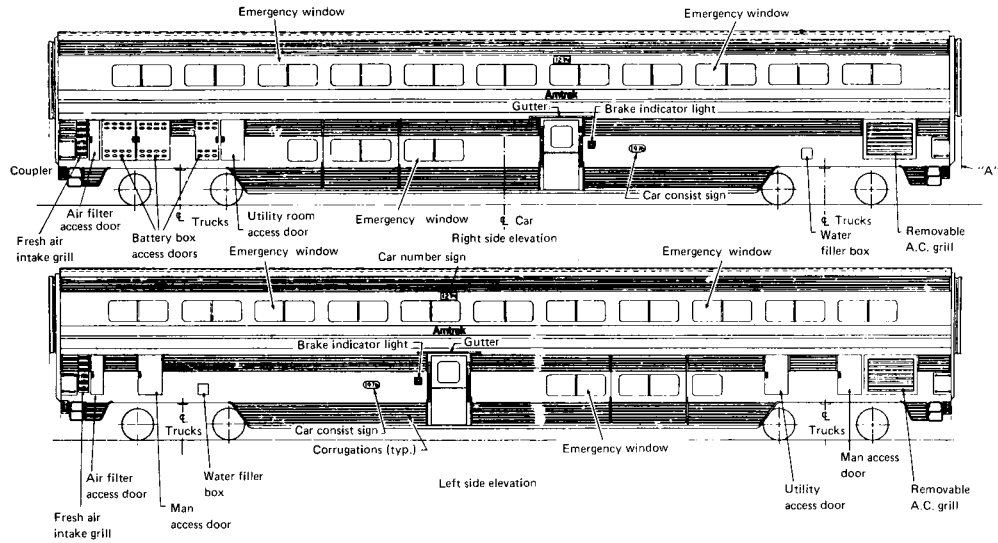


Fig. 11.2.20 Main-line passenger car.

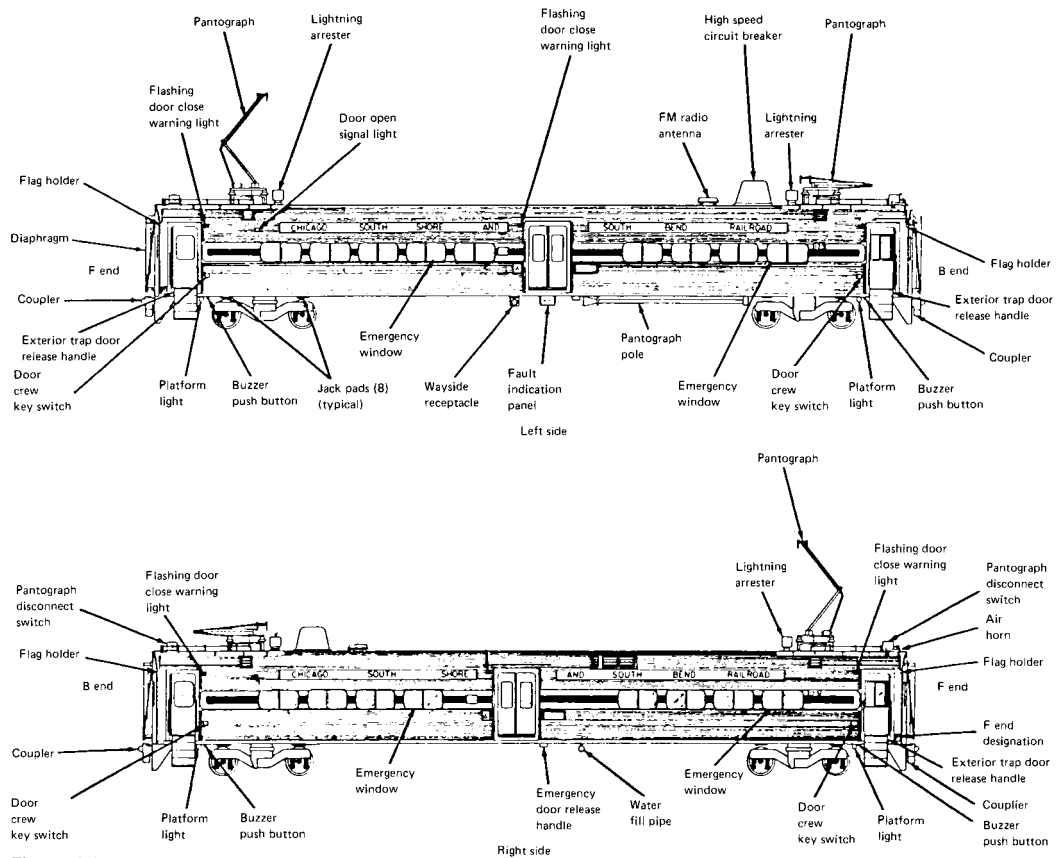


Fig. 11.2.21 Commuter rail car.

three-phase power supply for heating, ventilation, air conditioning, food car services, and other control and auxiliary power requirements. Figure 11.2.20 shows an Amtrak coach car of the Superliner class.

A few earlier high-speed main-line passenger cars (Metroliners) are equipped with special "hook"-type couplers which allow automatic connection of the pneumatic system as the cars are mechanically coupled together. During the past 10 years all of the major new Amtrak equipment has been equipped with the H-type coupler, a passenger version of the AAR standard coupler.

Trucks for passenger equipment are designed to provide a superior ride as compared to freight-car trucks. As a result, passenger trucks include a form of "primary" suspension to isolate the wheel set from the frame of the truck. A softer "secondary" suspension is provided to isolate the truck from the car body. In most cases, the primary suspension uses either coil springs, elliptical springs, or elastomeric components. The secondary suspension generally utilizes either large coil springs or pneumatic springs with special leveling valves to control the height of the car body. Hydraulic dampers are also applied to improve the vertical and lateral ride quality.

Commuter Rail Passenger Equipment Commuter rail equipment can be either locomotive-hauled or self-propelled (Fig. 11.2.21). Some locomotive-hauled equipment is arranged for "push-pull" service. This configuration permits the train to be operated with the locomotive either pushing or pulling the train. For push-pull service some of the passenger cars must be equipped with cabs to allow the engineer to operate the train from the end opposite the locomotive during the push operation. All cars must have control trainlines to connect the lead (cab) car to the trailing locomotive. Locomotive-hauled commuter rail cars use AAR-type H couplers. Self-propelled (single or multiple-unit) cars sometimes use other coupler designs which can be coupled to an AAR coupler with an adaptor.

Full-Scale Rapid Transit Equipment The equipment is used on traditional subway/elevated properties in such cities as Boston, New York, Philadelphia (Fig. 11.2.22), and Chicago in a semiautomatic mode of operation over dedicated rights-of-way which are constrained by limiting civil features. State-of-the-art subway-elevated properties include such cities as Washington, Atlanta, Miami, and San Francisco, where the equipment provides highly automated modes of operation on rights-of-way with generous civil alignments.

The cars can operate bidirectionally in multiple with as many as 12 cars controlled from the leading cab. They are electrically propelled,

usually from a dc third rail which makes contact with a shoe insulated from and supported by the frame of the truck. Occasionally, roof-mounted pantographs are used. Voltages range from 600 to 1000 V dc.

The cars range from 48 to 75 ft (14.6 to 22.9 m) over the anti-climbers, the longer cars being used on the newer properties. Passenger seating varies from 40 to 80 seats per car depending upon length and the local policy (or preference) regarding seated to standee ratio. Older properties require negotiation of curves as sharp as 50 ft (15.2 m) minimum radius with speeds up to only 50 mi/h (80 km/h) on tangent track, while newer properties usually have no less than 125 ft (38.1 m) minimum radius curves with speeds up to 75 mi/h (120 km/h) on tangent track.

All properties operate on standard-gage track with the exception of the 5 ft 6 in (1.7 m) San Francisco Bay Area Rapid Transit (BART), the 4 ft 10 7/8 in (1.5 m) Toronto Transit Subways, and the 5 ft 2 1/2 in (1.6 m) Philadelphia Southeastern Pennsylvania Transportation Authority (SEPTA) Market-Frankford line. Grades seldom exceed 3 percent, and 1.5 to 2.0 percent is the desired maximum.

Typically, newer properties require maximum acceleration rates of between 2.5 and 3.0 mi/(h·s) [4.0 to 4.8 km/(h·s)] as nearly independent of passenger loads as possible from 0 to approximately 20 mi/h (32 km/h). Depending upon the selection of motors and gearing, this rate falls off as speed is increased, but rates can generally be controlled at a variety of levels between zero and maximum.

Deceleration is typically accomplished by a blended dynamic and electropneumatic friction brake, although a few properties use an electrically controlled hydraulic friction brake. Either of these systems usually provides a maximum braking rate of between 3.0 and 3.5 mi/(h·s) [4.8 and 5.6 km/(h·s)] and is made as independent of passenger loads as possible by a load-weighting system which adjusts braking effort to suit passenger loads.

Dynamic braking is now generally used as the primary stopping mode and is effective from maximum speed down to 10 mi/h (16 km/h) with friction braking supplementation as the characteristic dynamic fade occurs. The friction brakes provide the final stopping forces. Emergency braking rates depend upon line constraints, car subsystems, and other factors, but generally rely on the maximum retardation force that can be provided by the dynamic and friction brakes within the limits of available wheel-to-rail adhesion.

Acceleration and braking on modern properties are controlled by a single master controller handle which has power positions in one direc-

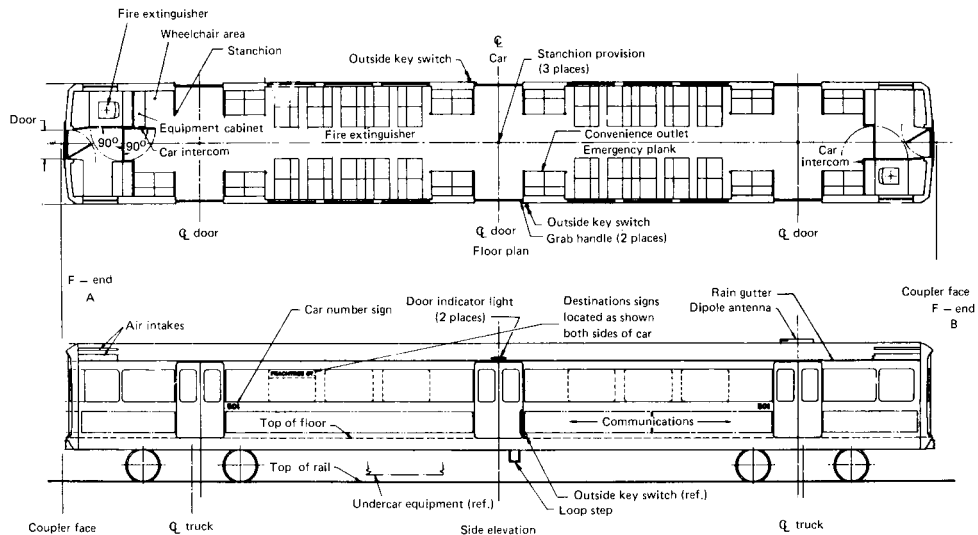


Fig. 11.2.22 Full-scale transit car.

11-36 RAILWAY ENGINEERING

tion and a coasting or neutral center position and braking positions in the opposite direction. The number of positions depends upon the property policy or preference and the control subsystems on the car. Control elements include motor-current sensors and some or all of the following: speed sensors, rate sensors, and load-weighting sensors. Signals are processed by an electronic control unit (ECU) which processes them and provides control functions to the propulsion and braking systems. The propulsion systems currently include pilot-motor-operated cams which actuate switches to control resistance steps, or chopper systems which electronically provide the desired voltages and currents at the motors.

Most modern cars are equipped with two trucks, each of which carries two series-wound dc traction motors. A few use motors with separately excited fields. Monomotor trucks are not used on full-scale rapid transit equipment. The motors are rated between 100 and 200 shaft hp at between 300 and 750 V dc, depending upon line voltage, series or series-parallel connections (electronic or electromechanical control), and performance level desired. The motors, gear units (right angle or parallel), and axles are joined variously through flexible couplings. Electronic-inverter control drives with ac motors have been employed in recent applications in Europe and North America.

In most applications, dynamic braking utilizes the traction motors as generators to dissipate energy through the on-board resistors also used in acceleration. It is expected that regenerative braking will become more common since energy can be returned to the line for use by other cars. Theoretically, 35 to 50 percent of the energy can be returned, but the present state-of-the-art is limited to a practical 20 percent on properties with large numbers of cars on close headways.

Bodies are made of welded stainless steel or **low-alloy high-tensile (LAHT)** steel of a design which carries structural loads (load bearing). Earlier problems with aluminum, primarily electrolytic action among dissimilar metals and welding techniques, have been resolved and aluminum is used on a significant number of new cars.

Trucks may be cast or fabricated steel with the frames and journal bearings either inside or outside the wheels. Axles are carried in roller-bearing journals connected to the frames so as to be able to move vertically against a variety of types of primary spring restraint. Metal springs or air bags are used as the secondary suspension between the trucks and the car body. Most wheels are solid cast or wrought steel. Resilient wheels have been tested but are not in general service on full-scale transit equipment.

All full-scale rapid transit systems use high-level loading platforms

to speed passenger flow. This adds to the civil construction costs, but is necessary to achieve the required level of service.

Light Rail Transit Equipment This equipment differs only slightly from full-scale rapid transit equipment since the term "light rail" means only that more severe civil restraints are acceptable to achieve about 80 percent of the capability at about 50 percent of the cost of full-scale rapid transit.

The cars are called light rail vehicles (Fig. 11.2.23 shows typical LRVs) and are used on a few remaining streetcar systems such as those in Boston, Philadelphia, and Toronto on city streets and on state-of-the-art subway, surface, and elevated systems such as those in Edmonton, Calgary, San Diego, and Portland (OR) in semiautomated modes over partially or wholly reserved rights-of-way.

As a practical matter, the LRV's track, signal systems, and power systems utilize the same subsystems as full-scale rapid transit and are not "lighter" in a physical sense.

The LRVs are designed to operate bidirectionally in multiple with up to four cars controlled from the leading cab. The LRV's are electrically propelled from an overhead contact wire often of catenary design which makes contact with a pantograph on the roof. For wayside safety reasons third-rail pickup is not used. Voltages range from 550 to 750 V dc.

The cars range from 60 to 65 ft (18.3 to 19.8 m) over the anticlimbers for single cars and from 70 to 90 ft (21.3 to 27.4 m) for articulated cars. The choice is determined by passenger volumes and civil constraints.

Articulated cars have been used in railroad and transit applications since the 1920s, but have found favor in light rail applications because of their ability to increase passenger loads in a longer car which can negotiate relatively tight-radius curves. These cars require the additional mechanical complexity of the articulated or hinged center section carried on a third truck which fits between two car-body sections.

Passenger seating varies from 50 to 80 seats per car depending upon length, placement of seats in the articulation and the policy regarding seated/standee ratio. Older systems require negotiation of curves down to 30 ft (9.1 m) minimum radius with speeds up to only 40 mi/h (65 km/h) on tangent track while newer systems usually have no less than 75 ft (22.9 m) minimum radius curves with speeds up to 65 mi/h (104 km/h) on tangent track.

The newer properties all use standard gage; however, existing older systems include 4 ft 10 $\frac{1}{8}$ in (1,495 mm) and 5 ft 2 $\frac{1}{2}$ in (1,587 mm) gages. Grades have reached 12 percent but 6 percent is now considered the maximum and 5 percent is preferred.

Typically, newer properties require maximum acceleration rates of

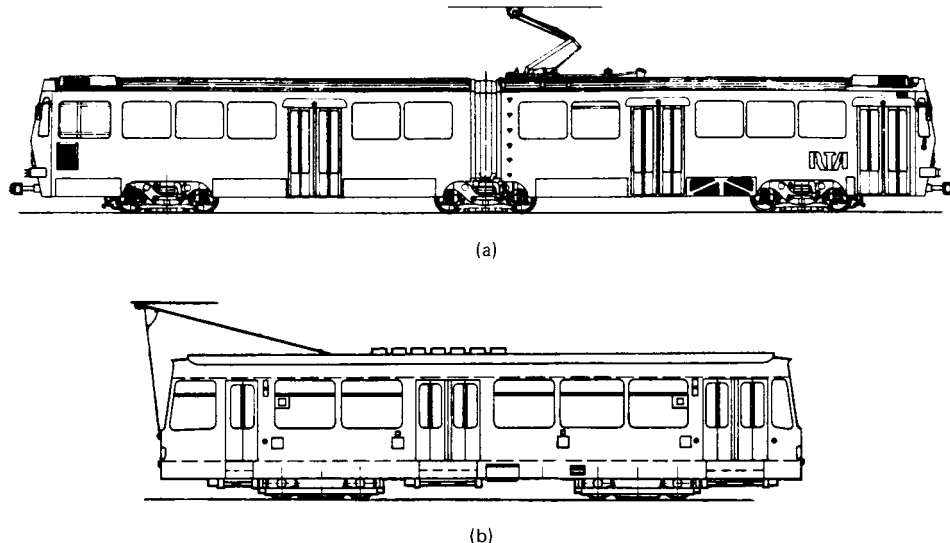


Fig. 11.2.23 Light-rail vehicle (LRV). (a) Articulated; (b) nonarticulated.

between 3.0 to 3.5 mi/(h·s) [4.8 to 5.6 km/(h·s)] as nearly independent of passenger load as possible from 0 to approximately 20 mi/h (32 km/h). Depending upon the selection of motors and gearing, this rate falls off as speed is increased, but the rates can generally be controlled at a variety of levels.

Unlike most full-scale rapid transit cars, LRVs incorporate three braking modes: dynamic, friction, and track brake which typically provide maximum service braking at between 3.0 and 3.5 mi/(h·s) [4.8 to 5.6 km/(h·s)] and 6.0 mi/(h·s) [9.6 km/(h·s)] maximum emergency braking rates. The dynamic and friction brakes are usually blended, but a variety of techniques exist. The track brake is intended to be used primarily for emergency conditions and may or may not be controlled with the other braking systems.

The friction brakes are almost exclusively disk brakes since LRVs use resilient wheels which can be damaged by tread-brake heat buildup. No single consistent pattern exists for the actuation mechanism. All-electric, all-pneumatic, electropneumatic, electrohydraulic, and electropneumatic over hydraulic are in common use.

Dynamic braking is generally used as the primary mode and is effective from maximum speed down to about 5 mi/h (8 km/h) with friction braking supplementation as the characteristic dynamic fade occurs.

As with full-scale rapid transit, the emergency braking rates depend upon line constraints, car-control subsystems selected, and other factors, but the use of track brakes means that higher braking rates can be achieved because the wheel-to-rail adhesion is not the limiting factor.

Acceleration and braking on modern properties are usually controlled by a single master controller handle which has power positions in one direction and a coasting or neutral center position and braking positions in the opposite direction. A few properties use foot-pedal control with a "deadman" pedal operated by the left foot, a brake pedal operated by the right foot, and an accelerator (power) pedal also operated by the right foot. In either case, the number of positions depends upon property policy and control subsystems on the car.

Control elements include motor-current sensors and some or all of the following: speed sensors, rate sensors, and load-weighting sensors. Signals from these sensors are processed by an electronic control unit (ECU) which provides control functions to the propulsion and braking systems.

The propulsion systems currently include pilot-motor-operated cams which actuate switches or electronically controlled unit switches to control resistance steps. Chopper systems which electronically provide the desired voltages and currents at the motors are also used.

Most modern LRVs are equipped with two powered trucks. In articulated designs (Fig. 11.2.23a), the third (center) truck is left unpowered but usually has friction and track brake capability. Some European designs use three powered trucks but the additional cost and complexity have not been found necessary in North America.

Unlike full-scale rapid transit, there are three major dc-motor configurations in use: the traditional series-wound motors used in bimotor trucks, the European-derived monomotor, and a hybrid monomotor with a separately excited field—the latter in chopper-control version only.

The bimotor designs are rated between 100 and 125 shaft hp per motor at between 300 and 750 V dc, depending upon line voltage and series or series-parallel control schemes (electronic or electromechanical control). The monomotor designs are rated between 225 and 250 shaft hp per motor at between 300 and 750 V dc (electronic or electro-mechanical control).

The motors, gear units (right angle or parallel), and axles are joined variously through flexible couplings. In the case of the monomotor, it is supported in the center of the truck, and right-angle gearboxes are mounted on either end of the motor. Commonly, the axle goes through the gearbox and connection is made with a flexible coupling arrangement. Electronic inverter control drives with ac motors have been applied in recent conversions and new equipment.

Dynamic braking is achieved in the same manner as full-scale rapid transit.

Unlike full-scale rapid transit, LRV bodies are made only of welded LAHT steel and are of a load-bearing design. Because of the semireversed right-of-way, the risk of collision damage with automotive vehicles is greater than with full-scale rapid transit and the LAHT steel has been found to be easier to repair than stainless steel or aluminum. Although the LAHT steel requires painting, this can be an asset since the painting can be done in a highly decorative manner pleasing to the public and appropriate to themes desired by the cities.

Trucks may be cast or fabricated steel with either inside or outside frames. Axles are carried in roller-bearing journals which are usually resiliently coupled to the frames with elastomeric springs as a primary suspension. Both vertical and a limited amount of horizontal movement occur. Since tight curve radii are common, the frames are usually connected to concentric circular ball-bearing rings, which, in turn, are connected to the car body. Air bags, solid elastomeric springs, or metal springs are used as a secondary suspension. Resilient wheels are used on virtually all LRVs.

With a few exceptions, LRVs have low-level loading doors and steps which minimize station platform costs.

TRACK

Gage The gage of railway track is the distance between the inner sides of the rail heads measured $\frac{3}{8}$ in (15.9 mm) below the top of rail. North American railways are laid with a nominal gage of 4 ft 8½ in (1,435 mm), which is known as **standard gage**. Rail wear causes an increase in gage. On sharp curves [over 8°, see Eq. (11.2.10)], it has been the practice to widen the gage to reduce rail wear.

Track Structure The basic track structure is composed of six major elements: rail, tie plates, fasteners, cross ties, ballast, and subgrade (Fig. 11.2.24).

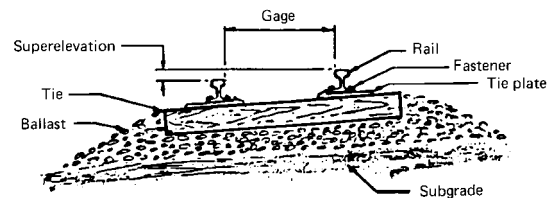


Fig. 11.2.24 Track structure.

Rail The Association of American Railroads has defined standards for the cross section of rails of various weights per yard. The **AREA standards** provide for rail weights varying from 90 to 140 lb/yd. A few railroads use special sections of their own design. The standard length in use is 39 ft (11.9 m) although some mills are now rolling 78 ft (23.8 m) or longer lengths.

The prevailing weight of rails used in main-line track is 112 to 140 lb/yd. Secondary and branch lines are generally laid with 75 to 100 lb/yd rail which has been previously used and partly worn in main-line service. In the past, rails were connected using bolted joint bars. Current practice is the use of **continuous welded rail (CWR)**. In general, rails are first welded into lengths up to 20 rails or more, then laid, and later field welded to eliminate conventional joints between rail strings and other track appliances. Electric-flash, gas-fusion, and Thermit welding processes are used. CWR requires the use of more rail anchors than bolted rail to clamp the base of the rail and position it against the sides of cross ties in order to prevent rail movement. This is necessary to restrain longitudinal forces which result from thermal expansion and contraction due to ambient temperature changes. Failure to adequately restrain the rail can result in track buckling either longitudinally, laterally, or both, in extremely hot weather or in rail "pull aparts" in extremely cold weather. Care must be exercised to install the rail at temperatures which do not approach high or low extremes.

A variety of heat-treating and alloying processes have been applied to produce rail that is more resistant to wear and less susceptible to fatigue

11-38 RAILWAY ENGINEERING

damage. Comprehensive studies indicate that gage face lubrication can dramatically reduce the wear rate of rail in curves (see publications of AAR Research and Test Department). This results in rail fatigue becoming the dominant cause for replacement at some longer life.

Tie Plates Rail is supported on tie plates which restrain the rail laterally, distribute the vehicle loads onto the cross tie, and position (cant) the rail for optimum vehicle performance. Tie plates cant the rail toward the gage side. Cants vary from 1:14 to 1:40, depending on service conditions and operating speeds.

Fasteners Rail and tie plates are fixed to the cross ties by fasteners. Conventional construction with wood cross ties utilizes steel spikes driven into the tie through holes in the tie plate. In some cases, screw-type fasteners are used to provide more resistance to vertical forces. Elastic, clip-type fasteners are used on concrete and, at times, on wooden cross ties to provide a uniform, resilient attachment and longitudinal restraint in lieu of anchors.

Cross Ties To retain gage and provide a further distribution of vehicle loads to the ballast, lateral cross ties are used. The majority of cross ties used in North America are wood. However, concrete cross ties are being used more and more frequently in areas where track surface and lateral stability are difficult to maintain and in high-speed passenger corridors.

Ballast Ballast serves to further distribute vehicle loads to the subgrade, restrain vertical and lateral displacement of the track structure, and provide for drainage. Typical main-line ballast materials are limestone, trap rock, granite, or slag. Lightly built secondary lines use gravel, cinders, or sand.

Subgrade The subgrade serves as the interface between the ballast and the native soil. Subgrade material is typically compacted or stabilized soil. Instability of the subgrade due to groundwater permeation is a concern in some areas. In some difficult locations, a semipermeable geotextile fabric is used to separate the ballast and subgrade and prevent subgrade material from fouling the ballast.

Track Geometry Railroad maintenance practices, state standards, AREA standards, and, more recently, FRA safety standards (CFR Title 49) specify limitations on geometric deviations for track structure. Among the characteristics considered are:

- Gage
- Alignment (the lateral position of the rails)
- Curvature
- Easement (the rate of change from tangent to curve)
- Superelevation
- Runoff (the rate of change in superelevation)
- Cross level (the relative height of opposite rails)
- Twist (the change in relative position of the rails about a longitudinal axis)

FRA standards specify maximum operating speeds by class of track ranging from Class I (poorest acceptable) to Class 6 (excellent). Track geometry is a significant consideration in vehicle suspension design.

Curvature The curvature of track is designated in terms of "degrees of curvature." The degree of curve is the number of degrees of central angle subtended by a chord of 100-ft length (measured on the track centerline). Equation (11.2.10) gives the approximate radius, R , in feet for ordinary railway curves.

$$R = \frac{5730}{\text{degrees per 100-ft chord}} \quad (11.2.10)$$

On important main lines where trains are operated at relatively high speed, the curves are ordinarily not sharper than 6 or 8°. In mountainous territory, in rare instances, main-line curves as sharp as 18° occur. Most diesel and electric locomotives are designed to traverse curves up to 21°. Most uncoupled cars will pass considerably sharper curves, the limiting factor in this case being the clearance of the truck components to car body structural members or equipment or the flexibility of the brake connections to the trucks (AAR "Manual of Standards and Recommended Practices," Sec. C).

Clearances The AREA standard clearance diagrams provide for a clear height of 22 ft (6.7 m) above the tops of the rail heads and for a width of 16 ft (4.9 m) on bridges and 15 ft (4.6 m) elsewhere. Where conditions require the minimum clearance, as in tunnels, these dimensions are much reduced. For tracks entering buildings, an opening 12 ft (3.7 m) wide and 17 ft (5.2 m) high will ordinarily suffice to pass the largest locomotives and cars. A standard clearance diagram for railway bridges (Fig. 11.2.25) represents the AAR recommendation for new construction. Since some clearances are dictated by state authorities, for specific clearance limitations on a particular railroad, refer to the official publication "Railway Line Clearances," Railway Equipment and Publishing Co.

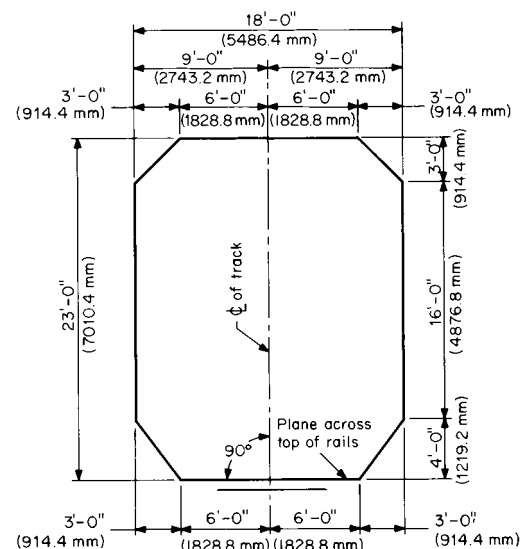


Fig. 11.2.25 Wayside clearance diagram. (AREA "Manual for Railway Engineering—Fixed Properties.")

Track Spacing The distance between centers of main-line track varies between 12 and 14 ft (3.6 and 4.3 m). Twelve-foot spacing exists, however, only on old construction. The prevailing spacing, 14 ft 0 in (4.3 m), has the implied endorsement of the AREA and is required by some states.

Turnouts Railway turnouts (switches) are described by frog number. The frog number is the cotangent of the frog angle, which is the ratio of the lateral displacement of the diverging track per unit of longitudinal distance along the nondiverging track. Typical turnouts in yard and industry trackage range from number 7 to number 10. For main-line service, typical turnouts range from number 10 to number 20. Generally, the higher the turnout number, the higher the allowable speed for a train traversing the diverging track. As a general rule, the allowable speed (in mi/h) is twice the turnout number.

Noise Allowable noise levels from railroad operation are prescribed by CFR40 §201.

VEHICLE-TRACK INTERACTION

Train Resistance The resistance to a train in motion along the track is of prime interest, as it is reflected directly in locomotive energy (fuel) requirements. This resistance is expressed in terms of "pounds per ton" of train weight. **Gross train resistance** is that force which must be overcome by the locomotives at the driving-wheel-rail interface. **Trailing train resistance** must be overcome at the locomotive rear drawbar.

There are two classes of resistance which must be overcome: "inherent" and "incidental." **Inherent resistance** includes the rolling resistance of bearings and wheels and aerodynamic resistance due to motion through still air. It may be considered equal to the force necessary to

maintain motion at constant speed on level tangent track in still air. **Incidental resistance** includes resistance due to grade, curvature, wind, and vehicle dynamics.

Inherent Resistance Of the elements of inherent resistance, at low speeds rolling resistance is dominant, but at high speeds aerodynamic resistance is the predominant factor. Attempts to differentiate and evaluate the various elements through the speed range are a continuing part of industry research programs to reduce train resistance. At very high speeds, the effect of air resistance can be approximately determined. This is an aid to studies in its reduction by means of cowling and fairing. The resistance of a car moving in still air on straight, level track increases parabolically with speed. Because the aerodynamic resistance is independent of car weight, the resistance in pounds per ton decreases as the weight of the car increases. The total resistance in pounds per ton of a 100-ton car is much less than twice as great as that of a 50-ton car under similar conditions. With known conditions of speed and car weight, inherent resistance can be predicted with reasonable accuracy. Knowledge of track conditions will permit further refining of the estimate, but for very rough track or extremely cold ambient temperatures, generous allowances must be made. Under such conditions normal resistance may be doubled. A formula proposed by Davis (*General Electric Review*, Oct. 1926) and revised by Tuthill "High Speed Freight Train Resistance," *Univ. of Illinois Engr. Bull.*, **376**, 1948) has been used extensively for inherent freight-train resistances at speeds up to 40 mi/h:

$$R = 1.3W + 29n + 0.045WV + 0.0005 AV^2 \quad (11.2.11)$$

where R = train resistance, lb/car; W = weight per car, tons; V = speed, mi/h; n = total number of axles; A = cross-sectional area, ft².

With freight-train speeds of 50 to 70 mi/h (80 to 112 km/h), it has been found that actual resistance values fall considerably below calculations based on the above formula. Several modifications of the Davis equation have been developed for more specific applications. All of these equations apply to cars trailing locomotives.

1. Davis equation modified by J. K. Tuthill (*University of Illinois Engr. Bull.*, **376**, 1948):

$$R = 1.3W + 29n + 0.045WV + 0.045V^2 \quad (11.2.12)$$

Note: In the Tuthill modification, the equation is augmented by a matrix of coefficients when the velocity exceeds 40 mi/h.

2. Modified by Canadian National Railway:

$$R = 0.6W + 20n + 0.01WV + 0.07V^2 \quad (11.2.13)$$

3. Modified by Canadian National Railway and Erie-Lackawanna Railroad for trailers and containers on flat cars:

$$R = 0.6W + 20n + 0.01WV + 0.2V^2 \quad (11.2.14)$$

Other modifications of the Davis equation have been developed for passenger cars by Totten ("Resistance of Light Weight Passenger Trains," *Railway Age*, **103**, Jul. 17, 1937). These formulas are for passenger cars pulled by a locomotive and do not include head-end air resistance.

1. Modified by Totten for streamlined passenger cars:

$$R = 1.3W + 29n + 0.045WV + [0.00005 + 0.060725 (L/100)^{0.88}]V^2 \quad (11.2.15)$$

2. Modified by Totten for nonstreamlined passenger cars

$$R = 1.3W + 29n + 0.045WV + [0.0005 + 0.1085 (L/100)^{0.7}]V^2 \quad (11.2.16)$$

where L = car length in feet.

Aerodynamic and Wind Resistance Wind-tunnel testing has indicated a significant effect on train resistance due to vehicle spacing, open tops of hopper and gondola cars, open boxcar doors, vertical side reinforcements on railway cars and intermodal trailers, and protruding appurtenances on cars. These effects can cause significant increases in train resistance at higher speeds. For example, spacing of intermodal trailers or containers greater than approximately 6 ft apart can result in a

new frontal area to be considered in determining train resistance. Frontal or cornering ambient wind conditions can also have an adverse effect on train resistance which is increased with discontinuities along the length of the train.

Curve Resistance Resistance due to track curvature varies with speed and degree of curvature. The behavior of railroad equipment in curve negotiation is the subject of several ongoing AAR studies. Lubrication of the rail gage face or wheel flanges is common practice for reducing friction forces and the resulting wheel and rail wear. Recent studies, in fact, indicate that flange and/or gage face lubrication can significantly reduce train resistance on tangent track as well (Allen, "Conference on the Economics and Performance of Freight Car Trucks," October 1983). In addition, a variety of special trucks (wheel assemblies) which reduce curve resistance by allowing axles to steer toward a radial position in curves have been developed. For general estimates of car resistance and locomotive hauling capacity on dry (unlubricated) rail with conventional trucks, speed and gage relief may be ignored and a figure of 0.8 lb/ton per degree of curvature used.

Grade resistance depends only on the angle of ascent or descent and relates only to the gravitational forces acting on the vehicle. It equates to 20 lb/ton for each "percent of grade" or 0.379 lb/ton for each foot per mile rise.

Acceleration Resistance The force (tractive effort) required to accelerate the train is the sum of the forces required for translation acceleration and that required to produce rotational acceleration of the wheels about their axle centers. A translatory acceleration of 1 mi/h · s (1.6 km/h · s) is produced by a force of 91.1 lb/ton. The rotary acceleration requirement adds 6 to 12 percent, so that the total is nearly 100 lb/ton (the figure commonly used) for each mile per hour per second. If greater accuracy is required, the following expression is used:

$$R_a = A(91.05W + 36.36n) \quad (11.2.17)$$

where R_a = the total accelerating force, lb; A = acceleration, mi/h · s; W = weight of train, tons; n = number of axles.

Acceleration and Distance If in a distance of S ft the speed of a car or train changes from V_1 to V_2 mi/h, the force required to produce acceleration (or deceleration if the speed is reduced) is

$$R_a = 74(V_2^2 - V_1^2)/S \quad (11.2.18)$$

The coefficient 74 corresponds to the use of 100 lb/ton above. This formula is useful in the calculation of the energy required to climb a grade with the assistance of stored energy. In any train-resistance calculation or analysis, assumptions with regard to acceleration will generally submerge all other variables; e.g., an acceleration of 0.1 mi/h · s (0.16 km/h · s) requires more tractive force than that required to overcome inherent resistance for any car at moderate speeds.

Starting Resistance Most railway cars are equipped with roller bearings with a starting force of 5 or 6 lb/ton.

Vehicle Suspension Design The primary consideration in the design of the vehicle suspension system is to isolate track input from the vehicle car body and lading. In addition, there are a few specific areas of instability which railway suspension systems must address, see AAR "Manual of Standards and Recommended Practice," Sec. C-II-M-1001, Chap. XI.

Harmonic roll is the tendency of a freight car with a high center of gravity to rotate about its longitudinal axis (parallel to the track). This instability is excited by passing over staggered low rail joints at a speed which causes the frequency of the input for each joint to match the natural roll frequency of the car. Unfortunately, in many car designs, this occurs for loaded cars at 12 to 18 mi/h (19.2 to 28.8 km/h), a common speed for trains moving in yards or on branch lines where tracks are not well maintained.

This adverse behavior is more noticeable in cars with truck centers approximately the same as the rail length. The effect of harmonic roll can be mitigated by improved track surface and by damping in the truck suspension.

Pitch and bounce are the tendencies of the vehicle to either translate vertically up and down (bounce), or rotate (pitch) about a horizontal

11-40 MARINE ENGINEERING

axis perpendicular to the centerline of track. This response is also excited by low track joints and can be relieved by increased truck damping.

Yaw is the tendency of the freight car to rotate about its axis vertical to the centerline of track. Yaw responses are usually related to truck hunting.

Truck hunting is an instability inherent in the design of the truck and dependent upon the stiffness parameters of the truck and the wheel conicity (tread profile). The instability is observed as a "parallelogramming" of the truck components at a frequency of 2 to 3 Hz causing the car body to yaw or translate laterally. This response is excited by the effect of the natural frequency of the "gravitational stiffness" of the wheel set when the speed of the vehicle approaches the kinematic velocity of the wheel set. This problem is discussed in analytic work available from the AAR Research and Test Department.

Superelevation As a train passes around a curve, there is a tendency for the cars to tip toward the outside of the curve due to the centrifugal force acting on the center of gravity of the car body (Fig. 11.2.26a). To compensate for this effect, the outside rail is superelevated, or raised, relative to the inside rail (Fig. 11.2.26b). The amount of superelevation for a particular curve is based upon the radius of the curve and the operating speed of the train. The "balance" or equilibrium speed for a given curve is that speed at which the centrifugal force on the car matches the component of gravity force resulting from the superelevation between the amount required for high-speed trains and the amount required for slower-operating trains. The FRA allows a railroad to operate with 3 in of outward unbalance, or at the speed at which equilibrium would exist if the superelevation were 3 in greater. The maximum superelevation is usually 6 in.

Longitudinal Train Action Longitudinal train (slack) action is a term associated with the dynamic action between individual cars in a train. An example would be the effect of starting a long train in which the couplers between each car had been compressed (i.e., bunched up). As the locomotive begins to pull the train, the slack between the locomotive and the first car must be traversed before the first car begins to

accelerate. Next the slack between the first and second car must be traversed before the second car begins to accelerate, and so on. Before the last car in a long train begins to move, the locomotive and the moving cars may be traveling at a rate of several miles per hour. This effect can result in coupler forces sufficient to cause the train to break in two.

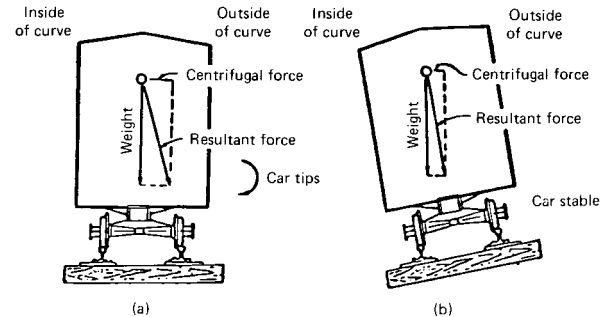


Fig. 11.2.26 Effect of superelevation on center of gravity of car body.

Longitudinal train action is also induced by serial braking, undulating grades, or by braking on varying grades. The Track Train Dynamics Program has published guidelines titled "Track Train Dynamics to Improve Freight Train Performance" which explain the causes of undesirable train action and how to minimize the effects. Analysis of the forces developed by longitudinal train action requires the application of the Davis equation to represent the resistance of each vehicle based upon its velocity and location on a grade or curve. Also, the longitudinal stiffness of each car and the tractive effort of the locomotive must be considered in equations which model the kinematic response of each vehicle in the train. Computer programs are available from the AAR to assist in the analysis of longitudinal train action.

11.3 MARINE ENGINEERING

by Michael C. Tracy

REFERENCES: Harrington, "Marine Engineering," SNAME, 1992. Lewis, "Principles of Naval Architecture," SNAME, 1988/89. Myers, "Handbook of Ocean and Underwater Engineering," McGraw-Hill, 1969. "Rules for Building and Classing Steel Vessels," American Bureau of Shipping. Rawson and Tupper, "Basic Ship Theory," American Elsevier, 1968. Gillmer and Johnson, "Introduction to Naval Architecture," Naval Institute, 1982. Barnaby, "Basic Naval Architecture," Hutchinson, London, 1967. *Jour. Inst. Environ. Sci.* Taggart, "Ship Design and Construction," SNAME, 1980. *Trans. Soc. Naval Architects and Marine Engrs.*, SNAME. *Naval Engrs. Jour.*, Am. Soc. of Naval Engrs., ASNE. *Trans. Royal Inst. of Naval Architects*, RINA. Figures and examples herein credited to SNAME have been included by permission of The Society of Naval Architects and Marine Engineers.

Marine engineering is an integration of many engineering disciplines directed to the development and design of systems of transport, warfare, exploration, and natural-resource retrieval which have one thing in common: operation in or on a body of water. Marine engineers are responsible for the engineering systems required to propel, work, or fight ships. They are responsible for the main propulsion plant; the powering and mechanization aspects of ship functions such as steering, anchoring, cargo handling, heating, ventilation, air conditioning, etc.; and other related requirements. They usually have joint responsibility with naval architects in areas of propulsor design; hull vibration excited by the propeller or main propulsion plant; noise reduction and shock hardening, in fact, dynamic response of structures or machinery

in general; cargo-handling pumping systems; and environmental control and habitability. Marine engineering is a distinct multidiscipline and characteristically a dynamic, continuously advancing technology.

THE MARINE ENVIRONMENT

Marine engineers must be familiar with their environment so that they may understand fuel and power requirements, vibration effects, and propulsion-plant strength considerations. The outstanding characteristic of the open ocean is its irregularity in storm winds as well as under relatively calm conditions. The **irregular sea** can be described by statistical mathematics based on the superposition of a large number of regular waves having different lengths, directions, and amplitudes. The characteristics of idealized regular waves are fundamental for the description and understanding of realistic, irregular seas. Actual sea states consist of a combination of many sizes of waves often running in different directions, and sometimes momentarily superimposing into an exceptionally large wave.

The effects of the marine environment also vary with water depth. As a ship passes from deep to shallow water, there is an appreciable change in the potential flow around the hull and a change in the wave pattern produced. Additionally, silt, sea life, and bottom growth may affect seawater systems or foul heat exchangers.

MARINE VEHICLES

The platform is additionally a part of marine engineers' environment. Ships are supported by a buoyant force equal to the weight of the volume of water displaced. For surface ships, this weight is equal to the total weight of the structure, machinery, outfit, fuel, stores, crew, and useful load. The principal sources of resistance to propulsion are skin friction and the energy lost to surface waves generated by moving in the interface between air and water. Minimization of one or both of these sources of resistance has generally been a primary objective in the design of marine vehicles.

Displacement Hull Forms

Displacement hull forms are the familiar monohull, the catamaran, and the submarine. The moderate-to-full-displacement **monohull** form provides the best possible combinations of high-payload-carrying ability, economical powering characteristics, and good seakeeping qualities. A more slender hull form achieves a significant reduction in wave-making resistance, hence increased speed; however, it is limited in its ability to carry topside weight because of the low transverse stability of its narrow beam. The **catamaran** provides a solution to the problem of low transverse stability. It is increasingly popular in sailing yachts and is under development for high-speed passenger ferries and research and small support ships. Sailing catamarans, with their superior transverse stability permitting large sail-plane area, gain a speed advantage over monohull craft of comparable size. A powered catamaran has the advantage of increased deck space and relatively low roll angles over a monohull ship. The **submarine**, operating at depths which preclude the formation of surface waves, experiences significant reductions in resistance compared to a well-designed surface ship of equal displacement.

Planing Hull Forms

The planing hull form, although most commonly used for yachts and racing craft, is used increasingly in small, fast commercial craft and in coastal patrol craft. The weight of the planing hull ship is partially borne by the dynamic lift of the water streaming against a relatively flat or V-shaped bottom. The effective displacement is hence reduced below that of a ship supported statically, with significant reduction in wave-making resistance at higher speeds.

High-Performance Ships

In a search for high performance and higher speeds in rougher seas, several advanced concepts to minimize wave-making resistance have been investigated. These concepts have been or are being developed in hydrofoil craft, surface-effect vehicles, and small water-plane-area twin hull (SWATH) forms (Fig. 11.3.1). The **hydrofoil craft** has a planing hull that is raised clear of the water through dynamic lift generated by an underwater foil system. The **surface-effect vehicles** ride on a cushion of compressed air generated and maintained in the space between the ve-

hicle and the surface over which it hovers or moves. The most practical vehicles employ a peripheral-jet principle, with flexible skirts for obstacle or wave clearance. A rigid sidewall craft, achieving some lift from hydrodynamic effects, is more adaptable to marine construction techniques. The **SWATH** gains the advantages of the catamaran, twin displacement hulls, with the further advantage of minimized wave-making resistance and wave-induced motions achieved by submarine-shaped hulls beneath the surface and the small water-plane area of the supporting struts at the air-water interface.

SEAWORTHINESS

Seaworthiness is the quality of a marine vehicle being fit to accomplish its intended mission. In meeting their responsibilities to produce seaworthy vehicles, marine engineers must have a basic understanding of the effects of the marine environment with regard to the vehicle's (1) **structure**, (2) **stability and motions**, and (3) **resistance and powering** requirements.

Units and Definitions

The introduction of SI units to the marine engineering field presents somewhat of a revolutionary change. Displacement, for instance, is a force and therefore is expressed in newtons (N) or meganewtons (MN); what for many years has been known as a 10,000-ton ship therefore becomes a 99.64-MN ship. To assist in the change, examples and data have been included in both USCS and SI units.

The **displacement** Δ is the weight of the water displaced by the immersed part of the vehicle. It is equal (1) to the buoyant force exerted on the vehicle and (2) to the weight of the vehicle (in equilibrium) and everything on board. Displacement is expressed in long tons equal to 1.01605 metric tons or 2,240 lb (1 lb = 4.448 N). The specific weight of seawater averages about 64 lb/ft; hence, the displacement in seawater is measured by the displaced volume ∇ divided by 35. In fresh water, divide by 35.9. (Specific weight of seawater = 10,053 N/m³; 1 MN = 99.47 m³; $\Delta = \nabla/99.47$ MN; in fresh water 1 MN = 102 m³.)

Two measurements of a merchant ship's earning capacity that are of significant importance to its design and operation are deadweight and tonnage. The **deadweight** of a ship is the weight of cargo, stores, fuel, water, personnel, and effects that the ship can carry when loaded to a specific load draft. Deadweight is the difference between the load displacement, at the minimum permitted freeboard, and the light displacement, which comprises hull weight and machinery. Deadweight is expressed in long tons (2,240 lb each) or MN. The volume of a ship is expressed in tons of 100 ft³ (2.83 m³) each and is referred to as its **tonnage**. Charges for berthing, docking, passage through canals and locks, and for many other facilities are based on tonnage. **Gross tonnage** is based on cubic capacity below the tonnage deck, generally the uppermost complete deck, plus allowances for certain compartments above,

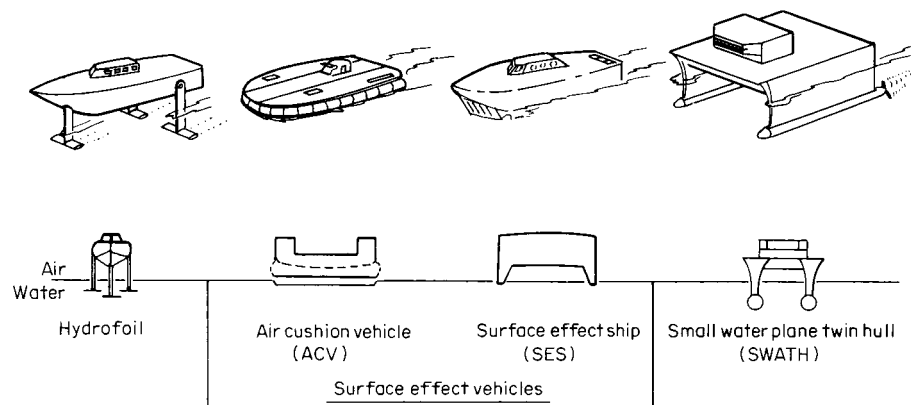


Fig. 11.3.1 Family of high-performance ships.

11-42 MARINE ENGINEERING

Table 11.3.1 Coefficients of Form

Type of vessel	$\frac{v}{\sqrt{gL}}$	C_B	C_M	C_P	C_{WP}	$\frac{\Delta}{(L/100)^3}$
Great Lakes ore ships	0.116–0.128	0.85–0.87	0.99–0.995	0.86–0.88	0.89–0.92	70–95
Slow ocean freighters	0.134–0.149	0.77–0.82	0.99–0.995	0.78–0.83	0.85–0.88	180–200
Moderate-speed freighters	0.164–0.223	0.67–0.76	0.98–0.99	0.68–0.78	0.78–0.84	165–195
Fast passenger liners	0.208–0.313	0.56–0.65	0.94–0.985	0.59–0.67	0.71–0.76	75–105
Battleships	0.173–0.380	0.59–0.62	0.99–0.996	0.60–0.62	0.69–0.71	86–144
Destroyer, cruisers	0.536–0.744	0.44–0.53	0.72–0.83	0.62–0.71	0.67–0.73	40–65
Tugs	0.268–0.357	0.45–0.53	0.71–0.83	0.61–0.66	0.71–0.77	200–420

which are used for cargo, passengers, crew, and navigating equipment. Deduction of spaces for propulsion machinery, crew quarters, and other prescribed volumes from the gross tonnage leaves the **net tonnage**.

The dimensions of a ship may refer to the molded body (or form defined by the outside of the frames), to general outside or overall dimensions, or to dimensions on which the determination of tonnage or of classification is based. There are thus (1) molded dimensions, (2) overall dimensions, (3) tonnage dimensions, and (4) classification dimensions. The published rules and regulations of the classification societies and the U.S. Coast Guard should be consulted for detailed information.

The **designed load waterline (DWL)** is the waterline at which a ship would float freely, at rest in still water, in its normally loaded or designed condition. The keel line of most ships is parallel to DWL. Some keel lines are designed to slope downward toward the stern, termed **designed drag**.

A vertical line through the intersection of DWL and the foreside of the stem is called the **forward perpendicular, FP**. A vertical line through the intersection of DWL with the afterside of the straight portion of the rudder post, with the afterside of the stern contour, or with the centerline of the rudder stock (depending upon stern configuration), is called the **aft perpendicular, AP**.

The **length** on the designed load waterline, L_{WL} , is the length measured at the DWL, which, because of the stern configuration, may be equal to the **length between perpendiculars, L_{PP}** . The **classification society length** is commonly noted as L_{PP} . The extreme length of the ship is the **length overall, L_{OA}** .

The **molded beam B** is the extreme breadth of the molded form. The extreme or overall breadth is occasionally used, referring to the extreme transverse dimension taken to the outside of the plating.

The **draft T** (molded) is the distance from the top of the keel plate or bar keel to the load waterline. It may refer to draft amidships, forward, or aft.

Trim is the longitudinal inclination of the ship usually expressed as the difference between the draft forward, T_F , and the draft aft, T_A .

Coefficients of Form Assume the following notation: L = length on waterline; B = beam; T = draft; ∇ = volume of displacement; A_{WP} = area of water plane; A_M = area of midship section, up to draft T ; v = speed in ft/s (m/s); and V = speed in knots.

Block coefficient, $C_B = \nabla/LBT$, may vary from about 0.38, for high-powered yachts and destroyers, to greater than 0.90 for slow-speed seagoing cargo ships and is a measure of the fullness of the underwater body.

Midship section coefficient, $C_M = A_M/BT$, varies from about 0.75 for tugs or trawlers to about 0.99 for cargo ships and is a measure of the fullness of the maximum section.

Prismatic coefficient, $C_P = \nabla/LA_M = C_B/C_M$, is a measure of the fullness of the ends of the hull, and is an important parameter in powering estimates.

Water-plane coefficient, $C_{WP} = A_{WP}/LB$, ranges from about 0.67 to 0.95, is a measure of the fullness of the water plane, and may be estimated by $C_{WP} \approx \frac{2}{3}C_B + \frac{1}{3}$.

Displacement/length ratio, $\Delta = \Delta/(L/100)^3$, is a measure of the slenderness of the hull, and is used in calculating the power of ships and in recording the resistance data of models.

A similar coefficient is the **volumetric coefficient, $C_V = \nabla/(L/10)^3$** , which is commonly used as this measure.

Table 11.3.1 presents typical values of the coefficients with representative values for Froude number = v/\sqrt{gL} .

Structure

The structure of a ship is a complex assembly of small pieces of material. Common hull structural materials for small boats are wood, aluminum, and fiberglass-reinforced plastic. Large ships are nearly always constructed of steel. Past practices of using aluminum in superstructures are usually nowadays limited to *KG*-critical ship designs.

The **analysis** of a ship structure is accomplished through the following simplified steps: (1) Assume that the ship behaves like a box-shaped girder supported on a simple wave system; (2) estimate the loads acting on the ship, using simplified assumptions regarding weight and buoyancy distribution; (3) calculate the static shear forces and bending moments; (4) analyze the resulting stresses; and (5) iterate the design until the stresses are acceptable. The maximum longitudinal bending stresses which result from such simplified loading assumptions are used as an indicator of the maximum stress that will be developed, and an approximate factor of safety is introduced to allow for stresses induced from other types of external loading, from local loadings, from stress concentration, and from material fatigue over the life of the ship.

Weight, buoyancy, and load curves (Figs. 11.3.2 and 11.3.3) are developed for the ship for the determination of shear force and bending moment. Several extreme conditions of loading may be analyzed. The weight curves include the weights of the hull, superstructure, rudder, and castings, forgings, masts, booms, all machinery and accessories, solid ballast, anchors, chains, cargo, fuel, supplies, passengers, and baggage. Each individual weight is distributed over a length equal to the distance between frames at the location of that particular weight.

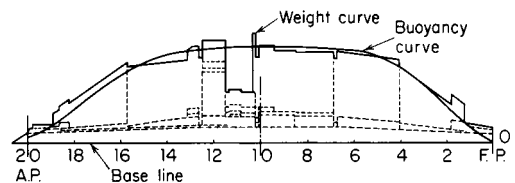


Fig. 11.3.2 Representative buoyancy and weight curves for a ship in still water.

The traditional method of calculating the **maximum design bending moment** involved the determination of weight and buoyancy distributions with the ship poised on a wave of trochoidal form whose length L_w is equal to the length of the ship, L_{PP} , and whose height $H_w = L_w/20$. To

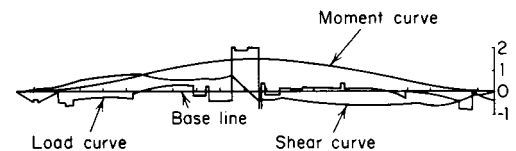


Fig. 11.3.3 Representative moment and net-load curves for a ship in still water.

more accurately model waves whose lengths exceed 300 ft, $H_w = 1.1\sqrt{L}$ is widely used (including standard use by the U.S. Navy), and others have been suggested and applied. With the wave crest amidships, the ship is in a **hogging** condition (Fig. 11.3.4a); the deck is in tension and the bottom shell in compression. With the trough amidships, the ship is

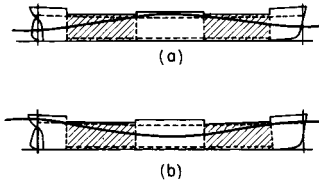


Fig. 11.3.4 Hogging (a) and sagging (b) conditions of a vessel. (From "Principles of Naval Architecture," SNAME, 1967.)

in a **sagging** condition (Fig. 11.3.4b); the deck is in compression and the bottom in tension. For normal cargo ships with the machinery amidships, the hogging condition produces the highest bending moment, whereas for normal tankers and ore carriers with the machinery aft, the sagging condition gives the highest bending moment.

The artificiality of the above assumption should be apparent; nevertheless, it has been an extremely useful one for many decades, and a great deal of ship data have been accumulated upon which to base refinements. Many advances have been made in the theoretical prediction of the actual loads a ship is likely to experience in a realistic, confused seaway over its life span. Today it is possible to predict reliably the bending moments and shear forces a ship will experience over a short term in irregular seas. Long-term prediction techniques use a probabilistic approach which associates load severity and expected periodicity to establish the design load.

In determining the **design section modulus** Z which the continuous longitudinal material in the midship section must meet, an **allowable bending stress** σ_{all} must be introduced into the bending stress equation. Based on past experience, an appropriate choice of such an allowable stress is $1.19 L^{1/3}$ tons/in² ($27.31 L^{1/3}$ MN/m²) with L in ft (m).

For ships under 200 ft (61 m) in length, strength requirements are dictated more on the basis of locally induced stresses than longitudinal bending stresses. This may be accounted for by reducing the allowable stress based on the above equation or by reducing the K values indicated by the trend in Table 11.3.2 for the calculation of the ship's bending moment. For aluminum construction, Z must be twice that obtained for steel construction. Minimum statutory values of section modulus are published by the U.S. Coast Guard in "Load Line Regulations." Shipbuilding classification societies such as the American Bureau of Shipping have section modulus standards somewhat greater.

Table 11.3.2 Constants for Bending Moment Approximations

Type	Δ tons (MN)	L ft (m)	K^*
Tankers	35,000–150,000 (349–1495)	600–900 (183–274)	35–41
High-speed cargo passenger	20,000–40,000 (199–399)	500–700 (152–213)	29–36
Great Lakes ore carrier	28,000–32,000 (279–319)	500–600 (152–183)	54–67
Destroyers	3,500–7,000 (35–70)	400–500 (122–152)	23–30
Destroyer escorts	1,600–4,000 (16–40)	300–450 (91–137)	22–26
Trawlers	180–1,600 (1.79–16)	100–200 (30–61)	12–18
Crew boats	65–275 (0.65–2.74)	80–130 (24–40)	10–16

* Based on allowable stress of $\sigma_{all} = 1.19 \sqrt[3]{L}$ tons/in² ($27.31 \sqrt[3]{L}$ MN/m²) with L in ft (m).

The **maximum bending stress** at each section can be computed by the equation

$$\sigma = M/Z$$

where σ = maximum bending stress, lb/in² (N/m²) or tons/in² (MN/m²); M = maximum bending moment, ft·lb (N·m) or ft·tons; Z = section modulus, in²·ft (m³); $Z = I/y$, where I = minimum vertical moment of inertia of section, in²·ft² (m⁴), and y = maximum distances from neutral axis to bottom and strength deck, ft (m).

The **maximum shear stress** can be computed by the equation

$$\tau = Vac/It$$

where τ = horizontal shear stress, lb/in² (N/m²); V = shear force, lb (N); ac = moment of area above shear plane under consideration taken about neutral axis, ft³ (m³); I = vertical moment of inertia of section, in²·ft² (m⁴); t = thickness of material at shear plane, ft (m).

For an approximation, the **bending moment** of a ship may be computed by the equation

$$M = \Delta L/K \quad \text{ft} \cdot \text{tons (MN} \cdot \text{m)}$$

where Δ = displacement, tons (MN); L = length, ft (m); and K is as listed in Table 11.3.2.

The above formulas have been successfully applied in the past as a convenient tool for the initial assessment of strength requirements for various designs. At present, computer programs are routinely used in ship structural design. Empirical formulas for the individual calculation of both still water and wave-induced bending moments have been derived by the classification societies. They are based on ship length, breadth, block coefficient, and effective wave height (for the wave-induced bending moment). Similarly, permissible bending stresses are calculated from formulas as a function of ship length and its service environment. Finite element techniques in the form of commercially available computer software packages combined with statistical reliability methods are being applied with increasing frequency.

For ships, the maximum longitudinal bending stresses occur in the vicinity of the midship section at the deck edge and in the bottom plating. Maximum shear stresses occur in the shell plating in the vicinity of the quarter points at the neutral axis. For long, slender girders, such as ships, the maximum shear stress is small compared with the maximum bending stress.

The structure of a ship consists of a grillage of stiffened plating supported by longitudinals, longitudinal girders, transverse beams, transverse frames, and web frames. Since the primary stress system in the hull arises from longitudinal bending, it follows that the longitudinally continuous structural elements are the most effective in carrying and distributing this stress system. The strength deck, particularly at the side, and the keel and turn of bilge are highly stressed regions. The shell plating, particularly deck and bottom plating, carry the major part of the stress. Other **key longitudinal elements**, as shown in Fig. 11.3.5, are longitudinal deck girders, main deck stringer plate, gunwale angle, sheer strake, bilge strake, inner bottom margin plate, garboard strake, flat plate keel, center vertical keel, and rider plate.

Transverse elements include deck beams and transverse frames and web frames which serve to support and transmit vertical and transverse loads and resist hydrostatic pressure.

Good structural design minimizes the structural weight while providing adequate strength, minimizes interference with ship function, provides for effective continuity of the structure, facilitates stress flow around deck openings and other stress obstacles, and avoids square corner discontinuities in the plating and other stress concentration "hot spots."

A longitudinally framed ship is one which has closely spaced longitudinal structural elements and widely spaced transverse elements. A transversely framed ship has closely spaced transverse elements and widely spaced longitudinal elements. Longitudinal framing systems are generally more efficient structurally, but because of the deep web frames supporting the longitudinals, it is less efficient in the use of internal space than the transverse framing system. Where interruptions

11-44 MARINE ENGINEERING

of open internal spaces are unimportant, as in tankers and bulk carriers, longitudinal framing is universally used. However, modern practice tends increasingly toward longitudinal framing in other types of ships also.

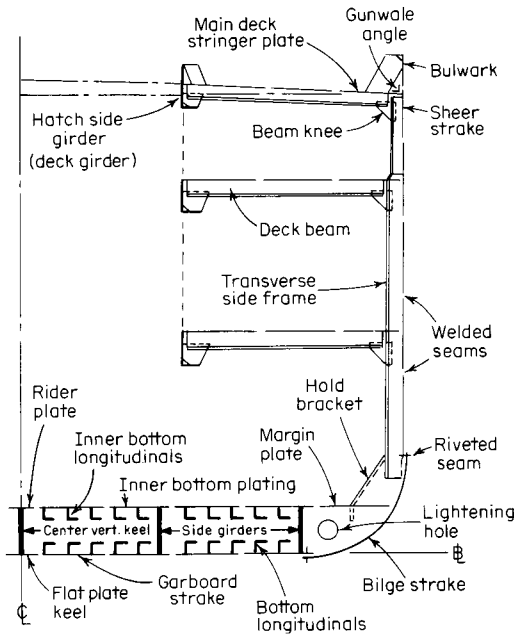


Fig. 11.3.5 Key structural elements.

Stability

A ship afloat is in vertical equilibrium when the force of gravity, acting at the ship's center of gravity G , is equal, opposite, and in the same vertical line as the force of buoyancy, acting upward at the center of buoyancy B . Figure 11.3.6 shows that an upsetting, transverse couple

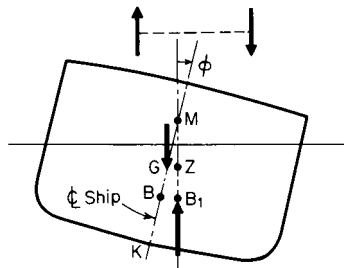


Fig. 11.3.6 Ship stability.

acting on the ship causes it to rotate about a longitudinal axis, taking a list ϕ . G does not change; however, B moves to B_1 , the centroid of the new underwater volume. The resulting couple, created by the transverse separation of the two forces (GZ), opposes the upsetting couple, thereby righting the ship. A static stability curve (Fig. 11.3.7), consisting of values for the righting arm GZ plotted against angles of inclination (ϕ), gives a graphic representation of the static stability of the ship. The primary indicator for the safety of a ship is the maximum righting arm it develops and the angle heel at which this righting arm occurs.

For small angles of inclination ($\phi < 10^\circ$), centers of buoyancy follow a locus whose instantaneous center of curvature M is known as the transverse metacenter. When M lies above G ($\overline{GM} > 0$), the resulting gravity-buoyancy couple will right the ship; the ship has positive stability. When G and M are coincident, the ship has neutral stability. When G

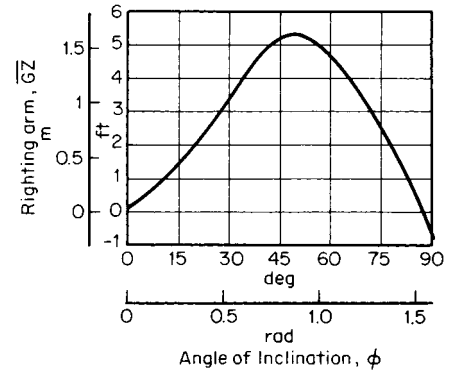


Fig. 11.3.7 Static stability curve.

is above M ($\overline{GM} < 0$), negative stability results. Hence \overline{GM} , known as the transverse metacentric height, is an indication of initial stability of a ship.

The transverse metacentric radius \overline{BM} and the vertical location of the center of buoyancy are determined by the design of the ship and can be calculated. Once the vertical location of the ship's center of gravity is known, then \overline{GM} can be found. The vertical center of gravity of practically all ships varies with the condition of loading and must be determined either by a careful calculation or by an inclining experiment.

Minimum values of \overline{GM} ranging from 1.5 to 3.5 ft (0.46 to 1.07 m), corresponding to small and large seagoing ships, respectively, have been accepted in the past. The \overline{GM} of passenger ships should be under 6 percent of the beam to ensure a reasonable (comfortable) rolling period. This relatively low value is offset by the generally large range of stability due to the high freeboard of passenger ships.

The question of longitudinal stability affects the trim of a ship. As in the transverse case, a longitudinal metacenter exists, and a longitudinal metacentric height \overline{GM}_L can be determined. The moment to alter trim 1 in, $MT1$, is computed by $MT1 = \Delta \overline{GM}_L / 12L$, ft · tons/in and moment to alter trim 1 m is $MT1 = 10^6 \Delta \overline{GM}_L / L$, N · m/m. Displacement Δ is in tons and MN, respectively.

The location of a ship's center of gravity changes as small weights are shifted within the system. The vertical, transverse, or longitudinal component of movement of the center of gravity is computed by $\overline{GG}_1 = w \times d / \Delta$, where w is the small weight, d is the distance the weight is shifted in a component direction, and Δ is the displacement of the ship, which includes w .

Vertical changes in the location of G caused by weight addition or removal can be calculated by

$$\overline{KG}_1 = \frac{\Delta \overline{KG} \pm w \overline{K}g}{\Delta_1}$$

where $\Delta_1 = \Delta \pm w$ and $\overline{K}g$ is the height of the center of gravity of w above the keel.

The free surface of the liquid in fuel oil, lubricating oil, and water storage and service tanks is deleterious to ship stability. The weight shift of the liquid as the ship heels can be represented as a virtual rise in G , hence a reduction in \overline{GM} and the ship's initial stability. This virtual rise, called the free surface effect, is calculated by the expression

$$\overline{GG}_v = \gamma_i i / \gamma_w \nabla$$

where γ_i , γ_w = specific gravities of liquid in tank and sea, respectively; i = moment of inertia of free surface area about its longitudinal centroidal axis; and ∇ = volume of displacement of ship. The ship designer can minimize this effect by designing long, narrow, deep tanks or by using baffles.

Seakeeping

The seakeeping qualities of a ship determine its ability to function normally in a seaway and are based on its motions in waves. These motions

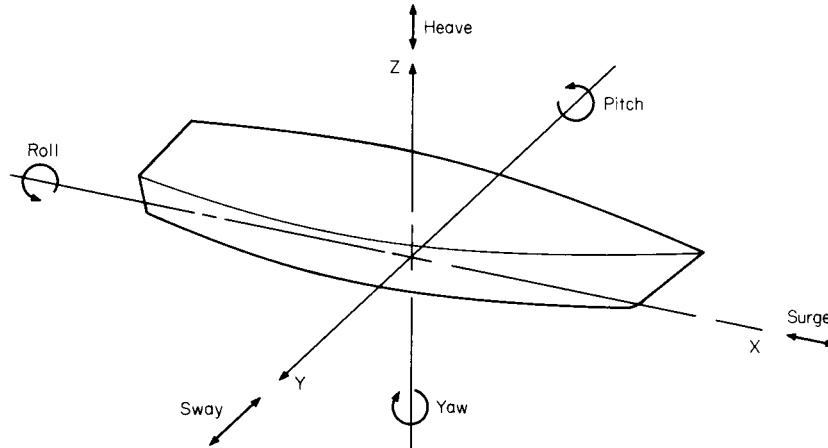


Fig. 11.3.8 Conventional ship coordinate axes and ship motions.

in turn directly affect the practices of marine engineers. The motion of a floating object has six degrees of freedom. Figure 11.3.8 shows the conventional ship coordinate axes and ship motions. Oscillatory movement along the x axis is called **surge**; along the y axis, **sway**; and along the z axis, **heave**. Rotation about x is called **roll**; about y , **pitch**; and about z , **yaw**.

Rolling has a major effect on crew comfort and on the structural and bearing requirements for machinery and its foundations. The natural period of roll of a ship is $T = 2\pi K/\sqrt{gGM}$, where K is the radius of gyration of virtual ship mass about a longitudinal axis through G . K varies from 0.4 to 0.5 of the beam, depending on the ship depth and transverse distribution of weights.

Angular acceleration of roll, if large, has a very distressing effect on crew, passengers, machinery, and structure. This can be minimized by increasing the period or by decreasing the roll amplitude. Maximum angular acceleration of roll is

$$d^2\phi/dt^2 = -4\pi^2(\phi_{\max}/T^2)$$

where ϕ_{\max} is the maximum roll amplitude. The period of the roll can be increased effectively by decreasing \overline{GM} ; hence the lowest value of \overline{GM} compatible with all stability criteria should be sought.

Pitching is in many respects analogous to rolling. The natural period of pitching, bow up to bow down, can be found by using the same expression used for the rolling period, with the longitudinal radius of gyration K_L substituted for K . A good approximation is $K_L = L/4$, where L is the length of the ship. The natural period of pitching is usually between one-third and one-half the natural period of roll. A by-product of pitching is **slamming**, the reentry of bow sections into the sea with heavy force.

Heaving and **yawing** are the other two principal rigid-body motions caused by the sea. The amplitude of heave associated with head seas, which generate pitching, may be as much as 15 ft (4.57 m); that arising from beam seas, which induce rolling, can be even greater. Yawing is started by unequal forces acting on a ship as it quarters into a sea. Once a ship begins to yaw, it behaves as it would at the start of a rudder-actuated turn. As the ship travels in a direction oblique to its plane of symmetry, forces are generated which force it into heel angles independent of sea-induced rolling.

Analysis of ship movements in a seaway is performed by using probabilistic and statistical techniques. The seaway is defined by a mathematically modeled wave energy density spectrum based on data gathered by oceanographers. This wave spectrum is statistically calculated for various sea routes and weather conditions. A ship response amplitude operator or transfer function is determined by linearly superimposing a ship's responses to varying regular waves, both experimentally and theoretically. The wave spectrum multiplied by the ship response

transfer function yields the ship response spectrum. The ship response spectrum is an energy density spectrum from which the statistical character of ship motions can be predicted. (See Edward V. Lewis, *Motions in Waves*, "Principles of Naval Architecture," SNAME, 1989.)

Resistance and Powering

Resistance to ship motion through the water is the aggregate of (1) wave-making, (2) frictional, (3) pressure or form, and (4) air resistances.

Wave-making resistance is primarily a function of Froude number, $Fr = v/\sqrt{gL}$, where v = ship speed, ft/s (m/s); g = acceleration of gravity, ft/s² (m/s²); and L = ship length, ft (m). In many instances, the dimensional speed-length ratio V/\sqrt{L} is used for convenience, where V is given in knots. A ship makes at least two distinct wave patterns, one from the bow and the other at the stern. There also may be other patterns caused by abrupt changes in section. These patterns combine to form the total wave system for the ship. At various speeds there is mutual cancellation and reinforcement of these patterns. Thus, a plot of total resistance of the ship versus Fr or V/\sqrt{L} is not smooth but shows humps and hollows corresponding to the wave cancellation or reinforcement. Normal procedure is to design the operating speed of a ship to fall at one of the low points in the resistance curve.

Frictional resistance is a function of Reynolds number (see Sec. 3). Because of the size of a ship, the Reynolds number is large and the flow is always turbulent.

Pressure or form resistance is a viscosity effect but is different from frictional resistance. The principal observed effects are boundary-layer separation and eddying near the stern.

It is usual practice to combine the wave-making and pressure resistances into one term, called the **residuary resistance**, assumed to be a function of Froude number. The combination, although not strictly legitimate, is practical because the pressure resistance is usually only 2 to 3 percent of the total resistance. The frictional resistance is then the only term which is considered to be a function of Reynolds number and can be calculated. Based on an analysis of the water resistance of flat, smooth planes, Schoenherr gives the formula

$$R_f = 0.5\rho S v^2 C_f$$

where R_f = frictional resistance, lb (N); ρ = mass density, lb/s²·ft⁴ (kg/m³); S = wetted surface area, ft² (m²); v = velocity, ft/s (m/s); and C_f is the frictional coefficient computed from the ITTC formula

$$C_f = \frac{0.075}{(\log_{10} Re - 2)^2}$$

and Re = Reynolds number = vL/ν .

11-46 MARINE ENGINEERING

Through towing tests of ship models at a series of speeds for which Froude numbers are equal between the model and the ship, **total model resistance** (R_{tm}) is determined. Residuary resistance (R_{rm}) for the model is obtained by subtracting the frictional resistance (R_{fm}). By **Froude's law of comparison**, the residuary resistance of the ship (R_{rs}) is equal to R_{rm} multiplied by the ratio of ship displacement to model displacement. Total ship resistance (R_{ts}) then is equal to the sum of R_{rs} , the calculated ship frictional resistance (R_{fs}), and a correlation allowance that allows for the roughness of ship's hull opposed to the smooth hull of a model.

$$\begin{aligned} R_{tm} &= \text{measured resistance} \\ R_{rm} &= R_{tm} - R_{fm} \\ R_{rs} &= R_{rm} (\Delta_s / \Delta_m) \\ R_{ts} &= R_{rs} + R_{fs} + R_a \end{aligned}$$

A nominal value of 0.0004 is generally used as the correlation allowance coefficient C_a . $R_a = 0.5 \rho S v^2 C_a$.

From R_{ts} , the **total effective power** P_E required to propel the ship can be determined:

$$P_E = \frac{R_{ts} v}{550} \quad \text{chp} \quad \left(P_E = \frac{R_{ts} v}{1,000} \quad \text{kW}_E \right)$$

where R_{ts} = total ship resistance, lb (N); v = velocity, ft/s (m/s); and $P_E = P_S \times P.C.$, where P_S is the shaft power (see Propulsion Systems) and $P.C.$ is the propulsive coefficient, a factor which takes into consideration mechanical losses, propeller efficiency, and the flow interaction with the hull. $P.C. = 0.45$ to 0.53 for high-speed craft; 0.50 to 0.60 , for tugs and trawlers; 0.55 to 0.65 , for destroyers; and 0.63 to 0.72 , for merchant ships.

Figure 11.3.9 illustrates the specific effective power for various displacement hull forms and planing craft over their appropriate speed regimes. Figure 11.3.10 shows the general trend of specific resistance versus Froude number and may be used for coarse powering estimates.

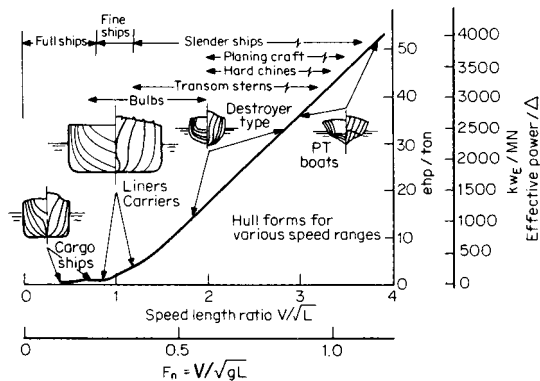


Fig. 11.3.9 Specific effective power for various speed-length regimes. (From "Handbook of Ocean and Underwater Engineering," McGraw-Hill, 1969.)

In early design stages, the hull form is not yet defined, and model testing is not feasible. Reasonably accurate power calculations are made by using preplotted series model test data of similar hull form, such as from Taylor's Standard Series and the Series 60. The Standard Series data were originally compiled by Admiral David W. Taylor and were based on model tests of a series of uniformly varied twin screw, cruiser hull forms of similar geometry. Revised Taylor's Series data are available in "A Reanalysis of the Original Test Data for the Taylor Standard Series," Taylor Model Basin, Rept. no. 806.

Air Resistance The air resistance of ships in a windless sea is only a few percent of the water resistance. However, the effect of wind can have a significant impact on drag. The wind resistance parallel to the ship's axis is roughly 30 percent greater when the wind direction is about 30° ($\pi/6$ rad) off the bow vice dead ahead, since the projected above-water area is greater. Wind resistance is approximated by $R_A =$

$0.002B^2V_R^2$ lb ($0.36B^2V_R^2$ N), where B = ship's beam, ft (m) and V_R = ship speed relative to the wind, in knots (m/s).

Powering of Small Craft The American Boat and Yacht Council, Inc. (ABYC) provides the following guide for determining the maximum safe brake power for pleasure craft.

Compute a length-width factor by multiplying the overall boat length in feet by the overall stern width in feet (widest part of stern excluding fins and sheer). For SI units, use length and width in metres times 10.76.

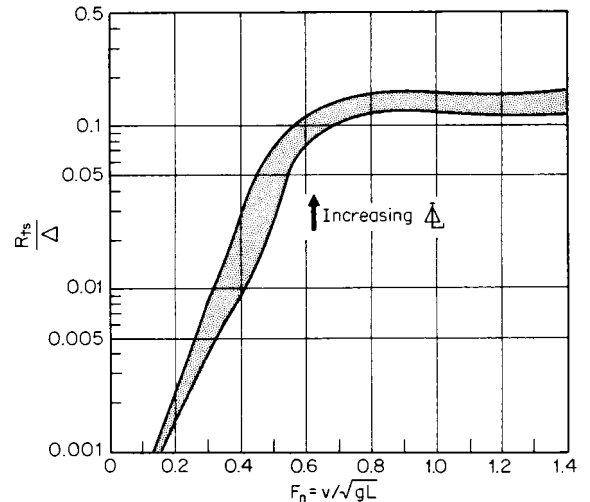


Fig. 11.3.10 General trends of specific resistance versus Froude number.

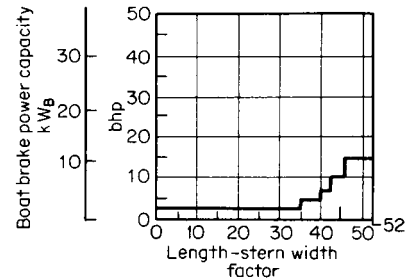


Fig. 11.3.11 Boat brake power capacity for length-width factor under 52. (From "Safety Standards for Small Craft," ABYC, 1974.)

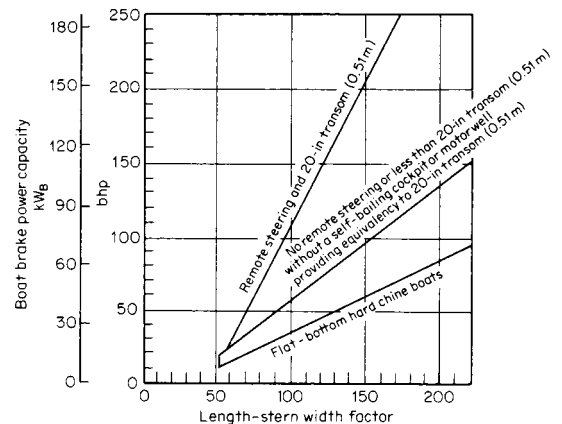


Fig. 11.3.12 Boat brake power capacity for length-width factor over 52. (From "Safety Standards for Small Craft," ABYC, 1974.)

Locate the factor in Fig. 11.3.11 or Fig. 11.3.12 and read the boat brake power capacity.

For powering canoes, the maximum should be 3.0 bhp (2.2 kW_B) for lengths under 15 ft (4.6 m); 5 bhp (3.7 kW_B) for 15 to 18 ft (4.6 to 5.5 m); and 7.5 bhp (5.6 kW_B) for over 18 ft (5.5 m).

ENGINEERING CONSTRAINTS

The constraints affecting marine engineering design are too numerous, and some too obvious, to include in this section. Three significant categories, however, are discussed. The geometry of the hull forms immediately suggests **physical constraints**. The interaction of the vehicle with the marine environment suggests **dynamic constraints**, particularly vibration, noise, and shock. The broad topic of **environmental protection** is one of the foremost engineering constraints of today, having a very pronounced effect on the operating systems of a marine vehicle.

Physical Constraints

Formerly, tonnage laws in effect made it economically desirable for the propulsion machinery spaces of a merchant ship to exceed 13 percent of the gross tonnage of the ship so that 32 percent of the gross tonnage could be deducted in computing net tonnage. In most design configurations, however, a great effort is made to minimize the space required for the propulsion plant in order to maximize that available to the mission or the money-making aspects of the ship.

Specifically, **space** is of extreme importance as each component of support equipment is selected. Each component must fit into the master compact arrangement scheme to provide the most efficient operation and maintenance by engineering personnel.

Weight constraints for a main propulsion plant vary with the application. In a tanker where cargo capacity is limited by draft restrictions, the weight of machinery represents lost cargo. Cargo ships, on the other hand, rarely operate at full load draft. Additionally, the low weight of propulsion machinery somewhat improves inherent cargo ship stability deficiencies. The weight of each component of equipment is constrained by structural support and shock resistance considerations. Naval shipboard equipment, in general, is carefully analyzed to effect weight reduction.

Dynamic Constraints

Dynamic effects, principally mechanical vibration, noise, shock, and ship motions, are considered in determining the dynamic characteristics of a ship and the dynamic requirements for equipment.

Vibration (See Sec. 9.) Vibration analyses are especially important in the design of the propulsion shafting system and its relation to the excitation forces resulting from the propeller. The main propulsion **shafting** can vibrate in longitudinal, torsional, and lateral modes. Modes of **hull vibration** may be vertical, horizontal, torsional, or longitudinal; may occur separately or coupled; may be excited by synchronization with periodic harmonics of the propeller forces acting either through the shafting, by the propeller force field interacting with the hull afterbody, or both; and may also be set up by unbalanced harmonic forces from the main machinery, or, in some cases, by impact excitation from slamming or periodic-wave encounter.

It is most important to reduce the excitation forces at the source. Very objectionable and serious vibrations may occur when the frequency of the exciting force coincides with one of the hull or shafting-system natural frequencies.

Vibratory forces generated by the propeller are (1) alternating pressure forces on the hull due to the alternating hydrodynamic pressure fields of the propeller blades; (2) alternating propeller-shaft bearing forces, primarily caused by wake irregularities; and (3) alternating forces transmitted throughout the shafting system, also primarily caused by wake irregularities.

The most effective means to ensure a satisfactory level of vibration is to provide adequate clearance between the propeller and the hull surface and to select the propeller revolutions or number of blades to avoid synchronism. Replacement of a four-blade propeller, for instance, by a

three- or five-blade, or vice versa, may bring about a reduction in vibration. Singing propellers are due to the vibration of the propeller blade edge about the blade body, producing a disagreeable noise or hum. Chamfering the edge is sometimes helpful.

Vibration due to variations in **engine torque reaction** is hard to overcome. In ships with large diesel engines, the torque reaction tends to produce an athwartship motion of the upper ends of the engines. The motion is increased if the engine foundation strength is inadequate.

Foundations must be designed to take both the thrust and torque of the shaft and be sufficiently rigid to maintain alignment when the ship's hull is working in heavy seas. Engines designed for foundations with three or four points of support are relatively insensitive to minor working of foundations. Considerations should be given to using flexible couplings in cases when alignment cannot be assured.

Torsional vibration frequency of the prime mover-shafting-propeller system should be carefully computed, and necessary steps taken to ensure that its natural frequency is clear of the frequency of the main-unit or propeller heavy-torque variations; serious failures have occurred. Problems due to resonance of engine torsional vibration (unbalanced forces) and foundations or hull structure are usually found after ship trials, and correction consists of local stiffening of the hull structure. If possible, engines should be located at the nodes of hull vibrations.

Although more rare, a **longitudinal vibration** of the propulsion shafting has occurred when the natural frequency of the shafting agreed with that of a pulsating axial force, such as propeller thrust variation.

Other forces inducing vibrations may be vertical inertia forces due to the acceleration of reciprocating parts of an unbalanced reciprocating engine or pump; longitudinal inertia forces due to reciprocating parts or an unbalanced crankshaft creating unbalanced rocking moments; and horizontal and vertical components of centrifugal forces developed by unbalanced rotating parts. Rotating parts can be balanced.

Noise The noise characteristics of shipboard systems are increasingly important, particularly in naval combatant submarines where remaining undetected is essential, and also from a human-factors point of view on all ships. Achieving significant reduction in machinery noise level can be costly. Therefore desired noise levels should be analyzed. Each operating system and each piece of rotating or reciprocating machinery installed aboard a submarine are subjected to intensive airborne (noise) and structureborne (mechanical) vibration analyses and tests. Depending on the noise attenuation required, similar tests and analyses are also conducted for all surface ships, military and merchant.

Shock In naval combatant ships, shock loading due to noncontact underwater explosions is a major design parameter. Methods of qualifying equipment as "shock-resistant" might include "static" shock analysis, "dynamic" shock analysis, physical shock tests, or a combination.

Motions Marine lubricating systems are specifically distinguished by the necessity of including list, trim, roll, and pitch as design criteria. The American Bureau of Shipping requires satisfactory functioning of lubricating systems when the vessel is permanently inclined to an angle of 15° (0.26 rad) athwartship and 5° (0.09 rad) fore and aft. In addition, electric-generator bearings must not spill oil under a momentary roll of 22½° (0.39 rad). Military specifications cite the same permanent trim and list as for surface ships but add 45° (0.79 rad) roll and 10° (0.17 rad) pitch requirements. For submarines, a requirement of 30° (0.52 rad) trim, 15° (0.26 rad) list, 60° (1.05 rad) roll, and 10° (0.17 rad) pitch is imposed.

Environmental Constraints

The **Refuse Act of 1899** (33 U.S.C. 407) prohibits discharge of any refuse material from marine vehicles into navigable waters of the United States or into their tributaries or onto their banks if the refuse is likely to wash into navigable waters. The term **refuse** includes nearly any substance, but the law contains provisions for sewage. The Environmental Protection Agency (EPA) may grant permits for the discharge of refuse into navigable waters.

The **Oil Pollution Act of 1961** (33 U.S.C. 1001-1015) prohibits the discharge of oil or oily mixtures (over 100 mg/L) from vehicles generally within 50 mi of land; some exclusions, however, are granted. (The Oil

11-48 MARINE ENGINEERING

Pollution Act of 1924 was repealed in 1970 because of supersession by subsequent legislation.)

The **Port and Waterways Safety Act of 1972** (PL92-340) grants the U.S. Coast Guard authority to establish and operate mandatory vehicle traffic control systems. The control system must consist of a VHF radio for ship-to-shore communications, as a minimum. The Act, in effect, also extends the provisions of the Tank Vessel Act, which protects against hazards to life and property, to include **protection of the marine environment**. Regulations stemming from this Act govern standards of tanker design, construction, alteration, repair, maintenance, and operation.

The most substantive marine environmental protection legislation is the **Federal Water Pollution Control Act (FWPCA)**, 1948, as amended (33 U.S.C. 466 et seq.). The 1972 and 1978 Amendments contain provisions which greatly expand federal authority to deal with **marine pollution**, providing authority for control of pollution by oil and hazardous substances other than oil, and for the assessment of penalties. **Navigable waters** are now defined as “. . . the waters of the United States, including territorial seas.”

“Hazardous substances other than oil” and harmful quantities of these substances are defined by the EPA in regulations. The Coast Guard and EPA must ensure removal of such discharges, costs borne by the responsible vehicle owner or operator if liable. **Penalties** now may be assessed by the Coast Guard for any discharge. The person in charge of a vehicle is to notify the appropriate U.S. government agency of any discharge upon knowledge of it.

The Coast Guard regulations establish **removal procedures** in coastal areas, contain regulations to **prevent discharges** from vehicles and transfer facilities, and regulations governing the **inspection of cargo vessels** to prevent hazardous discharges. The EPA regulations govern inland areas and non-transportation-related facilities.

Section 312 of the FWPCA as amended in 1972 deals directly with **discharge of sewage**. The EPA must issue standards for marine sanitation devices, and the Coast Guard must issue regulations for implementing those standards. In June, 1972, EPA published standards that now prohibit discharge of any sewage from vessels, whether it is treated or not. Federal law now prohibits, on all inland waters, operation with marine sanitation devices which have not been securely sealed or otherwise made visually inoperative so as to prevent overboard discharge.

The **Marine Plastic Pollution Control Act of 1987** (PL100-220) prohibits the disposal of plastics at sea within U.S. waters.

The **Oil Pollution Act of 1990** (PL101-380) provides extensive legislation on liability and includes measures that impact the future use of single-hull tankers.

PROPULSION SYSTEMS

(See Sec. 9 for component details.)

The basic operating requirement for the main propulsion system is to propel the vehicle at the required sustained speed for the range or endurance required and to provide suitable maneuvering capabilities. In meeting this basic requirement, the marine propulsion system integrates the power generator/prime mover, the transmission system, the propulsor, and other shipboard systems with the ship's hull or vehicle platform. Figure 11.3.13 shows propulsion system alternatives with the most popular drives for fixed-pitch and controllable-pitch propellers.

Definitions for Propulsion Systems

Brake power P_B , bhp (kW_B), is the power delivered by the output coupling of a prime mover before passing through speed-reducing and transmission devices and with all continuously operating engine-driven auxiliaries in use.

Shaft power P_S , shp (kW_S), is the net power supplied to the propeller shafting after passing through all reduction gears or other transmission devices and after power for all attached auxiliaries has been taken off. Shaft power is measured in the shafting within the ship by a torsionmeter as close to the propeller or stern tube as possible.

Delivered power P_D , dhp (kW_D), is the power actually delivered to the propeller, somewhat less than P_S because of the power losses in the

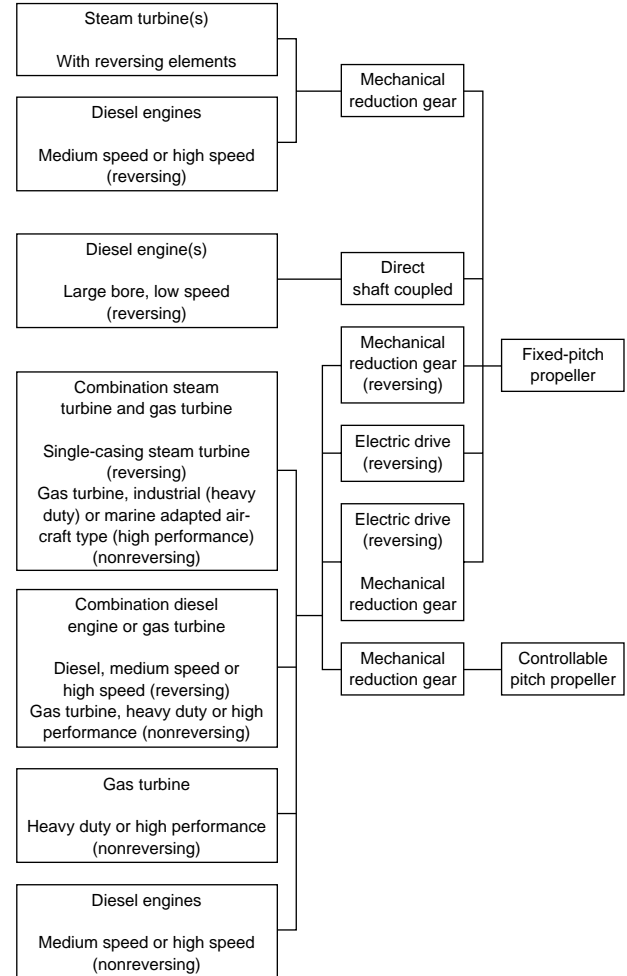


Fig. 11.3.13 Alternatives in the selection of a main propulsion plant. (From "Marine Engineering," SNAME, 1992.)

stern tube and other bearings between the point of measurement and the propeller. Sometimes called **propeller power**, it is also equal to the effective power P_E , ehp (kW_E), plus the power losses in the propeller and the losses in the interaction between the propeller and the ship.

Normal shaft power or **normal power** is the power at which a marine vehicle is designed to run most of its service life.

Maximum shaft power is the highest power for which propulsion machinery is designed to operate continuously.

Service speed is the actual speed maintained by a vehicle at load draft on its normal route and under average weather and sea conditions typical of that route and with average fouling of bottom.

Designed service speed is the speed expected on trials in fair weather at load draft, with clean bottom, when machinery is developing a specified fraction of maximum shaft power. This fraction may vary but is of order of 0.8.

MAIN PROPULSION PLANTS

Steam Plants

The basic steam propulsion plant contains main boilers, steam turbines, a condensate system, a feedwater system, and numerous auxiliary components necessary for the plant to function. A heat balance calculation, the basic tool for determining the effect of various configurations on

plant thermal efficiency, is demonstrated for the basic steam cycle. Both fossil-fuel and nuclear energy sources are successfully employed for marine applications.

Main Boilers (See Sec. 9.) The pressures and temperatures achieved in steam-generating equipment have increased steadily over recent years, permitting either a higher-power installation for a given space or a reduction in the size and weight of a given propulsion plant.

The **trend in steam pressures and temperatures** has been an increase from 600 psig (4.14 MN/m²) and 850°F (454°C) during World War II to 1,200 psig (8.27 MN/m²) and 950°F (510°C) for naval combatants in and since the postwar era. For merchant ships, the progression has been from 400 psig (2.76 MN/m²) and 750°F (399°C) gradually up to 850 psig (5.86 MN/m²) and 850°F (454°C) in the 1960s, with some boilers at 1,500 psig (10.34 MN/m²) and 1000°F (538°C) in the 1970s.

The **quantity of steam** produced by a marine boiler ranges from approximately 1,500 lb/h (680 kg/h) in small auxiliary boilers to over 400,000 lb/h (181,500 kg/h) in large main propulsion boilers. Outputs of 750,000 lb/h (340,200 kg/h) or more per boiler are practical for high-power installations.

Most marine boilers are **oil-fired**. Compared with other fuels, oil is easily loaded aboard ship, stored, and introduced into the furnace, and does not require the ash-handling facilities required for coal firing.

Gas-fired boilers are used primarily on power or drill barges which are fixed in location and can be supplied from shore (normally classed in the Ocean Engineering category). At sea, tankers designed to carry liquefied natural gas (LNG) may use the natural boil-off from their cargo gas tanks as a supplemental fuel (**dual fuel system**). The cargo gas boil-off is collected and pumped to the boilers where it is burned in conjunction with oil. The quantity of boil-off available is a function of the ambient sea and air temperatures, the ship's motion, and the cargo loading; thus, it may vary from day to day.

For economy of space, weight, and cost and for ease of operation, the trend in **boiler installations** is for fewer boilers of high capacity rather than a large number of boilers of lower capacity. The minimum installation is usually two boilers, to ensure propulsion if one boiler is lost; one boiler per shaft for twin-screw ships. Some large ocean-going ships operate on single boilers, requiring exceptional reliability in boiler design and operation.

Combustion systems include forced-draft fans or blowers, the fuel oil service system, burners, and combustion controls. Operation and maintenance of the combustion system are extremely important to the efficiency and reliability of the plant. The best combustion with the least possible excess air should be attained.

Main Turbines (See Sec. 9.) Single-expansion (i.e., single casing) marine steam turbines are fairly common at lower powers, usually not exceeding 4,000 to 6,000 shp (2,983 to 4,474 kW_S). Above that power range, the turbines are usually double-expansion (cross-compound) with high- and low-pressure turbines each driving the main reduction gear through its own pinion. The low-pressure turbine normally contains the reversing turbine in its exhaust end. The main condenser is either underslung and supported from the turbine, or the condenser is carried on the foundations, with the low-pressure turbine supported on the condenser.

The inherent **advantages** of the steam turbine have favored its use over the reciprocating steam engine for all large, modern marine steam propulsion plants. Turbines are not size-limited, and their high temperatures and pressures are accommodated safely. Rotary motion is simpler than reciprocating motion; hence unbalanced forces can be eliminated in the turbine. The turbine can efficiently utilize a low exhaust pressure; it is lightweight and requires minimum space and low maintenance.

The **reheat cycle** is the best and most economical means available to improve turbine efficiencies and fuel rates in marine steam propulsion plants. In the reheat cycle, steam is withdrawn from the turbine after partial expansion and is passed through a heat exchanger where its temperature is raised; it is then readmitted to the turbine for expansion to condenser pressure. Marine reheat plants have more modest steam conditions than land-based applications because of lower power ratings and a greater reliability requirement for ship safety.

The reheat cycle is applied mostly in high-powered units above 25,000 shp (18,642 kW_S) and offers the maximum economical thermal efficiency that can be provided by a steam plant. Reheat cycles are not used in naval vessels because the improvement in efficiency does not warrant the additional complexity; hence a trade-off is made.

Turbine foundations must have adequate rigidity to avoid vibration conditions. This is particularly important with respect to periodic variations in propeller thrust which may excite longitudinal vibrations in the propulsion system.

Condensate System (See Sec. 9.) The condensate system provides the means by which feedwater for the boilers is recovered and returned to the feedwater system. The major components of the condensate system of a marine propulsion plant are the **main condenser**, the **condensate pumps**, and the **deaerating feed tank or heater**. Both single-pass and two-pass condenser designs are used; the single-pass design, however, allows somewhat simpler construction and lower water velocities. The single-pass condenser is also adaptable to scoop circulation, as opposed to pump circulation, which is practical for higher-speed ships. The deaerating feedwater heater is supplied from the condensate pumps, which take suction from the condenser hot well, together with condensate drains from steam piping and various heaters.

The deaerating feed heater is normally maintained at about 35 psig (0.241 MN/m²) and 280°F (138°C) by auxiliary exhaust and turbine extraction steam. The condensate is sprayed into the steam atmosphere at the top of the heater, and the heated feedwater is pumped from the bottom by the feed booster or main feed pumps. In addition to removing oxygen or air, the heater also acts as a surge tank to meet varying demands during maneuvering conditions. Since the feed pumps take suction where the water is almost saturated, the heater must be located 30 to 50 ft (9.14 to 15.24 m) above the pumps in order to provide enough positive suction head to prevent flashing from pressure fluctuations during sudden plant load change.

Feedwater System The feedwater system comprises the pumps, piping, and controls necessary to transport feedwater to the boiler or steam generator, to raise water pressure above boiler pressure, and to control flow of feedwater to the boiler. **Main feed pumps** are so vital that they are usually installed in duplicate, providing a standby pump capable of feeding the boilers at full load. Auxiliary steam-turbine-driven centrifugal pumps are usually selected. A typical naval installation consists of three main feed booster pumps and three main feed pumps for each propulsion plant. Two of the booster pumps are turbine-driven and one is electric. Additionally, an electric-motor-driven emergency booster pump is usually provided. The total capacity of the main feed pumps must be 150 percent of the boiler requirement at full power plus the required recirculation capacity. Reliable feedwater regulators are important.

Steam Plant—Nuclear (See Sec. 9.) The compact nature of the energy source is the most significant characteristic of nuclear power for marine application. The fission of one gram of uranium per day produces about one megawatt of power. (One pound produces 608,579 horsepower.) In other terms, the fission of 1 lb of uranium is equivalent to the combustion of about 86 tons (87,380 kg) of 18,500 Btu/lb (43.03 MJ/kg) fuel oil. This characteristic permits utilization of large power plants on board ship without the necessity for frequent refueling or large bunker storage. Economic studies, however, show that nuclear power, as presently developed, is best suited for military purposes, where the advantages of high power and endurance override the pure economic considerations. As the physical size of nuclear propulsion plants is reduced, their economic attractiveness for commercial marine application will increase.

Major differences between the nuclear power and fossil-fuel plants are: (1) The **safety aspect** of the nuclear reactor system—operating personnel must be shielded from fission product radiation, hence the size and weight of the reactor are increased and maintenance and reliability become more complicated; (2) the steam produced by a pressurized-water reactor plant is saturated and, because of the **high moisture content** in the turbine steam path, the turbine design requires more careful attention; (3) the steam pressure provided by a pressurized-water reactor

11-50 MARINE ENGINEERING

plant varies with output, the maximum pressure occurring at no load and decreasing approximately linearly with load to a minimum at full power; hence, **blade stresses** in a nuclear turbine increase more rapidly with a decrease in power than in a conventional turbine. Special attention must be given to the design of the control stage of a nuclear turbine. The *N.S. Savannah* was designed for 700 psig (4.83 MN/m²) at no load and 400 psig (2.76 MN/m²) at full power.

Steam Plant—Heat Balance The heat-balance calculation is the basic analysis tool for determining the effect of various steam cycles on the thermal efficiency of the plant and for determining the quantities of steam and feedwater flow.

The thermal arrangement of a **simple steam cycle**, illustrated in Fig. 11.3.14, and the following simplified analysis are taken from "Marine Engineering," SNAME, 1992:

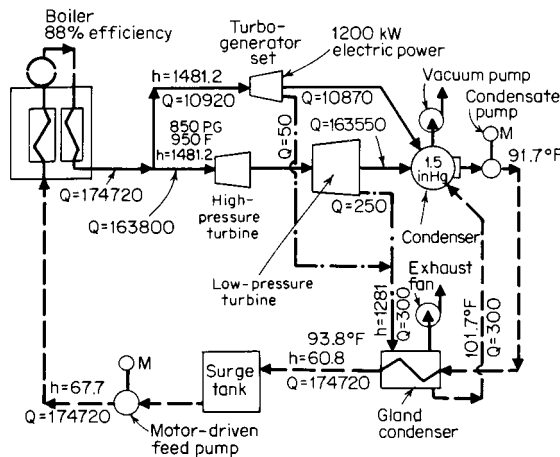


Fig. 11.3.14 Simple steam cycle. (From "Marine Engineering," SNAME, 1992.)

The unit is assumed to develop 30,000 shp (22,371 kW_S). The steam rate of the main propulsion turbines is 5.46 lb/(shp·h) [3.32 kg/(kW_S·h)] with throttle conditions of 850 psig (5.86 MN/m²) and 950°F (510°C) and with the turbine exhausting to the condenser at 1.5 inHg abs (5,065 N/m²). To develop 30,000 shp (22,371 kW_S), the throttle flow must be 163,800 lb/h (74,298 kg/h).

The generator load is estimated to be 1,200 kW, and the turbogenerator is thus rated at 1,500 kW with a steam flow of 10,920 lb/h (4,953 kg/h) for steam conditions of 850 psig (5.86 MN/m²) and 950°F (510°C) and a 1.5 inHg abs (5,065 N/m²) back pressure. The total steam flow is therefore 174,720 lb/h (79,251 kg/h).

Tracing the steam and water flow through the cycle, the flow exhausting from the main turbine is 163,800 - 250 = 163,550 lb/h (74,298 - 113 = 74,185 kg/h), 250 lb/h (113 kg/h) to the gland condenser, and from the auxiliary turbine is 10,870 lb/h (4,930 kg/h), 50 lb/h (23 kg/h) to the gland condenser. The two gland leak-off flows return from the gland leak-off condenser to the main condenser. The condensate flow leaving the main condenser totals 174,720 lb/h (79,251 kg/h).

It is customary to allow a 1°F (0.556°C) hot-well depression in the condensate temperature. Thus, at 1.5 inHg abs (5,065 N/m²) the condenser saturation temperature is 91.7°F (33.2°C) and the condensate is 90.7°F (32.6°C). Entering the gland condenser there is a total energy flow of 174,720 × 59.7 = 10,430,784 Btu/h (11,004,894,349 J/h). The gland condenser receives gland steam at 1,282 Btu/lb (2,979,561 J/kg) and drains at a 10°F (5.6°C) terminal difference or 101.7°F (38.6°C). This adds a total of 300 × (1,281 - 69.7) or 363,390 Btu/h (383,390,985 J/h) to the condensate, making a total of 10,794,174 Btu/h (11,388,285,334 J/h) entering the surge tank. The feed leaves the surge tank at the same enthalpy with which it enters.

The feed pump puts an amount of heat into the feedwater equal to the total power of the pump, less any friction in the drive system. This friction work can be neglected but the heat from the power input is a significant quantity. The power input is the total pump head in feet of feedwater, times the quantity pumped in pounds per hour, divided by the mechanical equivalent of heat and the efficiency. Thus,

Heat equivalent of feed pump work

$$= \frac{144 \Delta P v_f Q}{778 E} \quad \text{Btu/h} \quad \left(\frac{\Delta P v_f Q}{E} \quad \text{J/h} \right)$$

where ΔP = pressure change, lb/in² (N/m²); v_f = specific volume of fluid, ft³/lb (m³/kg); Q = mass rate of flow, lb/h (kg/h); and E = efficiency of pump.

Assuming the feed pump raises the pressure from 15 to 1,015 lb/in² abs (103,421 to 6,998,178 N/m²), the specific volume of the water is 0.0161 ft³/lb (0.001005 m³/kg), and the pump efficiency is 50 percent, the heat equivalent of the feed pump work is 1,041,313 Btu/h (1,098,626,868 J/h). This addition of heat gives a total of 11,835,487 Btu/h (12,486,912,202 J/h) entering the boiler. Assuming no leakage of steam, the steam leaves the boiler at 1,481.2 Btu/lb (3,445,219 J/kg), with a total thermal energy flow of 1,481.2 × 174,720 = 258,795,264 Btu/h (273,039,355,300 J/h). The difference between this total heat and that entering [258,795,264 - 11,835,487 = 246,959,777 Btu/h (260,552,443,098 J/h)] is the net heat added in the boiler by the fuel. With a boiler efficiency of 88 percent and a fuel having a higher heating value of 18,500 Btu/lb (43,030,353 J/kg), the quantity of fuel burned is

$$\begin{aligned} \text{Fuel flow rate} &= 246,959,777 / (18,500)(0.88) = 15,170 \text{ lb/h} \\ \text{or} &= 260,552,443,098 / (43,030,353)(0.88) = 6,881 \text{ kg/h} \end{aligned}$$

The specific fuel rate is the fuel flow rate divided by the net shaft power [15,170/30,000 = 0.506 lb/(shp·h) or 6881/22,371 = 0.308 kg/(kW_S·h)]. The heat rate is the quantity of heat expended to produce one horsepower per hour (one kilowatt per hour) and is calculated by dividing the net heat added to the plant, per hour, by the power produced.

Heat rate

$$\begin{aligned} &= (15,170 \text{ lb/h})(18,500 \text{ Btu/lb}) / 30,000 \text{ shp} = 9,335 \text{ Btu/(shp·h)} \\ \text{or} &= 296,091,858,933 / 22,371 = 13,235,522 \text{ J/(kW}_S \cdot \text{h)} \end{aligned}$$

This simple cycle omits many details that must necessarily be included in an actual steam plant. A continuation of the example, developing the details of a complete analysis, is given in "Marine Engineering," SNAME, 1992. A heat balance is usually carried through several iterations until the desired level of accuracy is achieved. The first heat balance may be done from approximate data given in the SNAME Technical and Research Publication No. 3-11, "Recommended Practices for Preparing Marine Steam Power Plant Heat Balances," and then updated as equipment data are known.

Diesel Engines

(See Sec. 9.)

While steam plants are custom-designed, diesel engines and gas turbines are selected from commercial sources at discrete powers. Diesel engines are referred to as being high, medium, or low speed. Low-speed diesels are generally categorized as those with engine speeds less than about 300 r/min, high-speed in excess of 1,200 r/min. Low-speed marine diesel engines are directly coupled to the propeller shaft. Unlike steam turbines and gas turbines, which require special reversing provisions, most direct-drive diesel engines are readily reversible.

Slow-speed diesel engines are well-suited to marine propulsion. Although larger, heavier, and initially more expensive than higher-speed engines, they generally have lower fuel, operating, and maintenance costs. Slow-speed engine parts take longer to wear to the same percentage of their original dimension than high-speed engine parts. Large-bore, low-speed diesel engines have inherently better combustion performance with lower-grade diesel fuels. However, a well-designed high-speed engine which is not overloaded can give equally good service as a slow-speed engine.

Medium- and High-Speed Diesels The number of medium- and high-speed diesel engines used in marine applications is relatively small compared to the total number of such engines produced. The medium- and high-speed marine engine of today is almost universally an adaptation of engines built in quantities for service in automotive and stationary applications. The automotive field contributes high-speed engine applications in the 400-hp (298-kW) range, with engine speeds commonly varying from 1,800 to 3,000 r/min, depending on whether use is continuous or intermittent. Diesels in the 1,200- to 1,800-r/min range are typical of off-highway equipment engines at powers from 500 to upward of 1,200 hp (373 to 895 kW). Medium-speed diesel engines in units from 6 to 20 cylinders are available at ratings up to and exceeding 8,000 hp (5,966 kW) from both locomotive and stationary engine manufacturers. These applications are not all-inclusive, but only examples of the wide variety of diesel ratings commercially available today.

Some of the engines were designed with **marine applications** in mind, and others require some modification in external engine hardware. The changes are those needed to suit the engine to the marine environment, meaning salt-laden air, high humidity, use of corrosive seawater for cooling, and operating from a pitching and rolling platform. It also may mean an installation made in confined spaces. In order to adapt to this environment, the prime requisite of the marine diesel engine is the ability to resist corrosion. Because marine engines may be installed with their crankshafts at an angle to the horizontal and because they are subjected to more motion than in many other applications, changes are also necessary in the lubricating oil system. The air intake to a marine engine may not be dust-free and dirt-free when operating in harbors, inland waters, or close offshore; therefore, it is as important to provide a good air cleaner as in any automotive or stationary installation.

Diesel engines are utilized in all types of marine vehicles, both in the merchant marine and in the navies of the world. The power range in which diesel engines have been used has increased directly with the availability of higher-power engines. The line of demarcation in horsepower between what is normally assigned to diesel and to steam has continually moved upward, as has the power installed in ships in general.

Small high-speed engines are commonly used in pleasure boats where the owner is safety-conscious and wants to avoid the use of gasoline. For the same reason, small boats in use in the Navy are usually powered by diesel engines, although the gas turbine is being used in special boats where high speed for short periods of time is the prime requirement. Going a little higher in power, diesels are used in many kinds of workboats such as fishing boats, tugs, ferries, dredges, river towboats and pushers, and smaller types of cargo ships and tankers. They are used in the naval counterparts of these ships and, in addition, for military craft such as minesweepers, landing ships, patrol and escort ships, amphibious vehicles, tenders, submarines, and special ships such as salvage and rescue ships and icebreakers. In the nuclear-powered submarine, the diesel is relegated to emergency generator-set use; however, it is still the best way to power a nonnuclear submarine when not operating on the batteries.

Diesel engines are used either singly or in multiple to drive propeller shafts. For all but high-speed boats, the rpm of the modern diesel is too fast to drive the propeller directly with efficiency, and some means of speed reduction, either mechanical or electrical, is necessary. If a single engine of the power required for a given application is available, then a decision must be made whether it or several smaller engines should be used. The decision may be dictated by the available space. The diesel power plant is flexible in adapting to specific space requirements. When more than one engine is geared to the propeller shaft, the gear serves as both a speed reducer and combining gear. The same series of engines could be used in an electric-drive propulsion system, with even greater flexibility. Each engine drives its own generator and may be located independently of other engines and the propeller shaft.

Low-Speed, Direct-Coupled Diesels Of the more usual prime mover selections, only low-speed diesel engines are directly coupled to the propeller shaft. This is due to the low rpm required for efficient pro-

PELLER operation and the high rpm inherent with other types of prime movers.

A rigid hull foundation, with a high resistance to vertical, athwartship, and fore-and-aft deflections, is required for the low-speed diesel. The engine room must be designed with sufficient overhaul space and with access for large and heavy replacement parts to be lifted by cranes.

Because of the low-frequency noise generated by low-speed engines, the operating platform often can be located at the engine itself. Special control rooms are often preferred as the noise level in the control room can be significantly less than that in the engine room.

Electric power may be produced by a generator mounted directly on the line shafting. Operation of the entire plant may be automatic and remotely controlled from the bridge. The engine room is often completely unattended for 16 h a day.

Gas Turbines

(See Sec. 9.)

The gas turbine has developed since World War II to join the steam turbine and the diesel engine as alternative prime movers for various shipboard applications.

In gas turbines, the efficiency of the components is extremely important since the compressor power is very high compared with its counterpart in competitive thermodynamic cycles. For example, a typical marine propulsion gas turbine rated at 20,000 bhp (14,914 kW_B) might require a 30,000 hp (22,371 kW) compressor and, therefore, 50,000 hp (37,285 kW) in turbine power to balance the cycle.

The basic **advantages** of the gas turbine for marine applications are its simplicity and light weight. As an internal-combustion engine, it is a self-contained power plant in one package with a minimum number of large supporting auxiliaries. It has the ability to start and go on line very quickly. Having no large masses that require slow heating, the time required for a gas turbine to reach full speed and accept the load is limited almost entirely by the rate at which energy can be supplied to accelerate the rotating components to speed. A further feature of the gas turbine is its low personnel requirement and ready adaptability to automation.

The relative simplicity of the gas turbine has enabled it to attain outstanding records of reliability and maintainability when used for aircraft propulsion and in industrial service. The same level of reliability and maintainability is being achieved in marine service if the unit is properly applied and installed.

Marine units derived from aircraft engines usually have the gas generator section, comprising the compressor and its turbine, arranged to be removed and replaced as a unit. Maintenance on the power turbine, which usually has the smallest part of the total maintenance requirements, is performed aboard ship. Because of their light weight, small gas turbines used for auxiliary power or the propulsion of small boats, can also be readily removed for maintenance.

Units designed specifically for marine use and those derived from industrial gas turbines are usually maintained and overhauled in place. Since they are somewhat larger and heavier than the aviation-type units, removal and replacement are not as readily accomplished. For this reason, they usually have split casings and other provisions for easy access and maintenance. The work can be performed by the usual ship repair forces.

Both **single-shaft** and **split-shaft** gas turbines can be used in marine service. Single-shaft units are most commonly used for generator drives. When used for main propulsion, where the propeller must operate over a very wide speed range, the single-shaft unit must have a controllable-pitch propeller or some equivalent variable-speed transmission, such as an electric drive, because of its limited speed range and poor acceleration characteristics. A multishaft unit is normally used for main propulsion, with the usual arrangement being a split-shaft unit with an independent variable-speed power turbine; the power turbine and propeller can be stopped, if necessary, and the gas producer kept in operation for rapid load pickup. The use of variable-area nozzles on the power turbine increases flexibility by enabling the compressor to be maintained at or near full speed and the airflow at low-power turbine

11-52 MARINE ENGINEERING

speeds. Nearly full power is available by adding fuel, without waiting for the compressor to accelerate and increase the airflow. Where low-load economy is of importance, the controls can be arranged to reduce the compressor speed at low loads and maintain the maximum turbine inlet and/or exhaust temperature for best efficiency. Since a gas turbine inherently has a poor part-load fuel rate performance, this variable-area nozzle feature can be very advantageous.

The physical arrangement of the various components, i.e., compressors, combustion systems, and turbines, that make up the gas turbine is influenced by the thermodynamic factors (i.e., the turbine connected to a compressor must develop enough power to drive it), by mechanical considerations (i.e., shafts must have adequate bearings, seals, etc.), and also by the necessity to conduct the very high air and gas flows to and from the various components with minimum pressure losses.

In marine applications, the gas turbines usually **cannot be mounted rigidly** to the ship's structure. Normal movement and distortions of the hull when under way would cause distortions and misalignment in the turbine and cause internal rubs or bearing and/or structural failure. The turbine components can be mounted on a subbase built up of structural sections of sufficient rigidity to maintain the gas-turbine alignment when properly supported by the ship's hull.

Since the gas turbine is a high-speed machine with output shaft speeds ranging from about 3,600 r/min for large machines up to 100,000 r/min for very small machines (approximately 25,000 r/min is an upper limit for units suitable for the propulsion of small boats), a **reduction gear is necessary** to reduce the speed to the range suitable for a propeller. Smaller units suitable for boats or driving auxiliary units, such as generators in larger vessels, frequently have a reduction gear integral with the unit. Larger units normally require a separate reduction gear, usually of the double- or triple-reduction type.

A gas turbine, in common with all turbine machinery, is **not inherently reversible** and must be reversed by external means. Electric drives offer ready reversing but are usually ruled out on the basis of weight, cost, and to some extent efficiency. From a practical standpoint there are two alternatives, a reversing gear or a controllable pitch (CRP) propeller. Both have been used successfully in gas-turbine-driven ships, with the CRP favored.

Combined Propulsion Plants

In some shipboard applications, diesel engines, gas turbines, and steam turbines can be employed effectively in various combinations. The prime movers may be combined either mechanically, thermodynamically, or both. The leveling out of specific fuel consumption over the operating speed range is the goal of most combined systems.

The gas turbine is a very flexible power plant and consequently figures in most possible combinations which include combined diesel and gas-turbine plants (CODAG); combined gas- and steam-turbine plants (COGAS); and combined gas-turbine and gas-turbine plants (COGAG). In these cycles, gas turbines and other engines or gas turbines of two different sizes or types are combined in one plant to give optimum performance over a very wide range of power and speed. In addition, combinations of diesel or gas-turbine plants (CODOG), or gas-turbine or gas-turbine plants (COGOG), where one plant is a diesel or small gas turbine for use at low or cruising powers and the other a large gas turbine which operates alone at high powers, are also possibilities. Even the combination of a small nuclear plant and a gas turbine plant (CONAG) has undergone feasibility studies.

COGAS Gas and steam turbines are connected to a common reduction gear, but thermodynamically are either independent or combined. Both gas- and steam-turbine drives are required to develop full power. In a thermodynamically independent plant, the boost power is furnished by a lightweight gas turbine. This combination produces a significant reduction in machinery weight.

In the thermodynamically combined cycle, commonly called STAG (steam and gas turbine) or RACER (Rankine cycle energy recovery), energy is recovered from the exhaust of the gas turbine and is used to augment the main propulsion system through a steam turbine. The prin-

cipal advantage gained by the thermodynamic interconnection is the potential for improved overall efficiency and resulting fuel savings. In this arrangement, the gas turbine discharges to a heat-recovery boiler where a large quantity of heat in the exhaust gases is used to generate steam. The boiler supplies the steam turbine that is geared to the propeller. The steam turbine may be coupled to provide part of the power for the gas-turbine compressor. The gas-turbine may be used to provide additional propulsion power, or its exhaust may be recovered to supply heat for various ship's services (Fig. 11.3.15).

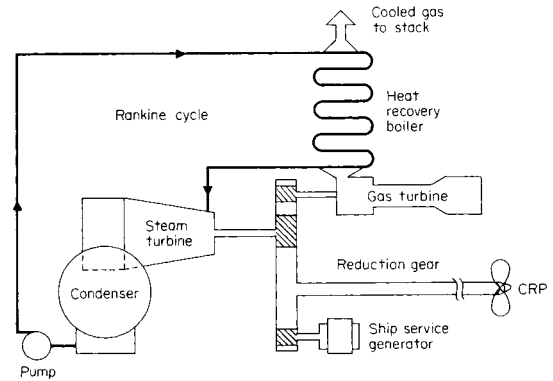


Fig. 11.3.15 COGAS system schematic.

Combined propulsion plants have been used in several applications in the past. **COGOG** plants have serviced some Navy patrol gunboats and the Coast Guard's Hamilton class cutters. Both **COGOG** and **COGAS** plants have been used in foreign navies, primarily for destroyer-type vessels.

PROPULSORS

The force to propel a marine vehicle arises from the rate of change of momentum induced in either the water or air. Since the force produced is directly proportional to the mass density of the fluid used, the reasonable choice is to induce the momentum change in water. If air were used, either the cross-sectional area of the jet must be large or the

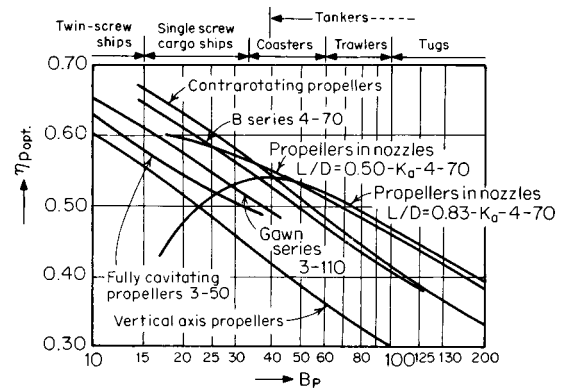


Fig. 11.3.16 Comparison of optimum efficiency values for different types of propulsors. (From "Marine Engineering," SNAME, 1992.)

velocity must be high. A variety of propulsors are used to generate this stream of water aft relative to the vehicle: screw propellers, controllable-pitch propellers, water jets, vertical-axis propellers, and other thrust devices. Figure 11.3.16 indicates the type of propulsor which provides the best efficiency for a given vehicle type.

Screw Propellers

The screw propeller may be regarded as part of a helicoidal surface which, as it rotates, appears to "screw" its way through the water, driving water aft and the vehicle forward. A propeller is termed "**right-handed**" if it turns clockwise (viewed from aft) when producing ahead thrust; if counterclockwise, "**left-handed.**" In a twin-screw installation, the starboard propeller is normally right-handed and the port propeller left-handed. The surface of the propeller blade facing aft, which experiences the increase in pressure, producing thrust, is the **face** of the blade; the forward surface is the **back**. The face is commonly constructed as a true helical surface of constant pitch; the back is not a helical surface. A **true helical surface** is generated by a line rotated about an axis normal to itself and advancing in the direction of this axis at constant speed. The distance the line advances in one revolution is the **pitch**. For simple propellers, the pitch is constant on the face; but in practice, it is common for large propellers to have a reduced pitch toward the hub and less usually toward the tip. The pitch at 0.7 times the maximum radius is usually a representative mean pitch; maximum lift is generated at that approximate point. Pitch may be expressed as a dimensionless ratio, P/D .

The **shapes** of blade outlines and sections vary greatly according to the type of ship for which the propeller is intended and to the designer's ideas. Figure 11.3.17 shows a typical design and defines many of the terms in common use. The **projected area** is the area of the projection of the propeller contour on a plane normal to the shaft, and the **developed area** is the total face area of all the blades. If the variation of helical cord length is known, then the true blade area, called **expanded area**, can be obtained graphically or analytically by integration.

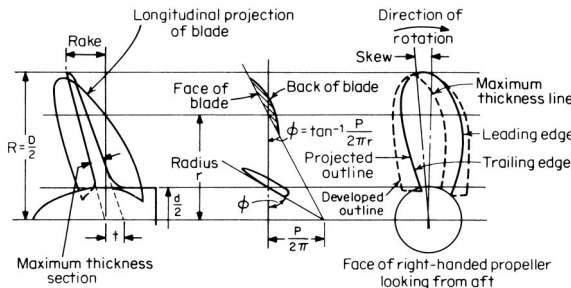


Fig. 11.3.17 Typical propeller drawing. (From "Principles of Naval Architecture," SNAME, 1988.)

- Diameter = D Pitch ratio = P/D Pitch = P
- Blade thickness ratio = t/D No. of blades = 4
- Pitch angle = ϕ
- Disk area = area of tip circle = $\pi D^2/4 = A_o$
- Developed area of blades, outside hub = A_D
- Developed area ratio = $DAR = A_D/A_o$
- Projected area of blades (on transverse plane) outside hub = A_p
- Projected area ratio = $PAR = A_p/A_o$
- Blade width ratio = $BWR = (\text{max. blade width})/D$
- Mean width ratio = $MWR = [A_D/\text{length of blades (outside hub)}]/D$

Consider a section of the propeller blade at a radius r with a pitch angle ϕ and pitch P working in an unyielding medium; in one revolution of the propeller it will advance a distance P . Turning n revolutions in unit time it will advance a distance $P \times n$ in that time. In a real fluid, there will be a certain amount of yielding when the propeller is developing thrust and the screw will not advance $P \times n$, but some smaller distance. The difference between $P \times n$ and that smaller distance is called the **slip velocity**. **Real slip ratio** is defined in Fig. 11.3.18.

A wake or a frictional belt of water accompanies every hull in motion; its velocity varies as the ship's speed, hull shape, the distance from the ship's side and from the bow, and the condition of the hull surface. For ordinary propeller design the **wake velocity** is a fraction w of the

ship's speed. Wake velocity = wV . The **wake fraction** w for a ship may be obtained from Fig. 11.3.19. The velocity of the ship relative to the ship's wake at the stern is $V_A = (1 - w)V$.

The **apparent slip ratio** S_A is given by

$$S_A = (Pn - V)/Pn = 1 - V/Pn$$

Although real slip ratio, which requires knowledge of the wake fraction, is a real guide to ship performance, the apparent slip ratio requires only ship speed, revolutions, and pitch to calculate and is therefore often recorded in ships' logs.

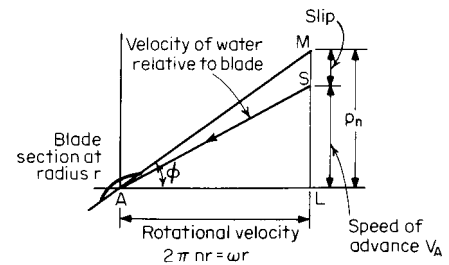


Fig. 11.3.18 Definition of slip. (From "Principles of Naval Architecture," SNAME, 1988.)

$$\tan \phi = Pn/2\pi nr = P/2\pi r$$

$$\text{Real slip ratio} = S_R = MS/ML = (Pn - V_A)/Pn = 1 - V_A/Pn$$

For P in ft (m), n in r/min, and V in knots, $S_A = (Pn - 101.3V)/Pn$; [$S_A = (Pn - 30.9V)/Pn$].

Propeller Design The design of a marine propeller is usually carried out by one of two methods. In the first, the design is based upon charts giving the results of open-water tests on a series of model propellers. These cover variations in a number of the design parameters such as pitch ratio, blade area, number of blades, and section shapes. A propeller which conforms with the characteristics of any particular series can be rapidly designed and drawn to suit the required ship conditions.

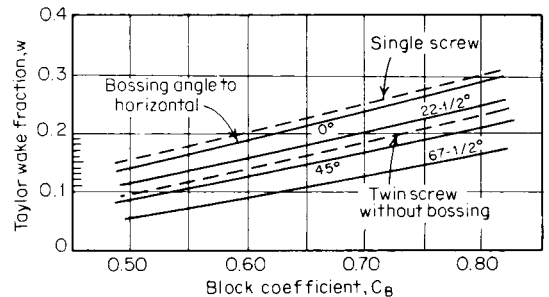


Fig. 11.3.19 Wake fractions for single- and twin-screw models. (From "Principles of Naval Architecture," SNAME, 1988.)

The second method is used in cases where a propeller is heavily loaded and liable to cavitation or has to work in a very uneven wake pattern; it is based on purely theoretical calculations. Basically this involves finding the chord width, section shape, pitch, and efficiency at a number of radii to suit the average circumferential wake values and give optimum efficiency and protection from cavitation. By integration of the resulting thrust and torque-loading curves over the blades, the thrust, torque, and efficiency for the whole propeller can be found.

Using the first method and **Taylor's propeller and advance coefficients** B_p and δ , a convenient practical design and an initial estimate of pro-

11-54 MARINE ENGINEERING

propeller size can be obtained

$$B_p = \frac{n(P_D)^{0.5}}{(V_A)^{2.5}} \left[\frac{1.158n(P_D)^{0.5}}{(V_A)^{2.5}} \right]$$

$$\delta = \frac{nD}{V_A} \left(\frac{3.281nD}{V_A} \right)$$

$$\eta_o = \frac{TV_A}{325.7P_D\eta_R} \left(\frac{TV_A}{1,942.5P_D\eta_R} \right)$$

where B_p = Taylor's propeller coefficient; δ = Taylor's advance coefficient; n = r/min; P_D = delivered power, dhp (kW_D); V_A = speed of advance, knots; D = propeller diameter, ft (m); T = thrust, lb (N); η_o = open-water propeller efficiency; η_R = relative rotative efficiency (0.95 < η_R < 1.0, twin-screw; 1.0 < η_R < 1.05, single-screw), a factor which corrects η_o to the efficiency in the actual flow conditions behind the ship.

Assume a reasonable value for n and, using known values for P_D and V_A (for a useful approximation, $P_D = 0.98P_s$), calculate B_p . Then enter Fig. 11.3.20, or an appropriate series of Taylor or Troost propeller charts, to determine δ , η_o , and P/D for optimum efficiency. The charts and parameters should be varied, and the results plotted to recognize the most suitable propeller.

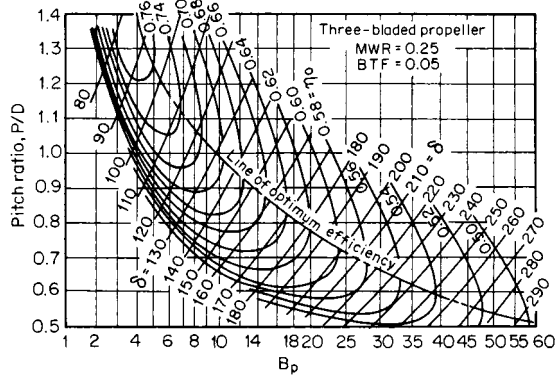


Fig. 11.3.20 Typical Taylor propeller characteristic curves. (From "Handbook of Ocean and Underwater Engineering," McGraw-Hill, 1969.)

Propeller cavitation, when severe, may result in marked increase in rpm, slip, and shaft power with little increase in ship speed or effective power. As cavitation develops, noise, vibration, and erosion of the propeller blades, struts, and rudders are experienced. It may occur either on the face or on the back of the propeller. Although cavitation of the face has little effect on thrust and torque, extensive cavitation of the back can materially affect thrust and, in general, requires either an increase in blade area or a decrease in propeller rpm to avoid. The erosion of the backs is caused by the collapse of cavitation bubbles as they move into higher pressure regions toward the trailing edge.

Avoidance of cavitation is an important requirement in propeller design and selection. The Netherlands Ship Model Basin suggests the following **criterion** for the minimum blade area required to avoid cavitation:

$$A_p^2 = \frac{T^2}{1,360(p_0 - p_v)^{1.5}V_A} \quad \text{or} \quad \left[\frac{T^2}{5.44(p_0 - p_v)^{1.5}V_A} \right]$$

where A_p = projected area of blades, ft² (m²); T = thrust, lb (N); p_0 = pressure at screw centerline, due to water head plus atmosphere, lb/in² (N/m²); p_v = water-vapor pressure, lb/in² (N/m²); and V_A = speed of advance, knots (1 knot = 0.515 m/s); and

$$\text{or} \quad \begin{matrix} p_0 - p_v = 14.45 + 0.45h & \text{lb/in}^2 \\ (p_0 - p_v = 99,629 + 10,179h & \text{N/m}^2) \end{matrix}$$

where h = head of water at screw centerline, ft (m).

A four-blade propeller of 0.97 times the diameter of the three-blade, the same pitch ratio, and four-thirds the area will absorb the **same power** at the same rpm as the three-blade propeller. Similarly, a two-blade propeller of 5 percent greater diameter is approximately equivalent to a three-blade unit. Figure 11.3.20 shows that propeller efficiency increases with decrease in value of the propeller coefficient B_p . A low value of B_p in a slow-speed ship calls for a large-diameter (optimum) propeller. It is frequently necessary to limit the diameter of the propeller and accept the accompanying loss in efficiency.

The number of propeller blades is usually three or four. Four blades are commonly used with single-screw merchant ships. Recently five, and even six, blades have been used to reduce vibration. Alternatively, highly skewed blades reduce vibration by creating a smoother interaction between the propeller and the ship's wake. Highly loaded propellers of fast ships and naval vessels call for large blade area, preferably three to five blades, to reduce blade interference and vibration.

Propeller fore-and-aft clearance from the stern frame of large single-screw ships at 70 percent of propeller radius should be greater than 18 in. The stern frame should be streamlined. The clearance from the propeller tips to the shell plating of twin-screw vessels ranges from about 20 in for low-powered ships to 4 or 5 ft for high-powered ships. U.S. Navy practice generally calls for a propeller tip clearance of 0.25 D . Many high-speed motorboats have a tip clearance of only several inches. The immersion of the propeller tips should be sufficient to prevent the drawing in of air.

EXAMPLE. Consider a three-blade propeller for a single-screw installation with $P_s = 2,950$ shp (2,200 kW_S), $V = 17$ knots, and $C_B = 0.52$. Find the propeller diameter D and efficiency η_o for $n = 160$ r/min.

From Fig. 11.3.19, the wake fraction $w = 0.165$. $V_A = V(1 - 0.165) = 14.19$ knots. $P_D = 0.98P_s = 2,891$ dhp (2,156 kW_D). At 160 r/min, $B_p = 160(2,891)^{0.5}/(14.19)^{2.5} = 11.34$. [1.158 × 160(2,156)^{0.5}/(14.19)^{2.5} = 11.34.] From Fig. 11.3.20, the following is obtained or calculated:

r/min	B_p	P/d	η_o	δ	D , ft (m)	P , ft (m)
160	11.34	0.95	0.69	139	12.33 (3.76)	11.71 (3.57)

For a screw centerline submergence of 9 ft (2.74 m) and a selected projected area ratio PAR = 0.3, investigate the cavitation criterion. Assume $\eta_R = 1.0$.

Minimum projected area:

$$T = 325.7 \eta_o \eta_R P_D/V_A = 325.7 \times 0.69 \times 1.0 \times 2,891/14.19 = 45,786 \text{ lb}$$

$$(T = 1942.5 \times 0.69 \times 2,156/14.19 = 203,646 \text{ N})$$

$$p_0 - p_v = 14.45 + 0.45(9) = 18.5 \text{ lb/in}^2$$

$$(p_0 - p_v = 99,629 + 10,179(2.74) = 127,519 \text{ N/m}^2)$$

$$A_p^2 = (45,786)^2/1,360(18.5)^{1.5}(14.19) = 1,365, A_p$$

$$= 36.95 \text{ ft}^2 \text{ minimum}$$

$$A_p^2 = (203,646)^2/5.44(127,519)^{1.5}(14.19) = 11.79, A_p$$

$$= 3.43 \text{ m}^2 \text{ minimum}$$

Actual projected area: PAR = $A_p/A_0 = 0.3$, $A_p = 0.3A_0 = 0.3\pi(12.33)^2/4 = 35.82 \text{ ft}^2$ (3.33 m²).

Since the selected PAR does not meet the minimum cavitation criterion, either the blade width can be increased or a four-blade propeller can be adopted. To absorb the same power at the same rpm, a four-blade propeller of about 0.97 (12.33) = 11.96 ft (3.65 m) diameter with the same blade shape would have an $A_p = 35.82 \times \frac{1}{4} \times (11.96/12.33)^2 = 44.94 \text{ ft}^2$ (4.17 m²), or about 25 percent increase. The pitch = 0.95 (11.96) = 11.36 ft (3.46 m). The real and apparent slip ratios for the four-blade propeller are:

$$S_R = 1 - (101.3)(14.19)/(11.36)(160) = 0.209$$

$$S_A = 1 - (30.9)(17.0)/(3.46)(160) = 0.051$$

that is, 20.9 and 5.1 percent (S_A calculated using SI values).

Since the projected area in the three-blade propeller of this example is only slightly under the minimum, a three-blade propeller with increased blade width would be the more appropriate choice.

Controllable-Pitch Propellers

Controllable-pitch propellers are screw propellers in which the blades are separately mounted on the hub, each on an axis, and in which the pitch of the blades can be changed, and even reversed, while the pro-

propeller is turning. The pitch is changed by means of an internal mechanism consisting essentially of hydraulic pistons in the hub acting on crossheads. Controllable-pitch propellers are most suitable for vehicles which must meet different operating conditions, such as tugs, trawlers, ferries, minesweepers, and landing craft. As the propeller pitch is changed, the engine can still run at its most efficient speed. Maneuvering is more rapid since the pitch can be changed more rapidly than could the shaft revolutions. By use of controllable-pitch propellers, neither reversing mechanisms are necessary in reciprocating engines, nor astern turbines in turbine-powered vehicles, especially important in gas-turbine installations. Except for the larger hub needed to house the pitch-changing mechanism, the controllable-pitch propeller can be made almost as efficient as the solid, fixed-blade propeller. The newest application is in the U.S. Navy's DDG 51 class destroyer, developing approximately 50,000 shp (24,785 kW_S) per shaft.

Water Jet

This method usually consists of an impeller or pump inside the hull, which draws water from outside, accelerates it, and discharges it astern as a jet at a higher velocity. It is a reaction device like the propeller but in which the moving parts are contained inside the hull, desirable for shallow-water operating conditions and maneuverability. The overall efficiency is lower than that of the screw propeller of diameter equal to the jet orifice diameter, principally because of inlet and ducting losses. Other disadvantages include the loss of volume to the ducting and impeller and the danger of fouling of the impeller. Water jets have been used in several of the U.S. Navy's hydrofoil and surface-effect vehicles.

Vertical-Axis Propellers

There are two types of vertical-axis propulsor systems consisting of one or two vertical-axis rotors located underwater at the stern. Rotor disks are flush with the shell plating and have five to eight streamline, spade-like, vertical impeller blades fitted near the periphery of the disks. The blades feather during rotation of the disk to produce a maximum thrust effect in any direction desired. In the **Kirsten-Boeing** system the blades are interlocked by gears so that each blade makes a half revolution about its axis for each revolution of the disk. The blades of the **Voith-Schneider** system make a complete revolution about their own axis for each revolution of the disk. A bevel gear must be used to transmit power from the conventional horizontal drive shaft to the horizontal disk; therefore, limitations exist on the maximum power that can be transmitted. Although the propulsor is 30 to 40 percent less efficient than the screw propeller, it has obvious maneuverability advantages. Propulsors of this type have also been used at the bow to assist in maneuvering.

Other Thrust Devices

Pump Jet In a pump-jet arrangement, the rotating impeller is external to the hull with fixed guide vanes either ahead and/or astern of it; the whole unit is enclosed in a duct or long shroud ring. The duct diameter increases from the entrance to the impeller so that the velocity falls and the pressure increases. Thus the impeller diameter is larger, thrust loading less, and the efficiency higher; the incidence of cavitation and noise is delayed. A penalty is paid, however, for the resistance of the duct.

Kort Nozzles In the Kort nozzle system, the screw propeller operates in a ring or nozzle attached to the hull at the top. The longitudinal sections are of airfoil shape, and the length of the nozzle is generally about one-half its diameter. Unlike the pump-jet shroud ring, the Kort nozzle entrance is much bigger than the propeller, drawing in more water than the open propeller and achieving greater thrust. Because of the acceleration of the water into the nozzle, the pressure inside is less; hence a forward thrust is exerted on the nozzle and the hull. The greatest advantage is in a tug, pulling at rest. The free-running speed is usually less with the nozzle than without. In some tugs and rivercraft, the whole nozzle is pivoted and becomes a very efficient steering mechanism.

Tandem and Contrarotating Propellers Two or more propellers arranged on the same shaft are used to divide the increased loading factor when the diameter of a propeller is restricted. Propellers turning in the same direction are termed **tandem**, and in opposite directions,

contrarotating. In tandem, the rotational energy in the race from the forward propeller is augmented by the after one. Contrarotating propellers work on coaxial, contrary-turning shafts so that the after propeller may regain the rotational energy from the forward one. The after propeller is of smaller diameter to fit the contracting race and has a pitch designed for proper power absorption. Such propellers have been used for years on torpedoes to prevent the torpedo body from rotating. Hydrodynamically, the advantages of contrarotating propellers are increased propulsive efficiency, improved vibration characteristics, and higher blade frequency. Disadvantages are the complicated gearing, coaxial shafting, and sealing problems.

Supercavitating Propellers When cavitation covers the entire back of a propeller blade, an increase of rpm cannot further reduce the pressure at the back but the pressure on the face continues to increase as does the total thrust, though at a slower rate than before cavitation began. Advantages of such fully cavitating propellers are an absence of back erosion and less vibration. Although the characteristics of such propellers were determined by trial and error, they have long been used on high-speed racing motor boats. The blade section design must ensure clean separation of flow at the leading and trailing edges and provide good lift-drag ratios for high efficiency. Introducing air to the back of the blades (**ventilated propeller**) will ensure full cavitation and also enables use at lower speeds.

Partially Submerged Propellers The appendage drag presented by a propeller supported below high-speed craft, such as planing boats, hydrofoil craft, and surface-effect ships, led to the development of partially submerged propellers. Although vibration and strength problems, arising from the cyclic loading and unloading of the blades as they enter and emerge from the air-water interface, remain to be solved, it has been demonstrated that efficiencies in partially submerged operation, comparable to fully submerged noncavitating operation, can be achieved. The performance of these propellers must be considered over a wide range of submergences.

Outboard Gasoline Engine Outboard gasoline engines of 1 to 300 bhp (0.75 to 225 kW_B), combining steering and propulsion, are popular for small pleasure craft. Maximum speeds of 3,000 to 6,000 r/min are typical, as driven by the propeller horsepower characteristics (see Sec. 9).

PROPULSION TRANSMISSION

In modern ships, only large-bore, slow-speed diesel engines are directly connected to the propeller shaft. Transmission devices such as mechanical speed-reducing gears or electric drives (generator/motor transmissions) are required to convert the relatively high rpm of a compact, economical prime mover to the relatively low propeller rpm necessary for a high propulsive efficiency. In the case of steam turbines, medium- and high-speed diesel engines, and gas turbines, speed reduction gears are used. Gear ratios vary from relatively low values for medium-speed diesels up to approximately 50:1 for a compact turbine design. Where the prime mover is unidirectional, the drive mechanism must also include a reversing mechanism.

Reduction Gears

Speed reduction is usually obtained with reduction gears. The simplest arrangement of a marine reduction gear is the **single-reduction**, single-input type, i.e., one pinion meshing with a gear (Fig. 11.3.21). This ar-

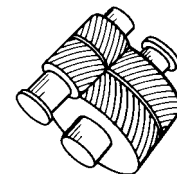


Fig. 11.3.21 Single-reduction, single-input gear. (From "Marine Engineering," SNAME, 1992.)

11-56 MARINE ENGINEERING

angement is used for connecting a propeller to a diesel engine or to an electric motor but is not used for propelling equipment with a turbine drive.

The usual arrangement for turbine-driven ships is the **double-reduction**, double-input, articulated type of reduction gear (Fig. 11.3.22). The two input pinions are driven by the two elements of a cross-compound turbine. The term *articulated* applies because a flexible coupling is generally provided between the first reduction or primary gear wheel and the second reduction or secondary pinion.

The **locked-train** type of double-reduction gear has become standard for high-powered naval ships and, because it minimizes the total weight and size of the assembly, is gaining increased popularity for higher-powered merchant ships (Fig. 11.3.23).

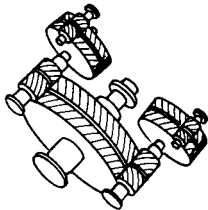


Fig. 11.3.22 Double-reduction, double-input, articulated gear. (From "Marine Engineering," SNAME, 1992.)

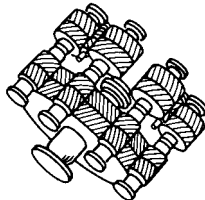


Fig. 11.3.23 Double-reduction, double-input, locked-train gear. (From "Marine Engineering," SNAME, 1992.)

Electric Drive

Electric propulsion drive is the principal alternative to direct- or geared-drive systems. The prime mover drives a generator or alternator which in turn drives a propulsion motor which is either coupled directly to the propeller or drives the propeller through a low-ratio reduction gear.

Among its **advantages** are the ease and convenience by which propeller speed and direction are controllable; the freedom of installation arrangement offered by the electrical connection between the generator and the propulsion motor; the flexibility of power use when not used for propulsion; the convenience of coupling several prime movers to the propeller without mechanical clutches or couplings; the relative simplicity of controls required to provide reverse propeller rotation when the prime mover is unidirectional; and the speed reduction that can be provided between the generator and the motor, hence between the prime mover and the propeller, without mechanical speed-reducing means.

The disadvantages are the inherently higher first cost, increased weight and space, and the higher transmission losses of the system. The advent of **superconductive electrical machinery** suitable for ship propulsion, however, has indicated order-of-magnitude savings in weight, greatly reduced volume, and the distinct possibility of lower costs. Superconductivity, a phenomenon occurring in some materials at temperatures near absolute zero, is characterized by the almost complete disappearance of electrical resistance. Research and development studies

have shown that size and weight reductions by factors of 5 or more are possible. With successful development of superconductive electrical machinery and resolution of associated engineering problems, mono-hulled craft, such as destroyers, can benefit greatly from the location flexibility and maneuverability capabilities of superconductive electric propulsion, but the advantages of such a system will be realized to the greatest extent in the new high-performance ships where mechanical-drive arrangement is extremely complex.

In general, electric propulsion drives are employed in marine vehicles requiring a high degree of maneuverability such as ferries, icebreakers, and tugs; in those requiring large amounts of special-purpose power such as self-unloaders, fireboats, and large tankers; in those utilizing nonreversing, high-speed, and multiple prime movers; and in deep-submergence vehicles. Diesel-electric drive is ideally adapted to bridge control.

Reversing

Reversing may be accomplished by stopping and reversing a reversible engine, as in the case of many reciprocating engines, or by adding reversing elements in the prime mover, as in the case of steam turbines. It is impracticable to provide reversing elements in gas turbines; hence a reversing capability must be provided in the transmission system or in the propulsor itself. Reversing reduction gears for such transmissions are available up to quite substantial powers, and CRP propellers are also used with diesel or gas-turbine drives. Electrical drives provide reversing by dynamic braking and energizing the electric motor in the reverse direction.

Marine Shafting

A main propulsion shafting system consists of the equipment necessary to transmit the rotative power from the main propulsion engines to the propulsor; support the propulsor; transmit the thrust developed by the propulsor to the ship's hull; safely withstand transient operating loads (e.g., high-speed maneuvers, quick reversals); be free of deleterious modes of vibration; and provide reliable operation.

Figure 11.3.24 is a shafting arrangement typical of multishaft ships and single-shaft ships with transom sterns. The shafting must extend outboard a sufficient distance for adequate clearance between the propeller and the hull. Figure 11.3.25 is typical of single-screw merchant ships.

The shafting located inside the ship is **line shafting**. The outboard section to which the propeller is secured is the **propeller shaft** or **tail shaft**. The section passing through the stern tube is the **stern tube shaft** unless the propeller is supported by it. If there is a section of shafting between the propeller and stern tube shafts, it is an **intermediate shaft**.

The principal dimensions, kind of material, and material tests are specified by the classification societies for marine propulsion shafting. The American Bureau of Shipping Rules for Steel Vessels specifies the minimum diameter of propulsion shafting, tail shaft bearing lengths, bearing liner and flange coupling thicknesses, and minimum fitted bolt diameters.

Tail or propeller shafts are of larger diameter than the line or tunnel shafting because of the propeller-weight-induced bending moment;

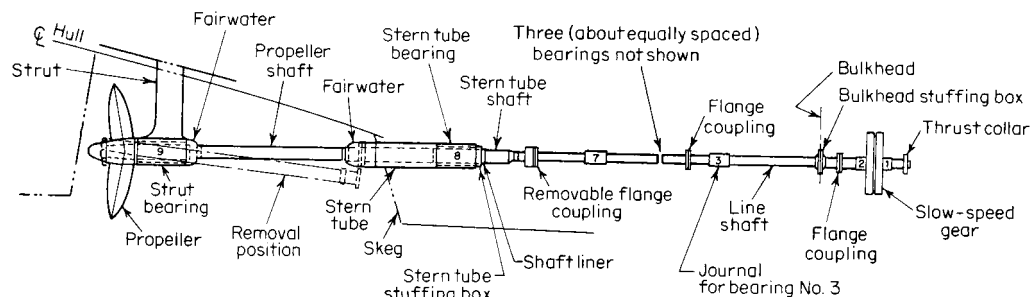


Fig. 11.3.24 Shafting arrangement with strut bearings. (From "Marine Engineering," SNAME, 1992.)

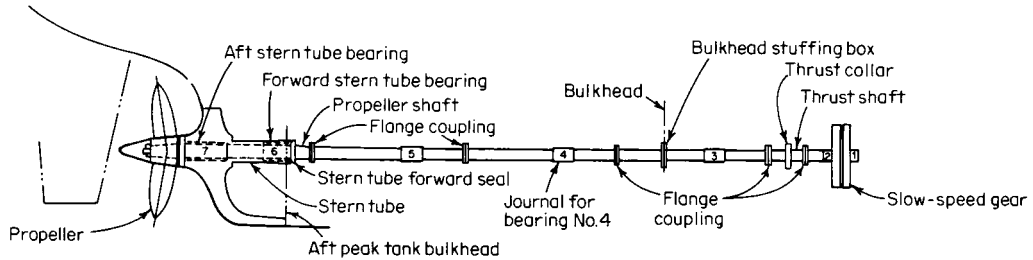


Fig. 11.3.25 Shafting arrangement without strut bearings. (From "Marine Engineering," SNAME, 1992.)

also, inspection during service is possible only when the vessel is dry-docked.

Propellers are fitted to shafts over 6 in (0.1524 m) diameter by a taper fit. Aft of the propeller, the shaft is reduced to 0.58 to 0.68 of its specified diameter under the liner and is fitted with a relatively fine thread, nut, and keeper. Propeller torque is taken by a long flat key, the width and total depth of which are, respectively, about 0.21 and 0.11 times the shaft diameter under the liner. The forward end of the key slot in the shaft should be tapered off in depth and terminate well aft of the large end of the taper to avoid a high concentrated stress at the end of the keyway. Every effort is made to keep saltwater out of contact with the steel tail shaft so as to prevent failure from corrosion fatigue.

A cast-iron, cast-steel, or wrought-steel-weldment **stern tube** is rigidly fastened to the hull. In single-screw ships it supports the propeller shaft and is normally provided with a packing gland at the forward end as seawater lubricates the stern-tube bearings. The aft stern-tube bearing is made four diameters in length; the forward stern-tube bearing is much shorter. A bronze liner, $\frac{3}{4}$ to 1 in (0.0191 to 0.0254 m) thick, is shrunk on the propeller shaft to protect it from corrosion and to give a good journal surface. Lignum-vitae inserts, arranged with the grain on end for medium and large shafts, are normally used for stern-tube bearings; the average bearing pressure is about 30 lb/in² (206,842 N/m²). Rubber and phenolic compound bearings, having longitudinal grooves, are also extensively used. White-metal oil-lubricated bearings and, in Germany, roller-type stern bearings have been fitted in a few installations.

The line or tunnel shafting is laid out, in long equal lengths, so that, in the case of a single-screw ship, withdrawal of the tail shaft inboard for inspection every several years will require only the removal of the next inboard length of shafting. For large outboard or water-exposed shafts of twin-screw ships, a bearing spacing up to 30 shaft diameters has been used. A greater ratio prevails for steel shafts of power boats. Bearings inside the hull are spaced closer—normally under 15 diameters if the shaft is more than 6 in (0.1524 m) diameter. Usually, only the bottom half of the bearing is completely white-metaled; oil-wick lubrication is common, but oil-ring lubrication is used in high-class installations.

Bearings are used to support the shafting in essentially a straight line between the main propulsion engine and the desired location of the propeller. Bearings inside the ship are most popularly known as line-shaft bearings, steady bearings, or spring bearings. Bearings which support outboard sections of shafting are stern-tube bearings if they are located in the stern tube and strut bearings when located in struts.

The propeller thrust is transmitted to the hull by means of a main thrust bearing. The main thrust bearing may be located either forward or aft of the slow-speed gear.

HIGH-PERFORMANCE SHIP SYSTEMS

High-performance ships have spawned new hull forms and propulsion systems which were relatively unknown just a generation ago. Because of their unique characteristics and requirements, conventional propellers are rarely adequate. The prime thrust devices range from those using water, to water-air mixtures, to large air propellers.

The total propulsion power required by these vehicles is presented in general terms in the Gabrielli and Von Karman plot of Fig. 11.3.26. Basically, there are those vehicles obtaining lift by displacement and

those obtaining lift from a wing or foil moving through the fluid. In order for marine vehicles to maintain a reasonable lift-to-drag ratio over a moderate range of speed, the propulsion system must provide increased thrust at lower speeds to overcome low-speed wave drag. The weight of any vehicle is converted into total drag and, therefore, total required propulsion and lift power.

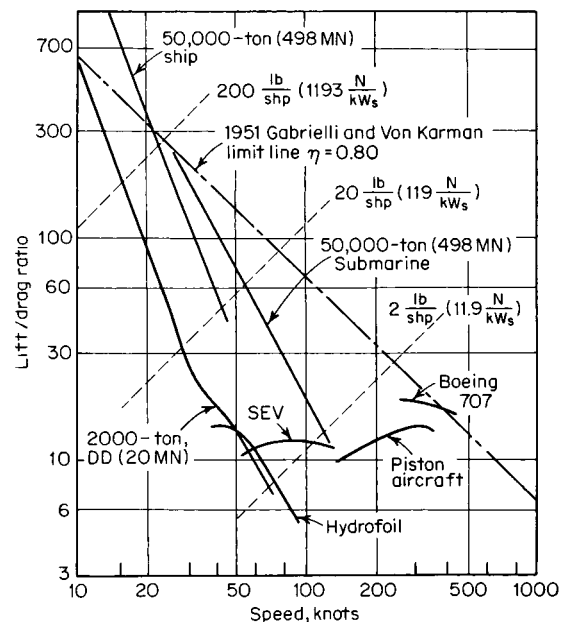


Fig. 11.3.26 Lift-drag ratio versus calm weather speed for various vehicles.

Lightweight, compact, and efficient propulsion systems to satisfy extreme weight sensitivity are achieved over a wide range of power by the marinized aircraft gas-turbine engine. Marinization involves addition of a power turbine unit, incorporation of air inlet filtration to provide salt-free air, addition of silencing equipment on both inlet and exhaust ducts, and modification of some components for resistance to salt corrosion. The shaft power delivered is then distributed to the propulsion and lift devices by lightweight shaft and gear power transmission systems.

A comparison of high-performance ship propulsion system characteristics is given in Table 11.3.3.

Hydrofoil Craft

Under foilborne conditions, the support of the hydrofoil craft is derived from the dynamic lift generated by the foil system, and the craft hull is lifted clear of the water. Special problems relating to operation and directly related to the conditions presented by waves, high fluid density, surface piercing of foils and struts, stability, control, cavitation, and ventilation of foils have given rise to foil system configurations defined in Fig. 11.3.27.

11-58 MARINE ENGINEERING

Table 11.3.3 U.S. Navy High-Performance Ship Propulsion System Characteristics

Ship	Engine	Propulsor/lift
Hydrofoil, PHM, 215 tons (2.1 MN), 50 knots	Foilborne: one LM-2500 GT, 22,000 bhp (15,405 kW _B), 3,600 r/min	Foilborne: one 2-stage axial-flow waterjet, twin aft strut inlets
Surface-effect ship, SES-200, 195 tons (1.94 MN), 30 + knots	Propulsion: two 16V-149TI diesel, 1,600 bhp (1,193 kW _B) Lift: two 8V-92TI diesel, 800 bhp (597 kW _B)	Two waterjet units Two double-inlet centrifugal lift fans
Air-cushion vehicle, LCAC, 150 tons (1.49 MN), 50 knots	Propulsion and lift: four TF-40B GT, 3,350 bhp (2,498 kW _B), 15,400 r/min	Two ducted-air propellers, 12 ft (3.66 m) dia., 1,250 r/min; four double-entry centrifugal lift fans, 1,900 r/min
SWATH, SSP, 190 tons (1.89 MN), 25 knots	Propulsion: two T-64 GT, 3,200 bhp (2,386 kW _B), 1,000 r/min at output of attached gearbox	Two subcavitating controllable-pitch propellers, 450 r/min

The hydrofoil craft has three modes of operation: **hullborne**, **takeoff**, and **foilborne**. The thrust and drag forces involved in hydrofoil operation are shown in Fig. 11.3.28. Design must be a compromise between the varied requirements of these operating conditions. This may be difficult,

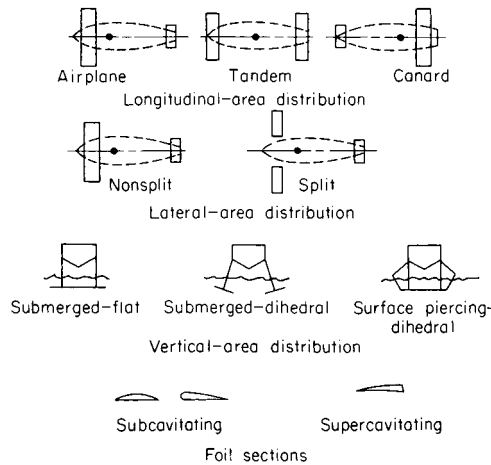


Fig. 11.3.27 Some foil arrangements and sections.

as with propeller design, where maximum thrust is often required at takeoff speed (normally about one-half the operating speed). A propeller designed for maximum efficiency at takeoff will have a smaller efficiency at design speeds, and vice versa. This is complicated by the

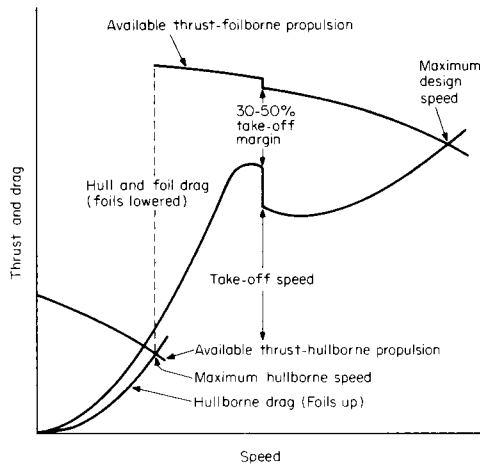


Fig. 11.3.28 Thrust and drag forces for a typical hydrofoil.

need for supercavitating propellers at operating speeds over 50 knots. Two sets of propellers may be needed in such a case, one for hullborne operation and the other for foilborne operation. The selection of a surface-piercing or a fully submerged foil design is determined from specified operating conditions and the permissible degree of complexity. A **surface-piercing system** is inherently stable, as a deviation from the equilibrium position of the craft results in corrective lift forces. **Fully submerged foil designs**, on the other hand, provide the best lift-drag ratio but are not stable by themselves and require a depth-control system for satisfactory operation. Such a control system, however, permits operation of the submerged-foil design in higher waves.

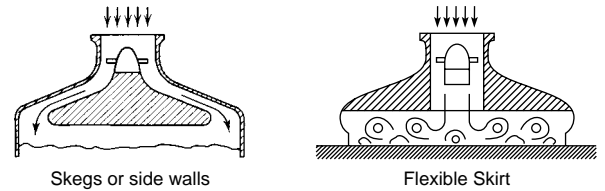


Fig. 11.3.29 Two configurations of the surface-effect principle.

Surface-Effect Vehicles (SEV)

The air-cushion-supported **surface-effect ship (SES)** and **air-cushion vehicle (ACV)** show great potential for high-speed and amphibious operation. Basically, the SEV rides on a cushion of air generated and maintained in the space between the vehicle and the surface over which it moves or hovers. In the SES, the cushion is captured by rigid sidewalls

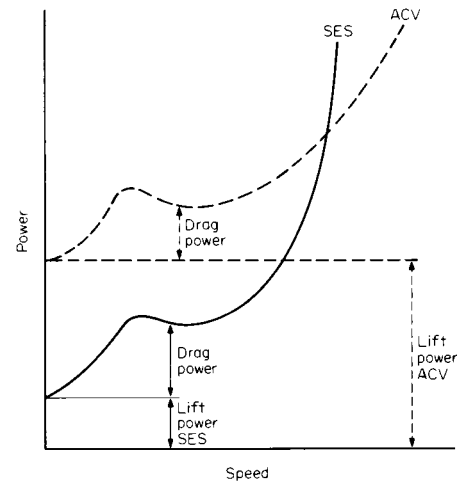


Fig. 11.3.30 Comparison of power requirements: SES versus ACV.

and flexible skirts fore and aft. The ACV has a flexible seal or skirt all around. Figure 11.3.29 illustrates two configurations of the surface-effect principle.

Since the ACV must rise above either land or water, the propulsors use only air for thrust, requiring a greater portion of the total power allocated to lift than in the SES design as shown in Fig. 11.3.30.

While SES technology has greatly improved the capability of amphibious landing vehicles, it is rapidly being developed for high-speed large cargo vessels.

Small Water-Plane Area Twin Hull

The **SWATH**, configured to be relatively insensitive to seaway motions, gains its buoyant lift from two parallel submerged, submarinelike hulls which support the main hull platform through relatively small vertical struts. In this configuration, a propulsion arrangement choice must be with regard to the location of the main engines: lower hull with the propulsor or upper hull with a suitable transmission system. In the U.S. Navy's semisubmerged platform (SSP), power from two independently operated gas turbines is transmitted down each aft strut by a group of three wide-belt chain drives with speed reduction to deliver 450 r/min to the propellers. By contrast, the 3,400-ton (33.87-MN), 11-knot T-AGOS 19 series SWATH vessels employ diesel-electric drive, with both motors and propulsors in the lower hull.

CARGO SHIPS

The development of containerization in the 1950s sparked a growth in ship size. More efficient cargo-handling methods and the desire to reduce transit time led to the emergence of the high-speed container vessel.

The Container Vessel

Because of low fuel costs in the 1950s and 1960s, early container vessel design focused on higher speed and container capacity. Rising fuel costs shifted emphasis toward ship characteristics which enhanced reduced operating costs, particularly as affected by fuel usage and trade route capacity. By the early 1980s, ships were generally sized for TEU (twenty-foot-equivalent-unit) capacity less than 2,500 and speeds of about 20 knots, lower if fuel was significant in the overall operating costs. Largely a function of the scale of trade route capacity, the weighted average full containership size is on the order of 1,000 TEU. The larger the trade capacity, the larger the containerships operating the route. However, many trade route scales do not support even moderately sized containership service.

The **on deck** and **under deck** container capacity varies with the type of vessel, whether a **lift on/lift off** vessel, a bulk carrier equipped for containers, or a **roll on/roll off** vessel. Extensive studies have been conducted to optimize the hull form and improve the operating efficiency for the modern containership.

11.4 AERONAUTICS

by M. W. M. Jenkins

REFERENCES: National Advisory Committee for Aeronautics, *Technical Reports* (designated *NACA-TR* with number), *Technical Notes* (*NACA-TN* with number), and *Technical Memoranda* (*NACA-TM* with number). British Aeronautical Research Committee *Reports and Memoranda* (designated *Br. ARC-R & M* with number). *Ergebnisse der Aerodynamischen Versuchsanstalt zu Göttingen*. Diehl, "Engineering Aerodynamics," Ronald. Reid, "Applied Wing Theory," McGraw-Hill. Durand, "Aerodynamic Theory," Springer. Prandtl-Tietjens, "Fundamentals of Hydro- and Aeromechanics," and "Applied Hydro- and Aeromechanics," McGraw-Hill. Goldstein, "Modern Developments in Fluid Dynamics," Oxford. Millikan, "Aerodynamics of the Airplane," Wiley. Von Mises, "Theory of Flight," McGraw-Hill. Hoerner, "Aerodynamic Drag," Hoerner. Glauert, "The Elements of Airfoil and Airscrew Theory," Cambridge. Milne-Thompson, "Theoretical Hydrodynamics," Macmillan. Munk, "Fluid Dynamics for Aircraft Designers," and "Principles of Aerodynamics," Ronald. Abraham, "Structural Design of Missiles and Spacecraft," McGraw-Hill. "U.S. Standard Atmosphere, 1962," U.S. Government Printing Office.

DEFINITIONS

Aeronautics is the science and art of flight and includes the operation of heavier-than-air aircraft. An **aircraft** is any weight-carrying device designed to be supported by the air, either by buoyancy or by dynamic action. An **airplane** is a mechanically driven fixed-wing aircraft, heavier than air, which is supported by the dynamic reaction of the air against its wings. A **helicopter** is a kind of aircraft lifted and moved by a large propeller mounted horizontally above the fuselage. It differs from the **autogyro** in that this propeller is turned by motor power and there is no auxiliary propeller for forward motion. A **ground-effect machine (GEM)** is a heavier-than-air surface vehicle which operates in close proximity to the earth's surface (over land or water), never touching except at rest, being separated from the surface by a cushion or film of air, however thin, and depending entirely upon aerodynamic forces for propulsion and control.

Aerodynamics is the branch of aeronautics that treats of the motion of air and other gaseous fluids and of the forces acting on solids in motion relative to such fluids. Aerodynamics falls into velocity ranges, depending upon whether the velocity is below or above the local speed of

sound in the fluid. The velocity range below the local speed of sound is called the **subsonic** regime. Where the velocity is above the local speed of sound, the flow is said to be **supersonic**. The term **transonic** refers to flows in which both subsonic and supersonic regions are present. The **hypersonic** regime is that speed range usually in excess of five times the speed of sound.

STANDARD ATMOSPHERE

The standard atmosphere of Table 11.4.1 is a revised U.S. Standard Atmosphere, adapted by the United States Committee on Extension to the Standard Atmosphere (COESA) in 1962.

The values given up to about 65,000 ft are designated as **standard**. The region from 65,000 to 105,000 ft is designated **proposed standard**. U.S. Standard Atmosphere, 1962, gives data out to 2,320,000 ft; however, the region from 105,000 to 295,000 ft is designated **tentative**, and that portion of the atmosphere above 295,000 ft is termed **speculative**.

The assumed sea-level conditions are: pressure, $p_0 = 29.91$ in (760 mm Hg) = 2,116.22 lb/ft²; mass density, $\rho_0 = 0.002378$ slugs/ft³ (0.001225 g/cm³); $T_0 = 59^\circ\text{F}$ (15°C).

UPPER ATMOSPHERE

High-altitude atmospheric data have been obtained directly from balloons, sounding rockets, and satellites and indirectly from observations of meteors, aurora, radio waves, light absorption, and sound effects. At relatively low altitudes, the earth's atmosphere is, for aerodynamic purposes, a uniform gas. Above 250,000 ft, day and night standards differ because of dissociation of oxygen by solar radiation. This difference in density is as high as 35 percent, but it is usually aerodynamically negligible above 250,000 ft since forces here will become less than 0.05 percent of their sea-level value for the same velocity.

Temperature profile of the COESA atmosphere is given in Fig. 11.4.1. From these data, other properties of the atmosphere can be calculated.

11-60 AERONAUTICS

Table 11.4.1 U.S. Standard Atmosphere, 1962

Altitude <i>h</i> , ft*	Temp <i>T</i> , °F†	Pressure ratio, <i>p/p</i> ₀	Density ratio, <i>ρ/ρ</i> ₀	(<i>ρ</i> ₀ / <i>ρ</i>) ^{0.5}	Speed of sound <i>V</i> _s , ft/s‡
0	59.00	1.0000	1.0000	1.000	1,116
5,000	41.17	0.8320	0.8617	1.077	1,097
10,000	23.34	0.6877	0.7385	1.164	1,077
15,000	5.51	0.5643	0.6292	1.261	1,057
20,000	-12.62	0.4595	0.5328	1.370	1,036
25,000	-30.15	0.3711	0.4481	1.494	1,015
30,000	-47.99	0.2970	0.3741	1.635	995
35,000	-65.82	0.2353	0.3099	1.796	973
36,089	-69.70	0.2234	0.2971	1.835	968
40,000	-69.70	0.1851	0.2462	2.016	968
45,000	-69.70	0.1455	0.1936	2.273	968
50,000	-69.70	0.1145	0.1522	2.563	968
55,000	-69.70	0.09001	0.1197	2.890	968
60,000	-69.70	0.07078	0.09414	3.259	968
65,000	-69.70	0.05566	0.07403	3.675	968
65,800	-69.70	0.05356	0.07123	3.747	968
70,000	-67.30	0.04380	0.05789	4.156	971
75,000	-64.55	0.03452	0.04532	4.697	974
80,000	-61.81	0.02725	0.03553	5.305	977
85,000	-59.07	0.02155	0.02790	5.986	981
90,000	-56.32	0.01707	0.02195	6.970	984
95,000	-53.58	0.01354	0.01730	7.600	988
100,000	-50.84	0.01076	0.01365	8.559	991

* × 0.3048 = metres.
 † × (°F - 32)/1.8 = °C.
 ‡ × 0.3048 = m/s.

Pressure and Density For all practical purposes, both decrease exponentially with altitude. The variations in *T* (Fig. 11.4.1) are accompanied by slight inflections in the curves of *p* and *ρ*, but the deviations from a mean curve are far less than the scatter in test data from various sources. For altitudes above 100,000 ft, pressure and density may be approximated by

$$\log p_0/p = 0.00001910h + 0.0140$$

$$\log \rho_0/\rho = 0.00001890h - 0.1000$$

where *h* is in ft. At *h* = 320,000 ft, or about 60 mi (96 km), *p* and *ρ* are about one-millionth of the sea-level values.

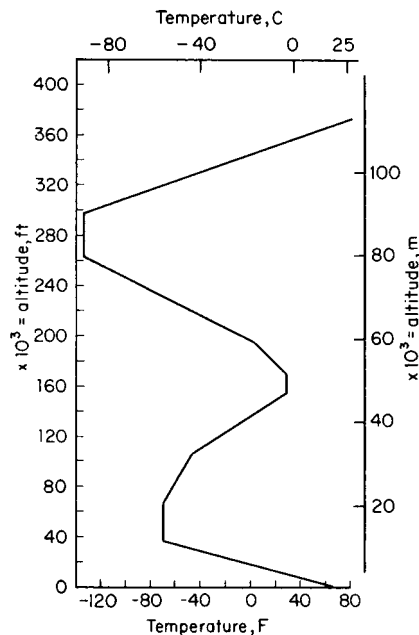


Fig. 11.4.1 Temperature as a function of altitude. (COESA.)

Speed in aeronautics may be given in knots (now standard for USAF, USN, and FAA), miles per hour, feet per second, or metres per second. The international nautical mile = 6,076.1155 ft (1,852 m). The basic relations are: 1 knot = 0.5144 m/s = 1.6877 ft/s = 1.1508 mi/h. For additional conversion factors see Sec. 1. Higher speeds are often given as **Mach number**, or the ratio of the particular speed to the speed of sound in the surrounding air. For additional data see "Supersonic and Hypersonic Aerodynamics" below.

Axes The forces and moments acting on an airplane (and the resultant velocity components) are referred to a set of three mutually perpendicular axes having the origin at the airplane center of gravity (cg) and moving with the airplane. Three sets of axes are in use. The basic difference in these is in the direction taken for the longitudinal, or *x*, axis, as follows:

Wind axes: The *x* axis lies in the direction of the relative wind. This is the system most commonly used, and the one used in this section. It is shown on Fig. 11.4.2.

Body axes: The *x* axis is fixed in the body, usually parallel to the thrust line.

Stability axes: The *x* axis points in the initial direction of flight. This results in a simplification of the equations of motion.

Absolute Coefficients Aerodynamic force and moment data are usually presented in the form of absolute coefficients. Examples of force coefficients are: lift $C_L = L/qS$; drag $C_D = D/qS$; side force $C_Y = Y/qS$; where *q* is the dynamic pressure $\frac{1}{2}\rho V^2$, *ρ* = air mass-density, and *V* = air speed. Examples of moment coefficients are $C_m = M/qSc$; roll $C_l = L/qSb$; and yaw $C_n = N/qSb$; where *c* = mean wing chord and *b* = wing span.

Section Coefficients NACA basic test data on wing sections are usually given in the form of section lift coefficient C_l and section drag coefficient C_d . These apply directly to an infinite aspect ratio or to two-dimensional flow, but aspect-ratio and lift-distribution corrections are necessary in applying to a finite wing. For a wing having an elliptical lift distribution, $C_L = (\pi/4)C_l$, where C_l is the centerline value of the local lift coefficient.

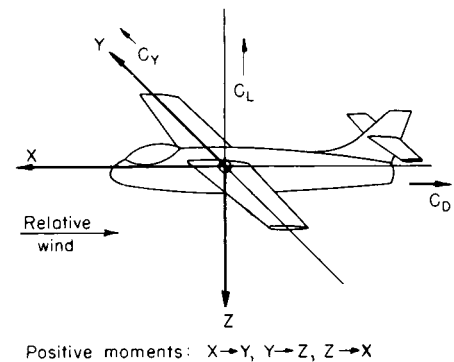


Fig. 11.4.2 Wind axes.

SUBSONIC AERODYNAMIC FORCES

When an airfoil is moved through the air, the motion produces a pressure at every point of the airfoil which acts normal to the surface. In addition, a frictional force tangential to the surface opposes the motion. The sum of these pressure and frictional forces gives the **resultant force R** acting on the body. The point at which the resultant force acts is defined as the **center of pressure, c.p.** The resultant force *R* will, in general, be inclined to the airfoil and the relative wind velocity *V*. It is resolved (Fig. 11.4.3) either along wind axes into

- L* = lift = component normal to *V*
- D* = drag or resistance = component along *V*, or along body axes into

N = normal force = component perpendicular to airfoil chord
 T = tangential force = component along airfoil chord

Instead of specifying the center of pressure, it is convenient to specify the moment of the air forces about the so-called *aerodynamic center*, a.c. This point lies at a distance a (about a quarter-chord length) back of the leading edge of the airfoil and is defined as the point about which the moment of the air forces remains constant when the angle of attack α is changed. Such a point exists for every airfoil. The force R acting at the c.p. is equivalent to the same force acting at the a.c. plus a moment equal to that force times the distance between the c.p. and the a.c. (see Fig. 11.4.3). The location of the aerodynamic center, in terms of the chord c and the section thickness t , is given for NACA 4- and 5-digit series airfoils approximately by

$$a/c = 0.25 - 0.40(t/c)^2$$

The distance $x_{c.p.}$ from the leading edge to the center of pressure expressed as a fraction of the chord is, in terms of the moment $M_{c/4}$ about the quarter-chord point,

$$M_{c/4} = (\frac{1}{4} - x_{c.p.}) \cdot cN$$

$$x_{c.p.} = \frac{1}{4} - \frac{M_{c/4}}{cN}$$

From dimensional analysis it can be seen that the air force on a body of length dimension l moving with velocity V through air of density ρ can be expressed as

$$F = \varphi \cdot \rho V^2 l^2$$

where φ is a coefficient that depends upon all the dimensionless factors of the problem. In the case of a wing these are:

1. **Angle of attack** α , the inclination between the chord line and the velocity V
2. **Aspect ratio** $A = b/c$, where b is the span and c the mean chord of the wing
3. **Reynolds number** $Re = \rho V l / \mu$, where μ is the coefficient of dynamic viscosity of air
4. **Mach number** V/V_s , where V_s is the velocity of sound
5. Relative surface roughness
6. Relative turbulence

The dependence of the force coefficient φ upon α and A can be theoretically determined; the variation of φ with the other parameters must be established experimentally, i.e., by model tests.

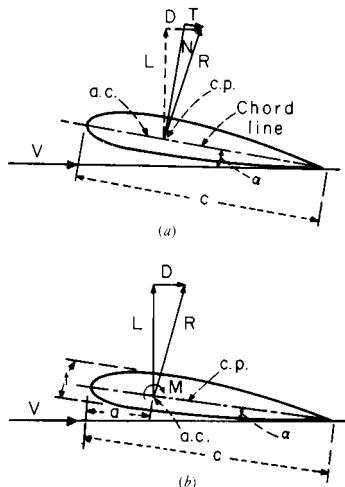


Fig. 11.4.3 Forces acting on an airfoil. (a) Actual forces; (b) equivalent forces through the aerodynamic center plus a moment.

AIRFOILS

Applying Bernoulli's equation to the flow around a body, if p represents the static pressure, i.e., the atmospheric pressure in the undisturbed air, and if V is superposed as in Fig. 11.4.4 and if p_1, V_1 represent the pressure and velocity at any point 1 at the surface of the body,

$$p + \frac{1}{2} \rho V^2 = p_1 + \frac{1}{2} \rho V_1^2$$

The maximum pressure occurs at a point s on the body at which the velocity is zero. Such a point is defined as the **stagnation point**. The maximum pressure increase occurs at this point and is

$$p_s - p = \frac{1}{2} \rho V^2$$

This is called the stagnation pressure, or **dynamic pressure**, and is denoted by q . It is customary to express all aerodynamic forces in terms of $\frac{1}{2} \rho V^2$, hence

$$F = \frac{1}{2} \varphi \rho V^2 l^2 = q \varphi l^2$$

For the case of a wing, the forces and moments are expressed as

$$\text{Lift} = L = C_L \frac{1}{2} \rho V^2 S = C_L q S$$

$$\text{Drag} = D = C_D \frac{1}{2} \rho V^2 S = C_D q S$$

$$\text{Moment} = M = C_M \frac{1}{2} \rho V^2 S c = C_M q S c$$

where S = wing area and c = wing chord.

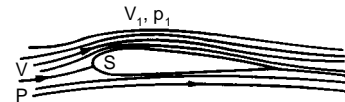


Fig. 11.4.4 Fluid flow around an airfoil.

The lift produced can be determined from the intensity of the circulatory flow or **circulation** Γ by the relation $L' = \rho V \Gamma$, where L' is the lift per unit width of wing. In a **wing of infinite aspect ratio**, the flow is two-dimensional and the lift reaction is at right angles to the line of relative motion. The **lift coefficient** is a function of the angle of attack α , and by mathematical analysis $C_L = 2\pi \sin \alpha$, which for small angles becomes $C_L = 2\pi \alpha$. Experiments show that $C_L = 2\pi \eta (\alpha - \alpha_0)$, where α_0 is the angle of attack corresponding to zero lift. $\eta \approx 1 - 0.64(t/c)$, where t is airfoil thickness.

In a **wing of finite aspect ratio**, the circulation flow around the wing creates a strong vortex trailing downstream from each wing tip (Fig.

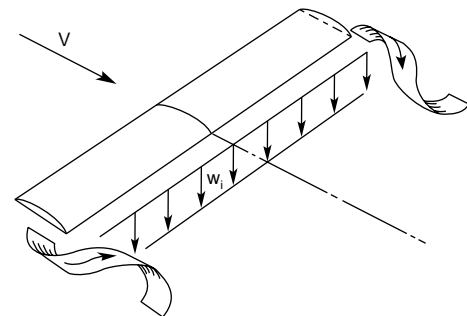


Fig. 11.4.5 Vortex formation at wing tips.

11.4.5). The effect of this is that the direction of the resultant velocity at the wing is tilted downward by an **induced angle of attack** $\alpha_i = w_i/V$ (Fig. 11.4.6). If friction is neglected, the resultant force R is now tilted to the rear by this same angle α_i . The lift force L is approximately the same as R . In addition, there is also a drag component D_i , called the **induced drag**, given by

$$D_i = L \tan \alpha_i = L w_i / V$$

11-62 AERONAUTICS

For a given geometrical angle of attack α the **effective angle of attack** has been reduced by α_i , and thus

$$C_L = 2\pi\eta(\alpha - \alpha_0 - \alpha_i)$$

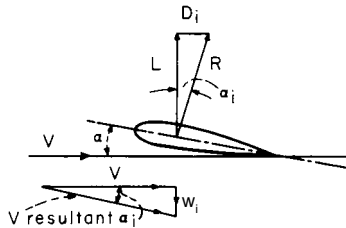


Fig. 11.4.6 Induced angle of attack.

According to the Lanchester-Prandtl theory, for wings having an elliptical lift distribution

$$\alpha_i = w_i/V = C_L/\pi A \quad \text{rad}$$

$$D_i = L^2/\pi b^2 q \quad \text{and} \quad C_{Di} = D_i/qS = C_L^2/\pi A$$

where b = span of wing and $A = b^2/S$ = aspect ratio of wing. These results also apply fairly well to wings not differing much from the elliptical shape. For **square tips**, correction factors are required:

$$\left. \begin{aligned} \alpha_i &= \frac{C_L}{\pi A} (1 + \tau) \quad \text{where } \tau = 0.05 + 0.02A \\ C_{Di} &= \frac{C_L^2}{\pi A} (1 + \sigma) \quad \text{where } \sigma = 0.01A - 0.01 \end{aligned} \right\} \text{for } A < 12$$

These formulas are the basis for transforming the characteristics of rectangular wings from an aspect ratio A_1 to an aspect ratio A_2 :

$$\alpha_2 = \alpha_1 + \frac{57.3C_L}{\pi} \left(\frac{1 + \tau_2}{A_2} - \frac{1 + \tau_1}{A_1} \right) \quad \text{deg}$$

$$C_{D2} = C_{D1} + \frac{C_L^2}{\pi} \left(\frac{1 + \sigma_2}{A_2} - \frac{1 + \sigma_1}{A_1} \right)$$

For elliptical wings the values of τ and σ are zero. Most wing-section data are given in terms of aspect ratios 6 and ∞ . For other values, the preceding formulas must be used.

Characteristics of Airfoils Airfoil characteristics are expressed in terms of the dimensionless coefficients C_L , C_D , and C_M and the angle of attack α . The NACA presents the results for wings of aspect ratio 6 and also corrected to aspect ratio ∞ (see Fig. 11.4.10).

The lift coefficient C_L is a linear function of the angle of attack up to a critical angle called the **stalling angle** (Fig. 11.4.7). The **maximum lift coefficient** C_{Lmax} which can be reached is one of the important characteristics of a wing because it determines the landing speed of the airplane.

The **drag of a wing** is made up of two components: the **profile drag** D_0 and the **induced drag** D_i . The profile drag is due principally to surface friction. At aspect ratio ∞ or at zero lift the induced drag is zero, and thus the entire drag is profile drag. In Fig. 11.4.8 the coefficient of induced drag $C_{Di} = C_L^2/\pi A$ is also plotted. The difference $C_D - C_{Di} = C_{D0}$, the profile-drag coefficient. Among the desirable characteristics of

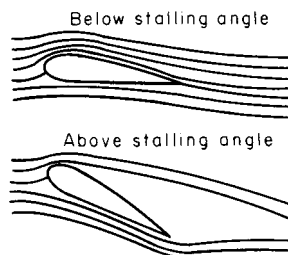


Fig. 11.4.7 Stalling angle of an airfoil.

an airfoil is a small value of the minimum profile-drag coefficient and a large value of C_L/C_D .

The moment characteristics of a wing are obtainable from the curve of the center of pressure as a function of α or by the **moment coefficient taken about the aerodynamic center** $C_{M.a.c.}$ as a function of C_L . A forward motion of the c.p. as α is increased corresponds to an unstable wing section. This instability is undesirable because it requires a large down-load on the tail to counteract it.

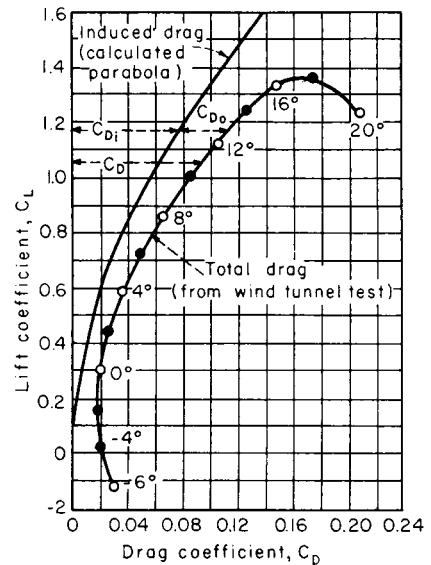


Fig. 11.4.8 Polar-diagram plot of airfoil data.

The characteristics of a wing section (Fig. 11.4.9) are determined principally by its **mean camber line**, i.e., the curvature of the median line of the profile, and secondly by the thickness distribution along the chord. In the NACA system of designation, when a four-digit number is used such as 2412, the significance is always first digit = maximum camber in percent of chord, second digit = location of position of maximum camber in tenths of chord measured from the leading edge (that is, 4 stands for 40 percent), and the last two figures indicate the maximum thickness in percent of chord. The NACA five-digit system is explained in *NACA-TR 610*.

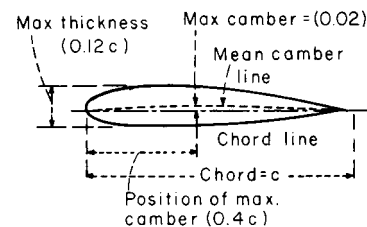


Fig. 11.4.9 Characteristics of a wing section.

Selection of Wing Section

In selecting a wing section for a particular airplane the following factors are generally considered:

1. Maximum lift coefficient C_{Lmax}
2. Minimum drag coefficient C_{Dmin}
3. Moment coefficient at zero lift C_{m0}
4. Maximum value of the ratio C_L/C_D

For certain special cases it is necessary to consider one or more factors from the following group:

5. Value of C_L for maximum C_L/C_D
6. Value of C_L for minimum profile drag

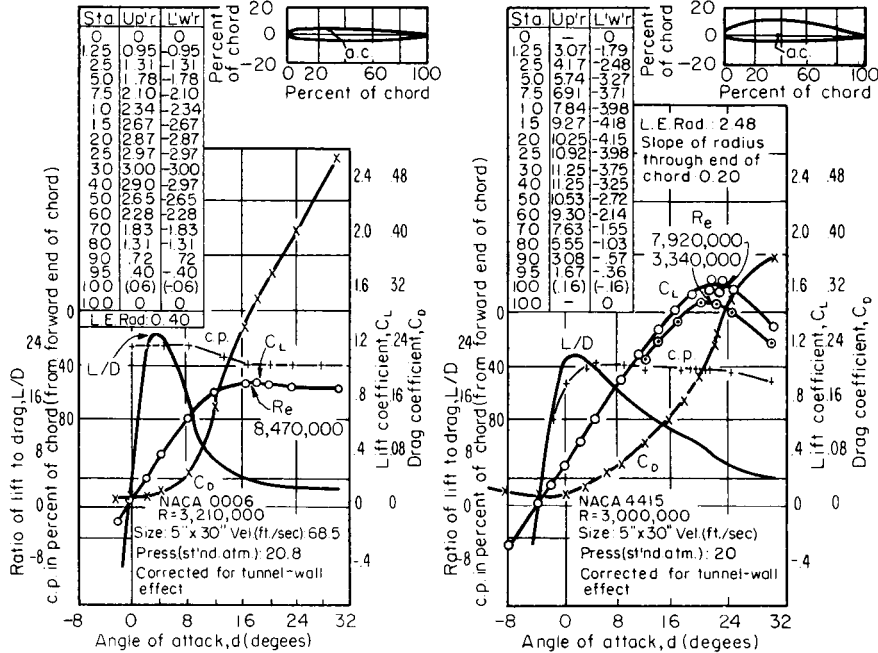


Fig. 11.4.10 Properties of an airfoil section.

7. Maximum value of $C_L^{3/2}/C_D$
 8. Maximum value of $C_L^{1/2}/C_D$
 9. Type of lift curve peak (stall characteristics)
 10. Drag divergence Mach number M_{DD}
- Characteristics of airfoil sections are given in *NACA-TR 586, 647, 669, 708, and 824*. Figure 11.4.10 gives data on two typical sections: 0006 is often used for tail surfaces, and 4415 is especially suitable for the wings of subsonic airplanes. For Mach numbers greater than 0.6 thin wings must be used.

The dimensionless coefficients C_L and C_D are functions of the **Reynolds number** $Re = \rho V l / \mu$. For wings, the characteristic length l is taken to be the chord. In standard air at sea level

$$Re = 6,378 V_{ft/s} \cdot l_{ft} = 9,354 V_{mi/h} \cdot l_{ft}$$

For other heights, multiply by the coefficient $K = (\rho/\mu)/(\rho_0/\mu_0)$. Values of K are as follows:

Altitude, ft*	0	5,000	10,000	15,000	20,000	25,000	30,000	40,000	50,000	60,000
K	1.000	0.884	0.779	0.683	0.595	0.515	0.443	0.300	0.186	0.116

* × 0.305 = m.

The variation of C_L and C_D with the Reynolds number is known as **scale effect**. These are shown in Figs. 11.4.11 and 11.4.12 for some typical airfoils. Figure 11.4.12 shows in dashed lines also the theoretical

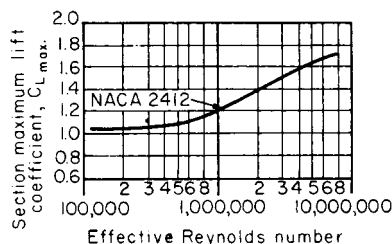


Fig. 11.4.11 Scale effect on section maximum lift coefficient.

variation of the drag coefficient for a smooth flat plate for laminar and turbulent flow, respectively, and also for the transition region.

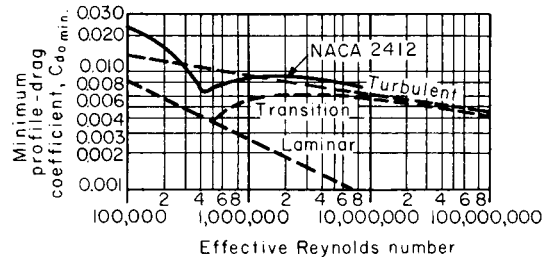


Fig. 11.4.12 Scale effect on minimum profile-drag coefficient.

In addition to the Reynolds number, airfoil characteristics also depend upon the **Mach number** (see "Supersonic and Hypersonic Aerodynamics" below).

Laminar-flow Wings NACA developed a series of **low-drag wings** in which the distribution of thickness along the chord is so selected as to maintain **laminar flow** over as much of the wing surface as possible.

The low-drag wing under controlled conditions of surface smoothness may have drag coefficients about 30 percent lower than those obtained on normal conventional wings. Low-drag airfoils are so sensitive to roughness in any form that the full advantage of laminar flow is unobtainable.

Transonic Airfoils At airplane Mach numbers of about $M = 0.75$, normal airfoil sections begin to show a greater drag, which increases sharply as the speed of sound is approached. Airfoil sections known as **transonic airfoils** have been developed which significantly delay this **drag rise** to Mach numbers of 0.9 or greater (Fig. 11.4.13). Advantage

11-64 AERONAUTICS

may also be taken of these airfoil sections by increasing the thickness of the airfoil at a given Mach number without suffering an increase in drag.

Wing sweepback (Fig. 11.4.14) or sweepforward also delays the onset of the drag rise to higher Mach numbers. The flow component normal to the wing leading edge, $M \cos \Gamma$, determines the effective Mach number felt by the wing. The parallel component, $M \sin \Gamma$, does not significantly influence the drag rise. Therefore for a flight Mach number M , the wing senses it is operating at a lower Mach number given by $M \cos \Gamma$.

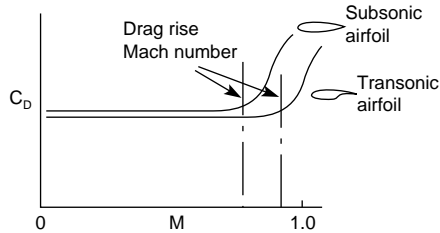


Fig. 11.4.13 Drag rise delay due to transonic section.

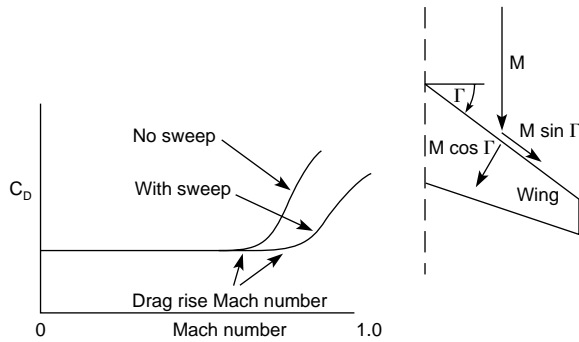


Fig. 11.4.14 Influence of wing sweepback on drag rise Mach number.

Flaps and Slots

The maximum lift of a wing can be increased by the use of **slots** on the leading edge or **flaps** on the trailing edge. **Fixed slots** are formed by rigidly attaching a curved sheet of metal or a small auxiliary airfoil to the leading edge of the wing. The trailing-edge flap is used to give increased lift at moderate angles of attack and to increase C_{Lmax} . Theoretical analyses of the effects are given in *NACA-TR 938* and *Br. ARC-R&M 1095*. Flight experience indicates that the four types shown in Fig. 11.4.15 have special advantages over other known types. Values of C_{Lmax} for these types are shown in Table 11.4.2. All flaps cause a diving

Table 11.4.2 Flaps*

Type of flap	Section C_{Lmax} (approx)	Finite wing C_{Lmax} (approx)	Remarks
Plain	2.4	1.9	$C_{p/c} = 0.20$. Sensitive to leakage between flap and wing.
Split	2.6	2.0	$C_{p/c} = 0.20$. Simplest type of flap.
Single slotted	2.8 3.0	2.2 2.4	$C_{p/c} = 0.25$. Shape of slot and location of deflected flap are critical.
Double slotted	3.0 3.4	2.4 2.7	$C_{p/c} = 0.25$. Shape of slot and location of deflected flap are critical.

* The data is for wing thickness $t/c = 0.12$ or 0.15 . Lift increment is dependent on the leading-edge radius of the wing.

moment ($-C_m$) which must be trimmed out by a download on the tail, and this download reduces C_{Lmax} . The correction is $\Delta C_{Lmax}(\text{trim}) = \Delta C_{mo}(l/c)$, where l/c is the tail length in mean chords.

Boundary-Layer Control (BLC) This includes numerous schemes for (1) maintaining laminar flow in the boundary layer in the flow over a

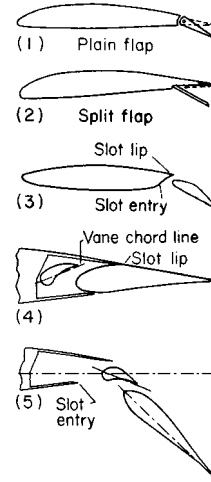


Fig. 11.4.15 Trailing-edge flaps: (1) plain flap; (2) split flap; (3) single-slotted flap; (4) double-slotted flap (retracted); (5) double-slotted flap (extended).

wing or (2) preventing flow separation. Schemes in the first category try to obtain the lower frictional drag of laminar flow either by providing favorable pressure gradients, as in the NACA "low-drag" wings, or by removing part of the boundary layer. The boundary-layer thickness can be partially controlled by the use of suction applied either to spanwise slots or to porous areas. The flow so obtained approximates the laminar skin-friction drag coefficients (see Fig. 11.4.12). Schemes in the second category try to delay or improve the stall. Examples are the leading-edge slot, slotted flaps, and various forms of suction or blowing applied through transverse slots. The slotted flap is a highly effective form of boundary-layer control that delays flow separation on the flap.

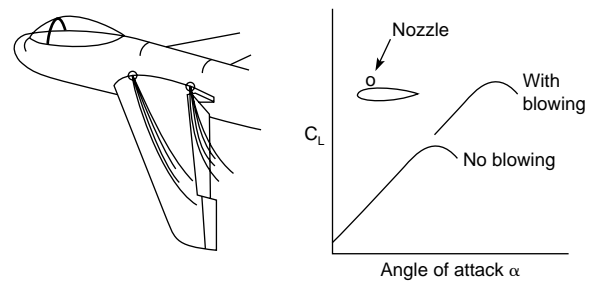


Fig. 11.4.16 Influence of spanwise blowing.

Spanwise Blowing Another technique for increasing the lift from an aerodynamic surface is spanwise blowing. A high-velocity jet of air is blown out along the wing. The location of the jet may be parallel to and near the leading edge of the wing to prevent or delay leading-edge flow separation, or it may be slightly behind the juncture of the trailing-edge flap to increase the lift of the flap. Power for spanwise blowing is sensitive to vehicle configuration and works most efficiently on swept wings. Other applications of this technique may include local blowing on ailerons or empennage surfaces (Fig. 11.4.16).

The **pressure distributions** on a typical airfoil are shown in Fig. 11.4.17. In this figure the ratio p/q is given as a function of distance along the chord. In Fig. 11.4.18 the effect of addition of an external airfoil flap is shown.

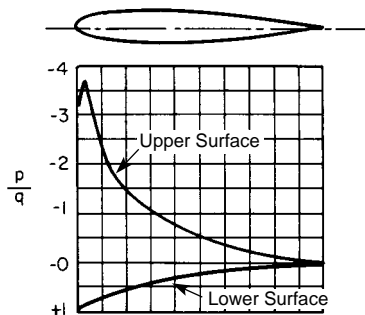


Fig. 11.4.17 Pressure distribution over a typical airfoil.

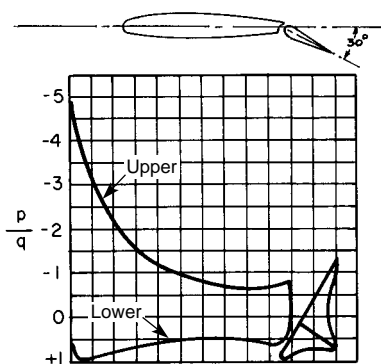


Fig. 11.4.18 Pressure distribution on an airfoil-flap combination.

Airplane Performance

In horizontal flight the lift of the wings must be equal to the weight of the airplane, or $L = W$, where W is the gross weight, lb (kg). This equation determines the minimum horizontal speed of an airplane since

$$W = C_{Lmax} \frac{1}{2} \rho V_{min}^2 S \quad \text{or} \quad V_{min} = \sqrt{2W/C_{Lmax} \rho S}$$

This corresponds to the **landing speed** without power, or the **stalling speed**.

In uniform horizontal flight the propeller thrust T must be exactly equal to the drag of the airplane, or $T = D$. Then $TV =$ power available from the propeller and $DV =$ power required for overcoming the drag of the airplane; for horizontal flight $TV = DV$. If the airplane climbs at a rate dh/dt , where $h =$ height, then an additional power $= W(dh/dt)$ is required to increase the potential energy of the airplane. The equilibrium condition becomes

$$TV = DV + W(dh/dt)$$

If the **thrust power available** P_{Ta} is measured in hp, D and W in lb, and V and dh/dt in ft/s,

$$P_{Ta} = \frac{1}{550} DV + \frac{1}{550} W(dh/dt) \quad (11.4.1)$$

The thrust horsepower available $P_{Ta} = \eta P_a$, where $P_a =$ **available engine horsepower** and η is the propeller efficiency. P_{Ta} is determined as a function of V from the engine and propeller characteristics. The **thrust horsepower required** to overcome the drag D is $P_{Tr} = DV/550$. The drag is the sum of the wing-profile drag D_0 , the wing induced drag D_i , and the parasite drag of the other airplane parts D_p . D_0 can be obtained from wing-profile tests corrected to full-scale Reynolds number, D_i from the induced drag formula $D_i = L^2/\pi q b^2$, and D_p by summation of the parasite drag components due to fuselage, tail surfaces, landing gear, etc.

From Eq. (11.4.1) the performance of an airplane can be obtained either graphically or analytically. In the graphical determination the curves of power available and power required are plotted for a fixed

altitude (Fig. 11.4.19). If $P_{Ta} > P_{Tr}$, the excess horsepower can be used either for horizontal acceleration to a higher speed or for climbing. The maximum speed V_{max} occurs when $P_{Ta} = P_{Tr}$. The rate of climb is determined by the equation $dh/dt = 550(P_{Ta} - P_{Tr})/W$. To calculate the

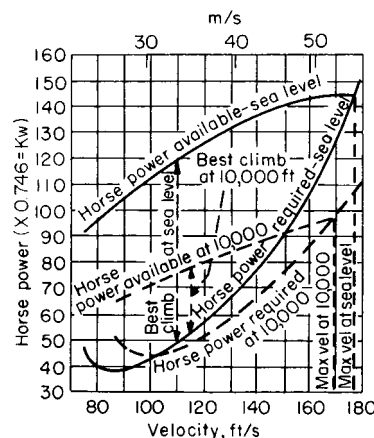


Fig. 11.4.19 Construction for determining airplane performance.

maximum velocity and rate of climb for another altitude, another set of curves of P_{Ta} and P_{Tr} versus V is constructed. At any altitude at which the air density is ρ and for a given angle of attack (corresponding to an unchanged lift/drag ratio), $L/D = L_0/D_0$. As the lift is equal to the weight, $L = L_0 = W$, therefore $D = D_0$ and

$$P_{Tr}/P_{Tr0} = VD/V_0 D_0 = V/V_0$$

But $C_L = C_{L0}$ and $C_L \cdot \frac{1}{2} \rho V^2 S = C_{L0} \frac{1}{2} \rho_0 V_0^2 S$. Therefore $V/V_0 = \sqrt{\rho_0/\rho}$. From this relation, new curves of P_{Tr} versus V may be constructed for various altitudes by **multiplying** both the ordinates and abscissas of the original curve by $\sqrt{\rho_0/\rho}$.

Figure 11.4.19 shows a performance chart for a 2,100-lb airplane. The maximum velocity at 10,000 ft altitude is 168.5 ft/s. At sea level $(P_{Ta} - P_{Tr})_{max} = 71$ and the rate of climb is $71 \times 33,000/2,100 = 1,120$ ft/min. At 10,000 ft altitude the rate is $30 \times 33,000/2,100 = 470$ ft/min.

When the curves of power required and power available become tangent to each other, there is only one speed at which the airplane can fly level and the rate of climb is zero. The corresponding altitude is the **absolute ceiling** H . It can be determined from the curve of maximum rate of climb as a function of altitude when this is approximated by a straight

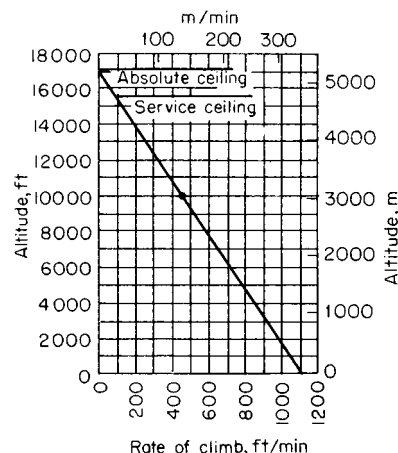


Fig. 11.4.20 Characteristic rate-of-climb curves.

11-66 AERONAUTICS

line (Fig. 11.4.20). The **service ceiling** h_s is defined as the altitude at which the rate of climb is 100 ft/min. For a linear decrease of rate of climb the following approximations hold:

$$\text{Absolute ceiling: } H = r_0 h / (r_0 - r)$$

where r_0 is the rate of climb at sea level and r is the rate of climb at altitude h .

$$\text{Service ceiling: } h_s = H(r_0 - 100)/r_0$$

Altitude climbed in t min,

$$h = H(1 - e^{-kt})$$

where $k = -r_0/H$.

Time to climb to altitude h ,

$$t = 2.303 \frac{H}{r_0} \log \frac{H}{H-h}$$

The maximum distance that an airplane can fly is called its **range**, and the length of time that it can remain flying, its **endurance**. If W_0 is the weight in pounds fully loaded and W_1 the weight after having consumed its fuel at the rate of C lb/(bhp · h), then for propeller-driven aircraft,

$$\text{Range} = 863.5 \frac{\eta}{C} \cdot \frac{L}{D} \cdot \log \frac{W_0}{W_1} \quad \text{mi}$$

$$\text{Endurance} = 750 \frac{\sqrt{W}}{V_c} \cdot \frac{\eta}{C} \cdot \frac{L}{D} \left(\frac{1}{\sqrt{W_1}} - \frac{1}{\sqrt{W_0}} \right) \quad \text{hours}$$

where η is the average propulsive efficiency and $L/D = C_L/C_D$ is the ratio of lift to drag. V_c is the cruising speed, mi/h, at any gross weight W , lb. See Table 11.4.3 for dimensions and performance of selected airplanes.

Power Available The maximum efficiency η_m and the diameter of a propeller to absorb a given power at a given speed and rpm are found from a propeller-performance curve. The thrust horsepower at maximum speed P_{Tm} is found from $P_{Tm} = \eta_m P_m$. The **thrust horsepower at any speed** can be approximately determined from the ratios given in the following table:

V/V_{\max}	0.20	0.30	0.40	0.50	0.60	0.70	0.80	0.90	1.00	1.10	
P_T/P_{Tm}	Fixed-pitch propeller	0.29	0.44	0.57	0.68	0.77	0.84	0.90	0.96	1.00	1.03
	constant-rpm propeller	0.47	0.62	0.74	0.82	0.88	0.93	0.97	0.99	1.00	1.00

The **brake horsepower** of an engine decreases with increase of altitude. The variation of P_T with altitude depends on engine and propeller characteristics with average values as follows:

h , ft	0	5,000	10,000	15,000	20,000	25,000
P_T/P_{T0} (fixed pitch)	1.00	0.82	0.66	0.52	0.41	0.30
P_T/P_{T0} (controllable pitch)	1.00	0.85	0.71	0.59	0.48	0.38

Performance with Jet Thrust In all cases where jet thrust constitutes either a part or all of the power source, it is necessary to use graphical methods, plotting thrust and drag as functions of speed at each altitude to be investigated. The major thrust corrections are those due to losses in (1) the air intake, (2) the ducting system, and (3) the tailpipe. (See Jet Propulsion and Aircraft Propellers.)

An excess thrust T , lb, at a speed V , mi/h, is equivalent to a thrust horsepower $P_T = TV/375$. The corresponding rate of climb is $dh/dt = 33,000P_T/W = 88TV/W$.

For jet-driven aircraft, range and endurance can be determined from

$$\text{Range} = 1.9285 \left(\frac{1}{\sqrt{\rho S}} \right) \cdot \frac{1}{C_i} \cdot \frac{C_L^2}{C_D} \cdot (W_0^{1/2} - W_1^{1/2}) \quad \text{mi}$$

and

$$\text{Endurance} = \frac{1}{C_i} \cdot \frac{C_L}{C_D} \cdot \log \left(\frac{W_0}{W_1} \right) \quad \text{hours}$$

where C_i is fuel consumption in lb/(lb thrust) · hour, S is wing area in ft², and ρ is the air density in slugs/ft³.

Parasite Drag

The drag of the nonlifting parts of an airplane is called the **parasite drag**. It consists of two components: the frictional and the eddy-making drag.

Frictional drag, or skin friction, is due to the viscosity of the fluid. It is the force produced by the viscous shear in the layers of fluid immediately adjacent to the body. It is always proportional to the wetted area, i.e., the total surface exposed to the air.

Eddy-making drag, sometimes called form drag, is due to the disturbance or wake created by the body. It is a function of the shape of the body.

The total drag of a body may be composed of the two components in any proportion, varying from almost pure skin friction for a plate edge-wise or a good streamline form to 100 percent form drag for a flat plate normal to the wind. A **streamline form** is a shape having very low form drag. Such a form creates little disturbance in moving through a fluid.

When air flows past a surface, the layer immediately adjacent to the surface adheres to it, or the tangential velocity at the surface is zero. In the transition region near the surface, which is called the **boundary layer**, the velocity increases from zero to the velocity of the stream. When the flow in the boundary layer proceeds as if it were made up of laminae sliding smoothly over each other, it is called a **laminar boundary layer**. If there are also irregular motions in the layers normal to the surface, it is a **turbulent boundary layer**. Under normal conditions the flow is laminar at low Reynolds numbers and turbulent at high Re with a transition range of values of Re extending between 5×10^5 and 5×10^7 . The profile-drag coefficients corresponding to these conditions are shown in Fig. 11.4.12.

For laminar flow the friction-drag coefficient is practically independent of surface roughness and for a flat plate is given by the Blasius equation,

$$C_{DF} = 2.656/\sqrt{\text{Re}}$$

The turbulent boundary layer is thicker and produces a greater frictional drag. For a smooth flat plate with a turbulent boundary layer

$$C_{DF} = 0.91/\log \text{Re}^{2.58}$$

For rough surfaces the drag coefficients are increased (see von Kármán, *Jour. Aeronaut. Sci.*, **1**, no. 1, 1934). The drag coefficients as given above are based on **projected area** of a double-surfaced plane. If **wetted area** is used, the coefficients must be divided by 2. The frictional drag is $D_F = C_{DF} qS$, where S is the **projected area**, or $D_F = \frac{1}{2} C_{DF} qA$, where A is the wetted area.

Values of C_{DF} for double-surfaced planes may be estimated from the following tabulation:

Laminar flow (Blasius equation):

Re	10	10 ²	10 ³	10 ⁴	10 ⁵	10 ⁶
C_{DF}	0.838	0.265	0.0838	0.0265	0.0084	0.0265

Turbulent flow:

Re	10 ⁵	10 ⁶	10 ⁷	10 ⁸	10 ⁹	10 ¹⁰
C_{DF}	0.0148	0.0089	0.0060	0.0043	0.00315	0.0024

These are double-surface values which facilitate direct comparison with wing-drag coefficients based on projected area. For calculations involving wetted area, use one-half of double-surface coefficients. In-

Table 11.4.3 Principal Dimensions and Performance of Typical Airplanes*

	Aero Commander	BAC	Beech	Bell	Boeing	Boeing	Lockheed	Douglas	McDonnell Douglas	Piper	Sikorsky
Designation model no.	680 F-P	One-Eleven	Bonanza S35	Ranger 47J2-A	747-200B	727	1011-1	DC-8 Series 5D	DC-10-10	Super Cub Pa 18-150	S-58
Type	Executive transport	Jet transport	Business plane	Executive helicopter	Passenger	Jet transport	Passenger	Jet transport	Passenger	Utility plane	Helicopter
No. passengers	5-7	63	4-6	4	374-500	70-114	256-400	116-176	255-380	2	12-18
Cargo capacity, lb	2,815	N.A.	270	1,120		8,550		20,850		50	
Span, ft	49.5	83.5	33.4	37.0†	195.6	108.6	155.3	142.3	155.3	35.3	56.0†
Overall length, ft	35.1	92.1	26.4	43.3	231.3	134.3	178.6	150.5	181.4	22.5	65.8
Overall height, ft	14.5	23.8	6.5	9.3	63.4	34.0	55.3	42.3	58	6.7	14.3
Wing area, ft ²	255	980	181	Rotor	5,500	1,650	3,456	2,868	3,861	178.5	Rotor
Weight empty, lb‡	5,185	58,000	1,885	1,730	361,216	86,000	234,275	124,529	231,779	930	7,900
Weight gross, lb	8,000	73,800	3,300	2,850	775,000	142,000	430,000	310,000	430,000	1,750	13,000
Power plant	(2) Lyc IGSO-540B1A	(2) RR Spey 2	Con IO-520-B	Lyc VO540	JT9D-3, -7	(3) PW JT8D-1	RB-211-22B	(4) PW JT3D-3	CF6-6D	Lyc O-320	WR R1820
High speed, knots	252	469	184	91	528	539	530	521	530	113	106
Cruise speed, knots	220	441	178	81	478	513	473	472	473	100	84
Landing speed, knots	91	N.A.	54	0	140	121	125	133	138	37	0
Range, nautical miles	1,310	1,700	1,145	260	5,748	2,320	2,500	8,600	2,110	460	247

* ft × 0.305 = m; ft² × 0.0929 = m²; lb m × 0.454 = kg.
 † Rotor diameter.
 ‡ Operating weight empty (includes trapped oil).
 N.A. Not available.

terpolations in the foregoing tables must allow for the logarithmic functions; i.e., the variation in C_{DF} is not linear with Re.

Drag Coefficients of Various Bodies

For **bodies with sharp edges** the drag coefficients are almost independent of the Reynolds number, for most of the resistance is due to the difference in pressure on the front and rear surfaces. Table 11.4.4 gives $C_D = D/qS$, where S is the maximum cross section perpendicular to the wind.

For **rounded bodies** such as spheres, cylinders, and ellipsoids the drag coefficient depends markedly upon the Reynolds number, the surface roughness, and the degree of turbulence in the airstream. A sphere and a cylinder, for instance, experience a sudden reduction in C_D as the Reynolds number exceeds a certain critical value. The reason is that at low speeds (small Re) the flow in the boundary layer adjacent to the body is laminar and the flow separates at about 83° from the front (Fig. 11.4.21). A wide wake thus gives a large drag. At higher speeds (large Re) the boundary layer becomes turbulent, gets additional energy from the outside flow, and does not separate on the front side of the sphere. The drag coefficient is reduced from about 0.47 to about 0.08 at a critical Reynolds number of about 400,000 in free air. Turbulence in the airstream reduces the value of the critical Reynolds number (Fig. 11.4.22). The Reynolds number at which the sphere drag $C_D = 0.3$ is

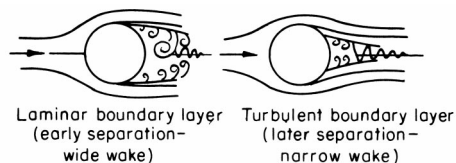


Fig. 11.4.21 Boundary layer of a sphere.

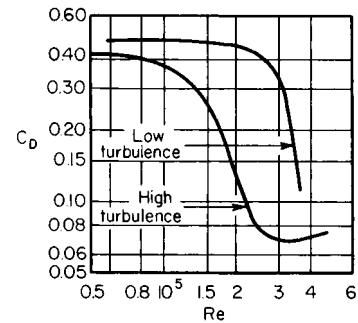


Fig. 11.4.22 Drag coefficients of a sphere as a function of Reynolds number and of turbulence.

taken as a criterion of the amount of turbulence in the airstream of wind tunnels.

Cylinders The drag coefficient of a cylinder with its axis normal to the wind is given as a function of Reynolds number in Fig. 11.4.23. Cylinder drag is sensitive to both Reynolds and Mach number. Figure 11.4.23 gives the Reynolds number effect for $M = 0.35$. The increase in C_D because of Mach number is approximately:

M	0.35	0.4	0.6	0.8	1.0
C_D increase, percent	0	2	20	50	70

(See NACA-TN 2960.)

Streamline Forms The drag of a streamline body of revolution depends to a very marked extent on the Reynolds number. The difference between extreme types at a given Reynolds number is of the same

Table 11.4.4 Drag Coefficients

Object	Proportions	Attitude	C_D
Rectangular plate, sides a and b	1		1.16
	4		1.17
	$\frac{a}{b} = 12.5$		1.23
	8		1.34
	25		1.57
	50		1.76
∞	2.00		
Two disks, spaced a distance l apart	1		0.93
	1.5		0.78
	$\frac{l}{d} = 2$		1.04
Cylinder	1		1.52
	2		0.91
	$\frac{l}{d} = 4$		0.85
	7		0.87
Circular disk		1.11	
		0.41	
Hemispherical cup, open back		1.35	
Hemispherical cup, open front, parachute		0.41	
		1.35	
Cone, closed base		$\alpha = 60^\circ, 0.51$	
		$\alpha = 30^\circ, 0.34$	

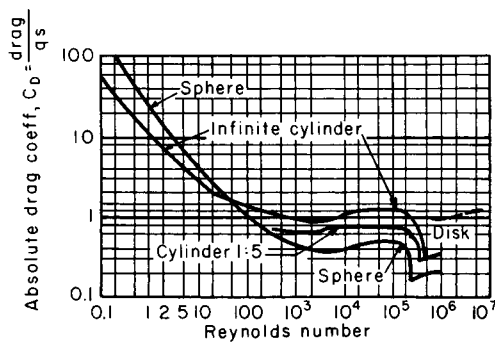


Fig. 11.4.23 Drag coefficients of cylinders and spheres.

order as the change in C_D for a given form for values of Re from 10^6 to 10^7 .

Tests reported in *NACA-TN 614* indicate that the shape for minimum drag should have a fairly sharp nose and tail. At $Re = 6.6 \times 10^6$ the best forms for a fineness ratio (ratio of length to diameter) 5 have a drag

$$D = 0.040qA = 0.0175qV^{2/3}$$

where A = max cross-sectional area and V = volume. This value is equivalent to about 1.0 lb/ft² at 100 mi/h. For $Re > 5 \times 10^6$, the drag coefficients vary approximately as $Re^{0.15}$.

Minimum drag on the basis of cross-sectional or frontal area is obtained with a fineness ratio of the order of 2 to 3. Minimum drag on the

basis of contained volume is obtained with a fineness ratio of the order of 4 to 6 (see *NACA-TR 291*).

The following table gives the ordinates for good streamline shapes: the Navy strut, a two-dimensional shape; and the Class C airships, a three-dimensional shape. Streamline shapes for high Mach numbers have a high fineness ratio.

Percent length of max ordinate	Navy strut	2.50	4.00	7.50	10.0	12.50
Class C airship	26	37.1	52.50	63.00	72.0	78.50

Percent length of max ordinate	Navy strut	40	60	80	90
Class C airship	91.1	99.5	86.1	56.2	33.8

Test data on the *RM-10* shape are given in *NACA-TR 1160*. This shape is a parabolic-arc type for which the coordinates are given by the equation $r_x = X/7.5(1.0 - X/L)$.

Struts Drag coefficients for streamline struts are given in the form

$$C_D = D/qS_f = D/qdl$$

where S_f is the projected frontal area; d is the thickness, ft; and l is the length, ft. The variation of C_D with Re for a Navy No. 1 strut of fineness ratio 3 is as follows:

$Re \times 10^{-5}$	0.75	1.0	1.25	1.5	2.0	3.0	4.0
C_D	0.114	0.102	0.093	0.088	0.085	0.077	0.073

Wing-Profile Drag For accurate basic values of profile drag it is necessary to refer to test data on the wing section employed. In the absence of test data, the following approximate values may be used:

Average t/c	0.10	0.12	0.14	0.16
Basic $\left\{ \begin{array}{l} C_{D0} \\ D_0/S \end{array} \right.$	0.0058	0.0060	0.0063	0.0067
Best wing $\left\{ \begin{array}{l} C_{D0} \\ D_0/S \end{array} \right.$	0.0078	0.0080	0.0083	0.0087
Average roughness $\left\{ \begin{array}{l} C_{D0} \\ D_0/S \end{array} \right.$	0.0098	0.0100	0.0103	0.0107
	0.25	0.256	0.264	0.274

The "basic" values are for a perfectly smooth wing of infinite aspect ratio, "best wing" values are for smooth full flush-riveted construction, and "average-roughness" values are for flush-riveted leading-edge with brazier head rivets back of the 20 percent chord point. C_{D0} is the profile-drag coefficient ($D_0 = C_{D0}qS$). The values of D_0/S are drags in lb/ft² of projected wing area at 100 mi/h in standard air ($q_0 = 25.58$ lb/ft²). t/c is the maximum wing thickness as a fraction of the chord.

Faired values of NACA data on **symmetrical sections** at $Re = 8 \times 10^6$ give the variation of minimum C_{D0} and C_{DA} with thickness as follows:

NACA section	0006	0009	0012	0015	0018	0021	0025	0030	0035
Min C_{D0}	0.0051	0.0056	0.0061	0.0067	0.0073	0.0080	0.0089	0.0103	0.0120
C_{DA} (see below)	0.085	0.062	0.050	0.045	0.041	0.038	0.036	0.034	0.034

NOTE: C_{DA} is the drag coefficient based on the frontal area. The 00 section is also suitable for use in struts or fairings. (See NACA-TR 628, 647, 669, 708.)

Drag of Tail Surfaces Owing to joints, control balances, and interference effects, the drag of a control surface is much higher than that of the basic section. The average value is about 0.40 lb/ft² at 100 mi/h in standard density.

Streamline Wire The drag coefficient of a standard streamline wire of lenticular or elliptical cross section is given as a function of Reynolds number in Fig. 11.4.24.

The drag coefficients of **wires and cables** are also shown in Fig. 11.4.24.

Elliptic Cylinders

Fineness ratio	C_D when Re is			
	3×10^4	6×10^4	1×10^5	2×10^5
1:1	1.20	1.22	1.22	1.23
2:1	0.62	0.57	0.46	0.35
4:1	0.32	0.32	0.30	0.24
8:1	0.27	0.23	0.22	0.21

The above data are for $M < 0.4$. For additional data see NACA-TR 619.

C_L and C_D for **inclined wires** are as follows:

Angle of attack, deg	0	15	30	45	60	75	90
C_L	0	0.09	0.25	0.39	0.42	0.27	0
C_D	0.01	0.05	0.17	0.46	0.77	1.01	1.12

C_L and C_D are based on the area $S = LD$, where L is the length and D the diam, ft.

(Additional data on prismatic cylinders are given in NACA-TR 619 and NACA-TN 3038.)

Engine Drag, Nacelle Drag The drag of an uncowlled air-cooled engine is approximately $D = 0.050d^2(V/100)^2$, where d is the overall diameter of the engine, in, and V is the speed, mi/h. The average drag

in pounds at 100 mi/h for a fixed-slot NACA-type cowl is as follows:

Engine diam, in	40	44	48	52	56
Drag, lb at 100 mi/h	28	34	40	47	54

If adjustable **cowl flaps** or controlled airflow is used, the engine drag need not vary as the square of the speed; it may remain substantially constant. Theoretically, it is possible to cool an engine by forced cooling at an expenditure of about 2 percent of the engine power.

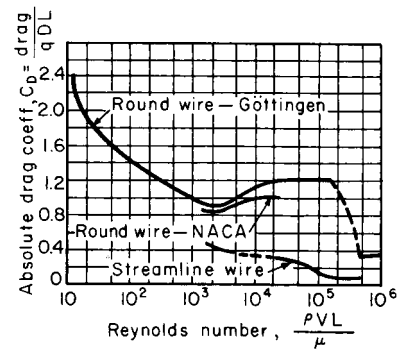


Fig. 11.4.24 Drag coefficients of wires.

The average drag coefficient of a nacelle is $C_D = 0.20$, based on frontal area. This is equivalent to about 5.0 lb/ft² at 100 mi/h. A very clean form may be as low as 3 lb/ft² at 100 mi/h. The drag of a pure streamline form would be of the order of 1 lb/ft² at 100 mi/h (see NACA-TR 313, 314, and 415).

Fuselage Drag Owing to various projections and irregularities in the surface, the drag of an average airplane fuselage is considerably greater than the drag of a pure streamline form. Since the increase is due in effect to a substantially constant drag increment, the drag per unit of cross-sectional area tends to decrease with increase in the size of the fuselage. At 100 mi/h the drag in lb/ft² will be approximately as follows:

A, ft ²	10	15	20	40	60
D/A , average	5.5	4.5	4.0	3.3	3.0
D/A , lower limit	4.0	3.3	3.0	2.4	2.3

Cockpit enclosures if properly designed and blended into fuselage lines, do not appreciably increase the fuselage drag coefficient. Sharp junctures must be avoided. The best fairing radius is approximately 25 percent of the enclosure height. Length of tail fairing should be $4 \times$ height (see NACA-TR 730).

Seaplane Floats, Flying-Boat Hulls The drag of a seaplane float is between 3 and 6 lb/ft² at 100 mi/h, depending on the lines. The step accounts for 5 to 10 percent of the drag.

The drag of a flying-boat hull is comparable to, but slightly higher than, the drag of a fuselage of the same cross-sectional area. Average values at 100 mi/h are as follows:

A, ft ²	40	60	80	100
D/A , lb/ft ²	4.5	4.3	4.1	4.0

11-70 AERONAUTICS

Wire Mesh Measurements on square pieces of exposed wire mesh have given the following results:

Percent area blocked	100	80	60	50	40	30	20
Percent flat plate, C_D	100	92	77	60	43	26	10

The pressure drop through a screen in a tube is given by

$$\Delta p = C_D q = \frac{1}{2} C_D \rho V^2$$

where C_D is a function of the percent area blocked as follows:

Percent area blocked	20	30	40	50	60	70
C_D	0.20	0.45	0.90	1.60	3.40	7.20

(See Br. ARC-R&M 1469.)

Interference Drag The total drag of two objects in close proximity is generally greater than the sum of the individual free-flow drags. The increase (or decrease) is known as interference drag. It is especially important where the wing is one component and the fuselage or a nacelle the other component. In this case it may be reduced to a minimum by an appropriate fairing or "fillet" in the path of the expanding flow (see NACA-TN 460).

The interference drag of two parallel streamline struts is as follows:

Spacing/thickness	5	4	3	2	1.5	1.25
D/D_0	1.00	1.06	1.12	1.25	2.25	2.87

The interference drag of a strut intersection with a flat surface is a function of the intersection angle θ . The drag increase, expressed as an equivalent length increase ΔL in diameters, is as follows:

θ , deg	90	70	60	50	40	30	20
ΔL	0	1.5	2.5	4.0	6.0	9.5	14.0

Nonintrusive flow field measurements about airfoils can be made by laser Doppler velocimeter (LDV) techniques. A typical LDV measurement system setup is shown in Fig. 11.4.25. A seeded airflow generates the necessary reflective particles to permit two-dimensional flow directions and velocities to be accurately recorded.

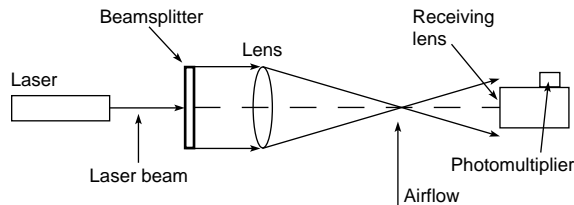


Fig. 11.4.25 Typical laser doppler velocimeter measurement system.

STABILITY AND CONTROL

Control An airplane is controlled in flight by imposing yawing, pitching, and rolling moments by use of rudders, elevators, and ailerons. This is known as the **three-control** system and is in almost universal use, although it is possible to dispense with either the ailerons or the rudders and so obtain a two-control system.

Controllability is separate and distinct from stability in physical significance, but not necessarily so in flight. An airplane may be made automatically stable by gyroscopic or other devices that actuate the controls mechanically; it is inherently stable if, on disturbance from any cause, the aerodynamic forces and moments induced always tend to return the airplane to its original attitude.

Stability may be either static or dynamic. An airplane is **statically stable** if the moments tend to return it to the original attitude. It is

statically stable if the oscillations produced by the static stability are rapidly damped out. If it is **statically unstable**, any departure tends to increase, there being an upsetting moment instead of a restoring moment. If it is **dynamically unstable**, the oscillations due to static stability tend to increase in amplitude with time. Static stability or a condition of stable equilibrium is necessary to obtain dynamic stability, but static stability does not ensure dynamic stability. Too much static stability may cause dynamic instability if damping is inadequate.

The common method of getting **static longitudinal stability** is by means of a tail surface. A wing alone has a lift force L acting at the a.c. and a moment M_0 about the a.c. (Fig. 11.4.26). The moment is measured

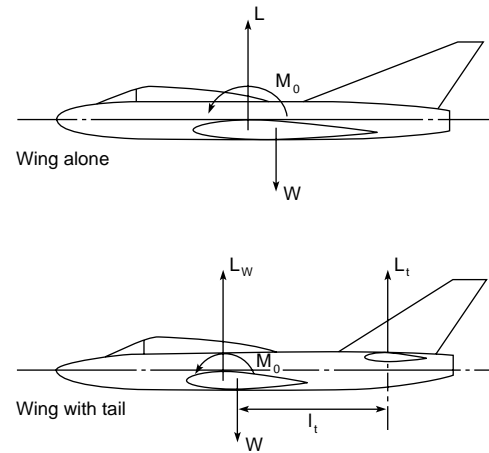


Fig. 11.4.26 Longitudinal stability of an airplane.

positively as airplane nose-up. Most wings alone are "unstable" (positive lift-curve slope), though possessing a small negative moment (diving moment). If there were no other air forces acting, this could be balanced by putting the center of gravity of the airplane behind the a.c. a distance δ such that $W\delta = M_0$. This arrangement would be in equilibrium but would be unstable. Upon a small increase in the angle of attack such as by a gust, the lift force will be increased. This gives a moment tending to increase further the angle of attack. The curve of the moment of the air forces on a wing about the center of gravity thus starts from the value M_0 and becomes positive for larger angles of attack. The curve is shown in Fig. 11.4.27. The positive slope of M versus α thus corresponds to an unstable moment. When a horizontal tail surface is added, a lift force also acts upon the tail. This gives a diving moment

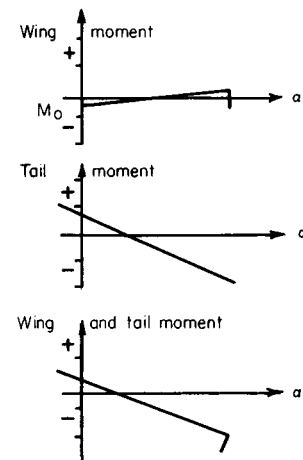


Fig. 11.4.27 Longitudinal stability. Wing and foil moments.

$M_t = -L_t \cdot l_t$. Upon an increase in the angle of attack α , the diving tail moment is increased more rapidly than the stalling moment of the wing. Thus, the combination is stable. The resultant curve of pitching moment against angle of attack has a small negative slope. Too steep a slope would indicate longitudinal stiffness and difficulty in control.

Rolling (or **banking**) does not produce any lateral shift in the center of the lift, so that there is no restoring moment as in pitch. However, when banked, the airplane sideslips toward the low wing. A fin placed above the center of gravity gives a lateral restoring moment that can correct the roll and stop the slip. The same effect can be obtained by **dihedral**, i.e., by raising the wing tips to give a transverse V. An effective dihedral of 1 to 3° on each side is generally required to obtain stability in roll. In low-wing monoplanes, 2° effective dihedral may require 8° or more of geometrical dihedral owing to interference between the wing and fuselage.

In a **yaw** or **slip** the line of action of the lateral force depends on the size of the effective vertical fin area. Insufficient fin surface aft will allow the skid or slip to increase. Too much fin surface aft will swing the nose of the plane around into a tight spiral. Sound design demands sufficient vertical tail surface for adequate directional control and then enough dihedral to provide lateral stability.

When moderate positive effective dihedral is present, the airplane will possess **static lateral stability**, and a low wing will come up automatically with very little yaw. If the dihedral is too great, the airplane may roll considerably in gusts, but there is little danger of the amplitude ever becoming excessive. **Dynamic lateral stability** is not assured by static stability in roll and yaw but requires that these be properly proportioned to the damping in roll and yaw.

Spiral instability is the result of too much fin surface and insufficient dihedral.

HELICOPTERS

REFERENCES: *Br. ARC-R & M* 1111, 1127, 1132, 1157, 1730, and 1859. *NACA-TM* 827, 836, 858. *NACA-TN* 626, 835, 1192, 3323, 3236. *NACA-TR* 434, 515, 905, 1078. *NACA Wartime Reports* L-97, L-101, L-110. NACA, "Conference on Helicopters," May, 1954. Gessow and Myers, "Aerodynamics of the Helicopter," Macmillan.

Helicopters derive lift, propulsion force, and control effect from adjustments in the blade angles of the rotor system. At least two rotors are required, and these may be arranged in any form that permits control over the reaction torque. The common arrangements are main lift rotor; auxiliary torque-control or tail rotor at 90°; two main rotors side by side; two main rotors fore and aft; and two main rotors, coaxial and oppositely rotating.

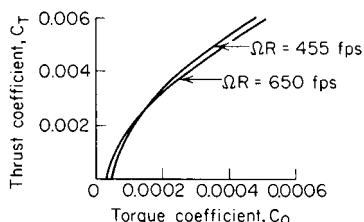


Fig. 11.4.28 Static thrust performance of NACA 8-H-12 blades.

The helicopter rotor is an actuator disk or momentum device that follows the same general laws as a propeller. In calculating the rotor performance, the major variables concerned are diameter D , ft (radius R); tip speed, $V_t = \Omega R$, ft/s; angular velocity of rotor $\Omega = 2\pi n$, rad/s; and rotor solidity q (= ratio of blade area/disk area). The rotor performance is usually stated in terms of coefficients similar to propeller coefficients. The rotor coefficients are:

$$\begin{aligned} \text{Thrust coefficient } C_T &= T/\rho(\Omega R)^2\pi R^2 \\ \text{Torque coefficient } C_Q &= Q/\rho(\Omega R)^2\pi R^3 \\ \text{Torque } Q &= 5,250 \text{ bhp/rpm} \end{aligned}$$

Hovering The **hovering flight** condition may be calculated from basic rotor data given in Fig. 11.4.28. These data are taken from full-scale rotor tests. Surface-contour accuracy can reduce the total torque coefficient 6 to 7 percent. The power required for hovering flight is greatly reduced near the ground. Observed flight-test data from various sources are plotted in Fig. 11.4.29. The ordinates are heights above the ground measured in rotor diameters.

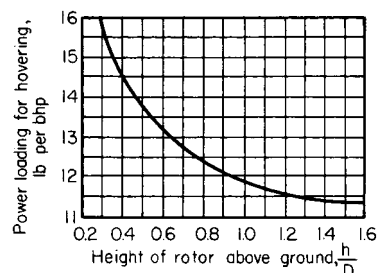


Fig. 11.4.29 Observed ground effect on Sikorsky-type helicopters.

Effect of Gross Weight on Rate of Climb Figure 11.4.30 from Tal-kin (*NACA-TN* 1192) shows the rate of climb that can be obtained by reducing the load on a helicopter that will just hover. Conversely, given the rate of climb with a given load, the curves determine the increase in load that will reduce the rate of climb to zero; i.e., they determine the maximum load for which hovering is possible.

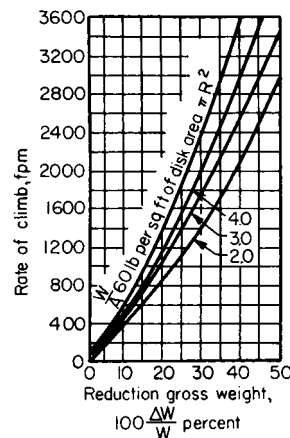


Fig. 11.4.30 Effect of gross weight on the rate of climb of a helicopter.

Performance with Forward Speed The performance of a typical single-main-rotor-type helicopter may be shown by a curve of C_{TR}/C_{QR} plotted against $\mu = v/\pi nD$, where v is the speed of the helicopter, as in Fig. 11.4.31. This curve includes the parasite-drag effects which are

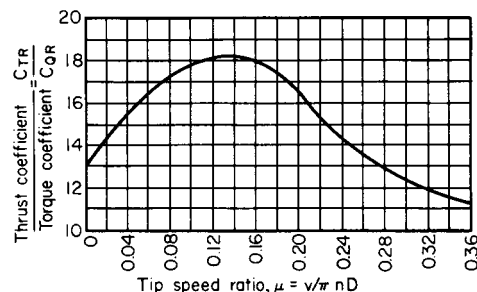


Fig. 11.4.31 Performance curve for a single-main-rotor-type helicopter.

11-72 AERONAUTICS

appreciable at the higher values of μ . It is only a rough approximation to the experimentally determined values. C_{TR} may be calculated to determine C_{QR} , from which Q is obtained.

The performance of rotors at forward speeds involves a number of variables. For more complete treatment, see *NACA-TN 1192* and *NACA Wartime Report L-110*.

GROUND-EFFECT MACHINES (GEM)

For data on air-cushion vehicles and hydrofoil craft, see Sec. 11.3 "Marine Engineering."

SUPERSONIC AND HYPERSONIC AERODYNAMICS

REFERENCES: Liepmann and Roshko, "Elements of Gas Dynamics," Wiley. "High Speed Aerodynamics and Jet Propulsion" 12 vols., Princeton. Shapiro, "The Dynamics and Thermodynamics of Compressible Fluid Flow," Vols. I, II, Ronald. Howarth (ed.), "Modern Developments in Fluid Mechanics—High Speed Flow," Vols. I, II, Oxford. Kuethe and Schetzer, "Foundations of Aerodynamics," Wiley. Ferri, "Elements of Aerodynamics of Supersonic Flows," Macmillan. Bonney, "Engineering Supersonic Aerodynamics," McGraw-Hill.

The effect of the compressibility of a fluid upon its motion is determined primarily by the **Mach number** M .

$$M = V/V_s \quad (11.4.2)$$

where V = speed of the fluid and V_s = speed of sound in the fluid which for air is $49.1\sqrt{T}$, where T is in °R and V_s in ft/s. The Mach number varies with position in the fluid, and the compressibility effect likewise varies from point to point.

If a *body moves through the atmosphere*, the overall compressibility effects are a function of the Mach number \bar{M} of the body, defined as

$$\bar{M} = \text{velocity of body/speed of sound in the atmosphere}$$

Table 11.4.5 lists the useful **gas dynamics relations** between velocity, Mach number, and various fluid properties for isentropic flow. (See also Sec. 4, "Heat.")

$$\begin{aligned} V^2 &= 2(h_0 - h) = 2C_p(T_0 - T) \\ \frac{V^2}{V_{s0}^2} &= \frac{M^2}{1 + \frac{\gamma-1}{2}M^2} \\ \left(\frac{p}{p_0}\right)^{(\gamma-1)/\gamma} &= \frac{T}{T_0} = \left(\frac{\rho}{\rho_0}\right)^{\gamma-1} = \left(\frac{V_s}{V_{s0}}\right)^2 = \frac{1}{1 + \frac{\gamma-1}{2}M^2} \\ \frac{1/2\rho V^2}{p_0} &= \frac{(\gamma/2)M^2}{\left(1 + \frac{\gamma-1}{2}M^2\right)^{\gamma/(\gamma-1)}} \quad (11.4.3) \\ \left(\frac{A}{A^*}\right)^2 &= \frac{1}{M^2} \left[\frac{2}{\gamma+1} \left(1 + \frac{\gamma-1}{2}M^2\right) \right]^{(\gamma+1)/(\gamma-1)} \end{aligned}$$

where h = enthalpy of the fluid, A = stream-tube cross section normal to the velocity, and the subscript $_0$ denotes the isentropic stagnation condition reached by the stream when stopped frictionlessly and adiabatically (hence isentropically). V_{s0} denotes the speed of sound in that medium.

The superscript * denotes the conditions occurring when the speed of the fluid equals the speed of sound in the fluid. For $M = 1$, Eqs. (11.4.2) become

$$\begin{aligned} \frac{T^*}{T_0} &= \left(\frac{V_s^*}{V_{s0}}\right)^2 = \frac{2}{\gamma+1} \\ \frac{p^*}{p_0} &= \left(\frac{2}{\gamma+1}\right)^{\gamma/(\gamma-1)} \\ \frac{\rho^*}{\rho_0} &= \left(\frac{2}{\gamma+1}\right)^{1/(\gamma-1)} \end{aligned} \quad (11.4.4)$$

For air $p^* = 0.52828p_0$; $\rho^* = 0.63394\rho_0$; $T^* = 0.83333T_0$.

For **subsonic regions** flow behaves similarly to the familiar hydraulics or incompressible aerodynamics: In particular, an increase of velocity is associated with a decrease of stream-tube area, and friction causes a pressure drop in a tube. There are no regions where the local flow velocity exceeds sonic speed. For **supersonic regions**, an increase of velocity is associated with an increase of stream-tube area, and friction causes a pressure rise in a tube. $M = 1$ is the dividing line between these two regions. For **transonic flows**, there are regions where the local flow exceeds sonic velocity, and this mixed-flow region requires special analysis. For **supersonic flows**, the entire flow field, with the exception of the regime near stagnation areas, has a velocity higher than the speed of sound.

The **hypersonic regime** is that range of very high supersonic speeds (usually taken as $M > 5$) where even a very streamlined body causes disturbance velocities comparable to the speed of sound, and stagnation temperatures can become so high that the gas molecules dissociate and become ionized.

Shock waves may occur at locally supersonic speeds. At low velocities the fluctuations that occur in the motion of a body (at the start of the motion or during flight) propagate away from the body at essentially the speed of sound. At higher subsonic speeds, fluctuations still propagate at the speed of sound in the fluid away from the body in all directions, but now the waves cannot get so far ahead; therefore, the force coefficients increase with an increase in the Mach number. When the Mach number of a body exceeds unity, the fluctuations instead of traveling away from the body in all directions are actually left behind by the body. These cases are illustrated in Fig. 11.4.32. As the supersonic speed is increased, the fluctuations are left farther behind and the force coefficients again decrease.

Where, for any reason, waves form an envelope, as at $M > 1$ in Fig. 11.4.32, a wave of finite pressure jump may result.

The speed of sound is higher in a higher-temperature region. For a compression wave, disturbances in the compressed (hence high-temperature) fluid will propagate faster than and overtake disturbances in the lower-temperature region. In this way shock waves are formed.

For a **stationary normal shock wave**, the fluid velocities V_1 before and V_2 after the shock are related by

$$V_1 V_2 = (V_s^*)^2 \quad (11.4.5)$$

Other properties are given by

$$p_2 - p_1 = \rho_1 V_1 (V_1 - V_2) \quad (11.4.6)$$

$$\begin{aligned} \frac{T_2}{T_1} &= \left(\frac{V_{s2}}{V_{s1}}\right)^2 \\ &= \left(\frac{2}{\gamma+1}\right)^2 \frac{1}{M_1^2} \left(1 + \frac{\gamma-1}{2}M_1^2\right) \left(\gamma M_1^2 - \frac{\gamma-1}{2}\right) \end{aligned} \quad (11.4.7)$$

$$M_2^2 = \left(1 + \frac{\gamma-1}{2}M_1^2\right) \left(\gamma M_1^2 - \frac{\gamma-1}{2}\right)^{-1} \quad (11.4.8)$$

$$\frac{p_{20}}{p_1} = \left(\frac{\gamma+1}{2}\right)^{(\gamma+1)/(\gamma-1)} M^2 \left(\gamma - \frac{\gamma-1}{2M_1^2}\right)^{-1/(\gamma-1)} \quad (11.4.9a)$$

$$\begin{aligned} \frac{p_{20}}{p_{10}} &= \left(\frac{\gamma+1}{2}\right)^{(\gamma+1)/(\gamma-1)} M^2 \\ &\times \left(1 + \frac{\gamma-1}{2}M^2\right)^{-\gamma/(\gamma-1)} \left(\gamma - \frac{\gamma-1}{2M^2}\right)^{-1/(\gamma-1)} \end{aligned} \quad (11.4.9b)$$

The subscript 20 refers to the stagnation condition after the shock, and the subscript 10 refers to the stagnation condition ahead of the shock.

In a normal shock M , V , and p_0 decrease; p , ρ , T , and s increase, whereas T_0 remains unchanged. These relations are given numerically in Table 11.4.6.

If the shock is moving, these same relations apply *relative to the shock*. In particular, if the shock advances into stationary fluid, it does so at the speed V_1 which is always greater than the speed of sound in the stationary fluid by an amount dependent upon the shock strength.

Table 11.4.5 Isentropic Gas Dynamics Relations

M	$\frac{p}{p_0}$	$\frac{V}{V_{s0}}$	$\frac{A}{A^*}$	$\frac{1/2\rho V^2}{p_0}$	$\frac{\rho V}{\rho_0 V_{s0}}$	$\frac{\rho}{\rho_0}$	$\frac{T}{T_0}$	$\frac{V_s}{V_{s0}}$
0.00	1.000	0.000	∞	0.000	0.000	1.000	1.000	1.000
0.05	0.998	0.050	11.59	0.002	0.050	0.999	0.999	1.000
0.10	0.993	0.100	5.82	0.007	0.099	0.995	0.998	0.999
0.15	0.984	0.150	3.91	0.016	0.148	0.989	0.996	0.998
0.20	0.972	0.199	2.964	0.027	0.195	0.980	0.992	0.996
0.25	0.957	0.248	2.403	0.042	0.241	0.969	0.988	0.994
0.30	0.939	0.297	2.035	0.059	0.284	0.956	0.982	0.991
0.35	0.919	0.346	1.778	0.079	0.325	0.941	0.976	0.988
0.40	0.896	0.394	1.590	0.100	0.364	0.924	0.969	0.984
0.45	0.870	0.441	1.449	0.123	0.399	0.906	0.961	0.980
0.50	0.843	0.488	1.340	0.148	0.432	0.885	0.952	0.976
0.55	0.814	0.534	1.255	0.172	0.461	0.863	0.943	0.971
0.60	0.784	0.580	1.188	0.198	0.487	0.840	0.933	0.966
0.65	0.753	0.624	1.136	0.223	0.510	0.816	0.922	0.960
0.70	0.721	0.668	1.094	0.247	0.529	0.792	0.911	0.954
0.75	0.689	0.711	1.062	0.271	0.545	0.766	0.899	0.948
0.80	0.656	0.753	1.038	0.294	0.557	0.740	0.887	0.942
0.85	0.624	0.795	1.021	0.315	0.567	0.714	0.874	0.935
0.90	0.591	0.835	1.009	0.335	0.574	0.687	0.861	0.928
0.95	0.559	0.874	1.002	0.353	0.577	0.660	0.847	0.920
1.00	0.528	0.913	1.000	0.370	0.579	0.634	0.833	0.913
1.05	0.498	0.950	1.002	0.384	0.578	0.608	0.819	0.905
1.10	0.468	0.987	1.008	0.397	0.574	0.582	0.805	0.897
1.15	0.440	1.023	1.018	0.407	0.569	0.556	0.791	0.889
1.20	0.412	1.057	1.030	0.416	0.562	0.531	0.776	0.881
1.25	0.386	1.091	1.047	0.422	0.553	0.507	0.762	0.873
1.30	0.361	1.124	1.066	0.427	0.543	0.483	0.747	0.865
1.35	0.337	1.156	1.089	0.430	0.531	0.460	0.733	0.856
1.40	0.314	1.187	1.115	0.431	0.519	0.437	0.718	0.848
1.45	0.293	1.217	1.144	0.431	0.506	0.416	0.704	0.839
1.50	0.272	1.246	1.176	0.429	0.492	0.395	0.690	0.830
1.55	0.253	1.274	1.212	0.426	0.478	0.375	0.675	0.822
1.60	0.235	1.301	1.250	0.422	0.463	0.356	0.661	0.813
1.65	0.218	1.328	1.292	0.416	0.443	0.337	0.647	0.805
1.70	0.203	1.353	1.338	0.410	0.433	0.320	0.634	0.796
1.75	0.188	1.378	1.387	0.403	0.417	0.303	0.620	0.788
1.80	0.174	1.402	1.439	0.395	0.402	0.287	0.607	0.779
1.85	0.161	1.425	1.495	0.386	0.387	0.272	0.594	0.770
1.90	0.149	1.448	1.555	0.377	0.372	0.257	0.581	0.762
1.95	0.138	1.470	1.619	0.368	0.357	0.243	0.568	0.754
2.00	0.128	1.491	1.688	0.358	0.343	0.230	0.556	0.745
2.50	0.059	1.667	2.637	0.256	0.219	0.132	0.444	0.667
3.00	0.027	1.793	4.235	0.172	0.137	0.076	0.357	0.598
3.50	0.013	1.884	6.790	0.112	0.085	0.045	0.290	0.538
4.00	0.007	1.952	10.72	0.074	0.054	0.028	0.238	0.488
4.50	0.003	2.003	16.56	0.049	0.035	0.017	0.198	0.445
5.00	0.002	2.041	25.00	0.033	0.023	0.011	0.167	0.408
10.00	0.00002	2.182	536.00	0.002	0.001	0.005	0.048	0.218

SOURCE: Emmons, "Gas Dynamics Tables for Air," Dover Publications, Inc., 1947.

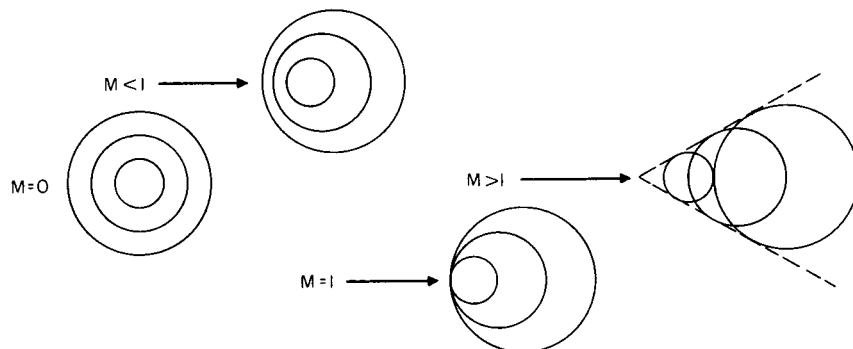


Fig. 11.4.32 Propagation of sound waves in moving streams.

11-74 AERONAUTICS

Table 11.4.6 Normal Shock Relations

M	p_2/p_1	p_{20}/p_1	p_{20}/p_{10}	M_2	V_{s2}/V_{s1}	V_2/V_1	T_2/T_1	p_2/p_1
1.00	1.000	1.893	1.000	1.000	1.000	1.000	1.000	1.000
1.05	1.120	2.008	1.000	0.953	1.016	0.923	1.033	1.084
1.10	1.245	2.133	0.999	0.912	1.032	0.855	1.065	1.169
1.15	1.376	2.266	0.997	0.875	1.047	0.797	1.097	1.255
1.20	1.513	2.408	0.993	0.842	1.062	0.745	1.128	1.342
1.25	1.656	2.557	0.987	0.813	1.077	0.700	1.159	1.429
1.30	1.805	2.714	0.979	0.786	1.091	0.660	1.191	1.516
1.35	1.960	2.878	0.970	0.762	1.106	0.624	1.223	1.603
1.40	2.120	3.049	0.958	0.740	1.120	0.592	1.255	1.690
1.45	2.286	3.228	0.945	0.720	1.135	0.563	1.287	1.776
1.50	2.458	3.413	0.930	0.701	1.149	0.537	1.320	1.862
1.55	2.636	3.607	0.913	0.684	1.164	0.514	1.354	1.947
1.60	2.820	3.805	0.895	0.668	1.178	0.492	1.388	2.032
1.65	3.010	4.011	0.876	0.654	1.193	0.473	1.423	2.115
1.70	3.205	4.224	0.856	0.641	1.208	0.455	1.458	2.198
1.75	3.406	4.443	0.835	0.628	1.223	0.439	1.495	2.279
1.80	3.613	4.670	0.813	0.617	1.238	0.424	1.532	2.359
1.85	3.826	4.902	0.790	0.606	1.253	0.410	1.573	2.438
1.90	4.045	5.142	0.767	0.596	1.268	0.398	1.608	2.516
1.95	4.270	5.389	0.744	0.586	1.284	0.386	1.647	2.592
2.00	4.500	5.640	0.721	0.577	1.299	0.375	1.688	2.667
2.50	7.125	8.526	0.499	0.513	1.462	0.300	2.138	3.333
3.00	10.333	12.061	0.328	0.475	1.637	0.259	2.679	3.857
3.50	14.125	16.242	0.213	0.451	1.821	0.235	3.315	4.261
4.00	18.500	21.068	0.139	0.435	2.012	0.219	4.047	4.571
4.50	23.458	26.539	0.092	0.424	2.208	0.208	4.875	4.812
5.00	29.000	32.653	0.062	0.415	2.408	0.200	5.800	5.000
10.00	116.500	129.220	0.003	0.388	4.515	0.175	20.388	5.714

SOURCE: Emmons, "Gas Dynamics Tables for Air," Dover Publications, Inc., 1947.

A shock wave may be oblique to a supersonic stream (see Fig. 11.4.33). If so, it behaves exactly like a normal shock to the normal component of the stream. The tangential component is left unchanged. Thus the resultant velocity not only drops abruptly in magnitude but also changes discontinuously in direction. Figure 11.4.34 gives the relations between M_1 , M_2 , θ_w , and δ .

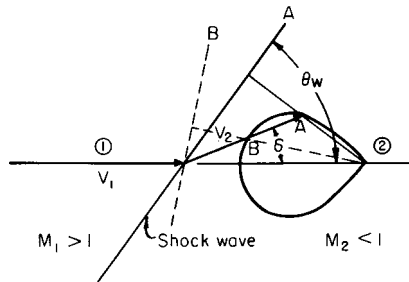


Fig. 11.4.33 Shock polar.

If, for a given supersonic stream, the velocities following all possible oblique shocks are plotted, a shock polar is obtained, as in Fig. 11.4.33. For any given stream deflection there are two possible shock angles. The supersonic flow past a wedge can, in principle, occur with either the strong shock B or the weak shock A attached to the leading edge; in practice only the weak shock occurs. The exact flow about the wedge may be computed by Eqs. (11.4.5) to (11.4.9) or more easily with the help of Fig. 11.4.34. For small wedge angles, the shock angle differs only slightly from $\sin^{-1}(1/M)$, the Mach angle, and the velocity component normal to this Mach wave is the speed of sound; the pressure jump is small and is given approximately by

$$p - p_1 = (\gamma p_1 \bar{M}_1^2 / \sqrt{\bar{M}_1^2 - 1}) \delta \quad (11.4.10)$$

where δ is the wedge semiangle.

Exact solutions also exist for supersonic flow past a cone. Above a certain supersonic Mach number, a conical shock wave is attached to the apex of the cone. Figures 11.4.35 and 11.4.36 show these exact relations; they are so accurate that they are often used to determine the Mach number of a stream by measuring the shock-wave angle on a cone of known angle. For small cone angles the shock differs only slightly from the Mach cone, i.e., a cone whose semiapex angle is the Mach angle; the pressure on the cone is then given approximately by

$$p - p_1 = \gamma p_1 \bar{M}_1^2 \delta^2 (\ln 2 / \delta \sqrt{\bar{M}_1^2 - 1}) \quad (11.4.11)$$

where δ is the cone semiangle.

A nozzle consisting of a single contraction will produce at its exit a jet of any velocity from $M = 0$ to $M = 1$ by a proper adjustment of the pressure ratio. For use as a subsonic wind-tunnel nozzle where a uniform parallel gas stream is desired, it is only necessary to connect the supply section to the parallel-walled or open-jet test section by a smooth gently curving wall. If the radius of curvature of the wall is nowhere less than the largest test-section cross-sectional dimension, no flow separation will occur and a good test gas stream will result.

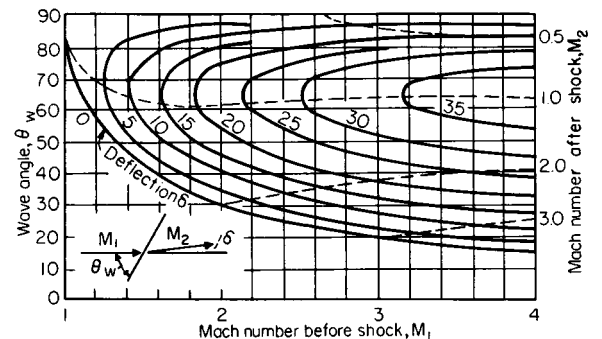


Fig. 11.4.34 Oblique shock wave relations.

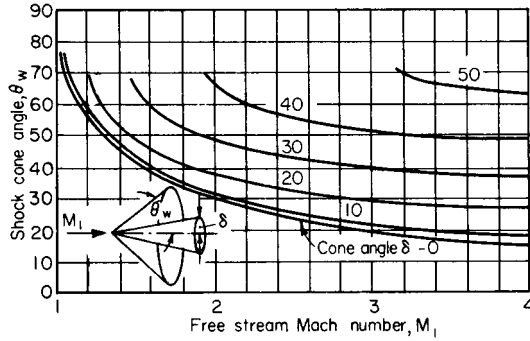


Fig. 11.4.35 Wave angles for supersonic flow around cones.

When a **converging nozzle** connects two chambers with the pressure drop beyond the critical $[(p/p_0) < (p^*/p_0)]$, the Mach number at the exit of the nozzle will be 1; the pressure ratio from the supply section to the nozzle exit will be critical; and all additional expansion will take place outside the nozzle.

A nozzle designed to supply a supersonic jet at its exit must converge to a minimum section and diverge again. The area ratio from the minimum section to the exit is given in the column headed A/A^* in Table 11.4.5. A converging-diverging nozzle with a pressure ratio $p/p_0 =$ (gas pressure)/(stagnation pressure), Table 11.4.5, gradually falling from unity to zero will produce shock-free flow for all exit Mach numbers from zero to the subsonic Mach number corresponding to its area ratio. From this Mach number to the supersonic Mach number corresponding to the given area ratio, there will be shock waves in the nozzle. For all smaller pressure ratios, the Mach number at the nozzle exit will not change, but additional expansion to higher velocities will occur outside of the nozzle.

To obtain a uniform parallel shock-free supersonic stream, the converging section of the nozzle can be designed as for a simple converging nozzle. The diverging or supersonic portion must be designed to produce and then cancel the expansion waves. A series of designs are given

in Table 11.4.7. These nozzles would perform as designed if it were not for the growth of the boundary layer. Experience indicates that these nozzles give a good first approximation to a uniform parallel supersonic stream but at a somewhat lower Mach number.

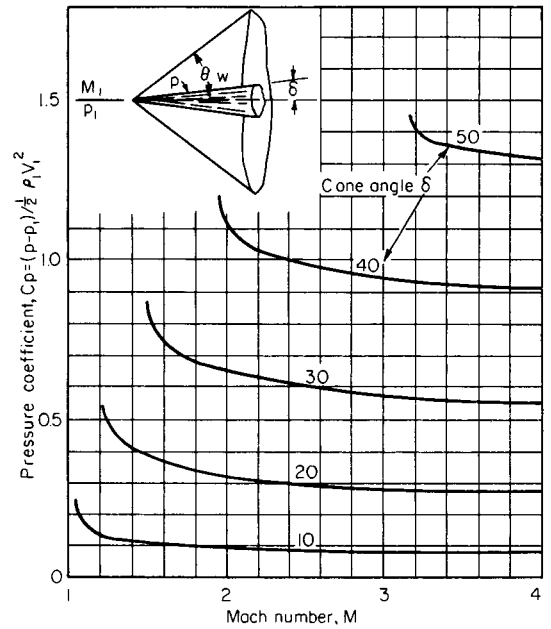


Fig. 11.4.36 Pressure calculations for supersonic flow around cones.

For **rocket nozzles** and other thrust devices the gain in thrust obtained by making the jet uniform and parallel at complete expansion must be balanced against the loss of thrust caused by the friction on the wall of the greater length of nozzle required. A simple conical diverging sec-

Table 11.4.7 Typical Nozzle Ordinates

A diagram of a conical diverging section of a nozzle. It shows a central axis with a conical wall. The distance from the vertex to the exit is x_t . The radius at the exit is y_t . The angle of the cone is θ_0 . The distance from the vertex to a point x is x , and the radius at that point is y .

M	1.99		2.42		2.82		3.24		3.62		4.04	
θ_0	7°		9°		12°		13°		14°		15°	
	x	y	x	y	x	y	x	y	x	y	x	y
	0	7.50	0	7.50	0	7.50	0	7.50	0	7.50	0	7.50
	4.38	7.42	4.52	7.42	5.62	7.40	4.94	7.41	5.52	7.40	5.94	7.40
	8.36	7.28	8.69	7.28	9.70	7.26	9.43	7.26	10.39	7.23	11.20	7.21
	11.97	7.09	12.47	7.08	13.38	7.07	13.47	7.05	14.89	7.00	16.10	6.96
	15.19	6.88	15.91	6.84	16.64	6.84	17.15	6.79	18.75	6.73	20.22	6.67
	18.06	6.62	19.04	6.56	19.67	6.57	20.41	6.50	22.24	6.42	23.94	6.34
	20.65	6.35	21.80	6.27	22.35	6.29	23.41	6.19	25.39	6.09	27.17	6.00
	21.84	6.20	24.34	5.96	24.80	5.99	26.03	5.87	28.08	5.76	30.11	5.64
			26.57	5.65	26.95	5.69	28.42	5.53	30.56	5.41	32.69	5.28
	x_t	4.48	27.48	5.49	28.90	5.37	30.46	5.21	32.73	5.07	34.95	4.92
					30.70	5.07	32.35	4.87	34.66	4.73	36.96	4.57
			x_t	3.06	32.20	4.77	33.99	4.56	36.35	4.40	38.69	4.23
					32.90	4.62	35.44	4.25	37.87	4.08	40.26	3.90
							36.13	4.09	39.20	3.77	41.62	3.58
					x_t	2.10			39.80	3.62	42.79	3.29
							x_t	1.41			43.32	3.15
									x_t	0.988		0.673

SOURCE: Puckett, Supersonic Nozzle Design, *Jour. Applied Mechanics*, 13, no. 4, 1948.

11-76 AERONAUTICS

tion, cut off experimentally for maximum thrust, is generally used (see also Sec. 11.5 "Jet Propulsion and Aircraft Propellers").

For transonic and supersonic flow, **diffusers** are used for the recovery of kinetic energy. They follow the test sections of supersonic wind tunnels and are used as inlets on high-speed planes and missiles for ram recovery. For the first use, the diffuser is fed a nonuniform stream from the test section (the nonuniformities depending on the particular body under test) and should yield the maximum possible pressure-rise ratio. In missile use the inlet diffuser is fed by a uniform (but perhaps slightly yawed) airstream. The maximum possible pressure-rise ratio is important but must provide a sufficiently uniform flow at the exit to assure good performance of the compressor or combustion chamber that follows.

In simplest form, a **subsonic diffuser** is a diverging channel, a nozzle in reverse. Since boundary layers grow rapidly with a pressure rise, subsonic diffusers must be diverged slowly, 6 to 8° equivalent cone angle, i.e., the apex angle of a cone with the same length and area ratio. Similarly, a **supersonic diffuser** in its simplest form is a supersonic nozzle in reverse. Both the convergent and divergent portions must change cross section gradually. In principle it is possible to design a shock-free diffuser. In practice shock-free flow is not attained, and the design is based upon minimizing the shock losses. Oblique shocks should be produced at the inlet and reflected a sufficient number of times to get compression nearly to $M = 1$. A short parallel section and a divergent section can now be added with the expectation that a weak normal shock will be formed near the throat of the diffuser.

An efficient diffuser for a supersonic inlet is illustrated in Fig. 11.4.37. The central body has stepped cones, each one of which produces an oblique conical shock wave. After two or three such weak shock compressions, the air flows at about $M = 1$ into an annular opening and is further compressed by an internal normal shock and by subsonic diffusion. *NACA-TM 1140* describes this diffuser. A ratio of pressure after diffusion to the total pressure in the atmosphere of as high as 0.6 is obtained with such diffusers at a Mach number of 3. The indications are that higher efficiencies are obtainable by careful design.

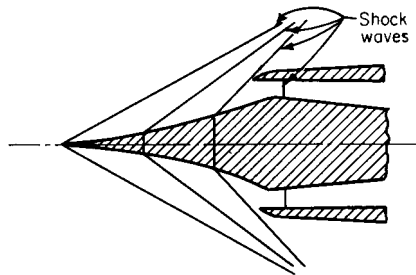


Fig. 11.4.37 Oblique-shock diffuser for ram recovery on a supersonic-plane air intake (Oswatitsch diffuser).

For a **supersonic wind tunnel**, the best way to attain the maximum pressure recovery at a wide range of operating conditions is to make the diffuser throat variable. The ratio of diffuser-exit static pressure to the diffuser-inlet (test-section outlet) total pressure is given in Table 11.4.8. These pressure recoveries are attained by the proper adjustment of the throat section of a variable diffuser on a supersonic wind-tunnel nozzle.

Table 11.4.8

M	1	1.5	2	3	4
p_e/p_0	0.83	0.69	0.50	0.23	0.10

A **supersonic wind tunnel** consists of a compressor or compressor system including precoolers or aftercoolers, a supply section, a supersonic nozzle, a test section with balance and other measuring equipment, a diffuser, and sufficient ducting to connect the parts. The **minimum pressure ratio** required from supply section to diffuser exit is given in Table

11.4.8. Any pressure ratio greater than this is satisfactory. The extra pressure ratio is automatically wasted by additional shock waves that appear in the diffuser. The compression ratio required of the compressor system must be greater than that of Table 11.4.8 by at least an amount sufficient to take care of the pressure drop in the ducting and valves. The latter losses are estimated by the usual hydraulic formulas.

After selecting a compressor system capable of supplying the required maximum pressure ratio, the test section area is computed from

$$A = 1.73 \frac{Q}{V_{s0}} \frac{A}{A^*} \frac{p_e}{p_0} \text{ ft}^2 \quad (11.4.12)$$

where Q is the inlet volume capacity of the compressors, ft^3/s ; V_{s0} is the speed of sound in the supply section, ft/s ; A/A^* is the area ratio given in Table 11.4.5 as a function of M ; p_e/p_0 is the pressure ratio given in Table 11.4.8 as a function of M .

The nozzle itself is designed for uniform parallel airflow in the test section. Such designs are given in Table 11.4.7, which covers only the part of the nozzle between the exit section and the maximum expansion angle. Since for each Mach number a different nozzle is required, the nozzle must be flexible or the tunnel so arranged that fixed nozzles can be readily interchanged.

The Mach number of a test is set by the nozzle selection, and the Reynolds number is set by the inlet conditions and size of model. The Reynolds number is computed from

$$Re = Re_0 D (p_0/14.7) (540/T_0)^{1.268} \quad (11.4.13)$$

where Re_0 is the Reynolds number per inch of model size for atmospheric temperature and pressure, as given by Fig. 11.4.38, D is model diam, in; p_0 is the stagnation pressure, lb/in^2 ; T_0 is the stagnation temperature, °R.

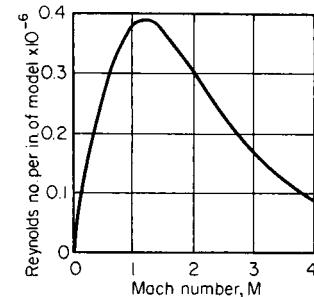


Fig. 11.4.38 Reynolds number–Mach number relation (for a fixed model size and stagnation condition).

For a closed-circuit tunnel, the Reynolds number can be varied independently of the Mach number by adjusting the mass of air in the system, thus changing p_0 .

Intermittent-wind tunnels for testing at high speeds do not require the large and expensive compressors associated with continuous-flow tunnels. They use either a large vacuum tank or a large pressure tank (often in the form of a sphere) to produce a pressure differential across the test section. Such tunnels may have steady flow for only a few seconds, but by careful instrumentation, sufficient data may be obtained in this time. A **shock tube** may be used as an intermittent-wind tunnel as well as to study shock waves and their interactions; it is essentially a long tube of constant or varying cross section separated into two parts by a frangible diaphragm. High pressure exists on one side; by rupturing the diaphragm, a shock wave moves into the gas with the lower pressure. After the shock wave a region of steady flow exists for a few milliseconds. Very high stagnation temperatures can be created in a shock tube, which is not the case in a wind tunnel, so that it is useful for studying hypersonic flow phenomena.

Wind-tunnel force measurements are subject to errors caused by the model support strut. Wall interference is small at high Mach numbers for which the reflected model head wave returns well behind the model.

Near $M = 1$, the wall interference becomes very large. In fact, the tunnel chokes at Mach numbers given in Table 11.4.5, at

$$\frac{A}{A^*} = \frac{1}{1 - \frac{\text{area of model projected on test-section cross section}}{\text{area of test-section cross section}}} \quad (11.4.14)$$

There are two choking points: one subsonic and one supersonic. Between these two Mach numbers, it is impossible to test in the tunnel. As these Mach numbers are approached, the tunnel wall interference becomes very large.

For tests in this range of Mach number, specially constructed **transonic wind tunnels** with perforated or slotted walls have been built. The object here is to produce a mean flow velocity through the walls that comes close to that which would have existed there had the body been moving at that speed in the open. Often auxiliary blowers are needed to produce the necessary suction on the walls and to reinject this air into the tunnel circuit in or after the diffuser section.

Drag is difficult to predict precisely from wind-tunnel measurements, especially in the transonic regime. **Flight tests** of rocket-boosted models which coast through the range of Mach numbers of interest are used to obtain better drag estimates; from telemetered data and radar or optical sighting the deceleration can be determined, which in turn yields the drag.

LINEARIZED SMALL-DISTURBANCE THEORY

As the speed of a body is increased from a low subsonic value (Fig. 11.4.39a), the local Mach number becomes unity somewhere in the fluid along the surface of the body, i.e., the lower critical Mach number is reached. Above this there is a small range of transonic speed in which a supersonic region exists (Fig. 11.4.39b). Shock waves appear in this region attached to the sides of the body (Fig. 11.4.39c) and grow with increasing speed. At still higher transonic speeds a detached shock wave appears ahead of the body, and the earlier side shocks either disappear or move to the rear (Fig. 11.4.39d). Finally, for a sharp-nosed body, the head wave moves back and becomes attached (Fig. 11.4.39e). The flow is now generally supersonic everywhere, and the transonic regime is replaced by the supersonic regime. With the appearance of shock waves there occurs a considerable alteration of the pressure distribution, and the center of pressure on airfoil sections moves from the one-fourth chord point back toward the one-half chord point. There is an asso-

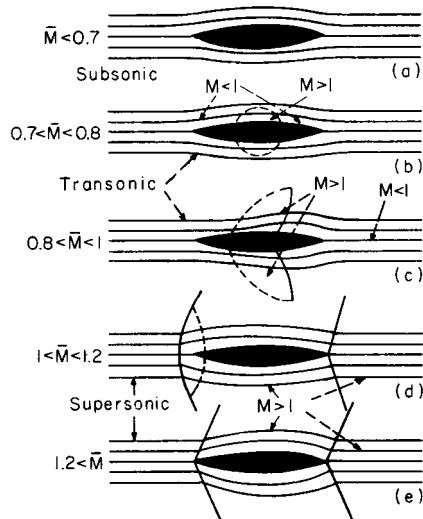


Fig. 11.4.39 Regions of flow about an airfoil (Mach numbers are approximate).

ciated increase of drag and, often, flow separation at the base of the shock.

The redistribution of pressures and the motion of shock waves over the wing surfaces through the transonic regime demands special consideration in the design of control surfaces so that they do not become ineffective by separation or inoperative by excessive loading.

If a body is slender (i.e., planes tangent to its surface at any point make small angles with the flight direction), the disturbance velocities caused by this body will be small compared with the flight speed and, excluding the hypersonic regime, small compared with the speed of sound. This permits the use of linearized small-disturbance theory to predict the approximate flow past the body. This theory relates the steady flow past the body at subsonic speeds to the incompressible flow past a distorted version of this body (the "generalized Prandtl-Glauert rule"). To find the velocity components in the **subsonic** flow about any slender body, first determine the velocity components, u, v, w (in the x, y, z directions, respectively), in the incompressible flow, at the same stream speed, about a stretched shape whose streamwise (x -axis direction) dimensions are $1/\beta$ times as great ($\beta = \sqrt{1 - M^2}$). The desired velocity components are then $\beta^{-2}u, \beta^{-1}v, \beta^{-1}w$ at corresponding points of the stretched and unstretched bodies. For **thin airfoil sections** this theory predicts

$$C_L = 2\pi\alpha/\sqrt{1 - M^2} \quad \alpha \text{ in radians} \quad (11.4.15)$$

where $L = C_L q S$ and $q = (\gamma/2)\rho_0 M^2$. For finite-span wings and for bodies, no such simple relations exist. However, an approximation to the overall **lift coefficient** for thin flat wings of rectangular platform is (see Fig. 11.4.41):

$$C_L = 2\pi A\alpha/[2 + \sqrt{4 + (\beta A)^2}] \quad (11.4.16)$$

and the drag is made up of the induced drag due to lift and the skin-friction drag (see above, "Airfoils").

$$C_D = (C_L/\pi A)(1 + 0.01\beta A) + C_{DF} \quad (11.4.17)$$

At supersonic speeds, the Prandtl-Glauert rule is also applicable if we replace β by $\lambda = \sqrt{M^2 - 1}$ and relate flow to flow past a stretched (or compressed) body at $M = \sqrt{2}$, where $\lambda = 1$. For **thin airfoil sections** (see Fig. 11.4.40) this theory predicts

$$C_L = 4\alpha/\sqrt{M^2 - 1} \quad \alpha \text{ in radians} \quad (11.4.18)$$

$$C_D = \frac{2}{\lambda} \int_0^1 \left[\left(\frac{dy_u}{dx} \right)^2 + \left(\frac{dy_l}{dx} \right)^2 \right] d \left(\frac{x}{c} \right) + \frac{4a^2}{\lambda} + C_{DF} \quad (11.4.19)$$

where dy_u/dx and dy_l/dx are the slopes of the upper and lower surfaces of the airfoil, respectively, and C_{DF} is again the skin-friction drag coefficient. Note that there is a drag due to thickness and a drag due to lift at supersonic speeds for an airfoil section where there is none at subsonic speeds. For symmetric double-wedge airfoil sections, the thickness drag coefficient becomes $(4/\lambda)(t/c)^2$, and for symmetric biconvex airfoil sections it is $(16/3\lambda)(t/c)^2$, where t is the maximum thickness.

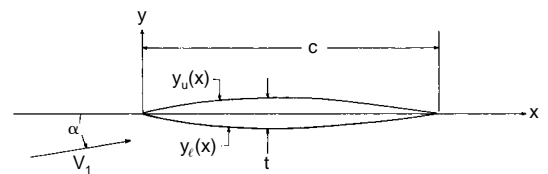


Fig. 11.4.40 Supersonic airfoil section.

Within the acoustic approximation, a disturbance at a point in supersonic flow can affect only the points in the **downstream Mach cone**, i.e., a conical region with apex at the point, axis parallel to the stream direction, and semicone angle equal to the Mach angle (see Fig. 11.4.32). Thus a rectangular wing with constant airfoil section has two-dimensional flow on all parts of the wing except the points within the tip Mach

11-78 AERONAUTICS

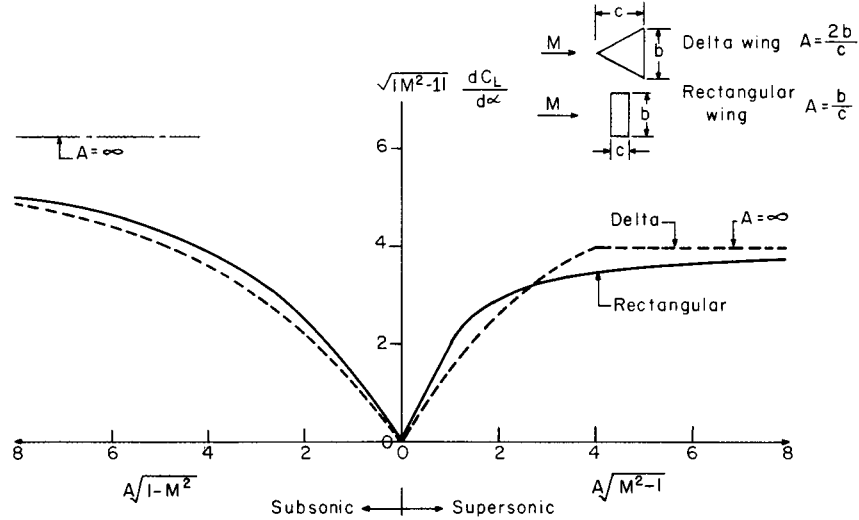


Fig. 11.4.41 Lift-coefficient curve slope for rectangular and delta wings (according to linearized theory).

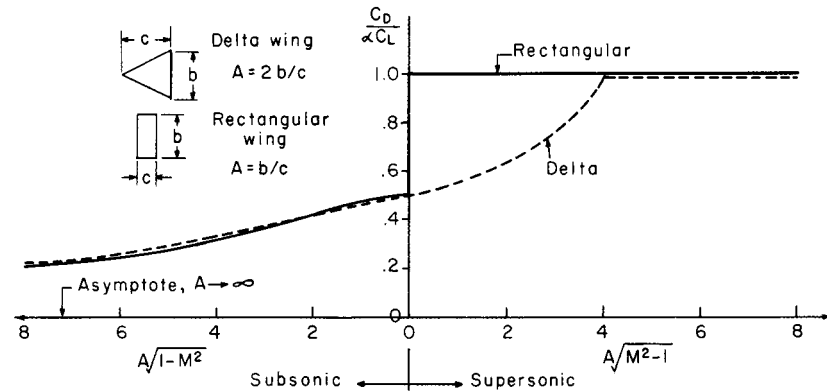


Fig. 11.4.42 Drag due to lift for rectangular and delta wings (according to linearized theory).

cones. At Mach numbers near unity these tip Mach cones cover nearly the entire wing, whereas at high Mach numbers they cover only a small part. Figure 11.4.41 shows the lift-curve coefficient slope for flat **rectangular and delta plan-form wings** at subsonic and supersonic speeds; these predictions of acoustic theory are inaccurate for high-aspect-ratio wings in the transonic regime, but elsewhere compare favorably with experiment. Figure 11.4.42 shows the drag due to lift for the same wings. The reduction in drag due to lift of the delta wing relative to the rectangular wing at moderate supersonic speeds, predicted by acoustic theory and shown in Fig. 11.4.42, is due to the fact that the delta-wing leading edge is **swept back**, and the component of velocity normal to the leading edge is subsonic. This creates a leading-edge suction which reduces the drag. This drag reduction is only partially realized in practice; a wing with a rounded leading edge realizes more of this reduction than a wing with a sharp leading edge. Figure 11.4.43 shows the thickness drag of the rectangular and delta wings, which occurs only at supersonic speeds. Note again that the leading-edge sweepback of the delta wing helps to reduce this drag at moderate supersonic speeds.

The lift of a slender **axially symmetric body** at small angle of attack is nearly independent of Mach number and is given approximately by

$$C_L = 2\alpha \quad (11.4.20)$$

where the lift coefficient is based on the cross-sectional area of the base. The drag for $\alpha = 0$ at subsonic speeds is made up of skin friction and

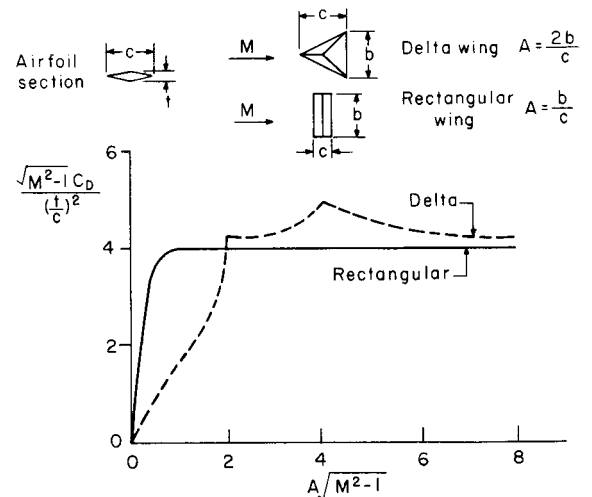


Fig. 11.4.43 Supersonic thickness drag coefficient for rectangular and delta wings with a symmetrical double-wedge airfoil section (according to linearized theory).

base drag; a dead-air region exists just behind the blunt base, and the pressure here is below ambient, causing a rearward suction which is the base drag. At supersonic speeds a wave drag is added, which represents the energy dissipated in shock waves from the nose. Figure 11.4.44 shows a typical drag-coefficient curve for a body of revolution where the **fineness ratio** (ratio of length to diameter) is 12.2. The skin-friction drag coefficient based on wetted area is the same as that of a flat plate, within experimental error.

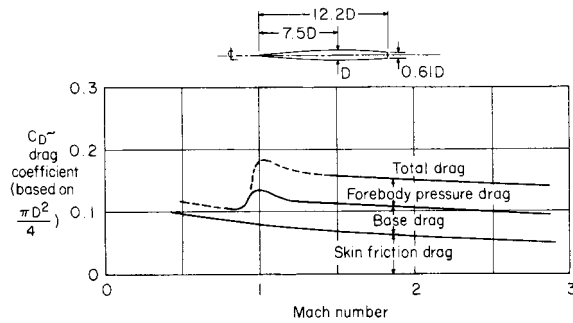


Fig. 11.4.44 Drag coefficients for parabolic-arc (NACA-RM 10) body (calculations from experimental data for a 30,000-ft altitude, $D = 12$ in, from NACR-TR 1160 and 1161, 1954).

At transonic and moderate supersonic speeds, the wave drag of a **wing body combination** can be effectively reduced by making the cross-sectional area distribution (including wings) a smooth curve when plotted versus fuselage station. This is the **area rule**; its application results in a decided indentation in the fuselage contour at the wing juncture. **Lift interference** effects also occur, especially when the body diameter is not small compared with the wing span. If the wing is attached to a cylindrical body, and if the wing-alone lift coefficient would have been C_L , then the lift carried on the body is $K_B C_L$, and the lift carried on the wing is $K_W C_L$. Figure 11.4.45 shows the variation of K_B and K_W with body diameter to wing-span ratio.

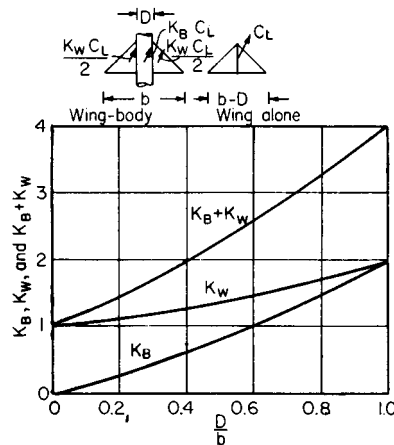


Fig. 11.4.45 Wing-body lift-interface factors.

The effect of **compressibility on skin-friction drag** is slight at subsonic speeds, but at supersonic speeds, a significant reduction in skin-friction coefficient occurs. Figure 11.4.46 shows the turbulent-boundary-layer mean skin-friction coefficient for a cone as a function of wall temperature and Mach number. An important effect at high speed is **aerodynamic heating**.

Figure 11.4.47 illustrates the velocity profile behind the shock wave of a body traveling at hypersonic speed. The shock-wave front repre-

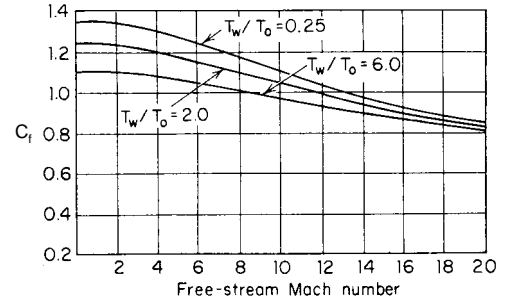


Fig. 11.4.46 Laminar skin-friction coefficient for a cone.

sents an area of high-temperature gas which radiates energy to the body, but boundary-layer convective heating is usually the major contributor. Behind this front is shown the velocity gradient in the boundary layer. The decrease in velocity in the boundary layer is brought about by the forces of interaction between fluid particles and the body (viscosity). This change in velocity is accompanied by a change in temperature and is dependent on the characteristics of the boundary layer. For example, heat transfer from a turbulent boundary layer may be of an order of magnitude greater than for laminar flow.

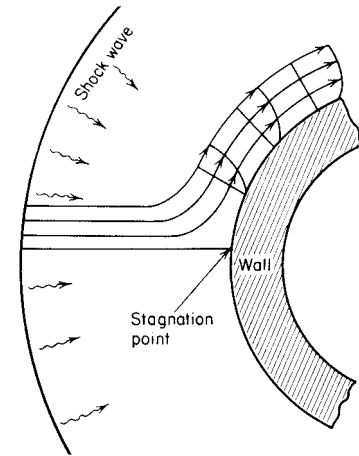


Fig. 11.4.47 Velocity profile behind a shock wave.

If the gas is brought to rest instantaneously, the total energy in the flow is converted to heat and the temperature of the air will rise. The resulting temperature is known as the **stagnation temperature** (see stagnation point, Fig. 11.4.47).

$$T_s = T_\infty \left(1 + \frac{\gamma - 1}{2} M^2 \right) \quad (11.4.21)$$

T_∞ is the ambient temperature of the gas at infinity, and γ is the specific-heat ratio of the gas. For undissociated air, $\gamma = 1.4$.

In general, this simple, one-dimensional relationship between velocity and temperature does not hold for temperature in the boundary layer. The laminae of the boundary layer are not insulated from each other, and there is cross conduction. This is associated with the **Prandtl number** Pr , which is defined as

$$Pr = C_p \mu / k_r \quad (11.4.22)$$

where k_r = thermal conductivity of fluid, C_p = specific heat of fluid at constant pressure, and μ = absolute viscosity of fluid.

Defining the **recovery factor** r as the ratio of the rise in the idealistic wall and stagnation temperature over the free-stream temperature,

$$r = (T_{aw} - T_\infty) / (T_s - T_\infty) = (Pr)^n \quad (11.4.23)$$

11-80 AERONAUTICS

For laminar flow, $r = (Pr)^{1/2}$; and for turbulent flow, $r = (Pr)^{1/3}$. Prandtl number Pr greatly complicates the thermal computations, but since it varies only over a small range of values, a recovery factor of 0.85 is generally used for laminar flow and 0.90 for turbulent flow.

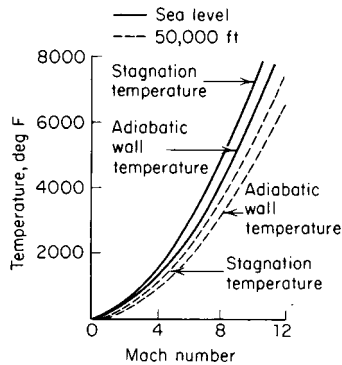


Fig. 11.4.48 Variation of stagnation and adiabatic wall temperature with Mach number.

For a thermally thin wall, the rate of change of the surface temperature is a function of the rate of total heat input and the surface's ability to absorb the heat.

$$dT_w/dt = q_T/wcb \quad (11.4.24)$$

where t = time, q_T = forced convective heating + radiation heating - heat radiation from the skin, w = density of skin material, c = specific heat of skin material, b = skin thickness, and T_w = skin temperature.

The heat balance may then be written

$$wcb \left(\frac{dT_w}{dt} \right) = k_c \left[T_0 \left(1 + r \frac{\gamma_B - 1}{2} M_0^2 \right) - T_w \right] + \alpha G_s A_p - \epsilon \sigma T_w^4 \quad (11.4.25)$$

where A_p = correction factor to account for area normal to radiation source, γ_B = specific heat ratio of boundary layer, ϵ = radiative emissivity of surface, σ = Stefan-Boltzmann constant [17.3×10^{-10} Btu/(h · ft² · °R⁴), α = surface absorptivity, G_s = solar irradiation Btu/(h · ft²).

For small time increments Δt ,

$$\frac{dT_w}{dt} = \frac{T_{w2} - T_{w1}}{\Delta t}$$

Then

$$T_{w2} = T_{w1} + \frac{\Delta t}{wcb} \left\{ h_c \left[T_0 \left(1 + \frac{\gamma_B - 1}{2} M_0^2 \right) - T_w \right] + \alpha G_s A_p - T_w^4 \right\} \quad (11.4.26)$$

The local heat-transfer coefficient h_c is defined as

$$h_c = \frac{k_r}{r^{4/3}} C_p C_f \rho_0 V g \quad (11.4.27)$$

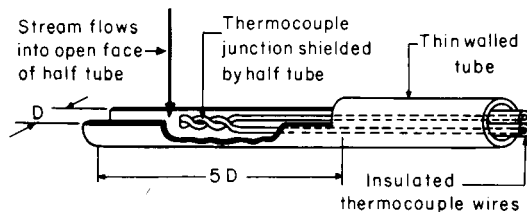


Fig. 11.4.49 Stagnation-temperature probe (recovery factor = 0.98).

where C_p = specific heat of air; C_f = local skin-friction coefficient; ρ_0 = density outside of boundary layer; V = velocity outside of boundary layer; g = acceleration of gravity.

For a cone, $k_r = 1,800$ (laminar $Re < 2 \times 10^6$) and $k_r = 1,800r^{4/3}$ (turbulent).

For a flat-plate transition, Reynolds number is 1×10^6 .

Figure 11.4.46 gives laminar-skin-friction coefficient for a cone. For a flat plate, multiply C_f by $\sqrt{3}/2$. For turbulent skin-friction coefficient for a cone,

$$\frac{0.242}{\sqrt{A^2 C_f T_w / T_0}} (\sin^{-1} \psi + \sin^{-1} \theta) = 0.41 \log \frac{Re}{2} C_f - 1.26 \log \frac{T_w}{T_0} \quad (11.4.28)$$

where

$$\psi = \frac{2A^2 - B}{\sqrt{B^2 + 4A^2}} \quad A^2 = \frac{(\gamma_0 - 1/2)M_0^2}{T_w/T_0}$$

$$\theta = \frac{B}{\sqrt{B^2 + 4A^2}} \quad B = \frac{1 + (\gamma_0 - 1/2)M_0^2}{T_w/T_0} - 1$$

For a flat plate, use Re instead of $Re/2$ in Eq. (11.4.28).

Figure 11.4.48 shows data on stagnation and adiabatic wall temperatures.

The primary measurements in aerodynamics are pressure measurements. A well-aligned pitot tube with an impact-pressure hole at its nose and static-pressure holes 10 diameters or more back from the nose will accurately measure the **impact pressure** and the **static pressure** of a uniform gas stream. Up to sonic speed the impact pressure is identical with stagnation pressure, but at supersonic speeds, a detached shock wave forms ahead of the probe, through which there is drop in stagnation pressure; the portion of the shock wave just ahead of the probe is normal, so that the equation for water flow in layer form over horizontal tubes (see "Transmission of Heat by Conduction and Convection" in Sec. 4) gives the relation of the measured impact pressure to the isentropic stagnation pressure.

Force measurements of total lift, drag, side force, pitching moment, yawing moment, and rolling moment on models are made on wind-

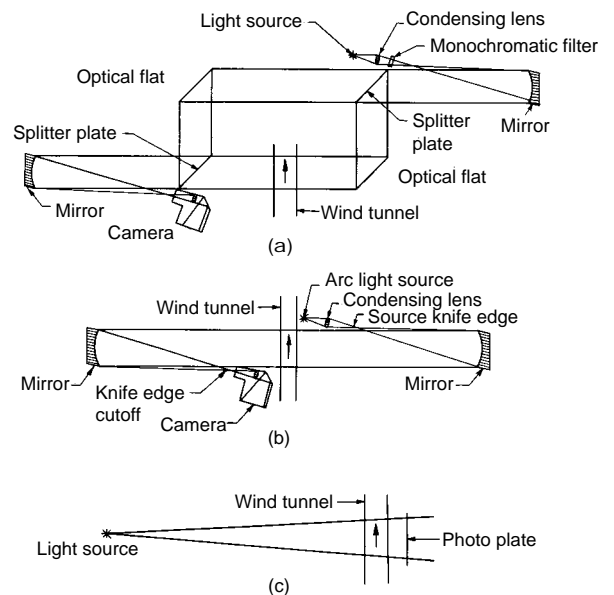


Fig. 11.4.50 Optical systems for observing high-speed flow phenomena. (a) Interferometer; (b) Schlieren (two-mirror) system; (c) shadowgraph.

tunnel balances just as at low speed. Small internal-strain-gage balances are often used to minimize strut interference.

An open thermocouple is unreliable for determining **stagnation temperature** if it is in a stream of high velocity. Figure 11.4.49 shows a simple temperature probe in which the fluid is decelerated adiabatically before its temperature is measured. The recovery factor used in equations, for this probe, accurately aligned to the stream, is 0.98.

Optical measurements in high-speed flow depend on the variation of index of refraction with gas density. This variation is given by

$$n = 1 + k\rho \quad (11.4.29)$$

where $k = 0.116 \text{ ft}^3/\text{slug}$ for air. A Mach-Zehnder **interferometer** (Fig. 11.4.50a), is capable of giving accurate density information for two-dimensional and axially symmetric flows. The **Schlieren** optical system (Fig. 11.4.50b) is sensitive to density gradients and is the most commonly used system to determine location of shock waves and regions of compression or expansion. The **shadowgraph** optical system is the simplest system (Fig. 11.4.50c) and is sensitive to the second space derivative of the density.

11.5 JET PROPULSION AND AIRCRAFT PROPELLERS

by Sanford Fleeter

REFERENCES: Zucrow, "Aircraft and Missile Propulsion," Vol. 2, Wiley. Hill and Peterson, "Mechanics and Thermodynamics of Propulsion," Addison-Wesley. Sutton, "Rocket Propulsion Elements," Wiley. Shorr and Zaehring, "Solid Propellant Technology," Wiley. Forestor and Kuskevics, "Ion Propulsion," AIAA Selected Reprints. Theodorsen, "Theory of Propellers," McGraw-Hill. Smith, "Propellers for High Speed Flight," Princeton. Zucrow, "Principles of Jet Propulsion," Wiley. "Aircraft Propeller Handbook," Depts. of the Air Force, Navy, and Commerce, U.S. Government Printing Office, 1956. Kerrebrock, "Aircraft Engines and Gas Turbines," MIT Press. Oates, ed., "The Aerothermodynamics of Aircraft Gas Turbine Engines," AFAPL-TR-78-52, 1978. Fleeter, "Aeroelasticity for Turbomachine Applications," *AIAA J. of Aircraft*, **16**, no. 5, 1979. Bathie, "Fundamentals of Gas Turbines," Wiley. Hagar and Vrabel, "Advanced Turboprop Project," *NASA SP 495*, 1988. "Aeronautical Technologies for the Twenty-First Century," National Academy Press. Mattingly, Heiser, and Daley, "Aircraft Engine Design," AIAA.

Newton's reaction principle, based on the second and third laws of motion, is the theoretical basis for all methods of propelling a body either in (or on) a fluid medium or in space. Thus, the aircraft propeller, the ships screw, and the jet propulsion of aircraft, missiles, and boats are all examples of the application of the reaction principle to the propulsion of vehicles. Furthermore, all jet engines belong to that class of power plants known as **reaction engines**.

Newton's second law states that a change in motion is proportional to the force applied; i.e. a force proportional to the rate of change of the velocity results whenever a mass is accelerated: $F = ma$. This can be expressed in a more convenient form as $F = d(mv)/dt$, which makes it clear that the application of the reaction principle involves the time rate of increase of the momentum (mv) of the body. It should be noted that the same force results from either providing a small acceleration to a large mass or a large acceleration to a small mass.

Newton's third law defines the fundamental principle underlying all means of propulsion. It states that for every force acting on a body there is an equal and opposite reaction force.

The application of this reaction principle for propulsion involves the indirect effect of increasing the momentum of a mass of fluid in one direction and then utilizing the reaction force for propulsion of the vehicle in the opposite direction. Thus, the reaction to the time rate of increase of the momentum of that fluid, called the **propulsive fluid**, creates a force, termed the **thrust**, which acts in the direction of motion desired for the propelled vehicle. The known devices for achieving the propulsion of bodies differ only in the methods and mechanisms for achieving the time rate of increase in the momentum of the propulsive fluid or matter.

The function of a propeller is to convert the power output of an engine into useful thrust. To do this it accelerates a mass of air in the direction opposite to the direction of flight, generating thrust via Newton's reaction principle. Figure 11.5.1 illustrates schematically, in the relative coordinate system for steady flow, the operating principle of the **ideal aircraft propeller**. Power is supplied to the propeller, assumed to be

equivalent to an **actuator disk**, which imparts only an axial acceleration to the air flowing through it. The rotation of the actuator disk produces a **slipstream** composed of the entire mass of air flowing in the axial direction through the area of the actuator disk, i.e., the circle swept by the propeller. Atmospheric air enters the slipstream with the flight speed V_0 and mass flow rate m_0 . It leaves the slipstream with the **wake velocity** w . The thrust is given in Eq. (11.5.5). Propulsion systems utilizing propellers will be termed **propeller propulsion**. (For detailed discussions of the airplane propeller, see the section "Aircraft Propellers.")

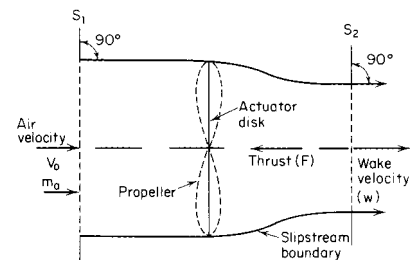


Fig. 11.5.1 Ideal propeller in the relative coordinate system.

Jet propulsion differs from propeller propulsion in that the propulsive fluid (or matter), instead of being caused to flow around the propelled body, is ejected from within the propelled body in the form of one or more high-speed jets of fluid or particles. In fact, the jet propulsion engine is basically designed to accelerate a large stream of fluid (or matter) and to expel it at a high velocity. There are a number of ways of accomplishing this, but in all instances the resultant reaction or thrust exerted on the engine is proportional to the time rate of increase of the momentum of the fluid. Thus, jet engines produce thrust in an analogous manner to the propeller and engine combination. While the propeller gives a small acceleration to a large mass of air, the jet engine gives a larger acceleration to a smaller mass of air.

Theoretically, there are no restrictions on either the type of matter, called the **propellant**, for forming a high-velocity jet or the means for producing the **propulsive jet**. The selection of the most suitable propellant and the most appropriate jet propulsion engine is dictated by the specific mission for the propelled vehicle. For example, in the case of the jet propulsion of a boat, termed **hydraulic jet propulsion**, the propulsive jet is formed from the water on which the boat moves. For the practical propulsion of bodies through either the atmosphere or in space, however, only two types of propulsive jets are suitable:

1. For propulsion within the atmosphere, there is the jet formed by expanding a highly heated, compressed gas containing atmospheric air as either a major or a sole constituent. Such an engine is called either an

11-82 JET PROPULSION AND AIRCRAFT PROPELLERS

airbreathing or a **thermal-jet engine**. If the heating is accomplished by burning a fuel in the air, the engine is a **chemical thermal-jet engine**. If the air is heated by direct or indirect heat exchange with a nuclear-energy source, the engine is termed a **nuclear thermal-jet engine**.

2. For propulsion both within and beyond the atmosphere of earth, there is the exhaust jet containing no atmospheric air. Such an exhaust jet is termed a **rocket jet**, and any matter used for creating the jet is called a **propellant**. A rocket may consist of a stream of gases, solids, liquids, ions, electrons, or a plasma. The assembly of all the equipment required for producing the rocket jet constitutes a **rocket engine**.

Modern airbreathing engines may be segregated into two principal types: (1) **ramjet engines**, and (2) **turbojet engines**. The turbojet engines are of two types: (1) the **simple turbojet engine**, and (2) the **turbofan**, or **bypass engine**.

Rocket engines can be classified by the form of energy used for achieving the desired jet velocity. The three principal types of rocket engines are (1) **chemical rocket engines**, (2) **nuclear heat-transfer rocket engines**, and (3) **electric rocket engines**.

The propulsive element of a jet-propulsion engine, irrespective of type, is the **exhaust nozzle** or orifice. If the exhaust jet is gaseous, the assembly comprising all the other components of the jet-propulsion engine constitutes a gas generator for supplying highly heated, high-pressure gases to the exhaust nozzle.

These classifications of jet-propulsion engines apply to the basic types of engines. It is possible to have combinations of the different types of thermal-jet engines and also combinations of thermal-jet engines with rocket engines; only the principal types are discussed here.

ESSENTIAL FEATURES OF AIRBREATHING OR THERMAL-JET ENGINES

In the subsequent discussions a *relative coordinate system* is employed wherein the atmospheric air flows toward the propulsion system with the flight speed V_0 , and the gases leave the propulsion system with the velocity w , *relative to the walls of the propulsion system*. Furthermore, steady-state operating conditions are assumed.

Ramjet Engine Figure 11.5.2 illustrates schematically the essential features of the simple ramjet engine. It comprises three major components: a diffusion or inlet system, (0–2); a combustion chamber (2–7); and an exhaust nozzle (7–9). In this simple ramjet engine, apart from the necessary control devices, there are no moving parts. However, for accelerating the vehicle or for operating at different Mach numbers, a variable geometry diffuser and exhaust may be required.

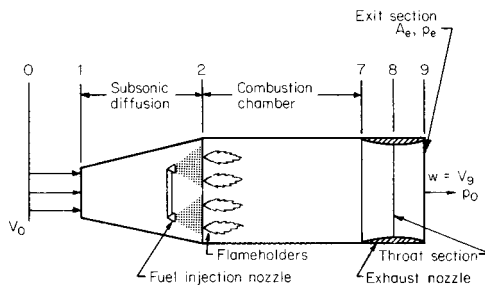


Fig. 11.5.2 Ramjet engine.

The operating principle of the ramjet engine is as follows. The free-stream air flowing toward the engine with a velocity V_0 and Mach number M_0 is decelerated by the inlet diffuser system so that it arrives at the entrance to the combustion chamber with a low Mach number, on the order of $M_2 = 0.2$. When the inlet-flow Mach number is supersonic, this diffuser system consists of a supersonic diffuser followed by a subsonic diffuser. The supersonic diffuser decelerates the inlet flow to approximately unity Mach numbers at the entrance to the subsonic diffuser; this deceleration is accompanied by the formation of shock waves and by an increase in the pressure of the air (diffusion). In the subsonic

diffuser the air is further diffused so that it arrives at the entrance to the combustion chamber with the required low Mach number. If P_0 is the total pressure of the free-stream air having the Mach number M_0 and P_2 that for the air entering the combustion system with the Mach number M_2 , then it is desirable that P_2/P_0 be a maximum.

In the combustion chamber a fuel is burned in the air, thereby raising the total temperature of the gases entering the exhaust nozzle (see Sec. 7) to approximately $T_7 = 4260^\circ\text{R}$ (2366 K). Most generally a liquid hydrocarbon fuel is used, but experiments have been conducted with solid fuels, liquid hydrogen, liquid methane, and "slurries" of metallic fuels in a liquid fuel. The combustion process is not quite isobaric because of the pressure drops in the combustion chamber, because of the increase in the momentum of the working fluid due to heat addition, and because of friction. The hot gases are discharged to the atmosphere, after expanding in the exhaust nozzle, with the relative velocity $w = V_g$.

Since the ramjet engine can function only if there is a ram pressure rise at the entrance to the combustion chamber, it is not self-operating at zero flight speed. It must, therefore, be accelerated to a flight speed which permits the engine to develop sufficient thrust for accelerating the vehicle it propels to the design flight Mach number. Consequently, a ramjet-propelled missile, for example, must either be launched by dropping it from an airplane or be **boosted** to the required flight speed by means of **launching**, or **booster**, rockets. It appears that the most appropriate flight regime for the ramjet is at low to moderate supersonic Mach numbers, between approximately $M_0 = 2$ and 5. The lower limit is associated with the necessary ram pressure rise while the upper limit is set by the problem of either cooling or protecting the outer skin of the engine body.

Scramjet Low-cost access to space is one of the major reasons for the interest in **hypersonic propulsion** (speeds above Mach 5). A vehicle to provide access to space must be capable of reaching very high Mach numbers, since orbital velocity (17,000 mi/h) is about Mach 24. The ramjet engine, which must slow the entering air to a low subsonic velocity, cannot be used much above Mach 5 or 6. The solution is to decelerate the flow in the engine to a supersonic Mach number lower than the flight Mach number but greater than the local speed of sound. This propulsion device is the **supersonic combustion ramjet**, or **scramjet**, which is capable, in principle, of operation to Mach 24. As shown schematically in Fig. 11.5.3, in contrast to the ramjet, the scramjet en-

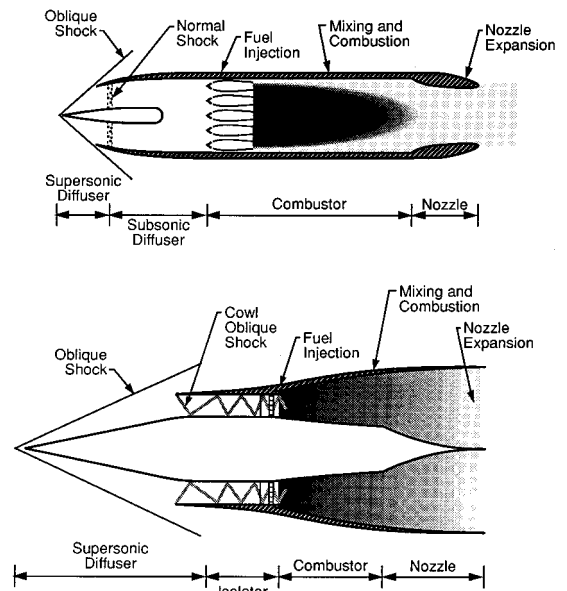


Fig. 11.5.3 Ramjet and scramjet flow configurations.

gine requires that fuel be added to the air, mixed, and burned, all at supersonic velocities, which is a significant technical challenge.

The advantage derived from supersonic combustion of the liquid fuel (usually liquid hydrogen) is that the diffuser of the scramjet engine is required to decelerate the air entering the engine from M_0 to only approximately $M_2 = 0.35 M_0$ instead of the $M_2 = 0.2$, which is essential with subsonic combustion. This elimination of the subsonic diffusion increases the diffuser efficiency, reduces the static pressure in the combustor (and, therefore, the engine weight and heat transfer rate), and increases the velocity in the combustor (thereby decreasing engine frontal area). It is the combination of the above effects that makes ramjet propulsion at high flight Mach numbers (>7) feasible.

Pulsejets may be started and operated at considerably lower speeds than ramjets. A pulsejet is a ramjet with an air inlet which is provided with a set of shutters loaded to remain in the closed position. After the pulsejet engine is launched, ram air pressure forces the shutters to open, fuel is injected into the combustion chamber, and is burned. As soon as the pressure in the combustion chamber equals the ram air pressure, the shutters close. The gases produced by combustion are forced out the jet nozzle by the pressure that has built up within the chamber. When the pressure in the combustion chamber falls off, the shutters open again, admitting more air, and the cycle repeats at a high rate.

Simple Turbojet Engine Figure 11.5.4 illustrates schematically the principal features of a simple turbojet engine, which is basically a gas-turbine engine equipped with a propulsive nozzle and diffuser. Atmospheric air enters the engine and is partially compressed in the diffusion system, and further compressed to a much higher pressure by the air compressor, which may be of either the axial-flow or centrifugal type. The highly compressed air then flows to a combustion chamber wherein sufficient fuel is burned to raise the total temperature of the gases entering the turbine to approximately $T_4 = 2160^\circ\text{R}$ (1200 K) for an uncooled turbine. The maximum allowable value for T_4 is limited by metallurgical and stress considerations; it is desirable, however, that T_4 be as high as possible. The combustion process is approximately isobaric. The highly heated air, containing approximately 25 percent of combustion products, expands in the turbine, which is directly connected to the air compressor, and in so doing furnishes the power for driving the air compressor. From the turbine the gases pass through a tailpipe which may be equipped with an **afterburner**. The gases are expanded in a suitably shaped exhaust nozzle and ejected to the atmosphere in the form of a high-speed jet.

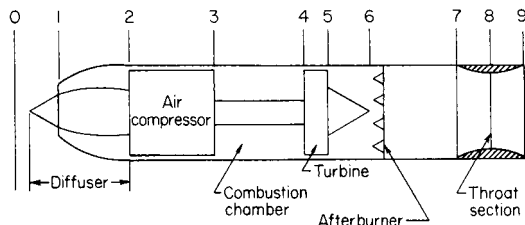


Fig. 11.5.4 Simple turbojet engine.

Like the ramjet engine, the turbojet engine is a continuous-flow engine. It has an advantage over the ramjet engine in that its functioning does not depend upon the ram pressure of the entering air, although the amount of ram pressure recovered does affect its overall economy and performance. The turbojet is the only airbreathing jet engine that has been utilized as the sole propulsion means for piloted aircraft. It appears to be eminently suited for propelling aircraft at speeds above 500 mi/h (805 km/h). As the design flight speed is increased, the ram pressure increases rapidly, and the characteristics of the turbojet engine tend to change over to those of the ramjet engine. Consequently, its top speed appears to be limited to that flight speed where it becomes more advantageous to employ the ramjet engine. It appears that for speeds above approximately 2,000 mi/h (3,219 km/h) it is advantageous to use some form of a ramjet engine.

The thrust of the simple turbojet engine increases rapidly with T_4 , because increasing T_4 increases the jet velocity V_j . Actually, V_j increases faster than the corresponding increase in T_4 . It is also an inherent characteristic of the gas-turbine engine which produces shaft power, called a **turboshaft** engine, that its useful power increases proportionally faster than a corresponding increase in its turbine inlet temperature T_4 . Because of the decrease in strength of turbine materials with increase in temperature, the turbine blades, stators, and disks require cooling at $T_4 > 2160^\circ\text{R}$ (1200 K) approximately. T_4 values are currently in the 2860 to 3260°R (1589 to 1811 K) range, and are being pushed toward the 4,600°R (2556 K) **stoichiometric** limit of JP4 fuel. The cooling air is bled from the compressor at the appropriate stage (or stages) and used to cool the stator blades or rotor blades by convective, film, or transpiration heat transfer. Up to 10 percent of the compressor air may be bled for turbine cooling, and this air is "lost" for turbine work for that blade row where it is used for cooling. Consequently "trade" studies must be made to "weigh" the increased complexity of the engine and the turbine work loss due to air bleed against the increased engine performance associated with increased T_4 .

As in the case of any gas-turbine power plant, the efficiencies of the components of the turbojet engine have an influence on its performance characteristics, but its performance is not nearly as sensitive to changes in the efficiency of its component machines as is a gas turbine which delivers shaft power. (See Sec. 9.)

As noted previously, two types of compressors are currently employed, the axial-flow compressor and the centrifugal compressor. Irrespective of the type, the objectives are similar. The compressor must be reliable, compact, easy to manufacture, and have a small frontal area. Because of the limited air induction capacity of the centrifugal compressor, also called the radial compressor, engines for developing thrusts above 7,000 lb (31 kN) at static sea level employ axial-flow compressors (see Sec. 14).

The turbojet engine exhibits a rather flat thrust-versus-speed curve. Because the ratio of the takeoff thrust to thrust in flight is small, certain operational problems exist at takeoff. Since the exhaust gases from the turbine contain considerable excess air, the jet velocity, and consequently the thrust, can be increased by burning additional fuel in the tailpipe upstream from the exhaust nozzle. By employing "**tailpipe burning**," or "**afterburning**," as it is called, the thrust can be increased by 35 percent and at 500 mi/h, in a tactical emergency, by approximately 60 percent. With afterburning, the temperature of the gases entering the nozzle T_7 , is of the order of 3800°R (2110 K).

Turbofan, or Bypass, Engine For a fixed turbine inlet temperature, the jet velocity from a simple turbojet engine propelling an airplane at subsonic speed is relatively constant. The propulsive efficiency depends on the ratio of the flight speed to the jet velocity and increases as the ratio increases. On the other hand, the thrust depends on the difference between the jet velocity and the flight speed; the larger the difference, the larger the thrust per unit mass of air induced into the engine. By reducing the jet velocity and simultaneously increasing the mass rate of airflow through the engine, the **propulsive efficiency** can be increased without decreasing the thrust. To accomplish this, a **turbofan** or **bypass engine** is required.

Figure 11.5.5 illustrates schematically the components of a turbofan engine. There are two turbines, a low-pressure turbine (LPT) and a high-pressure turbine (HPT); one drives the air compressor of the hot-gas generator and the other drives the fan. Air enters the fan at the rate of \dot{m}_{aF} and is ejected through the nozzle of area A_{7F} with the jet velocity $V_{jF} < V_j$, where V_j is the jet velocity attained by the air flowing through the hot-gas generator with the mass flow rate \dot{m}_{a1} ; the hot-gas generator is basically a turbojet engine.

A key parameter is the **bypass ratio**, defined as the ratio of the air mass flow rate through the fan bypass duct to that through the hot-gas generator ($\dot{m}_{aF}/\dot{m}_{a1}$). Bypass ratios of about 5 to 10 are in use, with values of about 5 utilized in modern large commercial transport engines, for example, the Pratt & Whitney 4000 and the General Electric CF-6. The hot-gas generator is basically a turbojet engine. The fuel is added to \dot{m}_{a1} at the rate \dot{m}_f . The hot-gas stream ($\dot{m}_{a1} + \dot{m}_f$) is discharged to the

11-84 JET PROPULSION AND AIRCRAFT PROPELLERS

atmosphere through A_7 with the velocity V_j . Both types of turbofan engine produce an "overall" jet velocity V_{jTF} which is smaller than that for a turbojet engine operating with the same P_3/P_2 and T_4 . The arrangements shown in Fig. 11.5.5 are for subsonic propulsion. Fuel can, of course, be burned in the fan air m_{aF} for increasing the thrusts of the

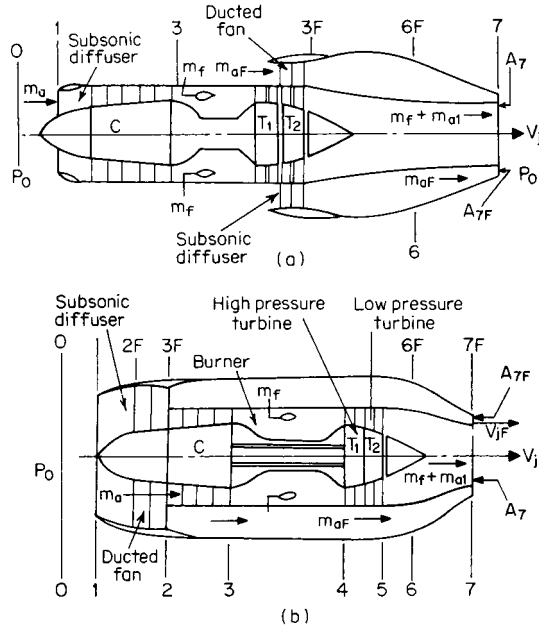


Fig. 11.5.5 Two different schematic arrangements of components of turbofan engines (subsonic flight). (a) Aft-fan turbofan engine; (b) ducted-fan turbofan engine.

engines. Practically all the newer commercial passenger aircraft are propelled by turbofan engines, and most of the older jet aircraft have been refurbished with new turbofan engines. The advantage of the lower effective jet velocity V_{jTF} is twofold: (1) It increases the propulsive efficiency η_p by reducing $v = V_{jTF}/V_0$ and, consequently, raises the value of η_0 . (2) The reduced jet velocity reduces the jet noise; the latter increases with approximately the eighth power of the jet speed.

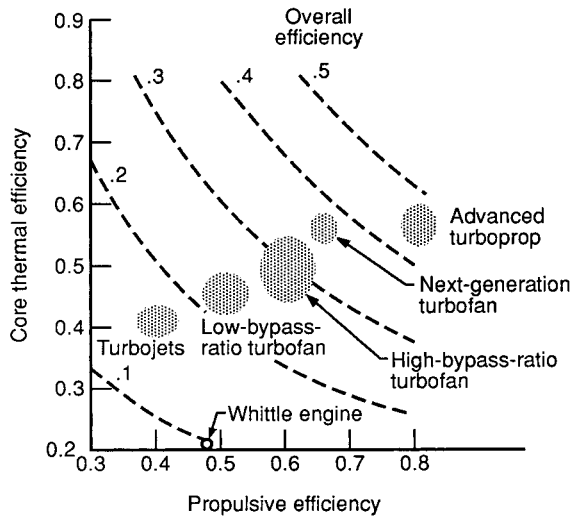


Fig. 11.5.6 Efficiency trends.

The next generation of large transport engines will be conventional high-bypass engines, but will have a larger thrust capability and will offer further improvements in specific fuel consumption, achieved by using even higher overall pressure ratios (over 40:1) and turbine inlet temperature (over 1850 K or 2870°F) combined with even more efficient components (Fig. 11.5.6). Beyond these conventional high-bypass engines, will be the **ultrahigh-bypass-ratio** engine in either a ducted or open rotor form (Fig. 11.5.7). The ducted ultrahigh-bypass-ratio engine features a counterrotating, reversible-pitch fan powered by a geared core engine with an overall 80:1 cycle pressure ratio. It is likely to be used on the larger aircraft, since it does not restrain the aircraft configuration or flight speed and will provide a 35 percent improvement in fuel burned over the most advanced current subsonic high-bypass engines.

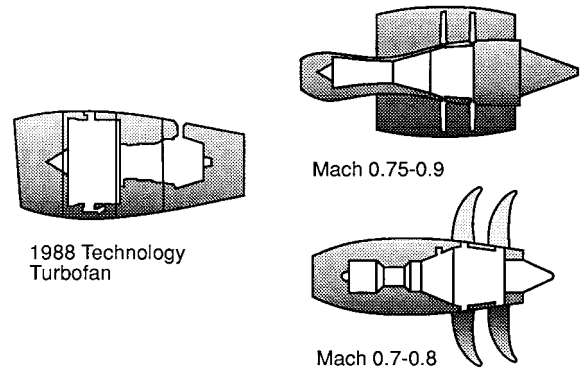


Fig. 11.5.7 Ultrahigh-bypass-ratio engine configurations.

A highly loaded, multiblade swept variable-pitch propeller, the **propfan** or **advanced turboprop**, could be combined with the latest turbine engine technology. The resulting advanced turboprop would offer a potential fuel saving of 50 percent over an equivalent-technology turbofan engine operating at competitive speeds and altitudes because of the turboprop's much higher installed efficiency. To eliminate the gearbox development for a 20,000 shaft horsepower engine, the propfans of the **unducted fan (UDF)** engine were directly driven with counterrotating turbine stages, a unique concept (Fig. 11.5.8). The projected specific

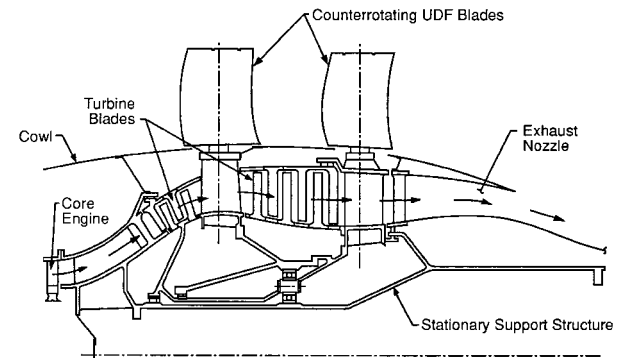


Fig. 11.5.8 UDF counterrotating turbine configuration.

fuel consumption at cruise for the resulting gearless, counterrotating UDF engine was 30 percent lower than that of the most modern turbofan engines, and about 50 percent lower than that of engines presently in use on 150-passenger airplanes. The tremendous fuel-saving potential of the turboprop has already been demonstrated. If economic conditions change, this concept could replace conventional high-bypass-ratio turbofans on small aircraft and military transports.

ESSENTIAL FEATURES OF ROCKET ENGINES

Figure 11.5.9 is a block-type diagram illustrating the essential features of a rocket engine, which comprises three main components: (A) a supply of propellant material contained in the rocket-propelled vehicle, (B) a propellant feed and metering system, and (C) a thrust chamber, also called a **rocket motor**, **thrustor**, or **accelerator**. In any rocket engine, energy must be added to the propellant as it flows through the thrustor.

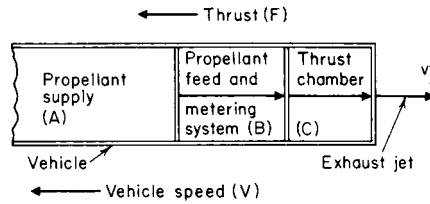


Fig. 11.5.9 Essential features of a rocket engine.

In Figure 11.5.9 propellant material from the supply is metered and fed to the thrust chamber, where energy is added to it. As a consequence of the energy addition, the propellant is discharged from the thrustor with the jet velocity V_j . The thrustor F acts in the direction opposite to that for the jet velocity V_j .

Chemical Rocket Engines

All chemical rocket engines have two common characteristics: (1) They utilize chemical reactions in a thrust chamber to produce a high-pressure, high-temperature gas at the entrance to a converging-diverging exhaust nozzle; (2) the hot propellant gas expands in flowing through the exhaust nozzle, and the expansion process converts a portion of the thermal energy, released by the chemical reaction, into the kinetic energy associated with a high-velocity gaseous-exhaust jet. Chemical rocket engines may be grouped into (1) liquid-bipropellant rocket engines, (2) liquid-monopropellant rocket engines, and (3) solid-propellant rocket engines.

Liquid-Bipropellant Rocket Engine Figure 11.5.10 illustrates the essential features of a liquid-bipropellant rocket engine employing **turbopumps** for feeding two propellants, an **oxidizer** and a **fuel**, to a rocket motor. The motor comprises (1) an injector, (2) a combustion chamber, and (3) a converging-diverging exhaust nozzle. The liquid propellants are fed under pressure, through the injector, into the combustion chamber, where they react chemically to produce large volumes of

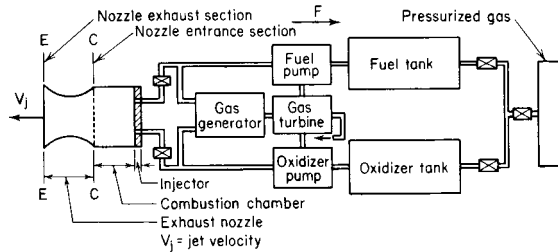


Fig. 11.5.10 Essential features of a liquid-bipropellant rocket engine.

high-temperature, high-pressure gases. For a given propellant combination, the **combustion temperature** T_c depends primarily on the oxidizer-fuel ratio (by weight), termed the **mixture ratio**, and to a lesser extent upon the combustion static pressure p_c . When the mass rate of flow of the liquid propellants equals that of the exhaust gases, the combustion pressure remains constant—the mode of operation that is usually desired.

If the bipropellants react chemically when their liquid streams come in contact with each other, they are said to be **hypergolic**. Propellants which are not hypergolic are said to be **diergolic**, and some form of ignition system is required to initiate combustion.

Except in those cases where the operating duration of the rocket motor is very short or where the combustion temperature is low, means must be provided for protecting the interior walls of the motor. The two most common methods are **ablative cooling** and **regenerative cooling**. In **ablative cooling** the inner surfaces of the thrust chamber are covered with an ablative material which vaporizes, thereby providing some cooling. Ordinarily, the material leaves a "char" which acts as a high-temperature insulating material. For high-performance engines which are to operate for relatively long periods, regenerative cooling is employed. In **regenerative cooling**, one of the propellants is circulated around the walls before injection into the motor. In some engines the regenerative cooling is combined with local liquid film cooling at critical areas of the thrust chamber. See Table 11.5.1 for bipropellant combinations.

Refer to Figure 11.5.10. By removing the oxidizer tank, the oxidizer pump, and the plumbing associated with the liquid oxidizer, one obtains the essential elements of a liquid-monopropellant rocket engine. Such an engine does not require a liquid oxidizer to cause the monopropellant to decompose and release its thermochemical energy.

There are basically three groups of monopropellants: (1) liquids which contain the fuel and oxidizer in the same molecule, e.g., hydrogen peroxide (H_2O_2) or nitromethane (CH_3NO_2); (2) liquids which contain either the oxidizer or the fuel constituent in an unstable molecular arrangement, e.g., hydrazine (N_2H_4); and (3) synthetic mixtures of liquid fuels and oxidizers. The most important liquid monopropellants are hydrazine and hydrogen peroxide (up to 98% H_2O_2). Hydrazine can be decomposed by a suitable metal catalyst, which is ordinarily packed in a portion of the thrust chamber at the injector end. The decomposition of hydrazine yields gases at a temperature of 2260°R (1265 K); the gases are a mixture of hydrogen and ammonia. Hydrogen peroxide can be readily decomposed either thermally, chemically, or catalytically. The most favored method is catalytically; a series of silver screens coated with samarium oxide is tightly packed in a decomposition chamber located at the injector end of the thrust chamber. At $P_c = 300$ psia, the decomposition of hydrogen peroxide (98%) yields gases having a temperature of 2260°R (1256 K).

The specific impulse obtainable for a liquid monopropellant is considerably smaller than that obtainable from liquid-bipropellant systems. Consequently, monopropellants are used for such auxiliary purposes as thrust vernier control, attitude reaction controls for space vehicles and missiles, and for gas generation.

Solid-propellant Rocket Engine Figure 11.5.11 illustrates schematically a solid-propellant rocket engine employing an **internal-burning case-bonded grain**; the latter burns radially outward at a substantially

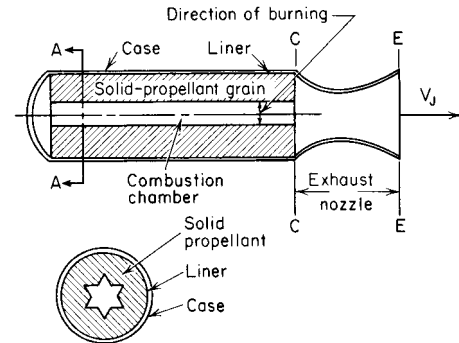


Fig. 11.5.11 Essential features of an internal-burning case-bonded solid-propellant rocket engine.

constant rate. A solid propellant contains both its fuel and the requisite oxidizer. If the fuel and oxidizer are contained in the molecules forming the solid propellant, the propellant is termed a **double-base propellant**. Those solid propellants wherein a solid fuel and a solid oxidizer form an intimate mechanical mixture are termed either **composite** or **heterogeneous** solid propellants. The chemical reaction of a solid propellant is

11-86 JET PROPULSION AND AIRCRAFT PROPELLERS

Table 11.5.1 Calculated Values of Specific Impulse for Liquid Bipropellant Systems^a
 $[P_c = 1,000 \text{ lbf/in}^2 (6,896 \times 10^3 \text{ N/m}^2) \text{ to } P_c = 1 \text{ atm}]$
 Shifting equilibrium; isentropic expansion; adiabatic combustion; one-dimensional flow

Oxidizer	Fuel	\dot{m}_o/\dot{m}_f	ρ	Temperature T_c		c^*	I (s)
				$^{\circ}\text{R}$	K		
Chlorine trifluoride (CTF) (ClF_3)	Hydrazine	2.80	1.50	6553	3640	5961	293.1
	MMH ^b	2.70	1.41	5858	3254	5670	286.0
	Pentaborane (B_5H_9)	7.05	1.47	7466	4148	5724	289.0
Fluorine (F_2)	Ammonia	3.30	1.12	7797	4332	7183	359.5
	Hydrazine	2.30	1.31	8004	4447	7257	364.0
	Hydrogen	7.70	0.45	6902	3834	8380	411.1
	Methane	4.32	1.02	7000	3889	6652	343.8
	RP-1	2.62	1.21	6839	3799	6153	318.0
Hydrogen peroxide (100% H_2O_2)	Hydrazine	2.00	1.26	4814	2674	5765	287.4
	MMH	3.44	1.26	4928	2738	5665	284.8
IRFNA ^c	Hydine ^d	3.17	1.26	5198	2888	5367	270.3
	MMH	2.57	1.24	5192	2885	5749	275.5
Nitrogen tetroxide (N_2O_4)	Hydrazine	1.30	1.22	5406	3002	5871	292.2
	Aerozine-50 ^e	2.00	1.21	5610	3117	5740	289.2
	MMH	2.15	1.20	5653	3141	5730	288.7
Oxygen (LOX) (O_2)	Hydrazine	0.91	1.07	5667	3148	6208	312.8
	Hydrogen	4.00	0.28	4910	2728	7892	291.2
	Methane	3.35	0.82	6002	3333	6080	310.8
	Pentaborane	2.21	0.91	7136	3964	6194	318.1
	RP-1	2.60	1.02	6164	3424	5895	300.0

^a Based on "Theoretical Performance of Rocket Propellant Combinations," Rocketdyne Corporation, Canoga Park, CA.
^b MMH: Monomethyl hydrazine ($\text{N}_2\text{H}_3\text{CH}_3$).
^c IRFNA: Inhibited red fuming nitric acid; 84.4% (HNO_3), 14% (N_2O_4), 1% (H_2O), 0.6% (HF).
^d Hydine: 60% UDMH^f, 40% Deta^g.
^e Aerozine-50: 50% UDMH^f, 50% hydrazine (N_2H_4).
^f UDMH: Unsymmetrical dimethylhydrazine (CH_3)₂ N_2H_4 .
^g DETA: Diethylenetriamine ($\text{C}_2\text{H}_{13}\text{N}_3$).

initiated by an igniter. In general, the configuration of a propellant grain can be designed so that the area of the burning surface of the propellant varies to give a prescribed thrust-versus-time curve.

Nuclear Heat-transfer Rocket Engine

Figure 11.5.12 illustrates schematically a nuclear heat-transfer rocket engine employing a **solid-core reactor**. The heat generated by the fissions of the uranium nucleus is utilized for heating a gaseous propellant, such as hydrogen, to a high temperature of 4000°R (2200 K) approx at the entrance section of the exhaust nozzle. The hot gas is ejected to the surroundings after expansion in a converging-diverging exhaust nozzle. The basic difference between the operating principles of a nuclear heat-transfer and a chemical rocket engine is the substitution of nuclear fission for chemical reaction as the source of heat for the propellant gas. Since the exhaust nozzle is the propulsive element, the remaining components of the nuclear heat-transfer rocket engine constitute the hot-gas generator.

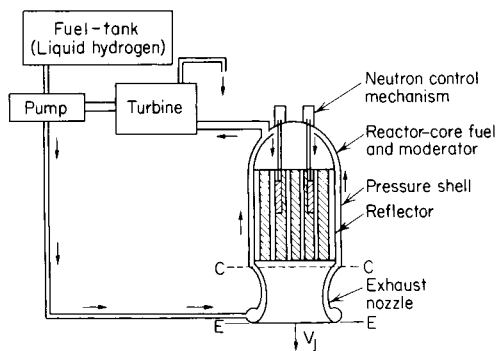


Fig. 11.5.12 Schematic arrangement of a nuclear heat-transfer rocket engine.

The propellant in a nuclear heat-transfer rocket engine functions basically as a fluid for cooling the solid-core nuclear reactor. Its reaction is not based on energy considerations alone, but on such properties as specific heat, latent heat, molecular weight, and liquid density and on certain practical considerations.

Electric Rocket Engines

Several different types of electric rocket engines have been conceived; the principal types are described below. All of them require some form of power plant for generating electricity. Thus the power plant may be nuclear, solar-cell batteries, thermoelectric, or other. The choice of the type of power plant depends upon the characteristics of both the electric rocket engine and the space-flight mission. Figure 11.5.13 illustrates diagrammatically an electric rocket engine, comprising (1) a **nuclear power source**, (2) an energy-conversion unit for obtaining the desired form of electric energy, (3) a propellant feed and metering system, (4) an electrically operated thruster, and (5) the requisite control devices. Electric rocket engines may be classified as (1) electrothermal, (2) electromagnetic, and (3) electrostatic.

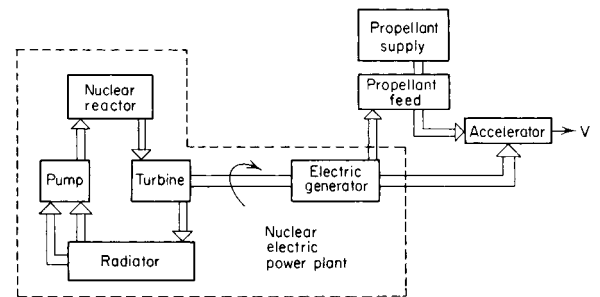


Fig. 11.5.13 Essential features of an electric rocket engine.

Electrothermal Rocket Engine Figure 11.5.14a illustrates the type of engine which uses electric power for heating gaseous propellant to a high temperature before ejecting it through a converging-diverging exhaust nozzle. If an electric arc is employed for heating the propellant, the engine is called a **thermal arc-jet rocket engine**.

Electromagnetic Rocket Engine Figure 11.5.14b illustrates an electromagnetic, or plasma, rocket engine. There is a wide variety of such engines, but all of them utilize the same operating principle. A plasma (a neutral ionized conducting gas) is accelerated by means of its interaction with either a stationary or a varying magnetic field. Basically, a plasma engine differs from a conventional electric motor by the substitution of a conducting plasma for a moving armature.

Electrostatic Rocket Engine Figure 11.5.14c illustrates schematically the electrostatic, or ion, rocket engine, comprising (1) an electric power plant; (2) a propellant supply; (3) ionization apparatus; (4) an ion accelerator; and (5) an electron emitter for **neutralizing** the ion beam ejected from the accelerator. Its operating principle is based on utilizing electrostatic fields for accelerating and ejecting electrically charged particles with extremely large velocities. The overall objective is to transform thermal energy into the kinetic energy associated with an extremely high-velocity stream of electrically neutral particles ejected from one or more thrusters. **Mercury ion engines** are currently being tested. The engine provides thrust by a rapid, controlled discharge of ions created by the ionization of atoms of the mercury fuel supply. Solar cells convert sunlight into electricity, which is then used to bombard the mercury with free electrons. This causes one electron to be stripped from each mercury atom, resulting in ionized mercury atoms. The ions mix with other mercury atoms to form a plasma. A magnetic field set up between two metal screens at the aft end of the engine draws the positively charged ions from the plasma and accelerates them at very high exit speeds out the back of the engine. This creates a high-velocity exit beam producing low-level but extremely long-term thrust.

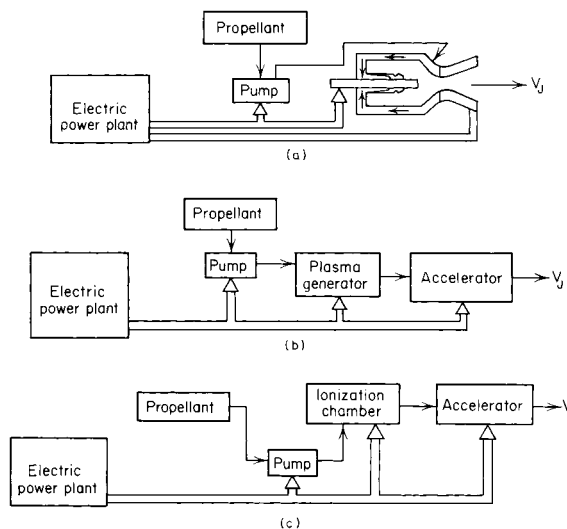


Fig. 11.5.14 Electric rocket engine. (a) Electrothermal rocket engine. (b) electromagnetic rocket engine. (c) electrostatic (ion) engine.

All electric rocket engines are low-thrust devices. The interest in such engines stems from the fact that chemical-rocket technology, for example, the space shuttle, is now so advanced that it has become feasible to place heavy *payloads*, such as a satellite equipped with an electric rocket engine, into an earth orbit. An electric rocket engine which is virtually inoperable terrestrially can be positioned in space and can then operate effectively because of the absence of aerodynamic drag and strong gravitational fields. Consequently, if a vehicle equipped with an

electric rocket engine is placed in an earth orbit, the low-thrust electric rocket engine, under the conditions in space, will accelerate it to a large vehicle velocity if the operating time for the engine is sufficiently long.

In a chemical rocket engine, the energy for propulsion, as well as the mass ejected through the exhaust nozzle, is provided by the propellants, but the energy which can be added to a unit mass of the propellant gas is a fixed quantity, limited by the nature of the chemical bonds of the reacting materials. For that reason, chemical rocket engines are said to be **energy-limited rocket engines**. Although a nuclear heat-transfer rocket engine is also energy-limited, the limitation is imposed by the amount of energy that can be added per unit mass of propellant without exceeding the maximum allowable temperature for the materials employed for the solid-core reactor.

In an electric rocket engine, on the other hand, the energy added to the propellant is furnished by an electric power plant. The power available for heating the propellant is limited by the maximum power output of the electric power plant, accordingly, electric rocket engines are **power-limited**.

Notation

- a = acoustic speed
- a_0 = acoustic speed in free-stream air
- a_2 = burning rate constant for solid propellant
- A_e = cross-sectional area of exit section of exhaust nozzle
- A_p = area of burning surface for solid propellant
- A_t = cross-sectional area of throat of exhaust nozzle
- c_p = specific heat at constant pressure
- c_v = specific heat at constant volume
- $c^* = P_c A_t / \dot{m}$ = characteristic velocity for rocket motor
- C_d = discharge coefficient for exhaust nozzle
- C_F = thrust coefficient
- C_{Fg} = gross-thrust coefficient for ramjet engine
- C_{Fn} = net thrust coefficient
- D or \mathcal{D} = drag
- $D_i = \dot{m}_a V_0$ = ram drag for airbreathing or thermal-jet engine
- d = diameter
- d_p = diameter of propeller
- E_{in} = rate at which energy is supplied to propulsion system
- E_f = calorific value of fuel
- E_p = calorific value of rocket propellants
- $f = \dot{m}_f / \dot{m}_a$ = fuel-air ratio
- $f' = f / \eta_B$ = fuel-air ratio for ideal combustion chamber
- F = force or thrust
- $F_i = m_e w - m_i V_0 + (p_e - p_0) A_e$ = thrust due to internal flow
- $F_j = m_e V_j$ = jet thrust
- $F_p = (p_e - p_0) A_e$ = pressure thrust
- $F = F_i$ = gross thrust for ramjet engine
- $F_g SFC_g$ = gross-thrust specific-fuel consumption for ramjet engine
- g_c = correction factor defined by Newton's second law of motion
- h = static specific enthalpy
- Δh_n = enthalpy change for exhaust nozzle
- H = total (stagnation) specific enthalpy
- ΔH_c = lower heating value of fuel
- I = specific impulse
- $I_a = F / g m_a$ = air specific impulse
- J = mechanical equivalent of heat; advance ratio, propeller
- $k = c_p / c_v$ = specific heat ratio
- L or \mathcal{L} = lift
- \mathcal{M} = mass
- m = mass rate of flow
- \dot{m}_a = mass rate of air consumption for thermal-jet engine
- \dot{m}_e = mass rate of flow of gas leaving propulsion system
- \dot{m}_f = mass rate of fuel consumption
- \dot{m}_i = mass rate of flow of gas into propulsion system
- \dot{m}_o = mass rate of oxidizer consumption for rocket engine
- $\dot{m}_p = \dot{m}_o + \dot{m}_f$ = mass rate of propellant consumption for rocket engine

11-88 JET PROPULSION AND AIRCRAFT PROPELLERS

\bar{m} = molecular weight
 M_e = momentum of gases leaving propulsion system in unit time
 M_i = momentum of gases entering propulsion system in unit time
 $M_0 = V_0/a_0$ = Mach number of free-stream air (flight speed)
 n = revolutions per unit time
 p = absolute static pressure; pitch of propeller blade
 p_c = absolute static pressure of gases in combustion chamber
 p_e = absolute static pressure in exit section of exhaust nozzle
 p_0 = absolute static pressure of free-stream ambient air
 P = absolute total (stagnation) pressure
 P_c = absolute total pressure at entrance to exhaust nozzle
 $P_0 = p_0 \left(1 + \frac{k-1}{2} M_0^2 \right)^{k/(k-1)}$ = absolute total pressure of free-stream air
 \mathcal{P} = propulsion power
 \mathcal{P}_L = leaving loss
 \mathcal{P}_T = thrust power
 $q = \rho V^2/2$ = dynamic pressure
 $q_0 = \rho_0 V_0^2/2 = k_0 p_0 M_0^2/2$ = dynamic pressure of free-stream air
 Q = torque
 Q_i = heat supplied to actual combustor
 Q'_i = heat supplied to ideal combustor (no losses)
 r_0 = linear burning rate for solid propellant
 $R = R_u/\bar{m}$ = gas constant
 R_u = universal gas constant = $\bar{m}R$
 t = absolute static temperature
 t_p = temperature of solid propellant prior to ignition
 T = absolute total (stagnation) temperature
 T_c = absolute total temperature of gas entering exhaust nozzle of rocket motor
 T_2 = absolute total temperature at entrance to air compressor (see Fig. 11.5.4)
 T_3 = absolute total temperature at exit section of air compressor (see Fig. 11.5.4)
 T'_3 = absolute total temperature at exit section of ideal compressor (see Fig. 11.5.4) operating between same pressure limits as actual compressor
 T_4 = absolute total temperature at entrance to turbine (see Fig. 11.5.4)
 T_5 = absolute total temperature at exit from turbine (see Fig. 11.5.4)
 T'_5 = absolute total temperature at exit from ideal turbine
 $u = \pi n d_p$ = propeller tip speed
 V = velocity
 V_F = forward speed of propeller
 V_j = effective jet velocity
 V_0 = velocity of free-stream air (flight speed)
 w = velocity of exit gases relative to walls of exhaust nozzle or velocity of air in ultimate wake of propeller
 \dot{W} = weight rate of flow
 \dot{W}_o = weight rate of flow of oxidizer
 \dot{W}_p = weight rate of flow of propellants

Greek

$\alpha = T_4/t_0 = \alpha_d \alpha_1$ = cycle temperature ratio; angle of attack
 $\alpha_d = T_2/t_0$ = diffusion temperature ratio
 $\alpha_1 = T_4/T_2$
 β = bypass ratio for turbofans; helix angle for propeller blade
 $\delta = P/P_{std}$ = corrected pressure
 η = efficiency
 $\eta_B = f'/f$ = efficiency of combustion for thermal-jet engine
 $\eta_c = (T'_3 - T_2)/(T_3 - T_2)$ = isentropic efficiency of compressor
 η_d = isentropic efficiency of diffuser
 $\eta_n = \varphi^2$ = isentropic efficiency of exhaust nozzle
 $\eta_o = \mathcal{P}_T/E_{in}$ = overall efficiency of propulsion system

$\eta_p = \mathcal{P}_T/(\mathcal{P}_T + \mathcal{P}_L)$ = ideal propulsive efficiency
 $\eta_i = (T_4 - T_5)/(T_4 - T'_5)$ = isentropic efficiency of turbine
 $\eta_{th} = \mathcal{P}/E_{in}$ = thermal efficiency of propulsion engine
 $\lambda = gI_a/\sqrt{2gJc_p t_0}$ = thrust parameter for turbojet engine; $1/2 + 1/2 \cos \phi$ = divergence coefficient for exhaust nozzle for rocket engines
 $\nu = V_0/w$ = speed ratio
 ρ = density
 $\bar{\rho}$ = mean density
 $\Omega = \sqrt{k} \left(\frac{2}{k+1} \right)^{(k-1)/(2k-1)}$
 ω = angular velocity of propeller shaft
 ω' = rate of rotation of slipstream at propeller
 ω'' = rate of rotation of slipstream in ultimate slipstream
 Φ = fan velocity coefficient = V_F/u
 ϕ = semiangle of exhaust-nozzle divergence; effective helix angle
 $\varphi = \sqrt{\eta_n}$ = velocity coefficient for exhaust nozzle
 ρ = density
 σ = solidity of propeller
 $\Theta = (P_3/P_0)^{(k-1)/k} = \Theta_d \Theta_c$ = cycle pressure ratio parameter
 $\Theta_c = (P_3/P_2)^{(k-1)/k}$ = compressor pressure-ratio parameter
 $\Theta_d = (P_2/P_0)^{(k-1)/k}$ = diffuser pressure-ratio parameter
 $\Theta_n = (P_7/P_0)^{(k-1)/k} = (P_7/p_9)^{(k-1)/k}$ = nozzle pressure-ratio parameter
 $\Theta_t = (P_4/P_5)^{(k-1)/k}$ = turbine pressure-ratio parameter
 $\theta = T/T_{std}$ = corrected temperature

Subscripts

(a) numbered

0 = free stream
 1 = entrance to subsonic diffuser
 2 = exit from subsonic diffuser
 3 = entrance to combustion chamber
 4 = entrance to turbine of turbojet engine
 5 = exit from turbine of turbojet engine
 6 = tail-pipe entrance
 7 = entrance to exhaust nozzle
 8 = throat section of exhaust nozzle
 9 = exit section of exhaust nozzle

(b) lettered

a = air
 B = burner or combustion chamber
 b = blade
 c = compressor
 d = diffuser
 e = exit section; effective
 F = fan
 f = fuel
 h = hydraulic
 n = nozzle
 o = overall or oxidizer
 p = propellant
 P = propulsive
 std = standard
 t = turbine or throat, as specified in text

Statement on Units The dynamic equation employed in the following sections are written for *consistent sets of units*, i.e., for sets in which 1 unit of force = 1 unit of mass \times 1 unit of acceleration. Consequently, the gravitational correction factor g_c in Newton's equation $F = (1/g_c)ma$ (see notation) has the numerical value unity and is omitted from the dynamic equations. When the equations are used for calculation purposes, g_c should be included and its appropriate value employed.

THRUST EQUATIONS FOR JET-PROPULSION ENGINES

Refer to Fig. 11.5.15, which illustrates schematically a rotationally symmetrical arbitrary propulsion engine immersed in a uniform flow field. Because of the reactions between the fluid flowing through the engine, called the **internal flow**, and the interior surfaces wetted by the internal flow a resultant **axial force** is produced, that is, a force collinear with the longitudinal axis of the engine. If an axial force acts in the **forward direction**, employing a relative coordinate system, it is called a **thrust**; if it acts in the **backward direction** it is called a **drag**. Similarly, the resultant axial force due to the **external flow**, the flow passing over the external surfaces of the propulsion system, is a thrust or drag depending upon whether it acts in the forward direction or the backward direction.

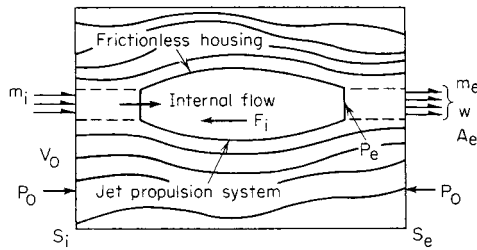


Fig. 11.5.15 Generalized jet-propulsion system.

Application of the momentum equation of fluid mechanics to the generalized propulsion system illustrated in Fig. 11.5.15 gives the following equation for the thrust F_i due to the **internal flow**. Thus, if it is assumed that the external flow is frictionless, there is no change in the rate of momentum for the external flow between S_i and S_e . Hence, the thrust $F = F_i$ is due entirely to the internal flow, and

$$F = F_i = m_e w - \dot{m}_i V_0 + (p_e - p_0) A_e \quad (11.5.1)$$

In Eq. (11.5.1), $\dot{m}_e w = F_j$ = **jet thrust**, $\dot{m}_i V_0 = D_i$ = **ram drag**, and $(p_e - p_0) A_e = F_p$ = **pressure thrust**. Hence,

$$F_i = F_j - D_i + F_p \quad (11.5.2)$$

It is convenient to introduce a fictitious **effective jet velocity** V_j , which is defined by

$$F = \dot{m}_e V_j - \dot{m}_i V_0 = \dot{m}_e w - \dot{m}_i V_0 + (p_e - p_0) A_e \quad (11.5.3)$$

If the gases are expanded completely, in the exhaust nozzle, then $w = V_j$ and $F_p = 0$. No appreciable error is introduced, in general, if it is assumed that $F_p = 0$. For **thermal jet engines**, $\dot{m}_i = \dot{m}_a$ (see notation), and $\dot{m}_e = \dot{m}_a + \dot{m}_f$. Let $f = \dot{m}_f / \dot{m}_a$, $v = V_0 / V_j$; then

$$F_i = \left(\frac{1+f}{v} - 1 \right) \dot{m}_a V_0 + (p_e - p_0) A_e \quad (11.5.4)$$

In the case of uncooled turbojet engines, \dot{m}_f is not significantly different from the fraction of \dot{m}_a utilized for cooling the bearings and turbine disk. Consequently, no significant error is introduced by assuming that $\dot{m}_e = \dot{m}_a + \dot{m}_f \approx \dot{m}_a = \dot{m}$. Hence, for a simple **turbojet engine**, one may write

$$F_e = \dot{m}_a (V_j - V_0) = \dot{m} V_0 (1/v - 1) \quad (11.5.5)$$

Equation (11.5.5) is also the thrust equation for an **ideal propeller**; in that case V_j is the **wake velocity** for the air leaving its slipstream. The trust equation for a hydraulic jet propulsion system has the same form as Eq. (11.5.5). Let V_0 denote the speed of a boat, and \dot{m}_w the mass rate of flow of the water entering the hydraulic pump and discharged by the exit nozzle with the velocity $w = V_j$ relative to the boat. Hence, for hydraulic jet propulsion

$$F = \dot{m}_w (V_j - V_0) = \dot{m}_w V_0 (1/v - 1) \quad (11.5.6)$$

where $v = V_0 / V_j$.

In the case of **rocket engines**, since they do not consume atmospheric air, $\dot{m}_a = 0$, and the flow of gas out of the rocket motor, under steady-state conditions, is equal to $\dot{m}_p - \dot{m}_o + \dot{m}_f$ (see notation).

The effective jet velocity V_j is larger than V_e = **exit velocity** if $p_e > p_0$; that is, if the gases are **underexpanded**. The effective jet velocity is a useful criterion because it can be determined accurately from the measured values of F_i and \dot{m}_p obtained from a static firing test of the rocket motor.

The ratio F_i / \dot{m}_p is denoted by I and called either the **specific thrust** or the **specific impulse**. Hence

$$I = F / \dot{m}_p = V_j / g_c \quad (11.5.7)$$

Although the dimensions of specific impulse are force/(mass)(s), it is conventional to state its units as **seconds**.

Equation (11.5.5) for the thrust of a **turbojet engine**, when expressed in terms of the effective jet velocity V_j , becomes

$$F = \dot{m}_a (V_j - V_0) \quad (11.5.8)$$

POWER AND EFFICIENCY RELATIONSHIPS

In a jet-propulsion engine the **propulsion element** is the **exhaust nozzle**, and the rate at which energy is supplied to it is called the **propulsion power**, denoted by \mathcal{P} . The rate at which the propulsion system does useful work is termed the **thrust power** \mathcal{P}_T and is given by

$$\mathcal{P}_T = F V_0 \quad (11.5.9)$$

Assume that $p_e = p_0$, and that the only energy loss in a propulsion system is the **leaving loss** $\mathcal{P}_L = \dot{m} (V_j - V_0)^2 / 2$, that is, the kinetic energy associated with the jet gases discharged from the system; then the propulsive power is given by

$$\mathcal{P} = \mathcal{P}_L + \mathcal{P}_T \quad (11.5.10)$$

The **ideal propulsive efficiency** is defined, in general, by

$$\eta_p = \mathcal{P}_T / (\mathcal{P}_T + \mathcal{P}_L) = \text{thrust power/propulsion power} \quad (11.5.11)$$

For a turbojet engine and hydraulic jet propulsion,

$$\eta_p = 2v / (1 + v) \quad (11.5.12)$$

For a chemical rocket engine,

$$\eta_p = 2v / (2 + v^2) \quad (11.5.13)$$

The propulsive efficiency η_p is of more or less academic interest. Of more importance is the overall efficiency η_o , which for airbreathing and rocket engines is defined by

$$\eta_o = \eta_{th} \eta_p \quad (11.5.14)$$

where

$$\eta_{th} = \mathcal{P} / E_{in} = \text{thermal efficiency of system} \quad (11.5.15)$$

and E_{in} is the rate at which energy is supplied to the propulsion system.

The overall efficiency of a hydraulic jet-propulsion system is given by

$$\eta_o = \eta_{th} \eta_p = \eta_{th} \eta_{th} [2v / (1 + v)] \quad (11.5.16)$$

where η_{th} is the thermal efficiency of the power plant which drives the water pump, and η_h is the hydraulic efficiency of the water pump. To achieve a reasonable fuel consumption rate, η_h must have a larger value.

For an airbreathing jet engine, $E_{in} = \dot{m}_f (E_f + V_0^2 / 2)$, and

$$\eta_o = \frac{2v}{1 + v} \frac{\mathcal{P}}{\dot{m}_f (E_f + V_0^2 / 2)} \quad (11.5.17)$$

The ratio \dot{m}_f / F is called the **thrust specific-fuel consumption (TSFC)** and is measured in mass of fuel per hour per unit of thrust. Hence,

$$TSFC = \dot{m}_f / F = f \dot{m}_a / F \quad (11.5.18)$$

11-90 JET PROPULSION AND AIRCRAFT PROPELLERS

For a rocket engine, $E_{in} = \dot{m}_p(E_p + V_0^2/2)$, so that

$$\eta_o = \frac{2\nu}{1 + \nu^2} \frac{\mathcal{P}}{\dot{m}_p(E_p + V_0^2/2)} \quad (11.5.19)$$

PERFORMANCE CHARACTERISTICS OF AIRBREATHING JET ENGINES

The Ramjet Engine In ramjet technology the thrust due to the internal flow F_i is called the **gross thrust** and denoted by F_g . Refer to Fig. 11.5.2 and assume $\dot{m}_0 \approx \dot{m}_9 \approx \dot{m}_a$. Then

$$F_g = F_i \approx \dot{m}_a(V_j - V_0) \quad (11.5.20)$$

In level unaccelerated flight F_g is equal to the external drag of the propelled vehicle and the ramjet body.

It is customary to express the thrust capabilities of the engine in terms of the **gross-thrust coefficient** C_{Fg} . If A_m is the maximum cross-sectional area of the ramjet engine, $q_0 = \rho_0 V_0^2/2 = k_0 \rho_0 M_0^2/2$ = the **dynamic pressure** of the free-stream air, then

$$C_{Fg} = \frac{F_g}{q_0 A_m} = \frac{2F_g}{A_m k_0 \rho_0 M_0^2} \quad (11.5.21)$$

In terms of the Mach numbers M_0 and M_9 ,

$$C_{Fg} = \frac{2A_9/A_m}{k_0 M_0^2} \left(\frac{P_9}{P_0} \frac{1 + k_9 M_9^2}{P_9/P_9} - 1 \right) - 2 \frac{A_0}{A_m} \quad (11.5.22)$$

In a fixed-geometry engine, M_9 depends upon the total temperature T_7 , the total pressure P_7 , the fuel-air ratio f , the nozzle area ratio A_e/A_t , and the efficiency of the nozzle η_n . For estimating purposes, $k_0 = 1.4$ and $k_9 = 1.28$, when the engine burns a liquid-hydrocarbon fuel. The manner in which C_{Fg} varies with altitude M_0 and fuel-air ratio f is shown schematically in Fig. 11.5.16.

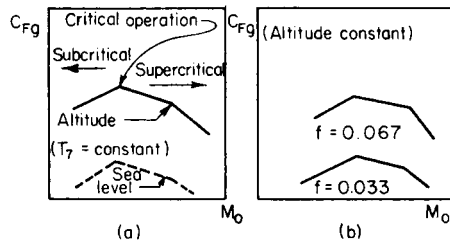


Fig. 11.5.16 Effect of altitude and fuel-air ratio on the gross-thrust coefficient of a fixed-geometry ramjet engine. (a) Effect of altitude; (b) effect of fuel-air ratio.

If $\alpha = T_7/t_0$ = cycle temperature ratio, and k_B is the mean value of k for the combustion gases, the rate at which heat is supplied to the engine is

$$Q_i = Q_i'/\eta_B = \dot{m}_a c_p b t_0 (\alpha - T_2)/\eta_B \quad (11.5.23)$$

It is readily shown that

$$Q_i = \frac{A_0 P_0 V_0}{\eta_B J} \frac{k_B}{k_B - 1} \left[\alpha - \left(1 + \frac{k_0 - 1}{2} M_0^2 \right) \right] \quad (11.5.24)$$

The **gross-thrust specific-fuel consumption** (F_g SFC) is, by definition,

$$F_g \text{ SFC} = \dot{m}_f/F_g \quad (11.5.25)$$

The principal sources of loss are aerothermodynamic in nature and cause a decrease in total pressure between stations 0 and 7. For estimating purposes, assuming $M_0 = 2.0$ and $T_6 = 3800^\circ\text{R}$ (2111 K), the total pressures across different sections of the engine may be assumed to be approximately those tabulated below.

Part of engine	Total pressure ratio
Supersonic diffuser (0-1)	$P_1/P_0 = 0.92$
Subsonic diffuser (1-2)	$P_2/P_1 = 0.90$
Flameholders (2-7)	$P_7/P_2 = 0.97$
Combustion chamber (2-7)	$P_7/P_2 = 0.92$
Exhaust nozzle (7-9)	$P_9/P_7 = 0.97$

The Simple Turbojet Engine A good insight into the design performance characteristics of the turbojet engine is obtained conveniently by making the following assumptions: (1) The mass rate of flow of working fluid is identical at all stations in the engine; (2) the thermodynamic properties of the working fluid are those for air; (3) the air is a perfect gas and its specific heats are constants; (4) there are no pressure losses due to friction or heat addition; (5) the exhaust nozzle expands the working fluid completely so that $p_9 = p_0$; and (6) the auxiliary power requirements can be neglected. Refer to Fig. 11.5.4 and let

$$\Theta = \left(\frac{P_3}{P_0} \right)^{(k-1)/k} \quad \Theta_d = \left(\frac{P_2}{P_0} \right)^{(k-1)/k} \quad \Theta_c = \left(\frac{P_3}{P_2} \right)^{(k-1)/k}$$

$$\Theta_t = \left(\frac{P_4}{P_5} \right)^{(k-1)/k} \quad \Theta_n = \left(\frac{P_7}{P_0} \right)^{(k-1)/k} = \left(\frac{P_7}{P_9} \right)^{(k-1)/k}$$

$$\alpha = T_4/t_0 \quad \alpha_d = T_2/t_0 \quad \alpha_1 = T_4/T_2$$

In view of the assumptions,

$$\Theta = \Theta_d \Theta_c = \Theta_t \Theta_n \quad (11.5.26)$$

and

$$\alpha = \alpha_d \alpha_1 \quad (11.5.27)$$

The diffuser pressure-ratio parameter Θ_d is given by

$$\Theta_d = 1 + \eta_d [(k-1)/2] M_0^2 \quad (11.5.28)$$

where η_d = isentropic efficiency of diffuser (0.75 to 0.90 for well-designed systems).

The turbine pressure-ratio parameter Θ_t is given by

$$1/\Theta_t = 1 - [(\Theta_c - 1)/\alpha_1 \eta_c \eta_t] \quad (11.5.29)$$

where η_t = the isentropic efficiency of the turbine (0.90 to 0.95).

Heat supplied, per unit mass of air, is

$$Q_i = (c_p/\eta_B)(T_4 - T_3)$$

or

$$Q_i = \frac{c_p t_0}{\eta_B \eta_c} \alpha_d \left(\alpha_d \eta_c - \eta_c - \Theta_c + 1 \right) \quad (11.5.30)$$

where η_c is the isentropic efficiency of the air compressor (0.85 to 0.90), and η_B is the efficiency of the burner (0.95 to 0.99).

The enthalpy change for the exhaust nozzle Δh_n is given by

$$\frac{\Delta h_n}{c_p t_0} = \frac{\eta_n}{\eta_c} [\alpha \eta_c - \alpha_d (\Theta_c - 1)]$$

$$\times \left\{ 1 - \frac{\alpha_1 \eta_c \eta_t}{\Theta_c [1 + \eta_d (\alpha_d - 1)] [\alpha_1 \eta_c \eta_t - (\Theta_c - 1)]} \right\} \quad (11.5.31)$$

The **specific thrust**, also called the **air specific impulse**, is

$$I_a = F_i/\dot{m}_{ag} = (\sqrt{2\Delta h_n} - V_0)/\dot{m}_a \quad (11.5.32)$$

The overall efficiency η_o is given by

$$\eta_o = \eta_{th} \eta_p = \frac{I_a V_0}{J Q_i}$$

$$= 2 \eta_B \eta_c \frac{\lambda M_0 \left(\frac{k-1}{2} \right)^{1/2}}{\alpha \eta_c - \left(1 + \frac{k-1}{2} M_0^2 \right) (\eta_c + \Theta_c - 1)} \quad (11.5.33)$$

where η_B ranges from 0.95 to 0.99 and λ is the dimensionless turbojet specific thrust parameter.

The *TSFC* for a turbojet engine is given by

$$TSFC = \frac{\dot{m}_f}{F} \quad (11.5.34)$$

It can be shown by dimensional analysis, if the effects of Reynolds numbers are neglected, that the variables entering into the performance of a given turbojet engine may be grouped as indicated in Table 11.5.2.

Table 11.5.2

Nondimensional group	Uncorrected form	Corrected form
Flight speed	$V_0/\sqrt{T_0}$	$V_0/\sqrt{\theta}$
Rotational speed	N/\sqrt{T}	$N/\sqrt{\theta}$
Air flow rate	$\dot{W}_a\sqrt{T}/D^2P$	$\dot{W}_a\sqrt{\theta}/\delta$
Thrust	F/D^2P	F/δ
Fuel flow rate	$\dot{W}_fJ\Delta H_c/D^2P\sqrt{T}$	$\dot{W}_f/\delta\sqrt{\theta}$

$\theta = T/T_{std} = T/519 (T/288) =$ corrected temperature (exact value for T_{std} is 518.699°R).
 $\delta = P/P_{std} = P/14.7 (P/1.013 \times 10^5) =$ corrected pressure.

Figure 11.5.17 is a design-point chart presenting λ and η_o as functions of α , P_3/P_2 , and Θ_c for the subsonic performance of simple turbojet engines. The curves apply to propulsion at 30,000 ft. (9.14 km) altitude for engines having characteristic data indicated in the figure. Curve A illustrates the effect of pressure ratio P_3/P_2 or Θ_c for engines operating with $\alpha = 5.0$. It is seen that increasing the compressor pressure ratio increases η_o but it approaches a maximum value at P_3/P_2

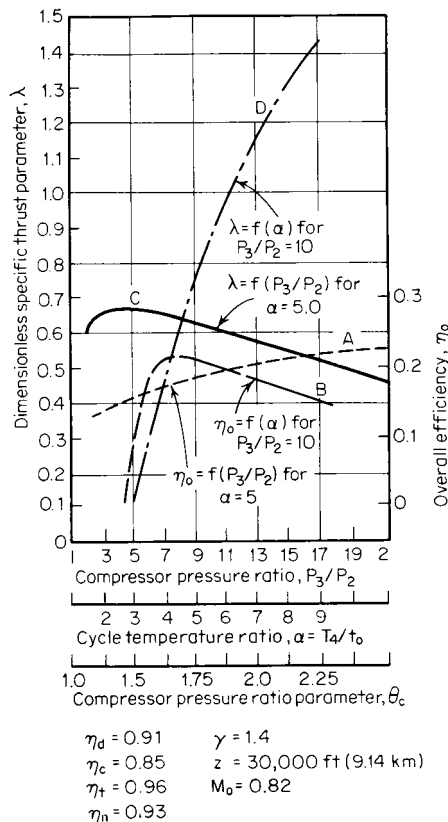


Fig. 11.5.17 Dimensionless thrust parameter λ and overall efficiency η_o as functions of the compressor pressure ratio (simple turbojet engine).

approximately equal to 19. Curve B applies to the design point of engines having a fixed compressor pressure ratio of 10:1 but having different values of α , that is, turbine inlet temperature. It shows that increasing α much above $\alpha = 5$ reduces the overall efficiency and consequently *TSFC*. Curve C presents the design-point characteristics for engines operating with $\alpha = 5$ but having different compressor pressure ratios. The maximum value of λ is obtained at a relatively low pressure ratio: approximately $P_3/P_2 = 5$. Curve D presents the design-point characteristics of engines having a fixed compressor pressure ratio of 10:1 but different cycle temperature ratios. Increasing α gives significant increases in λ . Hence, large values of turbine inlet temperature T_4 offer the potential for large thrusts per unit of frontal area for such turbojet engines.

Figure 11.5.18 presents the design-point characteristics for engines having $\eta_c = 0.85$, $\eta_t = 0.90$, $\eta_r = 0.93$, and $\eta_B = 0.99$. Different values of diffuser efficiency are presented for flight Mach numbers $M_o = 0.8$ ($\eta_d = 0.91$), $M_o = 1.60$ ($\eta_d = 0.90$) and $M_o = 2.4$ ($\eta_d = 0.88$). Two different classes of engines are considered, those with $P_3/P_2 = 4.0$ and those with $P_3/P_2 = 12.0$. The dimensionless thrust λ is plotted as a function of α with M_o as a parameter. It is evident that increasing λ , that is, the turbine inlet temperature T_4 , offers the advantage of a large increase in thrust per unit area of the engine under all the conditions considered in Fig. 11.5.18.

Figure 11.5.19 presents the effect of flight speed on the design-point performance, at 30,000 ft (9.14 km) altitude, for engines having $\eta_c = 0.85$, $\eta_t = 0.90$, $\eta_B = 0.95$, $T_4 = 2000^\circ\text{R}$ (1111 K) and burning a fuel having a heating value $\Delta H_c = 18,700 \text{ Btu/lbm}$ (10,380 kcal/kgm). The magnitude of the compressor pressure ratio P_3/P_2 approaches unity when V_o is approximately 1,500 mi/h, indicating that at higher speeds the compressor and turbine are superfluous; i.e., the propulsion requirements would be met more adequately by a ramjet engine. Raising T_4 tends to delay the aforementioned condition to a high value of V_o .

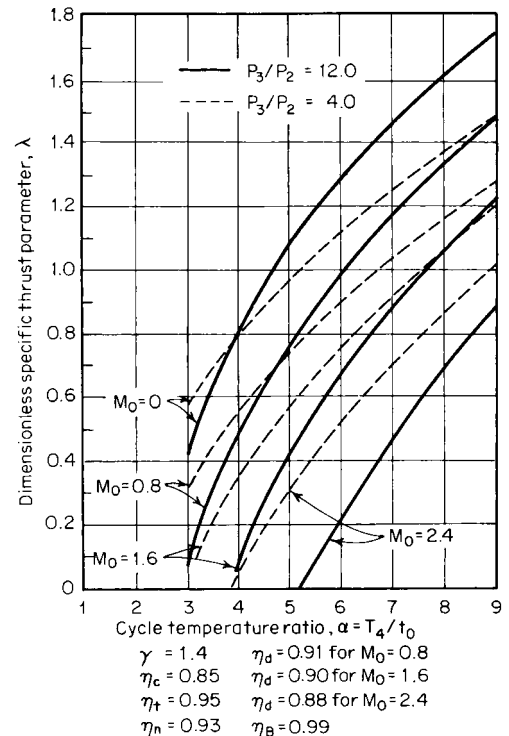


Fig. 11.5.18 Dimensionless thrust parameter λ for a simple turbojet engine and its overall efficiency η_o as functions of the cycle temperature ratio α , with the flight Mach number as a parameter.

11-92 JET PROPULSION AND AIRCRAFT PROPELLERS

It is a characteristic of turbojet engines, since $\eta_o = \eta_{th}\eta_p$, that for a given M_0 increasing η_{th} causes Δh_n to increase, and hence the jet velocity V_j . As a consequence, η_p is decreased. It is this characteristic which causes $\eta_o = f(\alpha)$, curve B of Fig. 11.5.17, to be rather flat for a wide range of values of $\alpha = T_4/t_0$.

The curves of Figs. 11.5.17 to 11.5.19 are design-point performance curves; each point on a curve is the design point for a different turbojet engine. The performance curves for a specific engine are either computed from experimental data pertaining to its components operating over a wide range of conditions or obtained from testing the complete turbojet engine. It is customary to present the data in standardized form.

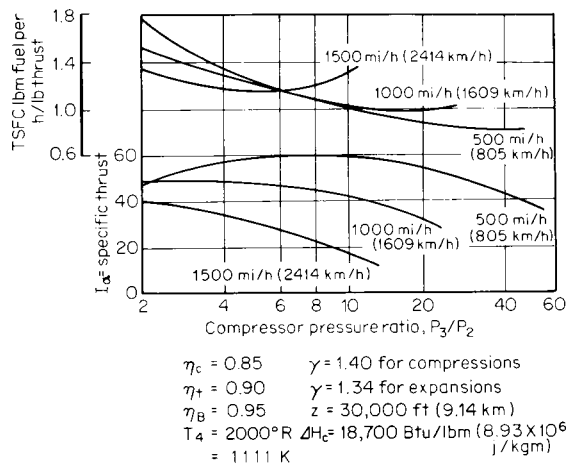


Fig. 11.5.19 TSFC and specific thrust I_a functions of the compressor pressure ratio, with flight speed as a parameter (simple turbojet engine).

The Turbofan or the Ducted-Fan Engine Refer to Fig. 11.5.5b. Assume that the hot-gas flow ($\dot{m}_{a1} + \dot{m}_f$) is ejected through the converging nozzle, area A_t , with the effective jet velocity V_j , and that the airflow \dot{m}_{aF} is ejected through the converging annular nozzle, area A_{7F} , with the jet velocity V_{jF} . Let $\beta = \dot{m}_{aF}/\dot{m}_{a1}$ denote the bypass ratio, approximately 5 for modern transport engines.

The thrust equation for the turbofan engine is

$$F = \dot{m}_{a1}(1 + f)V_j + \beta\dot{m}_{a1}V_{jF} - \dot{m}_{a1}(1 + \beta)V_0 \quad (11.5.35)$$

where $V_{jF} < V_j$. The thrust per unit mass of airflow, or air specific impulse, is

$$I_a = F/\dot{m}_{a1}(1 + \beta) \quad (11.5.36)$$

The TSFC is given by

$$TSFC = \dot{m}_f/F \quad (11.5.37)$$

One of the most important applications of turbofans is for **high-subsonic transport aircraft** where the fuel consumption in cruise is a major consideration. In general, as the bypass ratio increases, the TSFC decreases but the engine weight and external drag increase. The **optimum bypass ratio** for any particular application is determined by a trade-off between fuel weight, which is reduced by increasing the bypass ratio, and engine weight and external drag, which increase with bypass ratio for a given thrust. In general, the optimum value of β is that which makes the difference $(F - D_e)$ a maximum, where D_e is the external drag of the engine. Up to a certain point, the more sophisticated and efficient the engine, the larger the bypass ratio.

To achieve the maximum potential for the turbofan engine, high values of turbine inlet temperature T_4 are essential; i.e., cooled turbine stator and rotor blades must be developed. There is an upper limit to T_4 ; above it the TSFC begins to increase. As T_4 is increased, however, the optimum value of β must also be increased to avoid excessive leaving losses in the propulsive jet.

Mechanical Design

Blades New technologies being developed to achieve higher thrust-to-weight ratios in advanced gas turbine engines also cause higher vibratory blade row responses and stresses that delay engine development and may adversely affect engine reliability. In particular, the design trend toward higher stage loadings and higher specific flow are being attained through increased tip speeds, lower radius ratios, lower aspect ratios, and fewer stages. The resultant axial-flow compressor blade designs utilize thin, low-aspect-ratio blading with corresponding high steady-state stresses. Also, the mechanical damping is considerably reduced in newer rotor designs, particularly those with integral blade-disk configurations (**blisks**) and in those without shrouds. These are similar trends in turbine blading, but they are further complicated by increased inlet and cooling temperatures that have resulted in thin-walled, complex cooling passage designs. As a result, advanced axial-flow blade designs, both compressors and turbines, feature low-aspect-ratio blading which affect the **structural integrity** of the blading. These problems can be classified into two general categories: (1) **flutter** and (2) **forced response**. A fundamental parameter common to both categories is the **reduced frequency**, $k = \omega b/V$, where b is the blade semichord, ω the frequency of vibration, and V the relative free-stream velocity. For engine applications, the frequency corresponds generally to one of the lower-blade or coupled-blade disk **natural frequencies**.

Under certain conditions, a blade row operating in a completely uniform flow can enter into a self-excited vibrational **instability** termed **flutter**. The vibration is sustained by the extraction of energy from the uniform flow during each vibratory cycle. The outstanding feature of flutter is that **high stresses** exist in the blading, leading to short-term, high-cycle, **fatigue failures**. Its importance is evidenced by the fact that if a portion of a single blade fails due to flutter, the result may be instantaneous and total loss of engine power.

Figure 11.5.20 is a typical compressor map showing schematically the more common types of flutter. At subsonic Mach numbers, up to 0.8 to 0.9, either positive or negative **stall flutter** in the **bending** or **torsion** mode may occur. It is caused by operating beyond some critical airfoil angle of attack. A **critical reduced frequency** value of 0.8 has been cited for stall flutter; i.e., if $k < 0.8$ stall flutter is possible. **Choking flutter** usually occurs at negative incidence angles at a part-speed condition

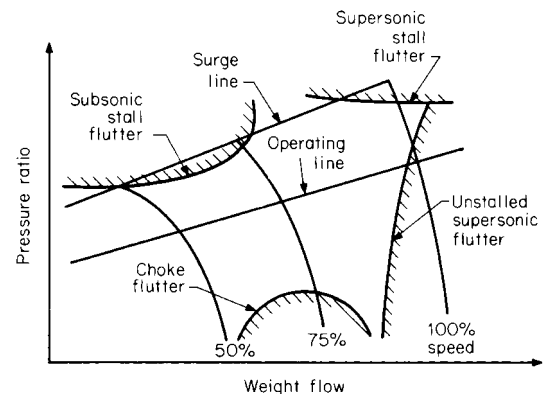


Fig. 11.5.20 Common types of compressor flutter.

with the blade operating either subsonically or transonically. The physical mechanism of choke flutter is not fully understood; both high negative incidence angles and choked flow are viable candidates. **Supersonic unstalled flutter** is largely associated with thin **fan blades** operating at supersonic relative flow velocities at the tip section. It is caused by a lagging of the unsteady aerodynamic forces relative to the blade motion and imposes a limit on the **high-speed operation** of the engine. The stress encountered during this type of flutter can be catastrophically large, decreasing rapidly as a constant speed line is traversed toward higher pressure ratios. High-speed operation near the surge line can lead to

supersonic stall flutter. Because this flutter is associated with **high pressure ratios**, there can be strong shocks present within the blade passages, and in some circumstances, ahead of the blade row.

Destructive aerodynamic **forced responses** have been noted in all engine blading. These failure-level vibratory responses occur when a periodic forcing functions, with frequency equal to a natural blade **resonant frequency**, acts on a blade row. Responses of sufficient magnitude to fail blades have been generated by a variety of sources including upstream and downstream blade rows, flow distortion, bleeds, and mechanical sources.

The importance of forced response lies in the **multiple sources** of excitation for any rotating system. The rotor speeds at which forced responses occur are predicted with “**Campbell**” or **speed-frequency** diagrams. These display the **natural frequency** of each blade mode versus rotor speed and, at the same time, the forcing function frequency (or **engine order** E lines) versus rotor speed, as indicated schematically in Fig. 11.5.21. These E lines represent the loci of available **excitation energy** at any rotational speed for 1, 2, 3, etc. excitations per revolution. Wherever these curves intersect, a potential source of destructive forced response exists. Not all intersections can be avoided. Design practice is

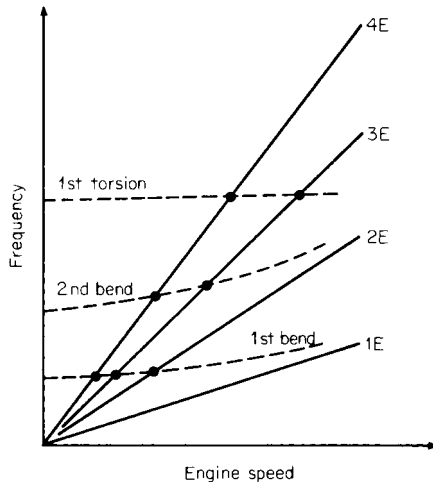


Fig. 11.5.21 Schematic speed-frequency diagram.

to eliminate the lower-order excitations from the operating range whenever possible. This is because the sources of most forced response energy usually result from these lower-order resonances, particularly the 2E line.

Environmental Issues

The increasing worldwide concern for the environment has led to two technical issues becoming significant: (1) airport noise and (2) the Earth's ozone layer.

Airport noise is now a major design criterion for commercial aircraft because of **Federal Aviation Rule, Part 36 (FAR-36)**, which sets maximum **takeoff, landing, and sideline** noise levels for certification of new turbofan-powered aircraft. Three measuring stations are referred to in FAR-36: (1) under the approach path 1 mi before touchdown, (2) under the takeoff path 3.5 mi from the start of the take-off roll, and (3) along the sides of the runway at a distance of 0.35 mi for four-engined aircraft. Since the power settings and aircraft height are variables, the noise at the approach and takeoff stations are dependent on the engines, the aircraft performance, and operational procedures. The sideline station is more representative of the intrinsic takeoff noise characteristics of the engine, since the engine is at full throttle and the station is at a fixed distance from the aircraft.

The **subsonic turbofan** radiates noise both forward and backward and also produces jet noise from both the fan-jet and the primary jet. How-

ever, because a low jet velocity gives good cruise propulsive efficiency, the jet noise can be reduced. Thus, for the subsonic high-bypass turbofan, **fan noise** is the most critical problem, both on approach and takeoff. For the supersonic turbojet engine, approach noise is not a major problem because it has a long inlet that can be **choked** on approach to suppress fan noise. The jet velocity at takeoff is high if the engine is optimized for cruise performance. However, one environmental barrier issue for the second-generation supersonic transport, the **high-speed civil transport (HSCT)**, is airport noise during the takeoff and landing. The prime contributor to an HSCT noise signature is the **jet exhaust**, and thus an approach to quieting the jet exhaust without seriously impacting nozzle aerodynamic performance, size, or weight must be developed.

With regard to aircraft propulsion, depletion of the Earth's **ozone layer** is attributed to the engine exhaust products, specifically the **nitric oxide (NO_x)** levels. Thus, combustor designs must evolve so as to produce ultralow levels of NO_x while at the same time not compromising combustion efficiency and operability.

CRITERIA OF ROCKET-MOTOR PERFORMANCE

In most applications of rocket motors the objective is to produce a large thrust for a limited period. The criteria of rocket-motor performance are, therefore, related to thrust-producing capabilities and operating duration. If \dot{W}_p denotes the rate at which the rocket motor consumes propellants, P_c the total pressure at the entrance to the exhaust nozzle, and C_w the **weight flow coefficient**, then

$$\dot{W}_p = C_w P_c A_t \quad (11.5.38)$$

Ordinarily, the values of C_w as a function of P_c and **mixture ratio** \dot{W}_o/\dot{W}_f are determined experimentally. If no experimental data are available, the values of C_w can be calculated with good accuracy from the calculated thermodynamic properties of the combustion gases. If T_c is the total temperature, and P_c the total pressure of the combustion gases at the entrance section of the nozzle, then, for steady operating conditions, $\dot{W}_p = \dot{W}_g$,

$$\dot{W}_g = C_d A_t P_c \Omega \sqrt{\frac{g}{RT_c}} \quad (11.5.39)$$

where

$$\Omega = \left(\frac{2}{k+1} \right)^{(k-1)/[2(k-1)]} \sqrt{k} \quad (11.5.40)$$

An equation similar to Eq. (11.5.38) can be written for the thrust developed by the rocket motor. Thus

$$F = C_F P_c A_t \quad (11.5.41)$$

The values of the **thrust coefficient** C_F for specific propellant combinations are determined experimentally as functions of P_c and the ratio \dot{W}_o/\dot{W}_f . When no experimental values are available, C_F can be calculated from the following equation. Therefore

$$C_F = C_d \lambda \phi \Omega \sqrt{\frac{2k}{k-1}} Z_t + \left(\frac{P_c}{P_c} - \frac{P_o}{P_c} \right) \frac{A_e}{A_t} \quad (11.5.42)$$

where

$$Z_t = 1 - \left(\frac{P_e}{P_c} \right)^{(k-1)/k}$$

Equation (11.5.42) shows that C_F is independent of the combustion temperature T_c and the molecular weight of the combustion gases. The nozzle area ratio A_e/A_t is given by the formula

$$\frac{A_e}{A_t} = \frac{(P_e/P_c)^{1/k}}{\left(\frac{k+1}{2} \right)^{1/(k-1)} \sqrt{[(k+1)/(k-1)] Z_t}} \quad (11.5.43)$$

Figure 11.5.22 presents C_F calculated by means of the preceding equations, as a function of the area ratio A_e/A_t , with P_c/P_o as a param-

11-94 JET PROPULSION AND AIRCRAFT PROPELLERS

ter, for gases having $k = 1.28$; the calculations assumed $\lambda = 0.983$ and $C_d = \varphi = 1.0$. The curves do not take into account the separation phenomena which occur when A_e/A_t is larger than that required to expand the gases to p_0 .

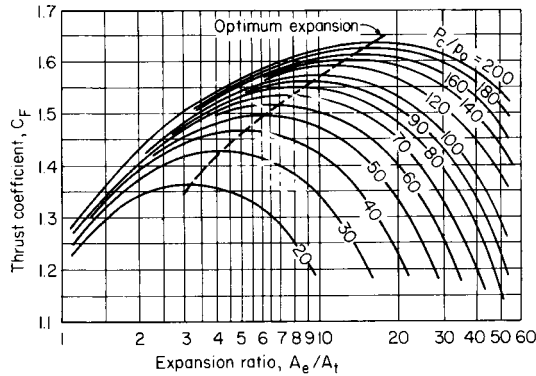


Fig. 11.5.22 Calculated thrust coefficient versus expansion ratio for different pressure ratios (based on $k = 1.28$, $\lambda = 0.9830$, $C_d = \varphi = 1.0$).

The specific impulse I is defined by Eq. (11.5.8) and can be shown to be given by

$$I = F/\dot{m}_p = C_F/C_w = V_j/g_c \quad (11.5.44)$$

A criterion which is employed for stating the performance of rocket motor is the characteristic velocity c^* . By definition

$$c^* = V_j/C_F = P_c A_t/\dot{m} = I/C_F \quad (11.5.45)$$

The values of c^* for a given propellant combination are determined experimentally. It should be noted that the value of c^* is independent of the thrust. Basically, c^* measures the effectiveness with which the thermochemical energy of the propellants is converted into effective jet kinetic energy. When no experimental data are available the value of c^* can be estimated quite closely from

$$c^* = \sqrt{RT_c/\Omega} \quad (11.5.46)$$

Table 11.5.1 presents values of specific impulse for some possible rocket-propellant combinations.

Solid-propellant rocket motors may be segregated into (1) **double-base powders** and (2) **composite, or heterogeneous, propellants**. Double-base powders are gelatinized colloidal mixtures of nitroglycerin and cellulose to which certain stabilizers have been added. Heterogeneous, or composite, propellants are physical mixtures of a solid oxidizer in powder form and some form of solid fuel, such as a plastic or rubberlike material.

Solid-propellant rocket motor technology has made tremendous strides. It is possible to produce solid propellants with a wide range of linear burning rates and with good physical properties. It has been demonstrated experimentally that large thrust rocket motors with chamber diameters of approximately 22 ft (6.7 m) are feasible. As a result, the solid-propellant rocket motor has displaced the liquid rocket engine from a large number of applications, which heretofore were considered the province of the liquid rocket engine. In military applications, there is a strong tendency to supplant liquid rocket engines with solid rocket engines. Only in such areas as the large thrust launching rockets for boosting manned vehicles into space have the liquid rocket engines reigned supreme; the space shuttle is equipped with liquid-bipropellant rocket engines, but it is boosted with auxiliary solid-propellant rocket motors.

The following considerations are what make solid-propellant rocket motors attractive: (1) They are simpler in construction than liquid rocket engines; (2) they are easier to handle in the field; (3) they have instant

readiness for use; (4) they have very good storage properties; (5) they have a larger average density $\bar{\rho}_p$ than most liquid-propellant combinations; (6) they have considerably fewer parts; and (7) their reliability in practice has been very good. Furthermore, once the performance characteristics and physical properties of a solid propellant have been established, it is a relatively straightforward engineering problem to design and develop solid-propellant rocket motors of widely different thrust levels and burning times t_R .

Rocket motors which burn double-base propellants find the greatest use in weaponry, e.g., artillery rockets, antitank weapons, etc.

Rocket motors burning heterogeneous, also called **composite**, solid propellants are used for propelling all kinds of military missiles and for sounding rockets. Modern composite propellants have three basic types of ingredients: (1) a fuel which is an organic polymer, called the **binder**; (2) a finely powdered oxidizer, ordinarily ammonium perchlorate (NH_4NO_3); and (3) various additives, for catalyzing the combustion process, for increasing the propellant density, for increasing the specific impulse (e.g., powdered aluminum), for improving the physical properties of the propellant, and the like. After the ingredients have been thoroughly mixed, the resulting viscous fluid is poured, usually under vacuum to prevent the formation of voids, directly into the chamber of the rocket motor which contains a suitable mandril for producing the desired configuration for the propellant grain. The propellant is cured by polymerization to form an elastomeric material. Some of the more common binders are butadiene copolymers and polyurethane.

Modern composite solid propellants have densities ranging from 1.60 to 1.70, depending upon the formulation, and specific impulse values of approximately 245 s, based on a combustion pressure of 1000 psia and expansion to 14.7 psia.

In the case of solid-propellant rockets the rate of propellant consumption \dot{m}_p is related to the **linear burning rate** for the propellant r_0 , that is, the rate at which the burning surface of the propellant recedes normal

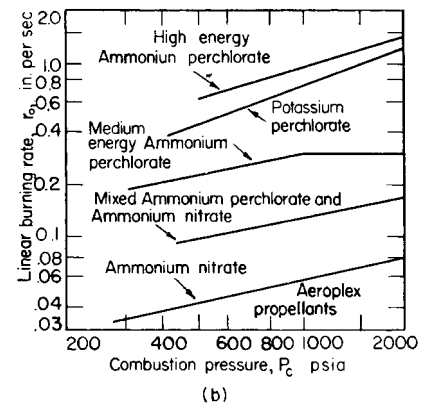
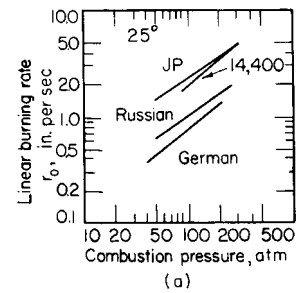


Fig. 11.5.23 (a) Linear burning rate as a function of combustion pressure for double-base propellants; (b) burning-rate characteristics of several heterogeneous propellants at 60°F (15.5°C). (Aerojet-General Corp.)

to itself as it burns. For practical purposes it can be assumed that the linear burning rate r_0 is given by

$$r_0 = a_2 p_c^n \quad (11.5.47)$$

where a_2 and n are constants which are determined by experiment.

If ρ_p denotes the density of the solid propellant and A_p the area of the burning surface, then the propellant consumption rate \dot{m}_p is given by

$$\dot{m}_p = A_p \rho_p r_0 = a_2 A_p \rho_p p_c^n \quad (11.5.48)$$

Figure 11.5.23 presents the linear burning rate as a function of the combustion pressure for several propellants.

The linear burning rate r_0 is influenced by the temperature of the solid propellant t_p prior to its ignition. Low values of t_p reduce the burning rate, and vice versa. Consequently, the temperature of the propellant must be given in presenting data on linear burning rates. Figure 11.5.24 presents r_0 as a function of p_c for $t_p = -40, 60,$ and 140°F for a composite propellant manufactured by the Aerojet-General Corp., Azusa, Calif.

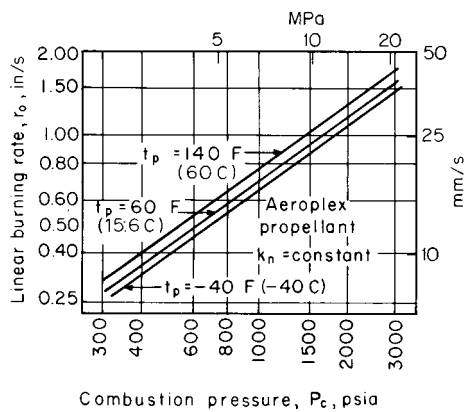


Fig. 11.5.24 Effect of propellant temperature on the linear burning rate of a heterogeneous propellant. (Aerojet-General Corp.)

AIRCRAFT PROPELLERS

The function of the aircraft propeller (or airscrew) is to convert the torque delivered to it by an engine into the thrust for propelling an airplane. If the airplane is in steady, level flight, the propeller thrust and the airplane drag equal each other. If the airplane is climbing, the thrust must overcome the drag plus the weight component of the airplane.

The propeller may be the sole thrust-producing element, but it can also be employed in conjunction with another thrust-producing device, such as the exhaust jet of a **turboprop** or **gas-turbine engine**. It may also be employed as a **windmilling** device for producing power.

The conventional propeller consists of two or more equally spaced radial blades, which are rotated at a substantially uniform angular velocity. At any arbitrary radius, the section of a blade has the shape of an airfoil, but as the hub is approached, the sections become more nearly circular because of considerations of strength rather than aerodynamic performance. The portions of the blades in the vicinity of the hub contribute, at best, only a small portion of the thrust developed by the propeller blades.

Each section of the propeller blade experiences the aerodynamic reactions of an airfoil of like shape moving through the air in a similar manner. Furthermore, at each radius, the section of one blade forms with the corresponding sections on the other blades a series of similar airfoils, which follow one another as the propeller rotates.

The torque of the rotating propeller imparts a rotational motion to the air flowing through it and, furthermore, causes the pressure immediately behind the propeller to increase while that in front of it is reduced; i.e., the air is sucked toward the front of the propeller and pushed away behind it. A slipstream is created as illustrated in Fig. 11.5.1. The ratio

of the cross-sectional area of the slipstream at any station to that of the actuator disk is termed the **slipstream contraction**.

The thrust produced by the propeller follows the relationships developed from the momentum theorem of fluid mechanics for jet engines as presented in Fig. 11.5.15 and Eq. (11.5.5). The thrust equation for the airbreathing engine (simplified) and the propeller is

$$F = \dot{m}(w - V_0) = \rho A V_0 (w - V_0) \quad (11.5.49)$$

In the case of a propeller the mass flow m is large and the velocity rise across the propeller is small, as compared with a jet engine of the same thrust. However, the thrust of propellers falls off rapidly as air compressibility effects on the propeller become large (flight speeds of 300 to 500 mi/h).

Propeller efficiency is defined as the useful work divided by the energy supplied to the propeller:

$$\eta_p = \frac{P_T}{P} = \frac{FV_0}{P} = \frac{m(v - V_0)V_0}{m/2(w^2 - V_0^2)} = \frac{2v}{1 + v} \quad (11.5.50)$$

where $v = V_0/w$.

Since w is only slightly larger than V_0 , the ideal efficiency is of the order of 0.95, and actual efficiencies are in the range of 0.5 to 0.9.

Propeller Theory

Axial-Momentum Theory The axial-momentum theory of the propeller is basically a special case of the generalized jet-propulsion system presented in Fig. 11.5.15. It is only a first approximation of the action of the propeller and cannot be employed for design purposes. It neglects such factors as the drag of the blades, energy losses due to slipstream rotation, blade interference, and air compressibility effects. Because of those losses, an actual propeller requires power to rotate at zero thrust, and at zero thrust its propulsive efficiency is, of course, zero.

Blade-Element Theory This theory, called **strip theory**, takes into account the profile losses of the blade sections. It is the theory most commonly employed in designing a propeller blade and for assessing the off-design performance characteristics of the propeller.

Each section of the propeller is considered to be a rotating airfoil. It is assumed that the radial flow of air may be neglected, so that the flow over a blade section is two-dimensional. Figure 11.5.25 illustrates diagrammatically the velocity vectors pertinent to a blade section of length dr , located at an arbitrary radius r . The projection of the axis of rotation is OO' , the plane of rotation is OC , the blade angle is β , the angle of attack for the air flowing toward the blade (in the relative coordinate system) with the velocity V_0 is α , the tangential velocity of the blade element is $u = 2\pi r\omega$, and the **pitch** or **advance angle** is ϕ . From Fig. 11.5.25.

$$\alpha = \beta - \phi \quad (11.5.51)$$

and

$$\phi = \tan^{-1}(V_0/\pi r\omega) \quad (11.5.52)$$

Figure 11.5.26 illustrates the forces acting on the blade element. If b denotes the width of the blade under consideration and C_L and C_D are

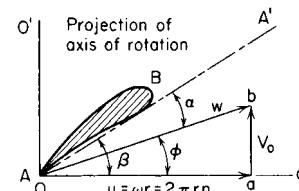


Fig. 11.5.25 Vector diagram for a blade element of a propeller.

the lift and drag coefficients of the blade (airfoil) section, then the thrust force dF acting on the blade element is given by

$$dF = \frac{1}{2} \rho V_0^2 b dr C_L \frac{\cos(\phi + \gamma)}{\cos \gamma \sin^2 \phi} \quad (11.5.53)$$

11-96 JET PROPULSION AND AIRCRAFT PROPELLERS

The corresponding torque force dQ is given by

$$dQ = \frac{1}{2} \rho V_0^2 b dr C_L \frac{\sin(\phi + \gamma)}{\cos \gamma \sin^2 \phi} \quad (11.5.54)$$

where

$$\tan \gamma = d\mathcal{D}/d\mathcal{L} = C_D/C_L = \mathcal{D}/\mathcal{L} \quad (11.5.55)$$

where \mathcal{D} and \mathcal{L} denote drag and lift, respectively.

The propulsion efficiency of the blade element, termed the **blading efficiency**, is defined by

$$\eta_b = \frac{V_0 dF}{u dQ} = \frac{\tan \phi}{\tan(\phi + \gamma)} = \frac{\mathcal{L}/\mathcal{D} - \tan \phi}{\mathcal{L}/\mathcal{D} + \cot \phi} \quad (11.5.56)$$

The value of ϕ which makes η_b a maximum is termed the **optimum advance angle** ϕ_{opt} . Thus

$$\phi_{opt} = \frac{\pi}{4} - \frac{\gamma}{2} = 45^\circ - \frac{57.3}{2(\mathcal{L}/\mathcal{D})} \quad (11.5.57)$$

The maximum blade efficiency is accordingly

$$(\eta_b)_{max} = \frac{2\gamma - 1}{2\gamma + 1} = \frac{2(\mathcal{L}/\mathcal{D}) - 1}{2(\mathcal{L}/\mathcal{D}) + 1} \quad (11.5.58)$$

A force diagram similar to Fig. 11.5.26 can be constructed for each element of the propeller blade, taking into account the variation in ϕ with the radius. The resultant forces acting on the propeller are obtained by summing (integrating) those forces acting on each blade element.

The integrated lift coefficient is

$$C_{Lr} = \int_{r/R}^{1.0} C_{Lr} \left(\frac{r}{R}\right)^3 d\left(\frac{r}{R}\right) \quad (11.5.59)$$

where C_{Lr} = propeller-blade-section lift coefficient and r/R = fraction of propeller-tip radius.

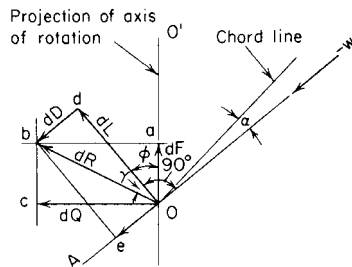


Fig. 11.5.26 Aerodynamic forces acting on a blade element.

The integrated lift coefficient is in the range 0.15 to 0.70. There is a dilemma in the design and selection of blade sections since high static thrust requires high C_{Lr} which gives relatively low η_p at cruise. Cruise conditions require low C_{Lr} for good η_p . Variable camber propellers permit optimization of C_{Lr} , but at the expense of weight and complexity.

Vortex Theory The simple two-dimensional blade-element theory can be further improved by taking account of the actual velocity distribution in the slipstream and thus determining the actual loading on the blading by the so-called *vortex theory*. The blades are represented by bound vortex filaments sweeping out vortex sheets to infinity. The vortex sheets are distorted both by the slipstream contraction and by the profile drag of the blades. If such distortions are neglected, the induced velocity in the wake can be calculated by assuming the vortex sheets to be tubular. Thus, in Fig. 11.5.25, the induced axial velocity becomes the arithmetic mean of the axial velocities at far distances upstream and downstream of the rotor disk; and the induced rotational velocity at the disk becomes $\omega - 0.5\omega'$, where ω' is the rotation of the slipstream in

the plane of the propeller. Hence, the angle of attack α for a rotor element is given by

$$\alpha = \beta - \tan^{-1}[V_F/r(\omega - 0.5\omega')] \quad (11.5.60)$$

where V_F is the induced axial velocity in the plane of the propeller.

The addition of the vortex effects improves the representation of the propeller by the blade sections. There are, however, three-dimensional flow effects which are not included, and the following coefficients have been suggested to include this effect (which reduces the lift coefficient).

Lift Curve Slope Correction Factors for Three-Dimensional Airfoils

Radial station (ratio r/R)	Correction factor
(0.2)(0.3)(0.45)(0.6)(0.7)	0.85
0.8	0.80
0.9	0.70
0.95	0.65

SOURCE: Departments of the Air Force, Navy, and Commerce, "Propeller Handbook."

Performance Characteristics

The pitch and the angle ϕ (Fig. 11.5.25) have different values at different radii along a propeller blade. It is customary, therefore, to refer to all parameters determining the overall characteristics of a propeller to their values at either $0.7r$ or $0.75r$.

For a given blade angle β , the angle of attack α at any blade section is a function of the **velocity coefficient** V_0/u , where $u = \pi n d_p$; it is customary, however, to replace V_0/u by its equivalent, the **advance ratio** $J = V_0/n d_p$.

For given values of β and n , the angle of attack α attains its maximum value when $V_0 = 0$, with $\phi = 0$. In other words, the propeller thrust F is maximum at takeoff. As V_0 increases, α decreases and so does the thrust. Finally, a forward speed is reached for which the thrust is zero.

Increasing $J = V_0/n d_p$, for a constant blade angle, causes the propeller to operate successively as a fan, propeller, brake, and windmill. Most of the operation, however, is conducted in the propeller state. At takeoff, the propeller is in the fan state. Windmilling must be avoided because it may overspeed the engine and damage it.

The lift coefficient C_L is a linear function of α up to the stalling angle, and C_D is a quadratic function of α . Furthermore, the lift \mathcal{L} is zero at a negative value for α . Figure 11.5.27 presents the \mathcal{L}/\mathcal{D} ratios of typical propeller sections. Figure 11.5.28 presents the blade (section) efficiency as a function of the pitch angle ϕ for different values of \mathcal{L}/\mathcal{D} . Propellers normally operate at \mathcal{L}/\mathcal{D} ratios of 20 or more. Supersonic propellers operate with \mathcal{L}/\mathcal{D} ratios of approximately 10, and from Fig. 11.5.27 it is apparent that they must operate close to the optimum pitch angle ϕ to obtain usable blade efficiencies.

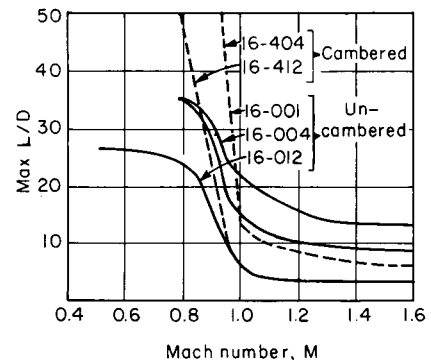


Fig. 11.5.27 Maximum lift-drag ratios for representative sections.

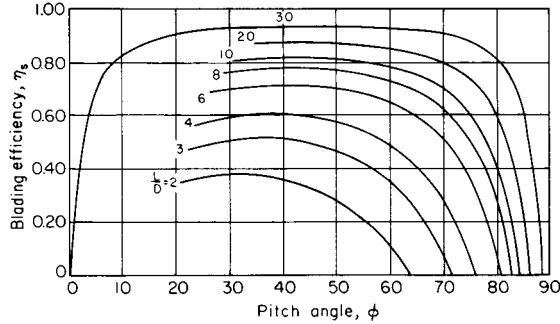


Fig. 11.5.28 Blade-element efficiency versus pitch angle.

Propeller Coefficients It can be shown, neglecting the compressibility of the air, that

$$f(V_0, n, d_p, \rho, F) = 0 \quad (11.5.61)$$

By dimensional analysis, the following coefficients are obtained for expressing the performances of propellers having the same geometry:

$$F = \rho n^2 d_p^4 C_F \quad Q = \rho n^2 d_p^5 C_Q \quad \mathcal{P} = \rho n^3 d_p^5 C_P \quad (11.5.62)$$

C_F , C_Q , and C_P are termed the **thrust**, **torque**, and **power coefficients**, respectively. They are independent of the size of the propeller. Consequently, tests of small-scale models can be employed for obtaining the values of F , Q , and \mathcal{P} for geometrically similar full-scale propellers. Hence, the ideal propulsive efficiency of a propeller is given by

$$\eta_p = \frac{FV_0}{\mathcal{P}} = \frac{C_F}{C_P} \frac{V_0}{d_p n} = J \frac{C_F}{C_P} \quad (11.5.63)$$

Other useful coefficients are the **speed-power coefficient** C_S and the **torque-speed coefficient** C_{QS} . Thus,

$$C_S = V_0 \sqrt{\rho} \mathcal{P} n^2 \quad C_{QS} = V_0 \sqrt{\rho} d_p^3 / Q \quad (11.5.64)$$

A commonly employed factor related to the geometry of a propeller is the **solidity** σ . By definition,

$$\sigma = c/p \quad (11.5.65)$$

The solidity varies from radius to radius; at a given radius, σ is proportional to the power-absorption capacity of the annulus of blade elements.

The **activity factor** of a blade AF is an arbitrary measure of the blade solidity and hence of its ability to absorb power. It takes the form

$$AF = \frac{100,000}{16} \int_{r_h/R}^{r/R=1.0} \frac{c}{d_p} \left(\frac{r}{R}\right)^3 d\left(\frac{r}{R}\right) \quad (11.5.66)$$

where $R = d_p/2$, $r =$ radius at any section, and $r_h =$ spinner radius.

Performance

Static Thrust From the simple axial-momentum theory, the static thrust F_0 of an actuator disk of diameter d_p is given by

$$F_0 = (\pi \rho / 2)^{1/3} (\mathcal{P} d_p)^{2/3} = 10.4 \text{ bhp} \times d_p^{2/3} \quad (\text{at sea level}) \quad (11.5.67)$$

The **thrust horsepower** (thp) is accordingly

$$\text{thp} = \frac{F_0}{\text{bhp}} = (38,400 / N d_p) (1/C_P^{1/3}) \quad (11.5.68)$$

Equations (11.5.67) and (11.5.68) assume uniform axial velocity, no rotation of the air, and no profile losses. Consequently, they may be in error by as much as 50 percent. Hesse suggests the use of the equations

$$\eta_{p \text{ static}} = \sqrt{\frac{2}{\pi}} \frac{C_F^{3/2}}{C_P} = 0.798 \frac{C_F^{3/2}}{C_P} \quad (11.5.69)$$

and

$$F = 10.42 [d_p (\eta_{p \text{ static}}) \text{shp}]^{2/3} (\rho/\rho_0)^{1/3} \quad (11.5.70)$$

together with data computed for a specific propeller, as illustrated in Fig. 11.5.29. The static thrust for a given power input increases with the diameter and the number of blades. Controllable pitch propellers selected for good overall performance will develop 3 to 4 lb of thrust per shp.

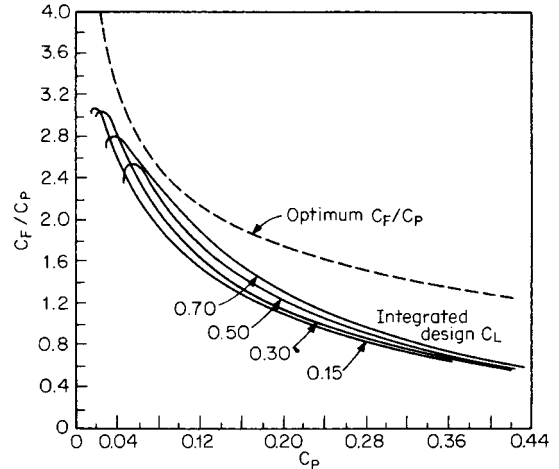


Fig. 11.5.29 Static-thrust performance of a propeller; four-bladed, 100 activity propellers of various integrated design C_L 's. (From Hamilton Standard Division, United Aircraft Corporation.)

At flight conditions the performance may be obtained from generalized charts presenting C_p as a function of the advance ratio J , with the propeller efficiency and blade pitch angle at 75 percent radius, $\theta_{3/4}$, as parameters. Figure 11.5.30 is such a chart.

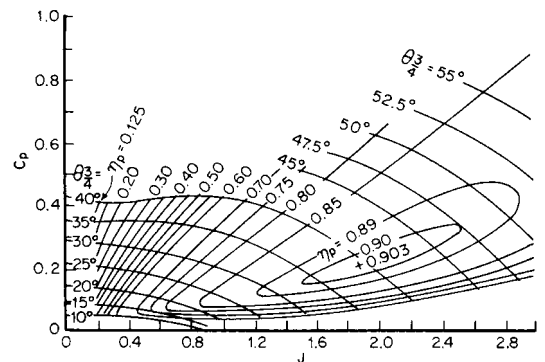


Fig. 11.5.30 Propeller performance—efficiency in forward flight; four-bladed, 100 activity factor, 0.500 integrated design C_L propeller. (From Hamilton Standard Division, United Aircraft Corporation.)

Reverse Thrust By operating the propeller blades at large negative angles of attack, reversed thrust can be developed. In that condition, the blades are stalled, and as in the case of static thrust, the forces acting on the blades cannot be calculated. In practice, the reverse-pitch stop is set by trial and error so that the propeller can absorb the rated power at zero speed, i.e., at $V_0 = 0$. With fixed-pitch reversing, the power absorbed when there is forward speed will be smaller than the rated value, but the reversed thrust is usually substantially larger than the static forward thrust corresponding to the rated power. The landing roll of an aircraft with reversed thrust plus brakes is approximately 45 percent of that with brakes alone.

Compressibility Effects As the relative velocity between an airfoil and the free-stream air approaches the sonic speed, the lift coefficient

11-98 JET PROPULSION AND AIRCRAFT PROPELLERS

C_L decreases rapidly, and simultaneously there is a large increase in the drag coefficient C_D . The propeller is subject to those effects. Since the acoustic speed decreases from sea level to the isothermal altitude, the effects appear at lower tip speeds at high altitude. Furthermore, the effect is more pronounced at higher tip speeds. Shock waves are formed at the leading edge of a propeller blade when its pitch-line velocity approaches the local sonic velocity of the air. As a consequence, the coefficient C_F is reduced and C_p is increased, thereby adversely affecting the propulsive efficiency of the propeller.

Because of the high propulsive efficiency of propellers, the application of advanced technologies may provide **turboprop**-powered transports with cruise speeds and other desirable characteristics comparable to advanced turbofan-powered transports, but with a 15 to 20 percent reduction in fuel consumption.

Advanced turboprop propeller blades operate at high power loading, are extremely thin, and have swept leading edges to minimize compressibility losses. Shaping the spinner and nacelle minimizes choking and compressibility losses. Efficiencies of about 70 percent at Mach 0.8 and design power loadings have been achieved in research propellers. Such propellers may be relatively noisy because the tips may be slightly supersonic at Mach 0.8 cruise. Attenuating the noise within the cabin wall will likely add airframe weight and reduce the fuel savings.

Mechanical Design

Blades The principal blade loadings are (1) steady tensile, due to centrifugal forces; (2) steady bending, due to the aerodynamic thrust and torque forces; and (3) vibratory bending, due to cyclic variations in airloads and other excitations originating in the engine. The most serious and limiting stresses usually result from the vibratory loadings. The principal vibratory loading results from the cyclic variation in angle of attack of the blades when the axis of rotation is pitched or yawed relative to airstream. When the axis is pitched up, such as when the aircraft is in a high-angle-of-attack climb, the blades are at a higher angle of attack on the downstroke than when on the upstroke. This results in a once per revolution, **1E**, variation in aerodynamic loading on the blades, usually referred to as **1E aerodynamic excitation**, and a steady **side force** and **yawing moment**, which are transmitted through the shaft to the aircraft.

The degree of pitch or yaw of the propeller axis is usually measured in terms of the **excitation factor**, defined as

$$\text{Excitation factor} = \psi(V_i/400)^2 \quad (11.5.71)$$

where ψ = angle of pitch or yaw, deg; V_i = indicated flight velocity, mi/h. Another factor sometimes used is Aq , where $A = \psi^2$, $q = 12\rho V_i^2$, Aq = excitation factor $\times 410$.

Because of the restoring moment of the **centrifugal loads** on the blade elements when the blade deflects in bending, centrifugal forces have the effect of apparently stiffening the blade in **bending**. In Fig. 11.5.31, the bending natural frequency increase with rpm. At some rpm, the bending natural frequency will come into resonance with the **1E** excitation, at which point small loadings will be greatly magnified (limited only by the damping present in the blade).

Propellers are designed so that the **1E** resonant speed is above any expected operating speed. However, there will always be some magnification of the vibratory loads (due to proximity to resonant speed), resulting in disproportionately high vibratory stresses. As indicated in Fig. 11.5.31, blades normally pass through a **2E** resonance in coming up to speed (usually not critical because it is a transient condition) and may pass through or be close to resonance with other modes.

The **natural frequencies** of the rotating propeller blade can be computed with good accuracy, but since the excitation varies from aircraft to aircraft and is usually not well defined, vibration surveys must be made of all new installations. These often result in the definition of ranges at which continuous operation should be avoided. **Allowable vibratory stresses** are limited by the fatigue strength of the material. Unlike the steady-stress limits, **fatigue strength** is not a unique function of the material but is a function of surface finish as well. A sharp notch in the

surface reduces the fatigue strength to a very low value. If propellers were designed to hold vibratory stresses below the lowest possible fatigue strength, the blades would be unacceptably heavy. Thus propellers are designed on the maintenance of a reasonably smooth surface finish. Since the blade surfaces are constantly subject to **store damage**, blades must be regularly inspected to make sure that the finish does not deteriorate below design standards.

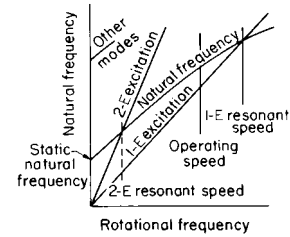


Fig. 11.5.31 Relation between blade natural frequency and major excitations.

Propeller blades are stalled when operating at low forward speeds and when reversing (see Performance, above). Under these conditions torsion-mode **stall flutter** can occur.

In general, **1E** considerations control the design of the **inboard** portions of a blade, and **stall flutter** the **outboard** sections.

There are five types of **blade construction** in common use today: **solid aluminum**; **fabricated steel**; **one-piece steel**; **monocoque, fiberglass construction**, supported on a steel shank; and a construction with a **hollow steel central spar and a lightweight fiberglass cover** that forms the aerodynamic contour of the blade. As in any beam designed on the basis of bending loads, it is desirable to concentrate the structural material at the maximum radii, as in the flanges of a simple I beam, and omit it from the center, where it carries no load. This is accomplished, with steel blades, by making them hollow. The structural material is concentrated in the outer fibers, or surface. In general, steel blades weigh about 80 to 85 percent of the equivalent solid aluminum blade. The advantage of steel increases with size. The blades normally constitute from one-third to one-half of the total propeller weight.

The **hub** retains the blades and contains the pitch-change motor. A **pitch-change mechanism** is provided so that the blades can be positioned at the proper angle of attack α to absorb the desired power at the desired rpm, regardless of flight speed. If the pitch is unchanged, as in Fig. 11.5.32, the angle of attack is excessive at low speed. This prevents the engine from reaching rated speed and delivering rated power. The centrifugal loads on the blade elements tend to rotate the blades toward flat pitch (see Fig. 11.5.33). The pitch-change motor acts against this moment by applying a pitch-increasing moment. The addition of **counterweights**, shown dotted in Fig. 11.5.33, reduces the moment and the size of the pitch-change motor. Counterweights, however, add to the radial

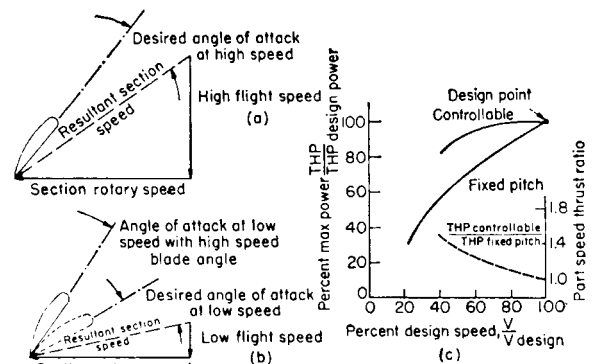


Fig. 11.5.32 Effect of flight speed on the desired blade angle.

centrifugal load of the blades, necessitating a heavier retention, and consequently do not necessarily reduce the net weight of the propeller.

Most pitch-change mechanisms employ a **hydraulic piston**, mounted on the hub, with feed through the propeller shaft and with rotation of the blades by means of gears or links. **Electric motors** and **direct mechanical drives** have been used successfully. In the past, the weight of all systems, when fully developed, has turned out to be about the same.

Action of the pitch-change motor is limited by **low-** and **high-pitch stops**. These prevent the blades from assuming negative angles with reverse thrust. On reciprocating engines, the low-pitch stop is set to allow the propeller to absorb approximately rated power at zero forward speed. A lower setting results in higher windmilling drags in gliding flight, which could be dangerous if carried too far. In reversing propellers the low-pitch stop is automatically removed when the controls are set for reverse pitch. The high-pitch stop prevents the propeller from reversing through the positive range. In feathering propellers it is set at the angle which gives zero aerodynamic moment about the shaft.

Propeller feathering is provided in order to reduce the drag of a dead engine. To accomplish it, the blade-angle range is extended to 90°, approximately. Auxiliary pitch-change power is provided to complete the feathering as the engine slows down and to unfeather when the engine is stationary.

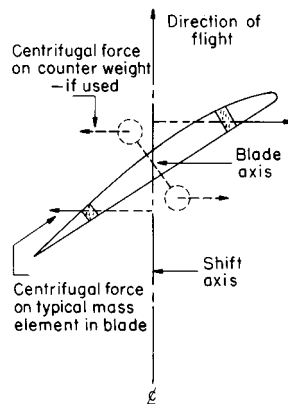


Fig. 11.5.33 Twisting effect of centrifugal loads on blades.

Reversing is provided in order to give propeller braking on the landing roll. It is accomplished by removing the flight low-pitch stop and driving the blades to a high negative **reverse-pitch angle**. The principal mechanical problem is to provide a mechanism which has the least possible chance of going into reverse inadvertently.

The **propeller control** is that portion of the system which regulates the blade angle. In light aircraft, this may consist merely of a mechanism which sets a given blade angle corresponding to a given position of the cockpit control. In such cases the propeller acts as a fixed-pitch propeller except when activated by the pilot. In most cases, the propeller control regulates blade angle so as to maintain a preset rotary rpm, irrespective of flight speed or shaft power. The **basic elements** of this system normally consist of a spring-balanced, engine-drive flyweight delivering an error signal which directs the servo, or pitch-change motor, to increase or decrease blade angle (Fig. 11.5.34). The control loop is closed by rpm feedback through the main engine. This basic system may be embellished with anticipating and delay devices to

maintain speed in rapid throttle movements, synchronizing to coordinate two or more engines, and with overriding features to activate the reversing and feathering sequences. (See also Sec. 16.)

Propeller **controls** are fundamentally the same, with several added secondary features. First, because the engine is capable of a very rapid increase or decrease in torque and because of the high gear ratio between the propeller and engine shaft, anticipating features are necessary to prevent overspeeds in the propeller from producing large overspeeds and possible failure in the turbine. Second, because of the high idle rpm needed to maintain the pressure ratio in the compressor, the low-pitch stop of the turboprop engine propeller must be set substantially lower than for a piston engine. This is not true of a free-turbine drive and is only partially true of a split-compressor engine. In the event of an **engine failure**, the propeller, sensing the loss in rpm, will govern down to the low-pitch stop. This may lead to large, often uncontrollable, negative thrust. To avoid this possibility, an engine-shaft torque signal is put into the control, a negative torque automatically activating the feathering system. This portion of the system is known as the **ENT (emergency negative-thrust)** system. Third, because of the high idle rpm characteristic of the turboprop engine, and the resulting low blade angles at low power in the ground-taxi regime, provision must be made to cut out the governing system and substitute direct blade-angle regulation (known as **beta control**). This is required because the propeller will not govern under these conditions as the torque-to-blade-angle relationship goes to zero. The propeller control of a turboprop engine is normally mechanically coordinated directly to the engine throttle, leaving only a single control, with so-called power lever, in the aircraft.

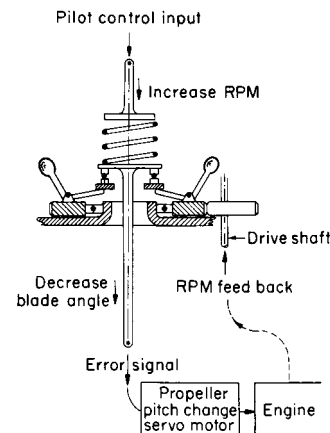


Fig. 11.5.34 Propeller-speed governor.

The shaft on which the propeller is mounted is subjected to the steady-thrust load, vibratory loads due to the propeller side, and **gyroscopic forces** (the $1E$ moment, acting on the blades, is reactionless in propellers with three or more blades). In large aircraft, the shaft size is usually determined by the propeller side force. In aircraft used for aerobatics, gyroscopic loads may become limiting. The **gyroscopic moment** on the propeller shaft is given by $2\omega_1 \cdot \omega_2(I_1 - I_2)$, where ω_1 = angular velocity of maneuver, ω_2 = angular velocity of shaft, I_1 = polar moment of inertia of propeller about shaft, I_2 = moment of inertia of propeller about diameter in plane of rotation. (See also Sec. 3.)

11.6 ASTRONAUTICS

by Aaron Cohen

REFERENCES: "Progress in Astronautics and Aeronautics," AIAA series, Academic Press. "Advances in Astronautical Sciences," American Astronautical Society series. "Handbook of the British Astronautical Association," Koelle, "Handbook of Astronautical Engineering," McGraw-Hill. Purser, Faget, and Smith, "Manned Spacecraft: Engineering Design and Operation," Fairchild Publications. Herrick, "Astrodynamics," Vol. 1, Van Nostrand Reinhold. Cohen, "Space Shuttle," Yearbook of Science and Technology, 1979, McGraw-Hill.

SPACE FLIGHT by Aaron Cohen

The science of astronautics deals with the design, construction, and operation of craft capable of flight through interplanetary or interstellar space. In addition to orbits around, and trajectories between, such bodies as stars, planets, and planetoids, the ascents from and descents to the surface of such bodies are considered to be part of the field.

The purposes of such craft are numerous and include the transportation of people and cargo, the transmission or relaying of signals, and the

carrying of instruments for the measurement of the characteristics of (1) the environment through which the craft flies, (2) the surface of the celestial body over which the craft flies, or (3) astronomical objects or phenomena. The commercial applications of space are now being realized. Many communication, weather, and earth-sensing satellites have been deployed. The space shuttle which provides a method to go to and from low earth orbits offers an expanded use of space.

Processing of materials in a microgravity environment is proving to be very reliable. In microgravity the effects of thermal convection and gravity are eliminated, hence purer materials can be manufactured. Containerless processing can also be accomplished which will lead to additional applications in microgravity materials technology. The space shuttle allows payloads up to 32,000 lb to be placed in earth orbit at altitudes of 150 to 200 nautical miles (nmi) and inclinations of 28.5° to 90°. A description of the space shuttle is contained in Table 11.6.1. Using expendable launch vehicles or the space shuttle and propulsion-assistance modules, satellites can be placed in various orbits. A polar orbit is one whose orbital plane includes the earth's axis and permits

Table 11.6.1 Specifications of the Space Shuttle System and Its Components

Component	Characteristic	Specifications	
Overall system	Length	184.2 ft (56.1 m)	
	Height	76.6 ft (23.3 m)	
	System weight		
	Due-east launch	4,490,800 lbm (2037.0 Mg)	
	104° launch azimuth	4,449,000 lbm (2018.0 Mg)	
	Payload weight		
	Due-east launch	65,000 lbm (29.5 Mg)	
	104° launch azimuth	32,000 lbm (14.5 Mg)	
	External tank		
External tank	Diameter	27.8 ft (8.5 m)*	
	Length	154.4 ft (47.1 m)	
	Weight		
	Launch	1,648,000 lbm (747.6 Mg)	
	Inert	70,990 lbm (32.2 Mg)	
	Solid rocket booster (SRB)		
Solid rocket booster (SRB)	Diameter	12.2 ft (3.7 m)	
	Length	149.1 ft (45.4 m)	
	Weight (each)		
	Launch	1,285,100 lbm (582.9 Mg)	
	Inert	176,300 lbm (80.0 Mg)	
	Launch thrust (each)	2,700,000 lbf (12.0 MN)	
Separation motors (each SRB), four aft, four forward	Thrust (each)	22,000 lbf (97.9 kN)	
Orbiter	Length	121.5 ft (37.0 m)	
	Wingspan	78.1 ft (23.8 m)	
	Taxi height	57 ft (17.4 m)	
	Weight		
	Inert	161,300 lbm (73.2 Mg)	
	Landing		
	With payload	203,000 lbm (92.1 Mg)	
Without payload	173,000 lbm (78.5 Mg)		
Payload bay	Cross range	1,100 nmi (2037.2 km)	
	Length	60 ft (18.3 m)	
Main engine (three)	Diameter	15 ft (4.6 m)	
	Vacuum thrust (each)	470,000 lbf (2090.7 kN)	
Orbital maneuvering system engines (two)	Vacuum thrust (each)	6,000 lbf (26.7 kN)	
Reaction control system engines			
	38 engines	Vacuum thrust (each)	870 lbf (3870 N)
	6 vernier rockets	Vacuum thrust (each)	24 lbf (111.2 N)

* Includes spray-on foam insulation.

line-of-sight contact between the spacecraft and every point on earth on a periodic basis. Synchronous orbits have angular rates equal to the rotational rate of the earth about its axis, providing a spacecraft locus of positions at nearly constant longitude. Orbital-parameter variation provides a wide variety of other orbits, permitting the selection of characteristics most suitable for the specific flight objective, such as communication relays, meteorological observations, earth surface monitoring, or interplanetary trajectories.

ASTRONOMICAL CONSTANTS OF THE SOLAR SYSTEM

by Michael B. Duke
NASA

REFERENCES: "Handbook of the British Astronautical Association." Blanco and McCuskey, "Basic Physics of the Solar System," Addison-Wesley. Clarke, Constants and Related Data for Use in Trajectory Calculations, *Tech*

Rep. 32-604, Jet Propulsion Lab., Pasadena. Francis, Constants for an Earth-Moon Transit, *Lockheed Rep. LAC/421571*. Krause, On a Consistent System of Astrodynamics Constants, NASA-TN D-1642. Makemson, Baker, and Westrom, Analysis and Standardization of Astrodynamics Constants, *Jour. Astro. Sci.*, Spring 1961. Townsend, "Orbital Flight Handbook," Martin Co. Space and Planetary Environment Criteria Guidelines for Use in Space Vehicle Development, 1982 Revision (Vols. I and II), *NASA Technical Memoranda 82478 and 82501*.

A greater number of astronomical constants is used in astrodynamics and astronautics than in classic astronomy because astronautics is a kind of experimental astronomy and its missions vary so greatly. A higher accuracy is also necessary because the astrodynamics missions include departure, landing, and flyby maneuvers. Some of the constants, given in relative and astronomical units in celestial mechanics, must be known in absolute units for astrodynamics purposes. Tables 11.6.2 to 11.6.4 provide the latest observed data for standardization of astrodynamics computations. See references for additional constants.

Table 11.6.2 General, Terrestrial, and Lunar Constants

1. Ephemeris second: $1 \text{ sec}_E = 1/31,556,925.9747$ of tropical year at 1900.0.
2. Mean solar day (culmination period of the mean sun):

$$1^d = 1^{d*}(.002\ 737\ 909\ 265 + 0^{d*}.589 \times 10^{-10}T = 24^{h*}03^{m*}56^{s*}.555\ 360\ 50 + 0^{s*}.050\ 89 \times 10^{-4}T$$

$$= 1^{\text{rot}}.002\ 737\ 811\ 891 - 0^{\text{rot}}.001\ 4 \times 10^{-10}T = (1 \pm 10^{-8})\frac{d}{2}$$
3. Mean sidereal day or mean equinoctial day (culmination period of the vernal equinox):

$$1^{d*} = 0^{d*}.997\ 269\ 566\ 414 - 0^{d*}.587 \times 10^{-10}T = 23^{h*}56^{m*}04^{s*}.090\ 538\ 17 - 0^{s*}.050\ 716\ 8 \times 10^{-4}T$$

$$= 0^{\text{rot}}.999\ 999\ 902\ 892 - 0^{\text{rot}}.589 \times 10^{-10}T$$
4. Mean stellar day or mean period of the earth's rotation (culmination period of an equatorial star without proper motion):

$$1_{st}^d = 1^{\text{rot}} = 1^{d*}.000\ 000\ 097\ 108 + 0^{d*}.589 \times 10^{-10}T$$

$$= 24^{h*}00^{m*}.008\ 390\ 13 + 0^{s*}.050\ 89 \times 10^{-4}T$$

$$= 0^{d*}.997\ 269\ 663\ 257 + 0^{d*}.001\ 4 \times 10^{-10}T = 23^{h*}56^{m*}04^{s*}.098\ 905\ 40 + 0^{s*}.001\ 21 \times 10^{-5}T$$
5. Tropical year (equinox to equinox):

$$P_{\text{trop}} = (365.242\ 198\ 78 - 0.000\ 006\ 138\ T)\frac{d}{2} = 365\frac{d}{2}05\frac{h}{2}48\frac{m}{2}45\frac{s}{2}.530\ T$$
6. Sidereal year (fixed star to fixed star):

$$P_{\text{sid}} = (365.256\ 360\ 42 + 0.000\ 000\ 11\ T)\frac{d}{2} = 365\frac{d}{2}06\frac{h}{2}09\frac{m}{2}09\frac{s}{2}.54 + 0\frac{s}{2}.010\ T$$
7. Synodic month (new moon to new moon):

$$P_{\text{syn}} = (29.530\ 588\ 2 - 0.000\ 000\ 2\ T)^d = 29^d\ 12^h\ 44^m\ 02^s.78 - 0^{s*}.017\ T$$
8. Tropical month (equinox to equinox):

$$P_{\text{trop}} = (27.321\ 581\ 7 - 0.000\ 000\ 2\ T)^d = 27^d\ 07^h\ 43^m\ 04^s.7 - 0^{s*}.017\ T$$
9. Sidereal month (fixed star to fixed star):

$$P_{\text{sid}} = (27.321\ 661\ 0 - 0.000\ 000\ 2\ T)^d = 27^d\ 07^h\ 43^m\ 11^s.47 - 0^{s*}.017\ T$$
10. Astronomical unit (mean earth-sun distance): $\text{au} = 149,598,700 \pm 400$ km.
11. Light year: $\text{ly} = (9.460\ 530 \pm 0.000\ 003) \times 10^{12}$ km = $63,239.39 \pm 0.15$ au.
12. Parsec: $\text{pc} = 206,264.806\ 247$ au = $(3.085\ 695 \pm 0.000\ 008) \times 10^{13}$ km.
13. Semimajor axis of the earth's orbit: $a_{\oplus} = 1.000\ 000\ 236$ au = $149,598,700 \pm 400$ km.
14. Mean orbital speed: $v_{\oplus} = 29,784.90 \pm 0.08$ m/sec.
15. Mass of the earth: $M_{\oplus} = (5.9761 \pm 0.004\ 3) \times 10^{24}$ kg.
16. Equatorial radius of the earth: $R_e_{\oplus} = 6,378\ 170 \pm 20$ m.
17. Flattening (oblateness, ellipticity): $f_{\oplus} = (R_e - R_p)/R_e = 0.003\ 352\ 55 = 1:(298.28 \pm 0.05)$.
18. Acceleration of gravity at the earth's surface:

$$g = g_e(1 + \beta \sin^2 \phi + \gamma \sin^2 2\phi) = 9.780\ 315(1 + 0.005\ 302\ 74 \sin^2 \phi - 0.000\ 005\ 9 \sin^2 2\phi) \text{ m/sec}^2$$
19. Moments of inertia of the earth:

$$A = (0.329\ 681_4 \pm 0.000\ 11) M_{\oplus} R_e^2 = (0.801\ 50 \pm 0.000\ 85) \times 10^{38} \text{ kg-m}^2$$

$$C = (0.330\ 763_9 \pm 0.000\ 11) M_{\oplus} R_e^2 = (0.804\ 13 \pm 0.000\ 85) \times 10^{38} \text{ kg-m}^2$$
20. Circular and escape velocities from the earth's surface at the equator.

$$v_{\text{cir}} = 7,905.39 \pm 0.06 \text{ m/sec} \quad v_{\text{esc}} = v_{\text{cir}} 2^{1/2} = 11,179.91 \pm 0.08 \text{ m/sec}$$
21. Mean observed distance of the perturbed moon from the earth:

$$\bar{r}_{\oplus} = 384,401.0 \pm 1.0 \text{ km} = (60.268\ 23 \pm 0.000\ 35) R_e_{\oplus} = 0.002\ 569\ 548 \pm 0.000\ 000\ 014 \text{ au}$$
22. Semimajor axis of the moon's orbit: $a_{\opl�} = 1.000\ 907\ 681\bar{r}_{\oplus} = 384\ 749.9 \pm 1.0$ km.
23. Mean orbital velocity: $v_{\opl�} = 1,024.089 \pm 0.003$ m/sec.
24. Mass of the moon: $M_{\opl�} = (7.353\ 4 \pm 0.007\ 5) \times 10^{22}$ kg = $M_{\opl�} (81.270 \pm 0.024)$.
25. Semiaxes of the moon ellipsoid: $a = 1,738,780 \pm 186$ m; $b = 1,738,452 \pm 209$ m; $c = 1,737,688 \pm 188$ m.

The time T is in Julian centuries of 36,525 days from 1900 Jan. 0.5 U.T. (universal time). The constants are given with probable errors (pe).

Copyright (C) 1999 by The McGraw-Hill Companies, Inc. All rights reserved. Use of this product is subject to the terms of its License Agreement. [Click here to view.](#)

11-102 ASTRONAUTICS

Table 11.6.3 Planetary Orbit Data

Planet	Number of satellites	Semimajor axis, au	Sidereal period, year	Synodic period, days	Mean daily motion, s/day	Eccentricity, e	Inclination to ecliptic, i , deg	Mean ascending node Ω , deg	Longitude perihelion, ω , deg	Orbital speed, km/s	Planetary escape speed, km/s	Gravity at surface, cm/s^2
Mercury ☿		0.387	0.2411	115.88	14,732.42	0.206	7.004	47.857	76.833	47.8	4.3	370
Venus ♀		0.723	0.6152	583.92	5767.2	0.007	3.394	76.320	131.008	35.0	10.3	887
Earth ☾	1	1.0000	1.0000		3548.19	0.017			102.253	29.8	11.2	982
Mars ♂	2	1.524	1.8822	779.94	1886.52	0.093	1.850	49.250	335.322	24.2	5.0	372
Jupiter ♃	16	5.203	11.86	398.88	299.13	0.048	1.305	99.44	12.72	13.1	61	2599
Saturn ♄	15	9.54	29.46	378.09	120.46	0.056	2.490	113.307	92.264	9.7	39.4	1290
Uranus ♅	5	19.2	84.0	369.66	42.23	0.50	0.773	73.796	170.011	6.8	21.2	830
Neptune ♆	2	30.1	164.8	367.49	21.53	0.009	1.774	131.340	44.274	5.4	23.8	1380
Pluto ♇	1	39.7	247.7	366.74	14.29	0.249	17.170	109.886	112.986	4.7	~ 1.3	

Table 11.6.4 Physical Data of Sun, Moon, and Planets

Name	Equatorial radius, km	Polar radius, km	Mass, kg	Mean density, g/cm ³	Visual albedo	Rotational period	Inclination of equator to orbit, deg
Sun	696,000		1.99×10^{30}	1.42		~ 27 days	7.25
Moon	1,738		7.35×10^{22}	3.34	0.067	27.322 days	6.65
Mercury	2,439		3.30×10^{23}	5.44	0.235	58.646 days	< 1
Venus	6,051		4.87×10^{24}	5.24	0.80	243.0 days	2.2
Earth	6,378	6,356	5.98×10^{24}	5.52	0.39	23.93 h	23.45
Mars	3,397	3,375	6.42×10^{23}	3.93	0.1-0.4	24.62 h	25
Jupiter	71,398	66,793	1.89×10^{27}	1.32	0.51	9.92 h	3.1
Saturn	60,330	55,020	5.68×10^{26}	0.71	0.45	10.66 h	26.7
Uranus	26,145	25,518	8.73×10^{25}	1.2	0.56	11-24 h	97.9
Neptune	24,700	24,060	1.03×10^{26}	1.67	0.57	~ 18 h	28.8
Pluto	1,600		$1.4-2 \times 10^{22}$	0.55-1.75	0.25-0.5	?	?

DYNAMIC ENVIRONMENTS

by Michael B. Duke

NASA

REFERENCES: Harris and Crede, "Shock and Vibration Handbook," McGraw-Hill. Beranek, "Noise Reduction," McGraw-Hill. Crandall, "Random Vibration," Technology Press, MIT. Neugebauer, The Space Environment, *Tech. Rep. 34-229*, Jet Propulsion Lab., Pasadena, 1960. Hart, Effects of Outer Space Environment Important to Simulation of Space Vehicles, *AST Tech Rep. 61-201*. Cornell Aeronautical Lab. Barret, Techniques for Predicting Localized Vibratory Environments of Rocket Vehicles, *NASA TN D-1836*. Wilhold, Guest, and Jones, A Technique for Predicting Far Field Acoustic Environments Due to a Moving Rocket Sound Source, *NASA TN D-1832*. Eldred, Roberts, and White, Structural Vibration in Space Vehicles, *WADD Tech. Rep. 61-62*. Bolt, Beranek, and Newman, Exterior Sound and Vibration Fields of a Saturn Vehicle during Static Firing and during Launching, *U.S.A. Ord. Rep. 764*.

The forces required to propel a space vehicle from the launch pad are tremendous. The dynamic pressures generated in the atmosphere by large rocket engines are exceeded only by nuclear blasts. Slow initial ascent from the launch pad is followed by rapid acceleration and high *g* loading, and acoustic and aerodynamic forces drive every point of the vehicle surface. The space-vehicle velocity quickly becomes supersonic and continues to hypersonic velocities. Gradually, as the space vehicle leaves the atmosphere, the aerodynamic forces recede. Then suddenly the rocket thrust decays and is followed by the ignition of another rocket, which quickly develops thrust and continues to accelerate the space vehicle. Finally, the space vehicle becomes weightless. In completing a mission, a space vehicle is subjected to the additional environmental extremes of planetary landings, escape, and earth reentry.

These environments represent basic criteria for space-vehicle design. For operational reliability, the most important are the shock, vibration, and acoustic environments which are present to varying magnitudes in all operational phases and which constitute major engineering problems.

It is not possible to have original environmental data prior to fabrication and testing of a particular structure. Vibration, shock, and acoustic noise adversely affect structural integrity and vehicle reliability. These environments must be considered prior to design and fabrication and then again for design verification through ground testing. Precise vibration and acoustic environmental predictions are complicated because of structural nonlinearities, random forcing functions, and multiple-degree-of-freedom systems. Current environmental-prediction techniques consist mainly of extrapolating measured data obtained from existing vehicles. Acoustic environments produced during ground test are important factors in evaluating ground-facility locations and design, personnel safety, and public relations.

A source of sound common to all jet and rocket-engine propulsion systems is the turbulent exhaust flow. This high-velocity flow produces pressure fluctuations, referred to as noise, and has adverse effects on the vehicle and its operations. Also, far-field uncontrolled areas may be subjected to intense acoustic-sound-pressure levels which may require personnel protection or sound-suppression devices. (See also Sec. 12.)

The sound-generation mechanism is presented in empirical and analytical form, utilizing measured sound pressures and the known engine operational parameters. This combination of empirical terms and analytical reasoning provides a generalized relationship to predict sound-pressure levels for the vehicle structure and also for far-field areas. It has been shown by Lighthill (*Proc. Royal Soc.*, 1961) that acoustic-power generation of a subsonic jet is proportional to $\rho V^8 D^2 / a_0^3$, where ρ is the density of the ambient medium, a_0 is the speed of sound in the ambient medium, V is the jet or rocket exit exhaust velocity, and D is a characteristic dimension of the engine. Attempts have been made to extend this relationship to allow supersonic-jet acoustic-power predictions to be made, but no one scheme is accepted for broad use.

From acoustic-data-gathering programs utilizing rocket engines, various trends have been noted which facilitate acoustic predictions. For rocket engines of up to 5×10^9 W mechanical power, the acoustic efficiency shows a nonlinear rate of increase. For greater mechanical power, the acoustic efficiency approaches a value slightly higher than 0.5 percent (Fig. 11.6.1).

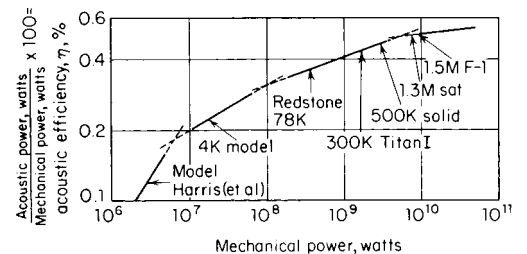


Fig. 11.6.1 Acoustic-efficiency trends.

Turbulent-exhaust-flow sound-source mechanisms also exhibit directional characteristics. Figure 11.6.2 shows data from a Saturn rocket vehicle launch with the microphone flush-mounted on the vehicle skin at approximately 100 ft above the nozzle plane.

During the period between on-pad firing and post-lifting-off or mainstage flight, the exhaust-flow direction changes. The directivity has also shifted 90° to retain its inherent relationship to the exhaust stream. The sound-pressure-level variation during a small time interval—between

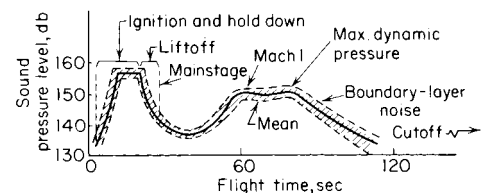


Fig. 11.6.2 Vehicle acoustic environment.

11-104 ASTRONAUTICS

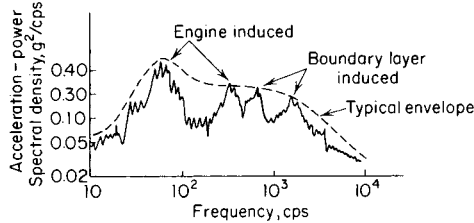


Fig. 11.6.3 Random-vibration spectrum of a space-vehicle structure.

on-pad condition and shortly after liftoff—depends on the changes which have occurred in the directivity and the jet-exhaust-velocity vector (Fig. 11.6.2). The change in sound-pressure level is 20 dB approximately in this case and is indicative of the significance of a sound source's directional properties, which depend on velocity and temperature of the jet.

The acoustic environments produced by a given conventional engine can be empirically described by that engine's flow parameters and geometry. It is difficult to predict the acoustic environments for nonconventional engines such as the plug-nozzle and expansion-deflection engines.

The turbulent-boundary-layer problem of high-velocity vehicle flights is difficult to evaluate in all but the simplest cases. Only for attached, homogeneous, subsonic flows can the boundary-layer noise be estimated with confidence.

The vibratory environment on rocket vehicles consists of total-vehicle bending vibrations, in which the vehicle is considered a non-uniform beam, with low-frequency responses (0 to 20 Hz) and localized vibrations with frequencies up to thousands of hertz. (See also Sec. 5.)

The response of a simple structure to a dynamic forcing function may be described by the universal equation of motion given as $M\ddot{x} + c\dot{x} + Kx = F(t)$ or $F(t)x(t) = (M - K\omega^2 - j(c/\omega))$ and is a complex function containing real and imaginary quantities. In the case of rocket-vehicle vibrations, $F(t)$ is a random forcing phenomenon. Thus, the motion responses must also be random. Random vibration may be described as vibration whose instantaneous magnitudes can be specified only by probability-distribution functions giving the probable fraction of the total time that the magnitude, or some sequence of magnitudes, lies within a specified range. In this type of vibration, many frequencies are present simultaneously in the waveform (Fig. 11.6.3). Power spectral density (PSD; in units of g^2/Hz) is defined as the limiting mean-square value of a random variable, in this case acceleration per unit bandwidth; i.e.,

$$PSD = \lim_{\Delta f \rightarrow 0} \bar{g}^2 / \Delta f = d\bar{g}^2 / df$$

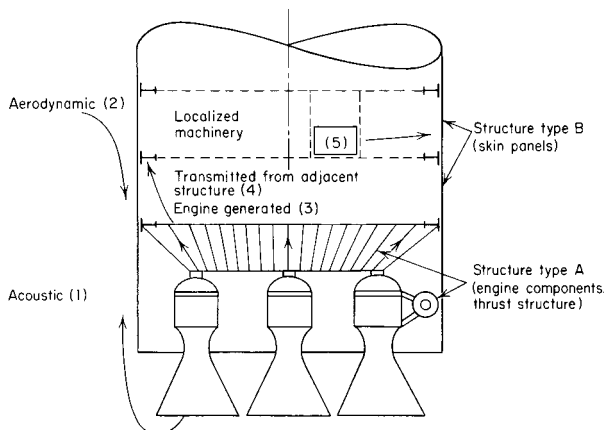


Fig. 11.6.4 Sources of vibration excitation.

The sources of vibration excitation are (1) acoustic pressures generated by rocket-engine operation; (2) aerodynamic pressures created by boundary-layer fluctuations; (3) mechanically induced vibration from rocket-engine pulsation, which is transmitted throughout the vehicle structure; (4) vibration transmitted from adjacent structure; and (5) localized machinery. Since the mean square acceleration is proportional to power, the total vibrational power at any point on the vehicle may be expressed as

$$P_v = P_v(1) + P_v(2) + P_v(3) + P_v(4) + P_v(5)$$

This is illustrated in Fig. 11.6.4 for an arbitrary vehicle. In many instances, the structure is principally excited by only one of these sources and the remaining can be considered negligible (Fig. 11.6.5). The vibration characteristics of structure B, taken from a skin panel, closely correspond to the trends of the acoustic pressures during flight. However, structure A, taken from a rocket-engine component, exhibits stationary trends, indicating no susceptibility to the impinging acoustic field. Thus, for this structure, it can be assumed that only $P_v(3)$ is significant, whereas for structure B, only $P_v(1)$ is the principal exciting source during the on-pad phase and only $P_v(2)$ is significant during the maximum dynamic-pressure phase. This also holds true for captive firings of the vehicle, in which only $P_v(1)$ is significant for structure B and $P_v(3)$ for structure A.

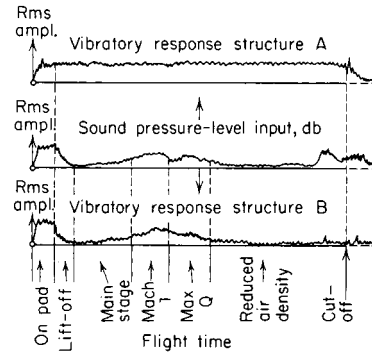


Fig. 11.6.5 Typical structural responses to a random-vibration environment.

SPACE-VEHICLE TRAJECTORIES, FLIGHT MECHANICS, AND PERFORMANCE

by O. Elnan, W. R. Perry, J. W. Russell, A. G. Kromis, and D. W. Fellenz

University of Cincinnati

REFERENCES: Russell, Dugan, and Stewart, "Astronomy," Ginn. Sutton, "Rocket Propulsion Elements," Wiley. White, "Flight Performance Handbook for Powered Flight Operations," Wiley. "U.S. Standard Atmosphere, 1962," NASA, USAF, U.S. Weather Bureau. Space Flight Handbooks, NASA SP-33, SP-34, and SP-35. Gazley, Deceleration and Heating of a Body Entering a Planetary Atmosphere from Space, "Visits in Astronautics," Vol. I, Pergamon. Chapman, An Approximate Analytical Method for Studying Entry into Planetary Atmospheres, NASA-TN 4276, May 1958. Chapman, An Analysis of the Corridor and Guidance Requirements for Super-circular Entry into Planetary Atmospheres, NASA-TN D-136, Sept 1959. Loh, "Dynamics and Thermodynamics of Planetary Entry," Prentice-Hall. Grant, Importance of the Variation of Drag with Lift in Minimization of Satellite Entry Acceleration, NASA-TN D-120, Oct. 1959. Lees, Hartwig, and Cohen, Use of Aerodynamic Lift during Entry into the Earth's Atmosphere, Jour. ARS, 29, Sept 1959. Gervais and Johnson, Abort during Manned Ascent into Space, AAS, Jan. 1962.

Notation

- A = reference area
- A_z = launch azimuth
- B = ballistic coefficient
- C_L = lift coefficient

- e = eccentricity
- f = stage-mass fraction (WP/W_A)
- H = total energy
- H_∞ = hyperbolic excess energy
- I = specific impulse
- Δ_i = plane-change angle
- L = lift force
- m = mass
- n = mean motion ($2\pi/p_{sid}$)
- p = ambient atmospheric pressure
- q = dynamic pressure
- R = earth's equatorial radius
- S = wing area
- T = transfer time, time, absolute temperature
- t_{pp} = time after perigee passage
- V_c = injection velocity
- V = velocity
- V_g = velocity loss to gravity
- \dot{W} = weight
- W_L = payload weight
- W_P = propellant weight
- Y = distance
- α_Ω = right ascension of the ascending node
- $\gamma = \theta - 90^\circ$ = flight-path angle used in reentry analysis
- v = true anomaly
- ω = earth's rotational velocity
- ψ = central angle
- $\sigma = \rho/\rho_0$ = relative atmospheric density
- Y = vernal equinox
- A_e = nozzle exit area
- a = semimajor axis
- C_D = drag coefficient
- D = drag force
- E = eccentric anomaly
- F = thrust
- g = acceleration due to gravity
- H_{esc} = escape energy
- h = altitude
- i = inclination
- J_2 = oblateness coefficient of the earth's potential (second-zonal harmonic)
- M = molecular weight, mean anomaly
- nm = nautical miles
- P = period of revolution
- P_e = nozzle exit pressure
- q_s = stagnation-point heat-transfer rate
- r = radius
- s = range
- t = time
- V_∞ = hyperbolic excess velocity
- V_{id} = ideal velocity
- ΔV = impulsive velocity
- W_A = stage weight ($W_O - W_L$)
- W_O = gross weight
- X = distance
- α = angle of attack, right ascension
- β = exponent of density-altitude function
- λ = longitude
- τ = hour angle
- ω = argument of perigee
- ϕ' = latitude
- ρ = atmospheric density
- θ = flight-path angle

Subscripts

- a = apogee
- e = entry
- f = final

- o = sea level conditions at 45° latitude
- s = space fixed
- vac = vacuum
- circ = circular orbital condition
- esc = escape
- i = initial
- p = perigee
- M = mean
- SL = sea level
- sid = sidereal

ORBITAL MECHANICS

by O. Elnan and W. R. Perry

University of Cincinnati

The motion of the planets about the sun, as well as that of a satellite in its orbit about a planet, is governed by the inverse-square force law for attracting bodies. In those cases where the mass of the orbiting body is small relative to the central attracting body, it can be neglected. This simplifies the analysis of the orbital motion. The shape of the orbit is always a conic section, i.e., ellipse, parabola, or hyperbola, with the central attracting body at one of the foci. Parabolic and hyperbolic orbits are open, terminate at infinity, and represent cases where the orbiting body escapes the central force field of the attracting body.

The laws of Kepler for satellite orbits are (1) the radius vector to the satellite from the central body sweeps over equal areas in equal times; (2) the orbit is an ellipse, with the central attracting body at one of its foci; and (3) the square of the period of the satellite is proportional to the cube of the semimajor axis of the orbit.

Six orbital elements are required to describe the orbit in the orbit plane and the orientation of the plane in inertial space. The three elements that define the orbit are the semimajor axis a , eccentricity e , and period of revolution P . The orientation of the orbit (Fig. 11.6.6) is defined by the

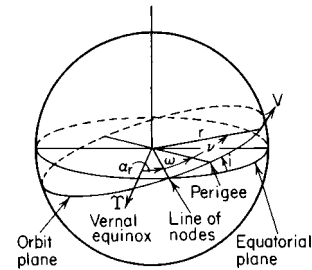


Fig. 11.6.6 Elements of satellite orbit around a planet.

right ascension of the ascending node α_Ω , inclination of the orbit plane to the earth's equatorial plane i , and the argument of perigee ω , which is the central angle measured in the orbit plane from ascending node to perigee. The following equations compute these orbital elements and other orbital parameters.

$$a = (r_a + r_p)/2 = \mu/V_a V_p = r_a/(1 + e) = r_p/(1 - e)$$

$$e = (r_a/a) - 1 = (V_p - V_a)/(V_p + V_a) = (r_p V_p^2/\mu) - 1$$

$$r = a(1 - e^2)/(1 + e \cos v)$$

$$r_a = a(1 + e) = r_p(1 + e)/(1 - e)$$

$$r_p = a(1 - e) = r_a(1 - e)/(1 + e)$$

$$V = [\mu(2/r - 1/a)]^{0.5}$$

$$P = 2\pi(a^3\mu)^{0.5} \quad (\text{for circular orbits, } r = a)$$

$$V_a = V_p(1 - e)/(1 + e) = [\mu(1 - e)/a(1 + e)]^{0.5}$$

$$V_p = V_a(1 + e)/(1 - e) = [\mu(1 + e)/a(1 - e)]^{0.5}$$

$$v = \cos^{-1}\{[2r_a r_p - r(r_a + r_p)]/r(r_a - r_p)\}$$

$$t_{pp} = (a^3/\mu)^{0.5}\{\cos^{-1}[(a - r)/ae] - e[1 - (a - r)^2/(ae)^2]^{0.5}\}$$

$$M = nt_{pp} = E - e \sin E$$

$$r = a(1 - e \cos E)$$

$$V_{esc} = (2\mu/r)^{0.5}$$

11-106 ASTRONAUTICS

The elements may be determined from known injection conditions. For example,

$$\begin{aligned} 1/a &= V_i^2 \mu - 2/r_i \\ e^2 &= \cos^2 V_i (r_i V_i^2 / \mu - 1)^2 + \sin^2 V_i \end{aligned}$$

General precession in longitude of vernal equinox:

$$x = 50''.2575 + 0''.0222T$$

where T is in Julian centuries of 36,525 mean solar days reckoned from 1900 Jan. 0.5 UT.

Measurement of Time

The concept of time is based on the position of celestial bodies with respect to the observer's meridian as measured along the geocentric celestial equator. The mean sun and the vernal equinox (Y) are used to define mean solar time and sidereal time. The mean sun, rather than the apparent (true) sun, is used since the latter's irregular motion from month to month gives a variation in the length of a day. The mean sun moves with uniform speed along the equator at a rate equal to the average of the true sun's angular motion during the year.

One sidereal day is the interval between two successive transits of the vernal equinox across the observer's meridian. A mean solar day is the interval between two successive transits of the mean sun. Local civil time (LCT) is defined to be the hour angle of the mean sun plus 12 h. Local sidereal time is the hour angle of the vernal equinox plus 12 h. For an observer at the Greenwich meridian, the local civil time is Greenwich mean time (GMT) or universal time (UT). The earth is divided into 24 time zones, each 15° of longitude wide. Each zone keeps the time of the standard meridian in the middle of the zone. (See Fig. 11.6.7.)

- Time $T = \tau + 12$ h
- Local sidereal time $LST = \tau_Y + 12$ h
- Greenwich sidereal time $GST = LST + \lambda(w)$
- Local civil time $LCT = \tau_M + 12$ h = mean solar time
- Equation of time $ET = \tau - \tau_M = \alpha_M - \alpha$
- Greenwich mean time $GMT = UT = \tau_M(\text{Greenwich}) + 12$ h = universal time

$$\begin{aligned} LCT &= UT - \lambda(w) \\ GMT &= ZT \pm \lambda^\circ/15 \end{aligned}$$

The "American Ephemeris and Nautical Almanac" gives the equation of time for every day of the year and conversions of mean solar time to and from sidereal time.

Hohmann Transfer This is a maneuver between two coplanar orbits where the elliptical transfer orbit is tangent at its perigee to the lower orbit and tangent at its apogee to the higher orbit. To transfer from a low circular orbit to a higher one, the impulsive velocity required is the difference between the velocities in the circular orbits and the velocities in the corresponding points on the transfer orbit. Using the general velocity equation above, the transfer velocities are $\Delta V_i = \{ \mu[2/r_i -$

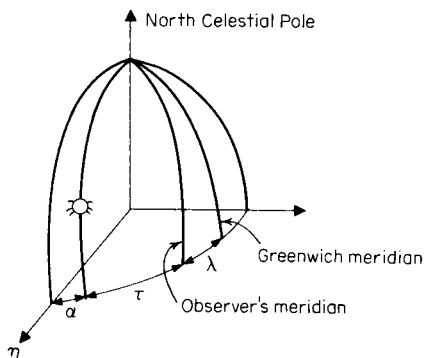


Fig. 11.6.7 Time-zone geometry.

$2/(r_i + r_f)]^{0.5} - (\mu/r_i)^{0.5}$ and $\Delta V_f = (\mu/r_f)^{0.5} - \{ \mu[2/r_f - 2/(r_i + r_f)] \}^{0.5}$, where V_i is the orbiting velocity in low orbit and V_f is the orbiting velocity in the high orbit.

Orbital Lifetime The satellite orbit will gradually decay to lower altitudes because of the drag effects of the atmosphere. This drag force has the form $D = 1/2 C_D A \rho V^2$, where values of the drag coefficient C_D may range from 2.0 to 2.5. The atmospheric density, as a function of altitude, can be used for computing an estimated orbital lifetime of a satellite (Fig. 11.6.8). (See NASA, "U.S. Standard Atmosphere" and "Space Flight Handbooks.")

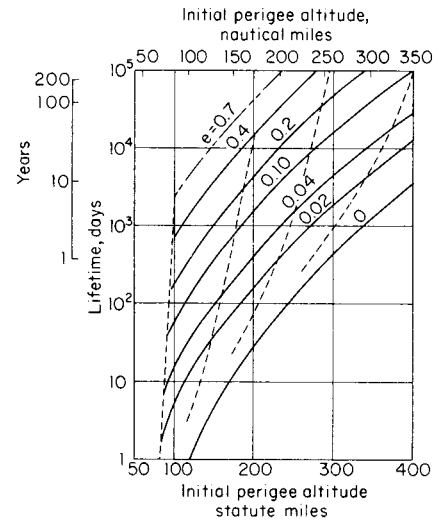


Fig. 11.6.8 Satellite lifetimes in elliptic orbits. $\rho = \text{ARDC, 1959}$; $B = C_D A / 2m = 1.0 \text{ ft}^2/\text{slug}$; $e = \text{initial eccentricity}$; --- = decay histories.

Perturbations of Satellite Orbits There are many secular and periodic perturbations of satellite orbits due to the effects of the sun, the moon, and some planets. The most significant perturbation on close-earth satellite orbits is caused by the oblateness of the earth. Its greatest effects are the precession of the orbit along the equator (nodal regression) and the rotation of the orbit in the orbit plane (advance of perigee). The nodal-regression rate is given to first-order approximation by

$$\dot{\alpha}_\Omega = -3/2 (\mu/a^3)^{0.5} J_2 [R/a(1 - e^2)]^2 \cos i$$

The mean motion of the perigee is

$$\dot{\omega} = J_2 n (2 - (5/2) \sin^2 i) / a^2 (1 - e^2)^2$$

LUNAR- AND INTERPLANETARY-FLIGHT MECHANICS

by J. W. Russell

University of Cincinnati

The extension of flight mechanics to the areas of lunar and interplanetary flight must include the effects of the sun, moon, and planets on the transfer trajectories. For most preliminary performance calculations, the "sphere-of-influence," or "patched-conic," method—whereby the multi-body force field is treated as a series of central force fields—provides sufficient accuracy. By this method, the trajectories in the central force field are calculated to the "sphere of influence" of each body as standard Keplerian mechanics, and the velocity and position of the extremals are then matched to give a continuous trajectory. After the missions have been finalized, the precision trajectories are obtained by numerically integrating the equations of motion which include all the perturbative elements. It is necessary to know the exact positions of the sun, moon, and planets in their respective orbits.

Lunar-Flight Mechanics The moon moves about the earth in an orbit having an eccentricity of 0.055 and an inclination to the ecliptic of about 5.145° . The sun causes a precession of the lunar orbit about the ecliptic, making the inclination of the lunar plane to the earth's equatorial plane oscillate between 18.5 and 28.5° over a period of 18.5 years approx. To compute precision earth-moon trajectories, it is necessary to know the precise launch time to be able to include the perturbative effects of the sun, moon, and planets. The data presented are based on the moon being at its mean distance from earth and neglect the perturbation of the sun and planets; they are therefore only to be considered as representative data. The injection velocity (see Gazley) at 100 nmi for earth-moon trajectories and the impulsive velocity for braking into a 100-nmi orbit about the moon are shown in Fig. 11.6.9 as a function of transfer time. Additional energy is required to offset losses due to gravity and aerodynamic drag as well as to provide plane-change and launch-window capabilities.

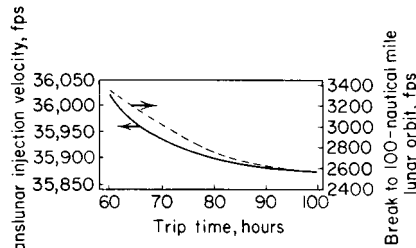


Fig. 11.6.9 Lunar-mission velocity requirements.

Interplanetary-Flight Mechanics The fact that planetary orbits about the sun are not coplanar greatly restricts the number of feasible interplanetary trajectories. The plane of the interplanetary trajectory must include the position of the departure planet at departure, the sun, and the position of the target planet at arrival. The necessary plane change can be prohibitive even though the relative inclinations of the planetary orbits are small. The impulsive velocity required to effect a plane change for a spacecraft departing earth can be approximated by $\Delta V = 195,350 \sin(\Delta_i/2)$, where Δ_i is the amount of plane change required and ΔV is in ft/s.

For interplanetary flight, the "ideal" total energy that must be imparted to the spacecraft is the energy required to escape the gravitational field of the departure planet plus the energy required to change path

Table 11.6.5 Hyperbolic-Excess-Velocity Requirements (ft/s) for Typical Mars Missions

Trip time, days	Opposition year				
	1982	1984	1986	1988	1990
100	27,241	23,012	18,070	15,569	19,955
150	15,940	13,088	11,437	10,520	13,792
200	12,268	10,021	11,486	9,308	12,463
250	10,510	12,688	13,410	10,480	15,784

SOURCE: Gammal, "Space Flight Handbooks."

about the sun so as to arrive at the target planet at the desired position and time. The energy required to escape the gravitational attraction of a planet can be determined by Keplerian mechanics to be $H_{esc} = \mu/r$, where μ is the gaussian gravitational constant and r is the distance from the center of the planet. After escaping the departure planet, the velocity must be altered in both magnitude and direction—in order to arrive at the target planet at the chosen time—by supplying additional energy, $H_\infty = \frac{1}{2}V_\infty^2$.

For determination of vehicle size necessary to inject the spacecraft into the interplanetary trajectory, it is convenient to express the total energy $H = H_{esc} + H_\infty$ in terms of the required injection velocity

$$V_c = \sqrt{2(H_{esc} + H_\infty)} \quad \text{or} \quad V_c \sqrt{2(\mu/r) + V_\infty^2}$$

Hyperbolic excess velocities V_∞ for earth-to-Mars missions are shown in Table 11.6.5 as a function of date. These velocities are near optimum for the trip time and year given but do not represent absolute-optimum trajectories. Mars has a cyclic period with respect to earth of 17 years approx; hence the energy requirements for Mars missions from earth also follow approximate 17-year cycles.

Figure 11.6.10 shows how the hyperbolic excess velocities of Table 11.6.5 can be converted to stage characteristic velocities for a vehicle leaving a 100-nmi earth parking orbit. These are simple cases. In many recent planetary missions, use has been made of planetary flybys to gain velocity and aim the space probe. These "gravity assists" significantly increase the capability of interplanetary flight.

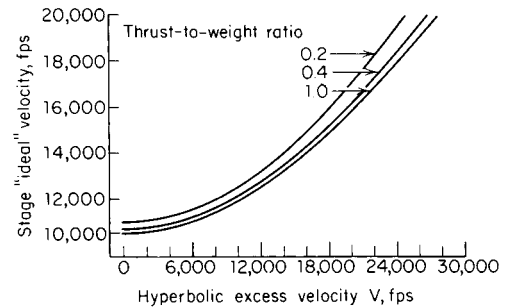


Fig. 11.6.10 Stage-velocity for earth departure from a 100-nmi parking orbit (specific impulse = 450 s).

ATMOSPHERIC ENTRY

by D. W. Fellenz

University of Cincinnati

A vehicle approaching a planet possesses a considerable amount of energy. The entry vehicle must be designed to dissipate this energy without exceeding its limits with respect to maximum decelerations or heating.

The trajectory parameters of an entering vehicle are determined largely by its initial trajectory conditions (suborbital, orbital, superorbital), by the ratio of gas-dynamic forces acting upon it, and by its mass (ballistic factor, lift-drag ratio) and the type of atmosphere it is entering.

Planetary atmospheres (Table 11.6.6) can be assumed, as a first ap-

Table 11.6.6 Planetary Atmospheres

Planet	V_{esc} , ft/s	Gases	M , gmol ⁻¹	T , K	β^{-1} , ft	$\beta\tau$	ρ_{SL} , lb/ft ³
Venus	34,300	2% N ₂ 98% CO ₂	40	250–350	2×10^4	1,006	1.0
Earth	36,800	78% N ₂ 21% O ₂	29	240	2.35×10^4	880	0.0765
Mars	16,900	95% N ₂ 3% CO ₂	28	130–300	6×10^4	132	0.0062
Jupiter	195,000	89% H ₂ 11% He	2.2	100–200	6×10^4	3,600	

11-108 ASTRONAUTICS

proximation, to have exponential density-altitude distributions: $\sigma = \rho/\rho_{SL} = e^{-\beta h}$, where

$$\beta = -(1/\rho)(d\rho/dh) = Mg/RT$$

For more exacting analyses, empirical atmospheric characteristics (e.g., U.S. Standard Atmosphere) have to be used.

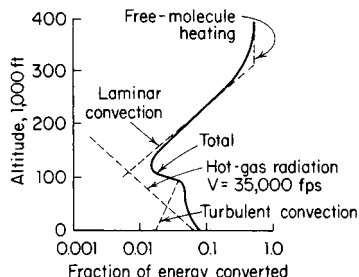


Fig. 11.6.11 Energy conversion during reentry. (After Gazley in Knoelle, "Handbook of Astronautical Engineering.")

The trajectory of the vehicle in flight-path fixed notation with the assumption of a nonrating atmosphere is described as $dV/dt = g \sin \gamma - (C_D A/m)(\rho/2)V^2$ and $(V/\cos \gamma)(d\gamma/dt) = g - (V^2/r) - (C_L A/m)(\rho/2)(V^2/\cos \gamma)$. Solutions exist for direct ($\gamma > 5^\circ$) ballistic entry and for equilibrium glide-lifting entry for $L/D > 1$. General solutions of the equations of motion have been obtained for shallow entry of both ballistic and lifting bodies. For a survey of analytical methods available, see Chapman, Loh, Grant, Lees, and Gervais.

The energy of an earth satellite at 200 mi altitude is about 13,000 Btu/lb, and a vehicle entering at escape velocity possesses twice this energy. This energy is transformed, through the mechanism of gas-dynamic drag, into thermal energy in the air around the vehicle, of which only a fraction enters the vehicle surface as heat. This fraction depends on the characteristics of the boundary-layer flow, which is determined by shape, surface condition, and Reynolds number. Figure 11.6.11 illustrates the energy conversion where it is necessary to manage a given amount of energy in a way that minimizes structural and heat-protection weights, operational restraints, and cost. It would be most desirable if this energy could be dissipated at a constant rate, but with constant vehicle parameters, decelerations vary proportionally to ρV^2 and heating rates proportionally to ρV^3 . The selection of a heat-protection system depends on the type of entry flown. Lifting entry from orbit results in relatively long flight times (in the order of 1/2 h) as compared with 10 min in the case of a steep ballistic entry. Radiative-heat-transfer systems favor low heating rates over long time periods. Ablative systems favor short heat pulses. In fact, longer soaking periods may melt the ablation coating without getting the benefit of heat absorption through multiple-phase changes. A more uniform dissipation of energy can be achieved by modulation of vehicle parameters.

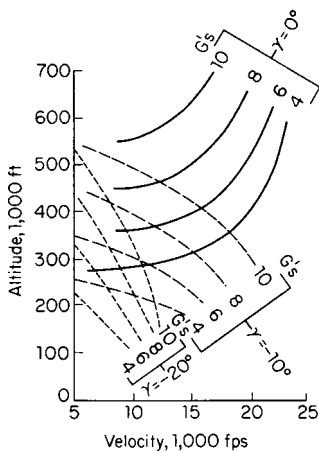


Fig. 11.6.12 Suborbital entry of a lifting vehicle. $W/C_D A = 28 \text{ lb/ft}^2$; $L/D = 0.7$.

Determination of an entry-vehicle configuration is a process of iteration. The entry-flight profile and the entry and recovery procedures are mainly determined by whether experiments or passengers are carried. The external shape is determined by requirements for hypersonic glide capability and subsonic handling and landing characteristics and also by the relations between aerodynamic shape, heat input, and structural-materials characteristics. Intermediate results are fed back into the evaluation of performance and operational effectiveness of the total transportation system.

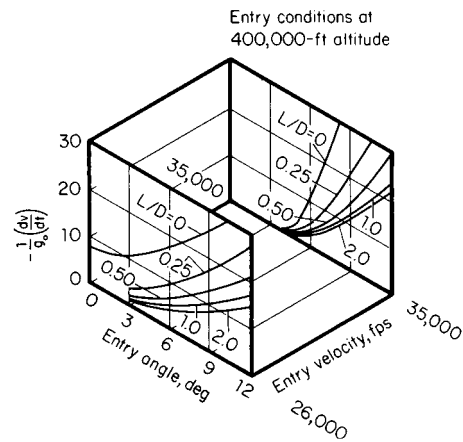


Fig. 11.6.13 Peak decelerations for entry at constant L/D .

If reentry capability from any point of the ascent trajectory is desired for a manned vehicle, vehicle constraints and trajectory requirements must be compatible. Performance-optimized trajectories encompass combinations of relatively small velocities and large flight-path angles, which would result in considerable decelerations. In such cases, either reshaping the ascent trajectory or adding velocity at the time of abort, resulting in lower entry-flight-path angles, is effective (see Fig. 11.6.12). Lower flight-path angles during ascent depress the trajectory and increase drag losses. Atmospheric entry is initiated by changing the vehicle-velocity vector so that the virtual perigee of the descent ellipse comes to lie inside the atmosphere. The retrovelocity requirement for entry from low orbit is between 250 and 500 ft/s, depending on the range desired from deorbit to landing. For nonlifting entry, maximum deceleration and heat input into the vehicle are largely a function of entry angle, with the ballistic factor $W/C_D A$ determining the alti-

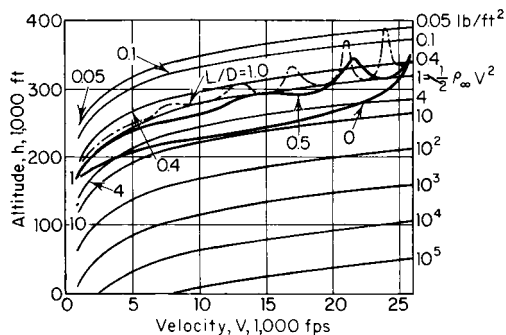


Fig. 11.6.14 Glide reentry, dynamic pressure. $W/C_D A = 1 \text{ lb/ft}^2$; $\gamma = 2^\circ$; $1/2 \rho_\infty V^2 = (W/C_D A)(1/2 \rho_\infty V^2)$; $h = h_1 - 23,500 \ln(W/C_D A)$; $V = V_1$.

Table 11.6.7

L/D	Lateral, nmi	Longitudinal, nmi
0.5	≈ 200	≈ 2,000
1	≈ 600	≈ 4,000
1.5	≈ 1,200	≈ 6,000
2	≈ 2,000	≈ 9,000

* Assumptions: $\gamma_e = 1^\circ$; $b_e = 400,000$ ft; $V_e = 26,000$ ft/s.

tude at which the maximum decelerations and heating rates occur. Deceleration can be readily determined through the approximate relation $-(1/g)(dv/dt) \approx q/(W/C_D A)$. Decelerations and temperatures are drastically reduced with increasing lift-drag ratio (Fig. 11.6.13) and decreasing $W/C_D A$ (Figs. 11.6.14 and 11.6.15). This effect is particularly beneficial at steeper entry angles. The combination of longer flight times with lower heating rates, however, may actually result in a larger total heat input into the vehicle.

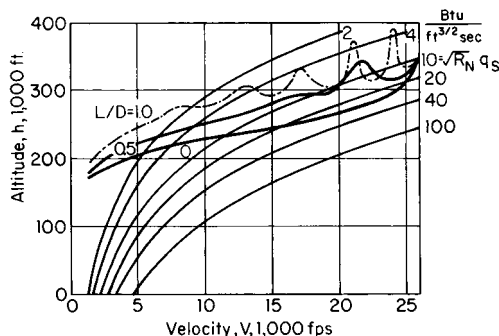


Fig. 11.6.15 Glide reentry, stagnation-heating rate. $W/C_D A = 1$ lb/ft²; $\gamma = 2^\circ$; $q_s = q_{s1} W/C_D A$; $h = h_1 - 23,500 \ln(W/C_D A)$; $V = V_1$.

The influence of lift on the reduction of decelerations is greatest for the step up to $L/D \approx 1$. The influence of $W/C_D A$ on decelerations disappears beyond $L/D \approx 0.6$. Higher, hypersonic L/D ratios serve to improve maneuverability. For entry from low orbit, the landing area selection (footprint) can be increased (see Table 11.6.7).

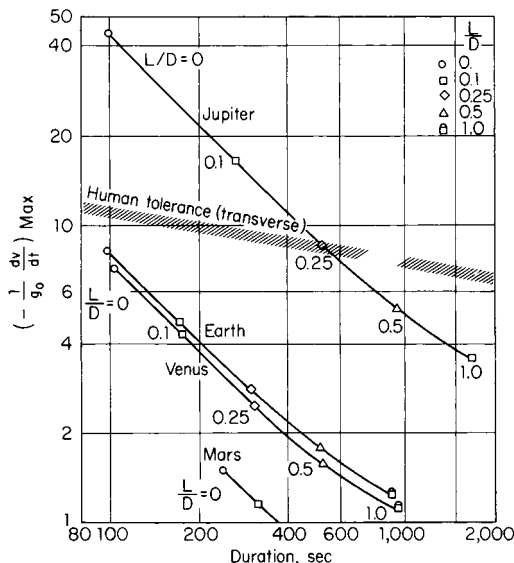


Fig. 11.6.16 Comparison of decelerations and duration for entry into various atmospheres from decaying orbits. (After Chapman.)

For entry at parabolic or hyperbolic speeds, it is necessary to dissipate sufficient energy so that the planet can capture the vehicle. Vehicle mass and aerodynamic characteristics determine the minimum allowable entry angle, the skip limit. The vehicle must be steered between the skip limit and the angle for maximum tolerable deceleration and heating. (See Figs. 11.6.16 and 11.6.17.)

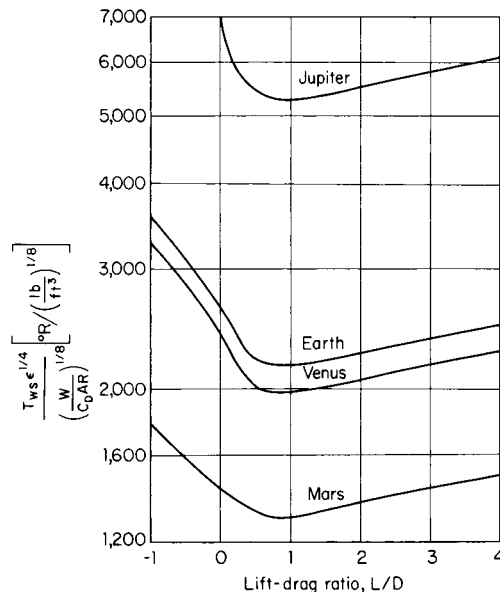


Fig. 11.6.17 Maximum surface temperature for entry into various planets from decaying orbits. (After Chapman.)

ATTITUDE DYNAMICS, STABILIZATION, AND CONTROL OF SPACECRAFT

by M. R. M. Crespo da Silva

University of Cincinnati

REFERENCES: Crespo da Silva, Attitude Stability of a Gravity-stabilized Gyrostat Satellite, *Celestial Mech.*, 2, 1970; Non-linear Resonant Attitude Motions in Gravity-stabilized Gyrostat Satellites, *Int. Jour. Non-linear Mech.*, 7, 1972; On the Equivalence Between Two Types of Vehicles with Rotors, *Jour. Brit. Int. Soc.*, 25, 1972. Thomson, Attitude Dynamics of Satellites, in Huang and Johnson (eds.), "Developments in Mechanics," Vol. 3, 1965. Kane, Attitude Stability of Earth Pointing Satellites, *AIAA Jour.*, 3, 1965. Kane and Mingori, Effect of a Rotor on the Attitude Stability of a Satellite in a Circular Orbit, *AIAA Jour.*, 3, 1965. Lange, The Drag-free Satellite, *AIAA Jour.*, 2, 1964. Fleming and DeBra, Stability of Gravity-stabilized Drag-free Satellites, *AIAA Jour.*, 9, 1971. Kendrick (ed.), TWR Space Book, 3d ed., 1967. Greensite, "Analysis and Design of Space Vehicle Flight Control Systems," Spartan Books, 1970.

A spacecraft is required to maintain a certain angular orientation, or attitude, in space in order to perform its mission adequately. For example, within a certain tolerance, it may be required to point a face toward the earth for communications and observation purposes, as well as a solar panel toward the sun for power generation. A vehicle in space is subject to several external forces which produce a moment about its center of mass tending to change its attitude. The environmental moments that can act on a spacecraft can be due to solar radiation pressure, aerodynamic forces, magnetic forces, and the gravity-gradient effect. The relative importance of each of the above moments depends on the spacecraft design and on how close it is to a central attracting body. Most often, the effect on the vehicle's attitude of the first three moments mentioned above is undesirable, although they have been used occasionally for attitude control (e.g., Mariner IV, Tiros, OAO). Micrometeorite impacts can also produce a deleterious effect on the vehicle's attitude.

11-110 ASTRONAUTICS

The most common ways to stabilize a vehicle's attitude in space are the gravity-gradient and the spin-stabilization methods. When a spacecraft is subject to the gravitational force of a central attracting body E , its mass element near the center of the gravity field will be subject to a greater force than that acting on the mass elements farther from E . This creates a moment about the center of mass, C , of the spacecraft, which depends on the inertia properties of the vehicle and also on the distance r from E to C . This gravity-gradient moment is given by

$$\mathbf{M} = (3GM_e/r^3)\hat{\mathbf{r}} \times (\mathbf{I} \cdot \hat{\mathbf{r}})$$

where \mathbf{I} is the inertia dyadic of the spacecraft, referred to its mass center, and $\hat{\mathbf{r}}$ is the unit vector in the direction from E to C . As a specific example, consider the elongated orbiting spacecraft shown in Fig. 11.6.18. The body-fixed x axis (yaw) departs an angle θ_3 from the local vertical, and the body-fixed z axis (pitch) remains normal to the orbital plane. The gravitational moment about C is readily found to be as given in the equation below (it is assumed that the maximum dimension of the vehicle is much smaller than the distance r).

$$\mathbf{M} = (3GM_e/2r^3)(I_x - I_y)(\sin 2\theta_3)\hat{\mathbf{z}}$$

(I_x and I_y are the spacecraft's moments of inertia about the x and y axes, respectively.) It is seen that unless the spacecraft's x axis is vertical or horizontal, this moment is nonzero, and for $I_x < I_y$ it tends to force the x axis of the vehicle to oscillate about the local vertical. Thus, the gravity-gradient moment provides a passive, and therefore very reliable, means for stabilizing the vehicle's attitude.

The orientation of a rigid body with respect to a reference frame is described by a set of three Euler angles. Figures 11.6.19 and 11.6.20 show a rigid body in orbit around a central attracting point E and the coordinate systems used to describe its attitude. The unit vectors $\hat{\mathbf{a}}_1$, $\hat{\mathbf{a}}_2$, and $\hat{\mathbf{a}}_3$, with origin at the spacecraft's center of mass, define the orbital reference frame. The vector $\hat{\mathbf{a}}_1$ points in the direction of the vector from E to C ; $\hat{\mathbf{a}}_3$ in the direction of the orbital angular velocity (whose magnitude is denoted by n); and $\hat{\mathbf{a}}_2$ is such that $\hat{\mathbf{a}}_2 = \hat{\mathbf{a}}_3 \times \hat{\mathbf{a}}_1$. The unit vectors $\hat{\mathbf{x}}$, $\hat{\mathbf{y}}$, and $\hat{\mathbf{z}}$ in Figs. 11.6.19 and 11.6.20 are directed along the three principal axes of inertia of the spacecraft. The attitude of the vehicle with respect to the orbiting frame is defined by the three successive rotations θ_1 (yaw), θ_2 (roll), and θ_3 (pitch) as shown in Fig. 11.6.20.

Using the above Euler angles, the gravity-gradient moment (about C) acting on the vehicle is given as

$$\mathbf{M} = \frac{3}{2}n^2[\hat{\mathbf{x}}(I_y - I_z) \sin 2\theta_2 \sin \theta_3 + \hat{\mathbf{y}}(I_x - I_z) \sin 2\theta_2 \cos \theta_3 + \hat{\mathbf{z}}(I_x - I_y) \cos^2 \theta_2 \sin 2\theta_3]$$

If the spacecraft is subject to an external (other than the gravitational attraction of E) torque $\mathbf{T} = T_x\hat{\mathbf{x}} + T_y\hat{\mathbf{y}} + T_z\hat{\mathbf{z}}$ about its center of mass C , and if its attitude deviations θ_1 , θ_2 , and θ_3 remain small, its linearized equations of motion are obtained as given in the following equations.

$$\begin{aligned} I_x \ddot{\theta}_1 + n\dot{\theta}_2(I_z - I_y - I_x) + n^2\theta_1(I_z - I_y) &= T_x \\ I_y \ddot{\theta}_2 + n\dot{\theta}_1(I_x - I_z + I_y) - 4n^2\theta_2(I_x - I_z) &= T_y \\ I_z \ddot{\theta}_3 + 3n^2(I_y - I_x)\theta_3 &= T_z \end{aligned}$$

Care must be taken in the design of a gravity-gradient stabilized satellite in order to guarantee that $I_x/I_z < I_y/I_z < 1$ for the attitude motions to be stable in the presence of the least amount of damping. For augmenting the gravity-gradient moments, booms are added to the satellite in order

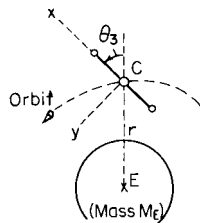


Fig. 11.6.18 Dumbbell satellite.

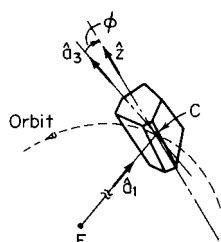


Fig. 11.6.19 Orbiting satellite.

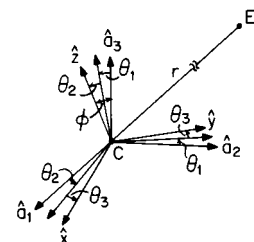


Fig. 11.6.20 Coordinate frames and Euler angles.

to make its inertia ellipsoid thinly shaped. It is interesting to note that theoretically stable motions can also be obtained when the axis of minimum moment of inertia is normal to the orbital plane. However, this orientation is unstable if damping is present, and this is what occurs in practice since all actual vehicles have parts that can move relative to each other, such as an antenna.

It is seen from the equations above that for infinitesimal oscillations the pitch motion of the satellite is uncoupled from its coupled roll-yaw motions. The natural frequency ω_p of the infinitesimal pitch oscillations is given by

$$\omega_p = n\sqrt{3(I_y - I_x)/I_z}$$

and those of the coupled roll-yaw oscillations are given by the roots of the polynomial $\omega^4 - a_2 n^2 \omega^2 - a_0 n^4 = 0$, where

$$\begin{aligned} a_2 &= 1 - [3 + (I_z - I_y)/I_x](I_x - I_z)/I_y \\ a_0 &= 4(I_z - I_y)(I_x - I_z)/(I_x I_y) \end{aligned}$$

For noninfinitesimal oscillations the pitch motion is coupled to the roll-yaw motion through nonlinear terms in the equations of motion. This coupling may give rise to an internal undesirable energy interchange between the modes of the oscillation, causing the roll-yaw motion, if uncontrolled, to oscillate slowly between two bounds. The upper bound of this nonlinear resonant roll-yaw motion may be much greater than (and independent of) the roll-yaw initial condition. For given values of I_x , I_y , and I_z , it can be decreased only by reducing the initial conditions of the pitch motion. This phenomenon can be excited if $\omega_p \approx 2\omega_1$ or $\omega_p \approx 2\omega_2$, where ω_1 and ω_2 are the two natural frequencies of the roll-yaw oscillations. The same phenomenon can also be excited if $\omega_p \approx \omega_1$ (or $\omega_p \approx \omega_2$). However, the observation of this latter resonance requires a much finer "tuning" between the modes of oscillation, and therefore it is of lesser importance.

As the altitude of the orbit increases, the gravity-gradient moment decreases rapidly. For precise pointing systems, spin stabilization is used. Historically, spin stabilization was the first method used in space and is still the most commonly employed today. Simplicity and reliability are the advantages of this method when only two-axis stabilization is needed. By increasing the spin rate, the vehicle can be made very stiff in resisting disturbance moments.

A rigid body spins in a stable manner about either its axis of maximum or of minimum moment of inertia. However, in the presence of energy dissipation, even if it is infinitesimal, a spin about the axis of minimum moment of inertia leads to an unstable roll-yaw motion. Spinning satellites are built in such a way as to achieve symmetry about the spin axis which, in practice, is the axis of maximum moment of inertia. A spin of a rigid body about its intermediate axis of inertia leads to an unstable roll-yaw motion. Since damping can destroy roll-yaw stability, an individual analysis of the equations of motion must be performed to guarantee the stability of the motions when the spacecraft houses a specific damper.

For planet-orbiting spinning satellites (for which the gravitational moment can now be viewed as a disturbance) the stability of the roll-yaw motion depends not only on the magnitude of the spin rate but also on the direction of its angular velocity (relative to the orbital reference frame) due to spin. Denoting the satellite's angular velocity due to spin by $\mathbf{s} = s \hat{\mathbf{z}}$, the following inequalities must be satisfied for the roll-yaw

motions of a spinning symmetric ($I_x = I_y$) satellite in a circular orbit to be stable in the presence of an infinitesimal amount of damping:

$$(1 + s/n) \frac{I_z}{I_x} - 1 > 0$$

$$(4 + s/n) \frac{I_z}{I_x} - 4 > 0$$

Very often, a spinning pitch wheel is added to a satellite to provide additional stiffness for resisting motions out of the orbital plane. Also, the inclusion of such a wheel provides more freedom to the spacecraft designer when specifying the range of the inertia ratios to guarantee that the attitude motions of the vehicle are stable.

Let us assume that a pitch wheel with axial moment of inertia I_w is connected to the spacecraft shown in Fig. 11.6.19. It is assumed that the wheel is driven by a motor at a constant angular velocity $s = s\hat{z}$ relative to the main body of the spacecraft. If the attitude deviations of the main body with respect to the orbiting reference frame remain small, the linearized equations for the attitude motion of the vehicle are now given as

$$I_x \ddot{\theta}_1 + n\theta_2(I_z - I_y - I_x + \beta I_z) + n^2\theta_1(I_z - I_y + \beta I_z) = T_x$$

$$I_y \ddot{\theta}_2 + n\dot{\theta}_1(I_x - I_z + I_y - \beta I_z) - n^2\theta_2[4(I_x - I_z) - \beta I_z] = T_y$$

$$I_z \ddot{\theta}_3 + 3n^2(I_y - I_x)\theta_3 = T_z$$

In these equations, the parameter β is defined as $\beta = I_w s / I_z n$, and I_x, I_y, I_z refer to the principal moments of inertia of the entire vehicle (rotor included).

Figure 11.6.21 shows a "stability chart" for this spacecraft when its center of mass, C , is describing a circular orbit around the central attracting point E . In this figure, a cut along the plane $\beta = 0$ produces the stability conditions for a gravity-gradient satellite, whereas a cut along the plane $K_1 + K_2 = 0$ (that is, $I_x = I_y$) gives rise to the inequalities for a spin-stabilized vehicle. Note that a rotor's spin rate with opposite sign to the orbital angular speed ($s < 0$) may destabilize the roll-yaw motions. Nonlinear resonances, as previously discussed, can also be excited in this vehicle. However, since the natural frequencies of the roll-yaw motions now also depend on the magnitude and sign of the internal angular momentum due to the rotor, the resonance lines are displaced in the region shown in Fig. 11.6.21 when the spin rate s of the rotor is changed to a different constant. Therefore, this phenomenon, when excited, can be avoided simply by changing the parameter β .

For a spacecraft to perform its mission adequately during a long period of time, an attitude control system to maintain the vehicle's attitude within specified limits is necessary. Typically, this is done by means of a set of mass expulsion jets mounted on the vehicle, which are actuated by the output of a controller that receives information from the attitude sensors.

Drag-Free Satellites For scientific applications that require the use

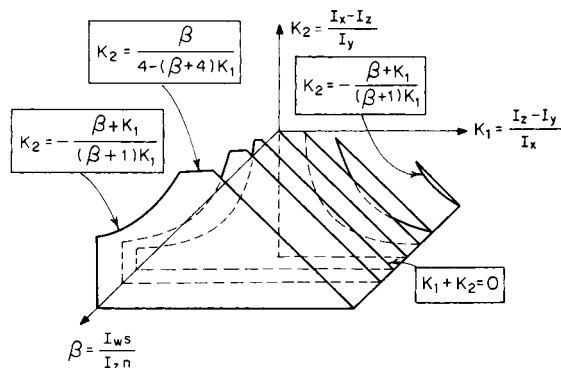


Fig. 11.6.21 Stable region of the vehicle parameter space.

of a satellite that follows a purely gravitational orbit, a translational control system is incorporated into the vehicle. Typical applications include satellite geodesy and navigation where accurate ephemeris prediction is needed. A drag-free satellite consists of a vehicle that contains a spherical cavity which houses an unsupported spherical proof mass. Sensors in the satellite detect the relative position of the proof mass inside the cavity and activate a set of thrusters placed in the vehicle, forcing it to follow the proof mass without touching it. Since the proof mass is shielded by the satellite from nongravitational forces, it follows a purely gravitational orbit.

METALLIC MATERIALS FOR AEROSPACE APPLICATIONS

by Stephen D. Antolovich
Revised by Robert L. Johnston
NASA

REFERENCES: MIL-HDBK-5C, "Metallic Materials and Elements for Aerospace Vehicle Structures," Sept. 1976. Wolf and Brown (eds.), "Aerospace Structural Metals Handbook," 1978, Mechanical Properties Data Center, Traverse City, Michigan. (This handbook gives information on mechanical, physical, and chemical properties; fabrication; availability; etc. in five published volumes encompassing ferrous, nonferrous, light metal alloys, and nonferrous heat-resistant alloys.) "Damage Tolerant Design Handbook," MCIC-HB-01, Metals and Ceramics Information Center, Battelle Columbus Laboratories, 1975, parts 1 and 2. (These two documents provide the most up-to-date and complete compilation of fracture-mechanics data for alloy steels, stainless steels, aluminum, and titanium alloys.) "Metals Handbook," 8th ed., 11 vols., American Society for Metals: Vol. I, Properties and Selection of Metals, 1961; Vol. II, Heat Treating, Cleaning and Finishing, 1964; Vol. III, Machinery, 1967; Vol. IV, Forming, 1969; Vol. V, Forging and Casting, 1970; Vol. VI, Welding and Brazing, 1971; Vol. VII, Atlas of Microstructures, 1972, Vol. VIII, Metallography, Structure and Phase Diagrams, 1973; Vol. IX, Fractography and Atlas of Fractographs, 1974; Vol. X, Failure Analysis and Prevention, 1975; Vol. XI, Nondestructive Testing and Quality Control, 1976. "Metals Handbook," 9th ed., 5 vols., American Society for Metals: Vol. I, Properties and Selection: Nonferrous Alloys and Pure Metals, 1979; Vol. III, Properties and Selection: Stainless Steels, Tool Materials and Special Purpose Metals, 1980; Vol. IV, Heat Treating; Vol. V, Surface Cleaning, Finishing and Coating. "Structural Alloys Handbook," Mechanical Properties Data Center, Belfour Stulen, Inc., Traverse City, Michigan, 1978. "Titanium Alloys Handbook," MCIC-HB-05, Metals and Ceramics Information Center, Battelle Columbus Laboratories, 1972.

A wide variety of materials are utilized in aerospace applications where performance requirements place extreme demands on the materials. Some of the more important engineering properties to be considered in the selection of materials are (1) strength-to-weight ratio, (2) density, (3) modulus of elasticity, (4) strength and toughness at operating temperature, (5) resistance to fatigue damage, and (6) environmental effects on strength, toughness, and fatigue properties. Factors such as weldability, formability, castability, quality control, and cost must be considered.

Although it is desirable to maximize the strength-to-weight ratio to achieve design goals, materials with high strength-to-weight ratios generally are sensitive to the presence of small cracks and may exhibit catastrophic brittle failure at stresses below the nominal design stress. The problem of premature brittle fracture is accentuated as the temperature decreases and the yield and ultimate strength increase. For these reasons it is imperative that the tendency toward brittle failure be given major consideration for low-temperature applications. For example, liquid oxygen, a common oxidizer, boils at -297°F (-183°C) whereas liquid hydrogen, an important fuel, boils at -423°F (-253°C), and the problem of brittle failure is predominant. The fracture-mechanics approach has gained wide acceptance, and nondestructive inspection (NDI) characterization of flaws allows safe operating stresses to be calculated. A considerable amount of fracture-mechanics data has been collected and evaluated ("Damage Tolerant Design Handbook"). Stress corrosion cracking and corrosion fatigue become important for repetitive-use components such as aircraft airframes, landing gear, fan shafts, fan and compressor blades, and disks, in addition to brittle fracture problems such as fatigue crack formation and propagation.

11-112 ASTRONAUTICS

Table 11.6.8 Effective Fiber Properties as Measured in Composites

Fiber	Modulus, 10 ⁶ lb/in ²	Tensile strength, ksi	Tensile failure strain, in/in	Specific gravity	Density, lb/in ³
Boron (4 mil)	60	460	0.8	2.60	0.094
Graphite (Thornel 300)	34	470	1.1	1.74	0.063
Graphite pitch	120	350	0.4	2.18	0.079
Kevlar 49	19	400	1.8	1.45	0.052
Kevlar 29	12	400	3.8	1.45	0.052
E glass	10.5	250–300	2.4	2.54	0.092
S glass	12.5	450	3.6	2.48	0.090

The presence of flaws must be assumed (they may occur either during processing or fabrication) and design must be based on **fatigue crack propagation** (FCP) properties (Sec. 5). FCP of many materials follows an equation of the form

$$da/dN = R(\Delta K)^n \quad (11.6.1)$$

where *a* refers to crack length, *N* is the number of cycles, *K* is the fluctuation in the stress-intensity parameter, and *R* and *n* are material constants. Equation (11.6.1) can be integrated to determine the cyclic life of a component provided that the stress-intensity parameter is known (Sec. 5). Although fatigue-crack initiation is generally retarded by having smooth surfaces, shot-peening, and other surface treatments, FCP of commercial aerospace alloys is relatively insensitive to metallurgical treatment and, to a reasonable approximation, whole classes of materials (i.e., aluminum alloys, high-strength steels, etc.) can be represented within the same scatter band.

It should be noted that increases in the plane-strain fracture toughness *K_{IC}* result in increased stress, through its linear relationship to the stress-intensity parameter, which in turn causes an exponential increase in the FCP rate and may introduce a fatigue problem where previously there was none.

The effect of environment on materials used for aerospace problems is usually to aggravate the FCP rate. It should be emphasized that fatigue loads have a synergistic effect on the environmental component of cracking and that the crack growth rate during corrosion fatigue is rarely the sum of the FCP and stress-corrosion cracking rates. In weldments of castings or wrought material, tests are needed to simulate anticipated use conditions and to prove weld soundness.

Materials in the turbine section of jet engines are subjected to deleterious gases such as O₂ and SO₂, high temperatures and stresses, and cyclic loads. Consequently the most significant metallurgical factors to consider are microstructural stability, resistance to oxidation and sulfidation, creep resistance, and resistance to low cycle fatigue. Nickel-base superalloys are generally used in the turbine section of the engine for both disks and blades. (See "Aerospace Structural Metals Handbook," Vols. II and IIA, for specific properties.) Although the Ni-base superalloys generally exhibit excellent strength and oxidation resistance at temperatures up to 1800°F (982.22°C), the interactive effects of sustained and cyclic loads are difficult to handle because, at high temperature, plastic deformation of these materials is time-dependent. An approach based on strain range partitioning is described in ASTM STP 520, 1973, pp. 744–782. The utility of this approach is that frequency and temperature dependence are incorporated into the analysis by the way in which the strain is partitioned and reasonable envelopes of the expected life can be calculated.

STRUCTURAL COMPOSITES

by Ivan K. Spiker

NASA

REFERENCES: MIL-HDBK-17, "Plastics for Aerospace Vehicles," Sept. 1973. Advanced Composites Design Guide, Vols. I–V, 3d ed., Sept. 1976.

Table 11.6.9 Matrix Temperature Limits

Material	Maximum use temperature, °F
Polyester	250
Polysulfone	250
Epoxy	350
Polyarylsulfone	400
Phenolic	450
Silicone	450
Polyimide	650
Aluminum	700
Magnesium	700
Glass	2500
Carbon* (W/C)	3200

* With oxidation-resistance.

Composite materials are fibrous materials embedded in a matrix to provide stiffnesses and strengths that neither of the components alone exhibits. There are three general classes of composites: fibers in organic matrices, fibers in metal matrices, and fibers in ceramic matrices.

The selection of a fiber is dictated by the specific strength and/or modulus of the fiber. Table 11.6.8 lists typical properties of the commonly used fibers for structural composites.

The parameter used for selecting the matrix material is normally the maximum use temperature; however, other environmental conditions such as chemical compatibility may dictate the selection of the matrix material. Table 11.6.9 lists matrix materials with their recommended temperature limits.

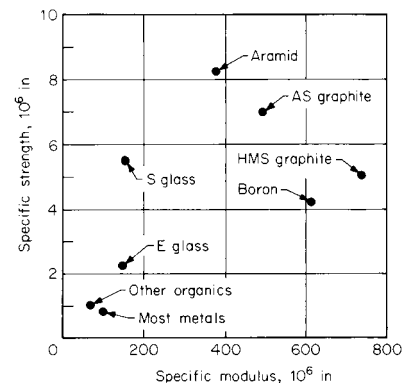


Fig. 11.6.22 Comparison of nonmetallic reinforcement materials with most metals. (Hercules Aerospace Co.)

A highly useful feature of composites is the ability to mold parts with complex shapes and multiple contours. A unique feature of designing with graphic composites is the ability to tailor the unidirectional coefficient of thermal expansion from -0.2×10^{-6} in/in \cdot °F to values comparable to those of metals.

Fig. 11.6.22 compares composites with homogeneous organics and metals based on their specific strengths and moduli. A comparison of the fatigue properties of unidirectional composites to an aluminum alloy is depicted in Fig. 11.6.23.

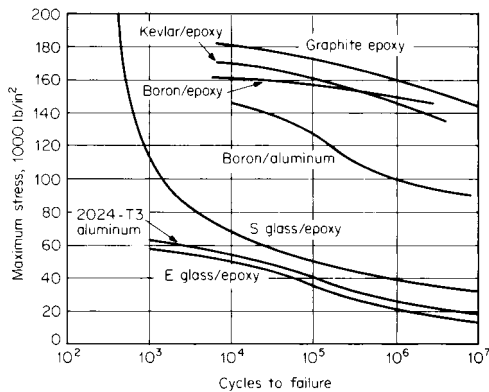


Fig. 11.6.23 Fatigue behavior of unidirectional composites and aluminum. (Hercules Aerospace Co.)

STRESS CORROSION CRACKING

by Samuel V. Glorioso

NASA

Stress corrosion cracking is caused by the interaction of sustained tensile or shear stresses and an aggressive environment which results in delayed cracking at stresses well below the yield strength of the material. The occurrence of cracking is dependent upon the duration and magnitude of the applied stress as well as the aggressiveness of the environment.

Sustained stresses can result from residual stresses, applied loads, or both. Residual stresses occur as a result of manufacturing and assembly

Table 11.6.10 Alloys with Low Resistance to Stress Corrosion Cracking

Alloy	Condition
Carbon steel (1000 series)	Above 200 ksi UTS
Low-alloy steel (4130, 4340, D6AC, etc.)	Above 200 ksi UTS
H-11 steel	Above 200 ksi UTS
400C stainless steel	All
AM 350 stainless steel	Below SCT 1000
AM 355 stainless steel	Below SCT 1000
Custom 455 stainless steel	Below H1000
PH 15-7 Mo stainless steel	All except CH900
17-7 PH stainless steel	All except CH900
2011 aluminum	T3, T4
2014 aluminum	All
2024 aluminum	T3, T4
7075 aluminum	T6
7175 aluminum	T6
Cartridge brass, 70% copper, 30% zinc	50% cold-rolled

operations with forming, forging, extrusion, welding, rolling, and assembly fit-up stress as frequent offenders.

Cracking occurs most rapidly for stresses in the material's short-transverse grain direction. Fracture can occur at stresses as low as 8,000 lb/in² for some aluminum alloys exposed to a moist air environment.

Conditions leading to stress corrosion include the exposure of copper to ammonia in condensers and heat exchangers and of stainless steels exposed to chloride-containing solutions. Table 11.6.10 lists some materials which are known to be susceptible. Table 11.6.11 includes materials which are considered to be resistant to stress corrosion cracking in

Table 11.6.11 Alloys with High Resistance to Stress Corrosion Cracking

Alloy	Condition
Carbon steel (1000 series)	Below 180 ksi UTS
Low-alloy steel (4130, 4340, etc.)	Below 180 ksi UTS
300-series stainless steel	All
A286 stainless steel	All
15-5 PA stainless steel	H1000 and above
Beryllium	
Hastelloy X	All
Incoloy 901	All
Inconel 600	Annealed
Inconel 718	All
Inconel x750	All
Monel K-500	All
1000 series aluminum	All
2024 bar, rod aluminum	T8
3000 series aluminum	All
5000 series aluminum	All
6000 series aluminum	All
7075	T73
99.9% copper	
Brass, 85% copper, 15% zinc	

moist salt air. Both tables were condensed from more extensive tables in NASA Specification MSFC-SPEC-522A entitled "Design Criteria for Controlling Stress Corrosion Cracking," which also contains a discussion of material selection and additional conditions under which stress corrosion can occur.

MATERIALS FOR USE IN HIGH-PRESSURE OXYGEN SYSTEMS

by Robert L. Johnston

NASA

Oxygen is relatively reactive at ambient conditions and extremely reactive at high pressures. The design of high-pressure oxygen systems requires special consideration of materials and designs. The types of potential ignition sources that could be present in even a simple component are quite varied. Sources of ignition include electrical failures, particle impact in high-flow regions, pneumatic shock, adiabatic compression, fretting or galling, and Helmholtz resonance in blind passages. Other sources of ignition energy are also possible. A comprehensive review of potential design problems is available in NASA Reference Publication 1113, A.C. Bond et al., "Design Guide for High Pressure Oxygen Systems."

Materials currently used in high-pressure oxygen systems range from ignition-resistant materials like Monel 400 to materials of widely vary-

11-114 ASTRONAUTICS

ing ignitability like butyl rubber and the silicones. The range of ignitability of various materials is shown in Figs. 11.6.24 and 11.6.25.

While material selection alone cannot preclude ignition, proper choices can markedly reduce the probability of ignition and limit propa-

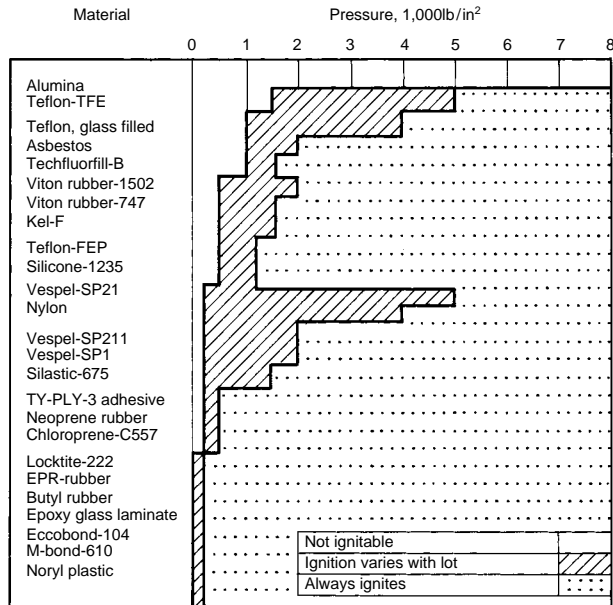


Fig. 11.6.24 Ignition variability of current oxygen-system nonmetallic materials.

gation. Selecting materials with small exothermic heats of combustion will reduce the possibility of propagation. Materials with high heats of combustion (stainless steels) or very high heats of combustion (aluminum) should be avoided. A summary of heats of combustion, as well as other design properties of a few currently used materials, is shown in Table 11.6.12.

The materials listed in Table 11.6.13 have superior resistance to ignition and fire propagation in high-pressure oxygen systems. Monel alloys are available in the necessary range of hardnesses. Springs can be made of Elgiloy. Sapphire poppet balls should replace tungsten carbide or steel balls because sapphire has a lower level of reactivity (and therefore is less combustible) than either tungsten carbide or steel and is more resistant than tungsten carbide to breakup under mechanical impact in an oxygen environment.

Titanium and its alloys, normally attractive as materials for pressure vessels, cannot be used for oxygen vessels because they are impact-sensitive in oxygen. Inconel is a good choice for vessels for high-pressure oxygen.

In no case should an alloy be used at an oxygen pressure above which it can be ignited by particle impact. This criterion would limit the use of aluminum alloys and stainless steels to pressures below 800 lb/in² to allow some margin for error in test results and impact predictions.

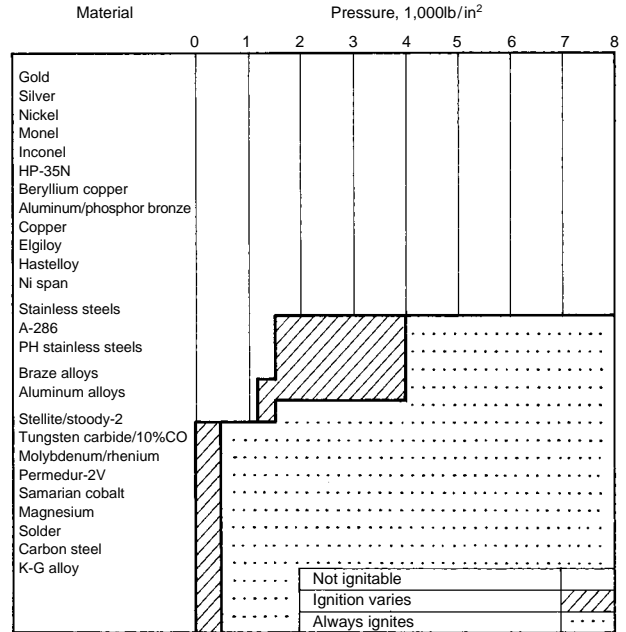


Fig. 11.6.25 Ignition variability of current oxygen-system metallic materials.

SPACE ENVIRONMENT

by L. J. Leger and Michael B. Duke

NASA

Materials in the space environment are exposed to vacuum, to temperature extremes, to radiation from the sun, and to the rarified earth atmosphere. Except for thermovacuum conditions, the most damaging aspects of the environment are solar-generated radiation at geosynchronous altitudes and bombardment of surfaces by atomic oxygen (the major constituent of the low-altitude earth atmosphere) in low earth orbit. For long-lived spacecraft impact on surfaces by meteoroids and space debris must be considered.

The vacuum of space may cause the evaporation of a material, or a volatile component of the material, and of the absorbed gases on surfaces. The evaporation rate of a pure material can be calculated by

$$G = \sqrt{\frac{M}{T}} \frac{P}{17.14}$$

where G = evaporation rate, g/(cm² · s); M = molecular weight; T = absolute temperature, K; and P = vapor pressure, mmHg at temperature T . (See Dushman, "Scientific Foundations of Vacuum Technique," Wiley.) This simple formula is not applicable to heterogeneous materials or even to a pure substance, such as a plasticizer in an elastomer, which is removed from a matrix of another substance. In this case, other factors, such as migration rate, influence the rate of loss. Although the evaporation of a component of a material may not reduce the effectiveness of the material, e.g., the plasticizer in the insulation of an electrical

Table 11.6.12 Physical Properties of Typical Oxygen System Metallic Materials

Property	Aluminum alloys	Stainless steel	Inconel 718	Monel 400
Density, lb/in ³	0.10	0.28	0.30	0.31
Tensile, ultimate, lb/in ²	40,000	140,000	180,000	145,000
Maximum use temperature, °F	350	950	1,200	1,000
Heat of combustion, Btu/lb	130,000	33,500	15,100	14,200
Maximum use pressure, lb/in ²	1,250	1,250	8,000	8,000

Table 11.6.13 Recommended Materials

Application	Material
Component bodies	Monel Inconel 718
Tubing and fittings	Monel Inconel 718
Internal parts	Monel Inconel 718
Springs	Beryllium copper Beryllium copper Elgiloy
Valve seats	Gold or silver over Monel or Inconel 718
Valve balls	Sapphire
Lubricants	Batch- or lot-tested Braycote 3L-38RP Batch- or lot-tested Everlube 812
O-seals and backup rings	Batch- or lot-tested Viton Batch- or lot-tested Teflon
Pressure vessels	Inconel

conductor, the deposition of the vapor on a colder surface may be intolerable. Metals do not usually evaporate in space at modest temperatures, but organic materials, including elastomers, plastics, coatings, adhesives, and lubricants, must be of very high molecular weight to avoid evaporation. A standard screening test (ASTM E595) has been developed to determine the acceptability of materials from an outgassing standpoint. This screening test addresses only contamination and, therefore, functional characteristic changes must be evaluated separately.

Spacecraft are exposed to electromagnetic radiation and particulate contamination in both low and geosynchronous altitudes; however, the large doses (5×10^{11} ergs/g per 30 years) of high-energy electrons and protons are experienced only at the higher altitudes. Metals and ionic compounds are relatively resistant to space-indigenous radiation. However, semiconductors are sensitive to permanent radiation damage, and other electrical materials are subject to permanent or transient damage. Organic materials are also susceptible to degradation by both electromagnetic and particle radiation, especially in vacuum. Organic polymers of high molecular weight may have such low vapor pressure that their evaporation in vacuum at reasonable temperatures is not significant. However, radiation, which may produce chain scission, yields fragments of reduced molecular weight and increased vapor pressure, which will result in the loss of the mass at the same temperature which did not affect the nonirradiated material (Table 11.6.14). Note the almost complete degradation of the tensile strength of neoprene and Buna N as a result of irradiation in vacuum. On the other hand, Viton A appears to be satisfactory for this environment on the basis of increased tensile strength; however, the decreased elongation would be an important consideration in the application of this material as a seal, particularly as a dynamic seal. Furthermore, Viton A is not suitable for very

low temperature applications, another component sometimes encountered in the space environment. Geosynchronous radiation may change thermal expansion characteristics of organic composite materials and this effect must, therefore, be considered for large space structures.

The better known organic liquid lubricants are subject to evaporation in space because of relatively high vapor pressures. A limited number of liquid film lubricants with sufficiently low vapor pressures are available; however, dry film lubricants are preferred. The most widely used dry film utilizes MoS_2 as the lubricating agent in either silicate or organic binders.

Moving electrical-contact surfaces such as brushes, slip rings, and make-break switches require either reliable isolation from the vacuum environment or special selection of materials, especially where long-time operation is involved. Composites of heavy-metal sulfides with silver or copper are promising possibilities for this application.

Spacecraft surfaces exposed in the low earth orbital environment experience 10^{14} to 10^{15} atomic oxygen impacts/($\text{cm}^2 \cdot \text{s}$) when facing into the velocity vector. For even relatively short missions (7 days) total fluence can be as much as 3×10^{20} atoms/(cm^2). This exposure leads to oxidation of the surface of some metals, the most active of which is silver, and to removal of a significant amount of organic material (approx $10 \mu\text{m}$), also by oxidation. The extent of reaction is dependent upon many parameters, including atmospheric density, vehicle velocity, attitude, and total exposure time. In turn, atmospheric density is dependent upon altitude and solar activity. Fully fluorinated polymers such as Teflon and silicone-based compounds appear to be more stable than other organic films by a factor of 10. This effect must be taken into account for long-duration flights at altitudes up to 600 km and for short-term low-altitude flights.

Meteoroids derived from comets, asteroids, and possibly larger satellites and planets are present in significant numbers in the inner solar system. These particles range in size from less than 10^{-12} g (cosmic dust) to asteroidal dimensions. In the vicinity of the earth, these particles travel with velocities on the order of 10 to 30 km/s, which makes even millimeter-sized particles potentially damaging to space structures. The current flux of meteoroids in the 1-mm size range is about $0.02/(\text{m}^2 \cdot \text{yr})$; at 1 cm, the flux is about 3 orders of magnitude lower. Some regions of space, for example, the asteroid belt or the vicinity of Saturn's rings, contain significantly higher numbers of solid particles.

The spectral energy distribution for the sun resembles a Planck curve with an effective temperature of 5,800 K, with most of the solar energy lying between 150 nm and 10 nm with a maximum near 450 nm. The radiant energy of the sun at 1 au is $1.37 \times 10^3 \text{ W/m}^2$. The sun's electromagnetic radiation at wavelengths shorter than visible includes significant fluxes of hard x-rays and gamma rays. The emission of the harder radiation varies with the solar cycle.

The sun also emits charged particles with velocities in the range of 500 to 700 km/s (solar wind) with fluxes on the order of 4×10^3 protons/($\text{cm}^2 \cdot \text{s}$). During solar flares, much higher energy particles are

Table 11.6.14 Effects of Vacuum and Radiation on Elastomers

Material	Test	Pressure, mmHg	Temp, °F	Radiation ergs, $\text{g}^{-1}/^\circ\text{C}$	Tensile strength, lb/in ²	Elongation, percent
Neoprene	Air	760	80	0	3,135	426
	Vacuum	1×10^{-5}	80	0	3,350	405
	Air and radiation	760	80	1.9×10^9	2,769	265
	Vac and radiation	5×10^{-6}	80	1.9×10^9	191	218
Buna N	Air	760	80	0	2,630	685
	Vacuum	1×10^{-5}	80	0	2,640	700
	Air and radiation	760	80	1.9×10^9	2,175	390
	Vac and radiation	5×10^{-6}	80	1.7×10^9	203	450
Viton A	Air	760	80	0	1,343	172
	Vacuum	1×10^{-5}	80	0	1,168	238
	Air and radiation	760	80	2×10^{10}	2,629	36
	Vac and radiation	5×10^{-7}	109	1.6×10^{10}	1,830	31

11-116 ASTRONAUTICS

emitted, ranging from 100 keV to 100 MeV energies, with typical proton fluxes at 1 au of 10 to 100 $\text{cm}^{-2} \cdot \text{ster}^{-1} \cdot \text{s}^{-1}$ at 10 MeV to less than 10 $\text{cm}^{-2} \cdot \text{ster}^{-1} \cdot \text{s}^{-1}$ at 30 MeV and higher. Total protons in a flare event are on the order of 10^7 to $10^{10}/\text{cm}^2$. Atomic nuclei ranging from protons to uranium nuclei are emitted in solar flares. Galactic cosmic rays, from outside the solar system, with 100-MeV to BeV energies are also observed.

In the vicinity of the earth, interactions between solar radiation and the earth's magnetic field lead to the phenomenon known as the Van Allen radiation belts, in which intense concentrations of radiation are observed in the form principally of protons and electrons, with energies on the order of a few electron volts. These lead to charging problems for spacecraft and structures embedded in the plasma. Beyond the earth's magnetic field, charging can occur, but is not a significant problem. In the vicinity of the earth, variations of charged-particle concentrations occur diurnally and with geographical variation of the magnetic field.

The vacuum of space in the inner solar system is limited by the presence of the solar wind, with the interplanetary pressure being about 10^{-13} mbar. Interaction of solar radiation with the gases at low earth orbital altitudes has been observed to produce ionized oxygen. This species and other ionized molecules may exist which can interact with spacecraft surfaces. In the local vicinity of spacecraft hardware, outgassing characteristics are generally the major determinant of the local pressure and the molecular composition.

Since the beginning of the space age, numerous artificial objects have been placed into earth orbit. Many of these remain in orbit, as does debris from the explosion or disaggregation of various spacecraft. This debris at about 1,000 km (the most intensely contaminated region) now approaches the natural meteoroid flux in the millimeter size range, and is predicted to grow in the future as additional space vehicles are launched into earth orbit. In the micrometer size range, numerous aluminum oxide particles resulting from the firing of upper-stage solid rocket motors are present and may be significantly more abundant than natural meteoroids. Thus, artificial debris from space flights is rapidly accumulating to levels which also present significant impact probabilities. There is widespread acceptance of the dual-wall technique of protecting a craft against particle impact damage. The outer wall, called the bumper, is detached from the load-carrying structural wall. The bumper dissipates some of the kinetic energy of the particle, but primarily it serves to fragment the particle into a fine spray so that the impact energy is spread over a larger area of the structural wall.

SPACE-VEHICLE STRUCTURES

by Thomas L. Moser and Orvis E. Pigg

NASA

REFERENCES: MIL-HDBK-5D, "Metallic Materials and Elements for Aerospace Vehicle Structures." Advanced Composites Design Guide, Sept. 1976, Library Accession no. AD916679 through AD916683. Ashton, Halpin, Pertit, "Primer on Composite Materials Analysis," Technomic Pub. Co. Aeronautical Structures Manual (Vols. I-III), NASA TMX-73305. Bruhn, "Analysis and Design of Flight Vehicle Structures." Tri-State Offset Co., Cincinnati. Barton, "Fundamentals of Aircraft Structures," Prentice-Hall, 1948. Roark, "Formulas for Stress and Strain," McGraw-Hill. "Nastran Theoretical Manual," Computer Software Management and Information Control (COSMIC), University of Georgia. Perry, "Aircraft Structures," McGraw-Hill. Gathwood, "Thermal Stress," McGraw-Hill. Zienkiewicz, "The Finite Element," McGraw-Hill. MIL-STD-810D, "Environmental Test Methods and Engineering Guidelines." Chapman, "Heat Transfer," Macmillan.

Space vehicles include a large variety of vehicle types, like their predecessors, earth vehicles. Airplanes were the first generation of space vehicles, and our definition of space vehicle has changed as the airplane approached the limits of the earth's atmosphere. Space, in this discussion, is the region beyond the earth's atmosphere.

Many space vehicles are hybrids since they are required to operate in the earth's atmosphere and beyond. The space shuttle orbiter is such a hybrid space vehicle. The Apollo command and service module is also a

hybrid, but the Apollo lunar module, which primarily functioned outside the earth's atmosphere, was a space vehicle.

The design procedure for any vehicle structure is basically the same:

1. Establish the design requirements and criteria
2. Define the loads and environments
3. Perform the design and analysis

4. Iterate the previous two steps (as required) because of the interrelation between configuration and loads

5. Verify the design

There are conditions and requirements which are unique for hybrid and space-vehicle structures.

Minimum weight and high reliability are significant but opposing requirements for space-vehicle structures which must be balanced to achieve an efficient, reliable structure design. Depending on the mission of the particular space vehicle, the ratio between the weight of the earth launch vehicle and the payload (e.g., interplanetary probe) can be as high as 400 to 1. The large weight leverages require that the design be as efficient as possible. Structural materials, therefore, must be stressed (or worked) as close to the capabilities as possible. Like aircraft structures, space-vehicle structures should be designed for a zero margin of safety (MS):

$$MS = \frac{(\text{material ultimate allowable})}{FS (\text{limit stress})} - 1$$

1. *Material ultimate allowable.* The stress at which the material will fail.

2. *FS (factor of safety).* This factor usually ranges between 1.25 and 1.50, for space structures, depending on the maturity of the design, the behavior of the material, the confidence in the loads, etc.

3. *Limit stress.* The maximum (reasonable) stress that the structural component would be expected to encounter.

Failure can be based on rupture, collapse, or yield as dictated by the functional requirements of the component. High reliability is necessary for most space vehicle structures since a failure is usually catastrophic or nonrepairable. Total structural reliability is composed of many of the design elements—loads, materials, allowables, load paths, factor of safety, analysis techniques, etc. If the reliability is specified and the statistical parameters are known for each design element, then the process is straightforward. A total structural reliability is seldom specified and good engineering practice is used for the solution of the reliability of each design element. Commonly used to assure structural reliability are (1) material allowables equivalent to A values from MIL-Handbook-5A for safe-life structure and B values for fail-safe structures; (2) limit loads which correspond to events and conditions which would not be exceeded more often than 3 times in 1,000 occurrences; (3) factor of safety equal to 1.4 for crew-carrying space vehicles and 1.25 for those without crews; and (4) verification of the structural design by test demonstration. A good structural design is one which has the correct balance between minimum weight and high reliability.

Space vehicles are usually manufactured and assembled on earth and transported to space. The launch environments of acceleration, vibration, aerodynamic pressure, rapid pressure change, and aerodynamic heating coupled with the space environments of extremely low pressure, wide ranges in temperature, meteoroids, and radiation dictate that the design engineers accurately define the magnitudes of these environments and the correct time-compatible combinations of these environments if realistic loads are to be determined. Many natural environments have been defined and are documented in the references. The induced environments, which are a function of the system and/or structural characteristics (e.g., dynamic pressure, vibration, etc.), must be determined by analysis, test, or extrapolation from similar space vehicles. Quantifying the induced loads for the structural designers is one of the major consumers of time and money in any aerospace program and one of the most important. Load determination can be a very complex task. For further guidance the reader is directed to the references.

For a space vehicle which is not exposed to the launch loads, the load determination is greatly simplified. In the absence of an appreciable atmosphere and gravitational accelerations the predominant external

force on a space-vehicle structure is that of the propulsion and attitude control systems and the resulting vibration loads. Even though not induced by an external force, thermal stresses and/or deflections can be a major design driver. Space vehicles commonly experience larger thermal gradients because of the time- or attitude-related exposure to solar radiation.

The thermal effects of stress and deflections of the structure require that temperature distributions be defined consistent with the strength and deflection requirements. From a strength integrity standpoint, temperature distribution on a space vehicle can be as important as the pressure distribution on an aircraft. The significance and sensitivity of thermal effects are greatly reduced by the use of composite materials for the structure. The materials can be layered to achieve, within limits, the desired thermal coefficient of expansion and thereby reduce the thermal effects.

Space vehicles which return to the earth must withstand the extremely high temperatures of atmospheric reentry. This produces dynamic temperature distributions which must be combined with the aerodynamic pressures and vehicle dynamic loads.

Innovative, clever, and efficient structural designs minimize the effects of loads associated with launch for a vehicle which is to remain in space. This is accomplished by attaching the space vehicle to the booster rocket to minimize scar weight and to reduce the aerodynamic loads by the use of shrouds, fairings, or controlling the attitude during atmospheric flight.

Efficiencies of weight-critical structures have been greatly improved by more accurately quantifying the loads and stress distributions in complex structural configurations. **Finite element methods (FEM)** of analysis and large capacity, high-speed digital computers have enabled the increased fidelity of analyses. In this process, the structure is modified with finite elements (beams, bars, plates, or solids) by breaking the structure into a group of nodal points and connecting the nodal points with the finite elements which best represent the actual structure. Loads are applied at the nodal points or on the elements which then distribute the loads to the nodal points. Constraints are also applied to the nodal points to support or fix the structure being analyzed. The finite-element program then assembles all the data into a number of linear simultaneous equations and solves for the unknown displacements and then for internal loads and stresses, as required. Many finite-element programs have been developed to perform a variety of structural analyses including static, buckling, vibration, and response.

The loads in a structure depend on the characteristics of the structure and the characteristics of the structure are largely dictated by the loads. This functional dependency between loads and structures requires an iterative design process.

Classically, when structures are worked to stresses near the capability of the materials, e.g., airplane structures, the design is verified by test demonstration. This method of verification was common before high-fidelity structural mathematical models were employed and is still used when practical to apply the design loads and environments to a dedicated test article to verify the design. Design deficiencies are then corrected depending on the importance and the manufacturing schedule.

Space-vehicle structures often do not lend themselves to the classical test approach because of the multitude of loads and environments which must be applied, because testing in earth's gravity precludes realistic loadings, and because of the size and configuration. Verification by analyses with complementary component tests and tests of selected load conditions are common.

VIBRATION OF STRUCTURES

by Lawrence H. Sobel

University of Cincinnati

REFERENCES: Crandall and McCalley, *Numerical Methods of Analysis*, chap. 28, in Harris and Crede (eds.), "Shock and Vibration Handbook," Vol. 2, McGraw-Hill. Hurty and Rubinstein, "Dynamics of Structures," Prentice-Hall. Meirovitch, "Analytical Methods in Vibrations," Macmillan. Przemieniecki, "Theory of Matrix Structural Analysis," McGraw-Hill. Wilkinson, "The Algebraic Eigenvalue Problem," Oxford.

As a result of the vast improvements in large-scale, high-speed digital computers, numerical methods are being used at an exponentially increasing rate to analyze complex structural vibration problems. The numerical methods most widely used in structural mechanics are the finite element method and the finite difference method. In the finite element method, the actual structure is represented by a finite collection, or assemblage, of structural components whereas, in the finite difference method, spatial derivatives in the differential equations governing the motion of the structure are approximated by finite difference quotients. With either method, the continuous structure with an infinite number of degrees of freedom is, in effect, approximated by a discrete system with a finite number of degrees of freedom (unknowns). The linear, undamped free and forced vibration analysis of such a discrete system is discussed herein. The analysis is most conveniently carried out with the aid of matrix algebra, which is well suited for theoretical and computational purposes. The following discussion will be brief, and the reader is referred to the cited references for more comprehensive treatments and examples.

Equation of Motion

Consider a conservative discrete system undergoing small motion about a state of equilibrium (neutral or stable). Let $q_1(t), \dots, q_n(t)$, where t is time, be the minimum number of independent coordinates (linear or rotational) that completely define the general dynamical configuration of the system and that are compatible with any geometrical constraints imposed on the system. Then the n coordinates q_1, \dots, q_n are called generalized coordinates, and the system is said to have n degrees of freedom. Let $\{\mathbf{Q}(t)\}$ be the vector of generalized forces, and let $\{\mathbf{q}(t)\}$ be the vector of generalized displacements, $\{\mathbf{q}(t)\} = \{q_1(t), \dots, q_n(t)\}$. Corresponding elements of the generalized force and displacement vectors are to be conjugate in the energy sense, which simply means that if one of the elements of $\{\mathbf{q}\}$ is a rotation (for instance), then the corresponding element of $\{\mathbf{Q}\}$ must be a moment, so that their product represents work or energy. Methods of computing $\{\mathbf{Q}\}$ are discussed in the references (e.g., Meirovitch). The matrix equation governing the small undamped motion of the system is given by

$$[M]\{\ddot{\mathbf{q}}\} + [K]\{\mathbf{q}\} = \{\mathbf{Q}\} \quad (11.6.2)$$

In this equation a dot denotes single differentiation in time, and $[M]$ and $[K]$ are the mass and stiffness matrices, respectively. $[M]$ and $[K]$ are real and constant matrices, which are assumed to be symmetric. Such symmetry will arise whenever an energy approach (e.g., Lagrange's equations) is employed to derive the equation of motion. The mass matrix is assumed always to be positive definite (and hence nonsingular, or can be made to be positive definite; see Przemieniecki).

Free-Vibration Analysis

The following equation governing the free vibration motion of the conservative system is obtained from Eq. (11.6.2) with $\{\mathbf{Q}\} = \{\mathbf{0}\}$: $[M]\{\ddot{\mathbf{q}}\} + [K]\{\mathbf{q}\} = \{\mathbf{0}\}$. To obtain a solution of this equation, we note that, for a conservative system, periodic motion may be possible. In particular, let us assume a harmonic solution for $\{\mathbf{q}\}$ in the form $\{\mathbf{q}\} = \{\mathbf{A}\} \cos(\omega t - \alpha)$. That is, we inquire whether it is possible for all coordinates to vibrate harmonically with the same angular frequency ω and the same phase angle α . This means that all points of the system will reach their extreme positions at precisely the same instant of time and pass through the equilibrium position at the same time. Substitution of this trial solution into the free vibration equation yields the eigenvector equation $[K]\{\mathbf{A}\} = \omega^2[M]\{\mathbf{A}\}$. In this equation $\{\mathbf{A}\}$ is called the eigenvector and ω^2 is the eigenvalue (the square of a natural frequency). This homogeneous equation always admits the trivial solution $\{\mathbf{A}\} = \{\mathbf{0}\}$.

Nontrivial solutions are possible provided that ω^2 takes on certain discrete values, which are obtained from the requirement that the determinant of the coefficient matrix of $\{\mathbf{A}\}$ vanishes. This yields the eigen-equation (frequency equation) $\Delta(\omega^2) = |[K] - \omega^2[M]| = 0$. It is an n th-degree polynomial in ω^2 , and its n roots are denoted by ω_r^2 , $r = 1, \dots, n$. The eigenvector $\{\mathbf{A}\}_r$, $r = 1, \dots, n$, corresponding to

11-118 ASTRONAUTICS

each eigenvalue is determined from $[K]\{\mathbf{A}\}_r = \omega_r^2[M]\{\mathbf{A}\}_r$. However, the homogeneous nature of this equation precludes the possibility of obtaining the explicit values of all the elements of $\{\mathbf{A}\}_r$. It is possible to determine only their relative values or ratios in terms of one of the components. Thus, we see that for each eigenvalue ω_r^2 there is a corresponding eigenvector $\{\mathbf{A}\}_r$, which has a unique shape (based on the relative values of its components) but which is determined only to within a scalar multiplicative factor that may be regarded as being the amplitude of the shape. This unique shape is called the mode shape, and it can be thought of as being the position of the system when it is in its extreme position, and hence momentarily stationary, as in a static problem. Each frequency along with its corresponding mode shape is said to define a so-called natural mode of vibration. Methods of determining these natural modes are presented in the references (e.g., Wilkinson). If the initial conditions are prescribed in just the right way, it is possible to excite just one of the natural modes. However, for arbitrary initial conditions all modes of vibration are excited. Thus, the general solution of the free-vibration problem is given by a linear combination of the natural modes, i.e.,

$$\{\mathbf{q}\} = \sum_{r=1}^n C_r \{\mathbf{A}\}_r \cos(\omega_r t - \alpha_r)$$

The $2n$ arbitrary constants C_r and α_r are determined through specification of the $2n$ initial conditions $\{\mathbf{q}(0)\}$, and $\{\dot{\mathbf{q}}(0)\}$. An explicit representation for $\{\mathbf{q}\}$ in terms of $\{\mathbf{q}(0)\}$ and $\{\dot{\mathbf{q}}(0)\}$ is given later.

Some of the properties of the natural modes of vibration will now be listed. Unless stated otherwise, the following properties are all consequences of the assumptions that $[M]$ and $[K]$ are real and symmetric and that $[M]$ is positive definite: (1) the n eigenvalues and eigenvectors are real. (2) If $[K]$ is positive definite (corresponding to vibration about a stable state of equilibrium), all eigenvalues are positive. (3) If $[K]$ is positive semidefinite (corresponding to vibration about a neutral state of equilibrium), there is at least one zero eigenvalue. All zero eigenvalues correspond to rigid-body modes. (4) Eigenvectors $\{\mathbf{A}\}_r$, $\{\mathbf{A}\}_s$ corresponding to different eigenvalues ω_r^2 , ω_s^2 ($\omega_r^2 \neq \omega_s^2$; $r \neq s$; $r, s = 1, \dots, n$) are orthogonal by pairs with respect to the mass and stiffness matrices (weighting matrices), that is, $\{\mathbf{A}\}_r^T [M] \{\mathbf{A}\}_s = 0$ and $\{\mathbf{A}\}_r^T [K] \{\mathbf{A}\}_s = 0$ for $r \neq s$; $r, s = 1, \dots, n$. Since the eigenvectors are orthogonal, and hence independent, they form a basis of the n -dimensional vector space. Thus, any vector in the space, such as the solution vector $\{\mathbf{q}\}$, can be represented as a linear combination of the eigenvectors (base vectors). This theorem (expansion theorem) is of vital importance for the response problem to be considered next.

Response Analysis

The response of the system due to arbitrary deterministic excitations in the form of initial displacements $\{\mathbf{q}(0)\}$, initial velocities (impulses) $\{\dot{\mathbf{q}}(0)\}$, or forcing functions $\{\mathbf{Q}(t)\}$ may be obtained by means of the above expansion theorem. That is, the displacement solution of the response problem is expanded with respect to the eigenvectors of the corresponding free-vibration problem. The time-dependent coefficients in this expansion are the so-called normal coordinates of the system. The equations of motion when expressed in terms of the n normal coordinates are uncoupled, and each one of the equations is mathematically identical in form to the equation governing the motion of a simple one-degree-of-freedom spring-mass system. Hence solutions of these equations are readily obtained for the normal coordinates. The normal coordinates are then inserted into the eigenvector expansion to obtain the following explicit solution for displacement response $\{\mathbf{q}(t)\}$ (Przemieniecki) for undamped constrained or unconstrained (free) structures:

$$\{\mathbf{q}(t)\} = \sum_{r=1}^m \frac{\{\mathbf{A}\}_{ro} \{\mathbf{A}\}_{ro}^T}{\{\mathbf{A}\}_{ro}^T [M] \{\mathbf{A}\}_{ro}} \left([M] (\{\mathbf{q}(0)\} + t \{\dot{\mathbf{q}}(0)\}) + \int_{\tau=0}^{\tau=t} \int_{\tau_1=0}^{\tau_2=t} \{\mathbf{Q}(\tau_1)\} d\tau_1 d\tau_2 \right) + \sum_{r=m+1}^n \frac{\{\mathbf{A}\}_{re} \{\mathbf{A}\}_{re}^T}{\{\mathbf{A}\}_{re}^T [M] \{\mathbf{A}\}_{re}} \left([M] \left(\{\mathbf{q}(0)\} \cos \omega_r t + \frac{1}{\omega_r} \{\dot{\mathbf{q}}(0)\} \sin \omega_r t \right) + \frac{1}{\omega_r} \int_{\tau=0}^{\tau=t} \{\mathbf{Q}(\tau)\} \sin \omega_r (t - \tau) d\tau \right) \quad (11.6.3)$$

From this equation, it is seen that the displacement response is expressed directly in terms of the arbitrary excitations and the free-vibration frequencies and eigenvectors. The eigenvectors have been separated into two types denoted by $\{\mathbf{A}\}_{ro}$ and $\{\mathbf{A}\}_{re}$. The "rigid-body" eigenvectors $\{\mathbf{A}\}_{ro}$ correspond to the m rigid-body modes (if there are any) for which $\omega_r = 0$, $r = 1, \dots, m$. The "elastic" eigenvectors $\{\mathbf{A}\}_{re}$ correspond to the remaining $n - m$ eigenvectors, for which $\omega_r \neq 0$, $r = m + 1, \dots, n$. The general solution given by Eq. (11.6.3) is very useful provided that the second integral (Duhamel's integral) can be evaluated. (The first integral is easier to evaluate.) Closed-form solutions of this integral for some of the simpler types of elements of $\{\mathbf{Q}(t)\}$, such as step functions, ramps, etc., are available (see Przemieniecki). Solutions of Duhamel's integral for more complicated forcing functions can be obtained through superposition of solutions for the simpler cases or, of course, from direct numerical integration.

The displacement response obtained from Eq. (11.6.3) may be employed to obtain other response variables of interest, such as velocities, accelerations, stresses, strains, etc. Velocities and accelerations are obtained from successive time differentiations of Eq. (11.6.3). The method used to evaluate the stresses depends on the type of spatial discretization employed to approximate the structural continuum. For example, difference quotients are used in the finite difference approach. Note that the rigid-body components do not contribute to the stress or strain response and hence the first summation in Eq. (11.6.3) can be omitted for computation of these responses.

SPACE PROPULSION

by Henry O. Pohl

NASA

The propulsion system provides the maneuverability, speed, and range of a space vehicle. Modern propulsion systems have diverse forms, however, they all convert an energy source into a controlled high velocity stream of particles to produce force. Among the many possible energy sources, five are considered useful for space-vehicle propulsion:

1. Chemical reaction
2. Solar energy
3. Nuclear energy
4. Electrical energy
5. Stored energy (cold gas)

Accordingly, the various propulsion devices are categorized into chemical energy propulsion, nuclear energy propulsion, stored energy propulsion, solar energy propulsion and electrical energy propulsion.

Chemical propulsion can be further categorized into liquid propulsion or solid propulsion systems. Many combinations of fuels and oxidizers are available. Likewise, electrical energy propulsion can be subdivided into systems using resistive heating, arc heating, plasma, or ion propulsion. Nuclear energy and solar energy are external energy sources used to heat a gas (usually hydrogen).

All space propulsion systems, with the exception of ion propulsion, use nozzle expansion and acceleration of a heated gas as the mechanism for imparting momentum to a vehicle. The fundamental relationships of space propulsion systems are commonly expressed by a number of parameters as follows: The basic performance equation can be derived from the classical newtonian equation $F = MA$. It is defined as

$$F = \left(\frac{\dot{W}}{g} \right) V_e + A_e (P_e - P_a)$$

where F = thrust, lbf; \dot{W} = propellant weight flow rate; g = gravitational acceleration; V_e = exhaust velocity; A_e = nozzle exit area; P_e = pressure at nozzle exit; and P_a = ambient external pressure.

Table 11.6.15 Specific Impulse for Representative Space Propulsion Systems

Engine type	Working fluid	Specific impulse
Chemical (liquid)	Hydrogen peroxide-hydrazine	110–140
		220–245
Bipropellant	O ₂ -H ₂	440–480
	O ₂ -hydrocarbon	340–380
	N ₂ O ₄ -Monomethyl hydrazine	300–340
Chemical (solid)	Fuel and oxidizer	260–300
Nuclear	H ₂	600–1000
Solar heating	H ₂	400–800
Arc jet	H ₂	400–2000
Cold gas	N ₂	50–60
Ion	Cesium	5000–25,000

The specific impulse is one of the more important parameters used in rocket design. It is defined as $I_s = F/W$, where I_s = specific impulse in seconds, F = thrust, and W = propellant weight flow rate per second of operation. I_s increases in engines using gas expansion in a nozzle as the pressure and temperature increase and/or the molecular weight of the gas decreases. The specific impulse values for representative space propulsion systems are shown in Table 11.6.15.

The total impulse $I_t = \int F(t) dt$ is useful to determine candidate rocket firing duration and thrust combinations required to satisfy a given change in momentum, where F = thrust and t = time.

Mass fraction is the ratio of propellant to total weight of the vehicle and is defined as $\gamma = (W_i - W_f)/W_i$, where γ = mass fraction; W_i = total weight of the vehicle including the propellant, structure, engine, etc., at the start of operation; and W_f = total weight of the vehicle less the weight of propellant consumed.

In the simplified case of a vehicle operating free of atmospheric drag and gravitational attractions, the velocity increment obtained from a propulsion system is defined as $\Delta V = I_{sg} \ln (W_i/W_f)$, where ΔV = velocity increment obtained; W_i = total weight of vehicle including propellant, structure, engine, etc., at start of operation; and W_f = total weight of vehicle less weight of propellant consumed during operations. This equation brings together the mission parameters, vehicle parameters and rocket-engine parameters.

Figure 11.6.26 graphically shows the effect specific impulse and mass fraction have on the ability of a propulsion system to change the velocity of a payload in space.

Chemical Propulsion Only chemical energy has found wide acceptance for use in space propulsion systems. Modern materials and current technologies have made it possible to operate rockets at relatively high pressures. When these rockets are fitted with very large expansion-ratio nozzles (nozzle exits 40 to 200 times the area of the throat) the force produced per unit of propellant consumed is greatly increased when operating in the vacuum of space.

Solid-propellant rocket motors are used for moderate total impulse requirements, in spite of their low specific impulse, provided that the total impulse requirements can be precisely set before the rocket is built. The low specific impulse for these applications is largely offset by the high mass fraction (ratio of propellant weight to total propulsion system weight including propellant weight). They are simple to start, have good storage characteristics and multiple velocity requirements can be accommodated by staging, i.e., using a separate motor for each burn.

Liquid-propellant systems are generally used for moderate to high total impulse requirements, multiple burns, velocity-controlled thrust terminations, variable thrust requirements or for applications where the total impulse requirement is likely to change after the rocket is built or launched.

Bipropellant systems are the most commonly desired systems to satisfy moderate to high total impulse requirements. A fuel and oxidizer are injected into a combustion chamber where they burn, producing large volumes of high-temperature gases. Oxygen and hydrogen produce the

highest specific impulse of any in-service chemical rocket (440 to 460 s). These systems also have good mass fractions (0.82 to 0.85). Oxygen and hydrogen, as stored in the rocket propellant tanks, are cryogenic, with boiling points of -296.7°F and -442°F respectively. Storing these propellants for long periods of time requires thermally

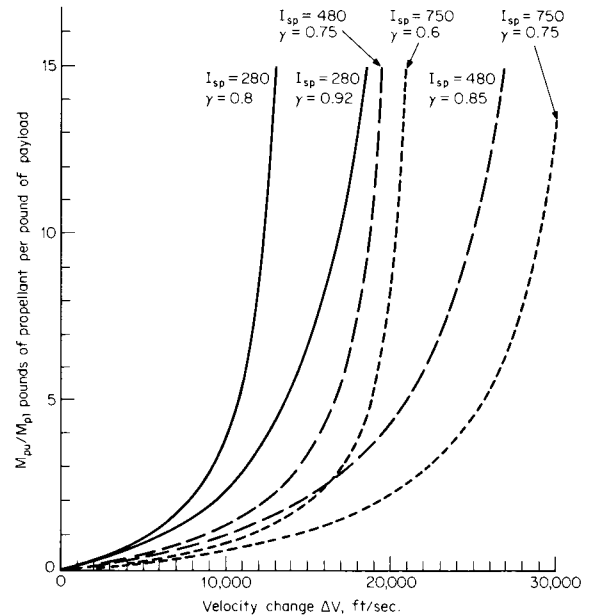


Fig. 11.6.26 Performance curves for a range of specific impulse and mass fractions.

insulated propellant containers and specially designed thermodynamic vents or refrigeration systems to control boil-off losses. The low density of hydrogen (4.4 lb/ft^3) requires the use of bulky containers. Because of these characteristics, oxygen/hydrogen rocket systems can best satisfy moderate to high total-impulse requirements. Where designs are constrained by volume, very long durations of time between firings, many short burns, or precise impulse requirements, nitrogen tetroxide and monomethylhydrazine are often preferred, if the total impulse requirements are moderate.

Monopropellant systems generally use a single propellant that decomposes in the presence of a catalyst. These are usually low total-impulse systems used to provide attitude control of a spacecraft or vernier velocity corrections. For attitude control, small thrusters are arranged in clusters around the perimeter of the vehicle. These small thrusters may, in the course of a single mission, produce over 1,000,000 impulses, to keep the vehicle oriented or pointed in the desired direction.

Solar-heating propulsion would use a solar collector to heat the working fluid which is exhausted through a conventional nozzle. The concentrated solar energy heats the rocket propellant directly through the heat exchanger. The heated propellant is then exhausted through the nozzle to produce thrust. Many design problems make the practical development of the solar-heating rocket quite difficult. For example, the solar collector must be pointed toward the sun at all times and the available solar energy varies inversely with the square of the distance from the sun. Using hydrogen as a working fluid, this type system would have a specific impulse of 400 to 800 s and could satisfy very high total impulse requirements at low thrust levels.

Nuclear propulsion is similar to solar-heating propulsion except that the energy source is replaced by a nuclear reactor. A propellant is injected into the reactor heat exchanger, where the propellant is heated under pressure and expanded through the nozzle. Liquid hydrogen is the best choice for the nuclear rocket's working fluid because its low molecular weight produces the highest exhaust velocity for a given nozzle-inlet temperature. For example, for a given entrance nozzle pressure of

11-120 ASTRONAUTICS

43 atm and temperatures of 1650, 3300, and 4950 K the following specific impulses are obtainable: 625, 890, and 1,216 s respectively. The nuclear rocket engine is started by adjusting the reactor neutron-control drums to increase the neutron population. Propellant flow is initiated at a low reactor-power level and is increased in proportion to the increasing neutron population until the design steady-state reactor power output is obtained.

For shutdown of the engine, control drums are adjusted to poison the core and decrease the neutron population. Steady-state reactor thermal power, in megawatts, is determined by the relation $P1 = Kw (h_{out} - h_{in})$, where w and h are core flow rate and enthalpy, respectively, and K is the appropriate conversion factor to megawatts.

The reactor is a high-power-density, self-energizing heat exchanger which elevates the temperature of the hydrogen propellant to the limit of component materials.

SPACECRAFT LIFE SUPPORT AND THERMAL MANAGEMENT
by Walter W. Guy

NASA

REFERENCES: NASA SP-3006, "Bioastronautics Data Book." Chapman, "Heat Transfer," Macmillan. Purser, Faget, and Smith, "Manned Spacecraft: Engineering Design and Operation," Fairchild.

Life Support—General Considerations

To sustain human life in a spacecraft two functions must be provided. The first is to replenish those substances which humans consume and the second is to control the conditions of the environment at levels consistent with human existence. Humans consume oxygen, water, and food in the metabolism process. As a by-product of this metabolism, they generate CO₂, respired and perspired water, urine, and feces (Table 11.6.16). The provisioning of man's necessities (and the elimination of his wastes) is a primary function of life support. However, an equally important function is the maintenance of the environment in which he lives.

There are three aspects of environmental control—ambient pressure, atmospheric composition, and thermal condition of the environs. In a typical spacecraft design the ambient pressure is maintained generally in the range between 1/3 atm and sea-level pressure, with the oxygen partial pressure varying in accordance with Fig. 11.6.27 in order to provide the appropriate partial pressure of oxygen in the lungs for breathing.

The other constituents of concern in the atmosphere are the diluent, CO₂, water vapor, and trace amounts of noxious and toxic gases. The percent of the diluent in the atmosphere (or indeed whether a diluent is present at all) is selectable after proper consideration of the design parameters. For instance, short-duration spacecraft can take advantage of human adaptability and use atmospheric pressures and compositions significantly different from those at sea level, with the attendant advantage of system design simplicity. The Mercury, Gemini, and Apollo spacecrafts utilized 5-lb/in² pure oxygen as the basic cabin atmosphere. Skylab used an oxygen-nitrogen mixture although at a reduced pressure, while the shuttle is designed for an essentially sea-level equivalent at-

mosphere. When selecting the pressure and composition, it is important to remember that although a two-gas system adds complexity, it can eliminate the concerns of (1) flammability in an oxygen-rich environment, (2) oxygen toxicity of the crew, and (3) decreased atmospheric cooling potential for electronic equipment in a reduced-pressure cabin. In the selection of a diluent, nitrogen should be considered first, since its properties and effects on humans and equipment are well understood. However, other diluents, such as helium, which have characteristics attractive for a special application, are available.

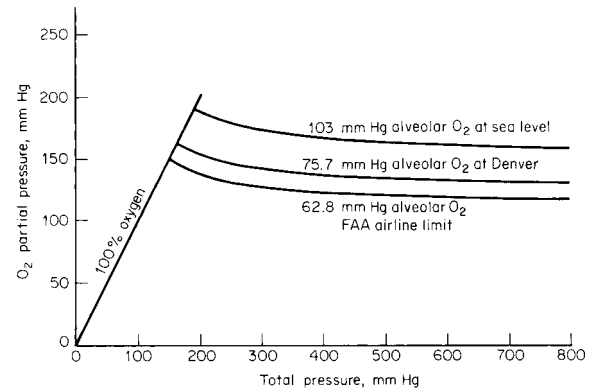


Fig. 11.6.27 Atmospheric oxygen pressure requirements for humans.

The other atmospheric constituents—CO₂, water vapor, and trace gases—must be controlled within acceptable ranges for comfort and well-being. Although the partial pressure of CO₂ is less than half a millimeter of mercury in an ambient earth environment, humans are generally insensitive to CO₂ levels up to 1 percent of the atmosphere (or 7.6 mmHg) unless mission durations increase to more than a month. As spacecraft missions are further extended, the partial pressure of CO₂ should approach the earth ambient level to ensure physiological acceptance. Atmospheric water vapor (or humidity) should be maintained high enough to prevent drying of the skin, eyes, and mucous membranes, but low enough to facilitate evaporation of body perspiration, maximizing crew comfort. The generally accepted range for design is 40 to 70 percent relative humidity. In the closed environment of the spacecraft, cabin noxious and toxic gases are of particular concern. It should be noted that 8-h/day industrial exposure limits are not appropriate for the continuous exposure which results from a sealed spacecraft cabin. Therefore, materials which can offgas should be screened and limited in the crew compartment. The small quantities which cannot be completely eliminated, as well as certain undesirable products of metabo-

Table 11.6.16 Metabolic Balance for Humans

Consumed		Produced	
Oxygen	1.84	Carbon dioxide	2.20
Drinking water	5.18	Perspiration	2.00
Food (2/3 H ₂ O)	3.98	Respiration	2.00
		Urine	4.53
		Feces	0.27
	11.00		11.00

NOTE: Metabolic rate = 11,200 Btu/human-day and RQ = 0.87; RQ (respiratory quotient) = vol CO₂ produced/vol O₂ consumed. All values are in units of lb/human-day.

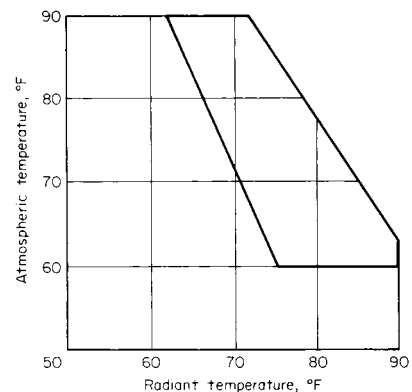


Fig. 11.6.28 Thermal comfort envelope for humans. (Note: metabolic rate 300–600 Btu/h; air velocity 15–45 ft/min; pressure 14.7 lb/in².)

lism, must be actively removed by the life-support system to maintain an acceptable atmosphere for the crew.

The third of the environmental control aspects—atmospheric thermal condition—is subject to several design variables, all of which must be taken into account. Thermal comfort is a function of the temperature and relative humidity of the surrounding atmosphere, the velocity of any ventilation present, and the temperature and radiant properties of the cabin walls and equipment. The interrelationship of these parameters is shown in Fig. 11.6.28 for a reasonable range of flight clothing ensembles. Because of the effective insulations available to the vehicle designers, the problem of thermal control in the spacecraft cabin is generally one of heat removal. Utilizing increased ventilation rates to enhance local film coefficients is one means of improving thermal comfort within the cabin. However, the higher power penalties associated with gas circulation blowers, as compared to liquid pumps, should suggest using the spacecraft thermal control liquid circuit in reducing the temperature of the radiant environment as potentially a lower-power alternative. However, if the walls or equipment are chilled below the dew point, condensation will occur.

As an additional benefit, maintaining an acceptable thermal environment through radiative means reduces the psychological annoyance of a drafty, noisy environment. Ventilation rates between 15 and 45 ft/min are generally considered comfortable, and exceeding this range should be avoided.

Life Support—Subsystems Selection

In designing the life-support system for a spacecraft, subsystems concepts must be selected to accomplish each of the required functions. This process of selection involves many design criteria. Size, weight, power consumption, reliability of operation, process efficiency, service and maintenance requirements, logistics dependency, and environmental sensitivity may each be very important or inconsequential depending on the spacecraft application. In general, for life support subsystems, the dominant selection criterion is mission duration. Various subsystem choices for accomplishing the life support functions are shown in Fig. 11.6.29.

To illustrate the relationship between mission duration and subsystem selection, the various concepts for removal of CO₂ from the atmosphere shown in Fig. 11.6.29b will be discussed. The simplest method of controlling the level of CO₂ in the spacecraft cabin is merely to purge a small amount of the cabin atmosphere overboard. This concept is simple and reliable and requires almost no subsystem hardware, although it does incur a fairly significant penalty for atmospheric makeup. For missions such as Alan Sheppard's first Mercury flight, this concept is probably optimum. However, even a minor increase in mission duration will result in a sizable weight penalty to the spacecraft. By adding a simple chemical absorption bed to the spacecraft ventilation loop (with a chemical such as lithium hydroxide as the absorbent), the expendable penalty for CO₂ removal can be reduced to the weight of the chemical canisters consumed in the absorption process. This concept was used on the Apollo spacecraft. The penalty for this type of concept also becomes prohibitive if mission durations are further extended. For missions such as Skylab, the expendable chemical absorbent can be replaced by a regenerable adsorbent. This change eliminates the lithium hydroxide weight penalty but incurs a small atmospheric ullage loss during the vacuum regeneration of the adsorbent. In addition, the regenerable system is more complex, requiring redundant beds (one for adsorption while the alternate bed desorbs), and mechanical-timing circuits and switching valves. This result is typical in that reducing expendable requirements is generally at the expense of system complexity.

The three CO₂ removal concepts discussed above all prevent the subsequent use of the collected CO₂ after removal from the atmosphere. Should the CO₂ be required for reclaiming the metabolic oxygen (such as will be the case for a space station design), the regenerable concepts can be adapted to accommodate retrieval of the CO₂ during desorption. However, this enhancement further complicates the subsystem design. There is an alternative CO₂ removal concept available which utilizes a fuel-cell-type reaction to concentrate the CO₂ in the atmosphere through

electrochemical means. This process is mechanically simple (as compared to the adsorption-desorption system) but does require more electrical power. However, it has an integration advantage in that it provides the CO₂ collected from the atmosphere mixed with hydrogen, which makes its effluent a natural feedstock for either one of several CO₂ reduction subsystems (which will be required for oxygen recovery on a space station). Although Figure 11.6.29 identifies the various life-support subsystem choices for candidate spacecraft designs of different mission durations, this information should be used only as a guide. The crew size as well as other design parameters can skew the range of applicability for each subsystem (e.g., a large crew can render expendable dependent subsystems inappropriate even for relatively short missions).

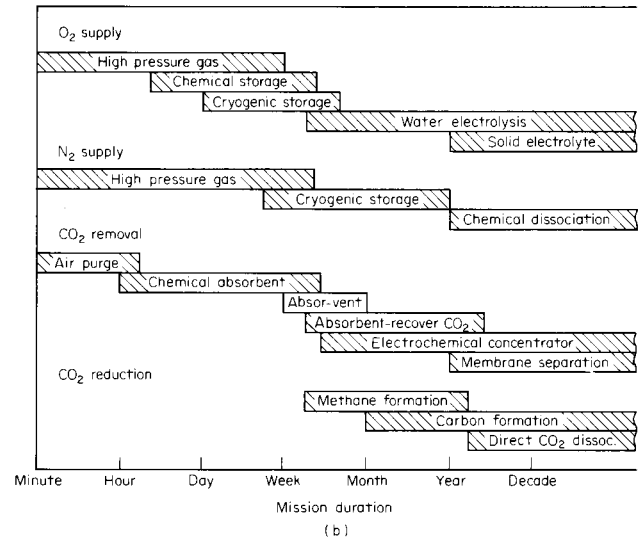
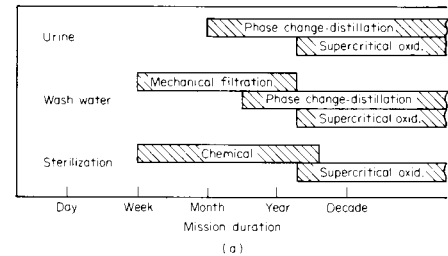


Fig. 11.6.29 Concepts to accomplish the life-support function. (a) Water recovery; (b) atmospheric revitalization.

There is another major aspect of life support system design for spacecraft (in addition to subsystem selection) and that is process integration and mass balance. For example, a space-station-class life-support system design must accommodate wastewater with a wide range of contamination levels—from humidity condensate which includes only minor airborne contamination to various wash and rinse waters (including personal hygiene, shower, clothes washing, and dish washing) and urine. The degree of contamination generally influences the reclamation process selection; therefore, multiple contaminated sources tend to result in multiple subsystem processes. For example, highly contaminated water, such as urine, is most reliably reclaimed through a distillation process since evaporation and condensation can be more effectively utilized to separate dissolved and particulate material from the water, while less contaminated wash waters can be effectively reclaimed through osmotic and mechanical filtration techniques at significantly less power penalties in watts/lb H₂O recovered. Regardless of the tech-

11-122 ASTRONAUTICS

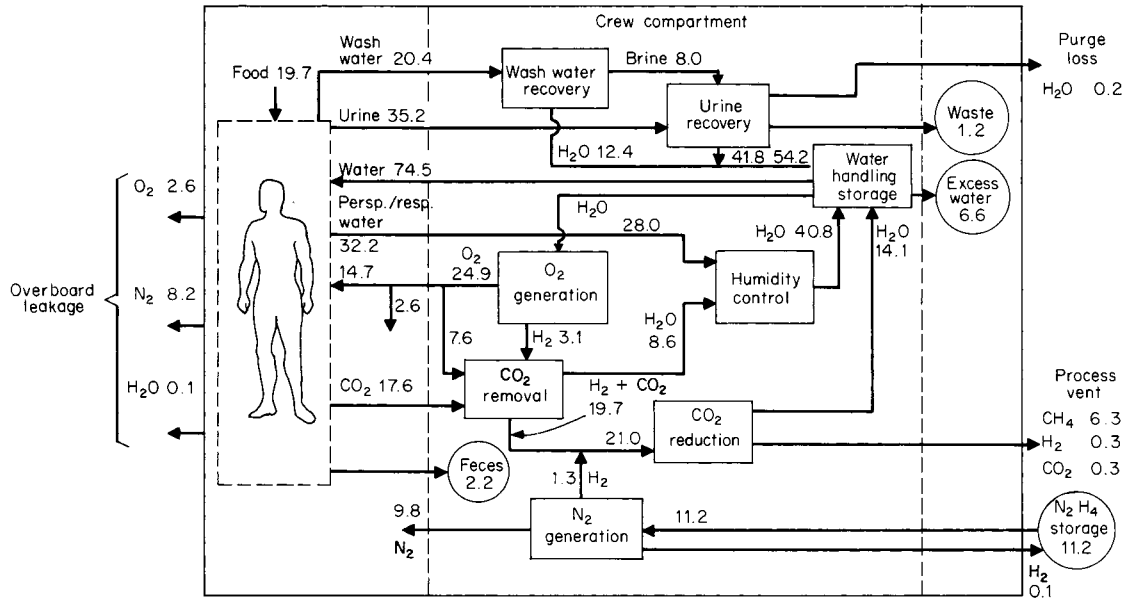


Fig. 11.6.30 Life-support systems mass balance. (All values are in pounds per day for an eight-person crew.)

niques selected, water must be made available for drinking, food preparation, and cleaning the crew and the equipment they use, as well as for generating the oxygen they breathe. In fact, the space station life-support design process can be looked upon, in one respect, as a multifaceted water balance since the dissociation of CO₂ and generation of O₂ both involve water in the respective processes. Figure 11.6.30 is a typical space station schematic depicting the interrelationship of the subsystems and the resulting mass balance.

Thermal Management—General Considerations

Although there is an aspect of life support associated with thermal comfort, the area of spacecraft thermal management encompasses a much broader scope. In the context of this section, thermal management includes the acquisition and transport of waste heat from the various sources on the spacecraft, and the disbursing of this thermal energy at vehicle locations requiring it, as well as the final rejection of the net waste heat to space. Although there are thermal implications to the design of most spacecraft hardware, the Life Support and Thermal Management section only deals with the integration of the residual thermal requirements of the various vehicle subsystems to provide an energy-efficient spacecraft design (i.e., one which utilizes waste heat to the maximum and therefore minimizes requirements for the vehicle heat rejection system).

Thermal management systems are typically divided into two parts. The first, associated with the spacecraft cabin, has design requirements associated with maintaining the crew environment and equipment located in the cabin at acceptable temperatures, and in addition has special requirements imposed on its design because of the location of the system in the pressurized compartment and its proximity to humans. These additional requirements are usually dominant. Any cooling medium which is used in the crew compartment must have acceptable toxicological and flammability characteristics in order to not impose a hazard to the crew in the event of malfunction or leakage. Although there are thermal control fluids which have low toxicity potential, reasonable flammability characteristics and adequate thermal transport properties, none are better than water.

The second aspect of the thermal management system involves those spacecraft systems located outside the cabin. The dominant design criteria in thermal control fluid selection for these systems are thermal

transport efficiency and low-temperature characteristics. The thermal transport efficiency is important since the size, weight, and power requirements of the pumping and distribution system depend on this parameter. However, in the environs of deep space the potential exists for very low temperatures. Therefore, for maximum system operating flexibility, the characteristics of the thermal transport fluid must be such that operation of the system can continue even in a cold environment; thus, low-temperature properties become a fluid selection constraint. Although the range of acceptable fluids is broader here, several fluids in the Freon family meet these requirements. For single-phase, pumped-fluid systems, the temperature levels of the heat sources are important in determining the optimum sequence for locating equipment in the thermal circuit. The equipment with the lowest-temperature heat sink requirements are accommodated by placing them immediately after the heat rejection devices, while equipment which can accept a higher-temperature heat sink are located downstream. Also, those subsystems which require heating must be located at a point in the circuit which can provide the thermal energy at the required temperature level.

Typically spacecraft heat sources include cabin-atmosphere heat exchangers, the avionics system as well as other electronic black boxes, power generation and storage equipment, etc., while heat sinks include propulsion system components, various mechanical equipment requiring intermittent operation, dormant fluid systems which have freezing potential, etc. The ultimate elimination of the net thermal energy (i.e., sources minus sinks) is by rejection to space. This is accomplished through expendables or radiation.

Recent developments in thermal management technology have resulted in the consideration of a two-phase acquisition, transport, and rejection system. This concept uses the heat of evaporation and condensation of the transport fluid to acquire and reject thermal energy, reducing by several orders of magnitude the amount of fluid required to be pumped to the various heat sources and sinks within the spacecraft. This concept has the added advantage of operating nearly isothermally, permitting the idea of a thermal "bus" to be included in future spacecraft design, with indiscriminate sequencing of the heat sources and sinks within the vehicle.

Thermal Management Subsystem Selection

The subsystem selection process associated with the thermal management area depends largely on the magnitude of thermal energy being

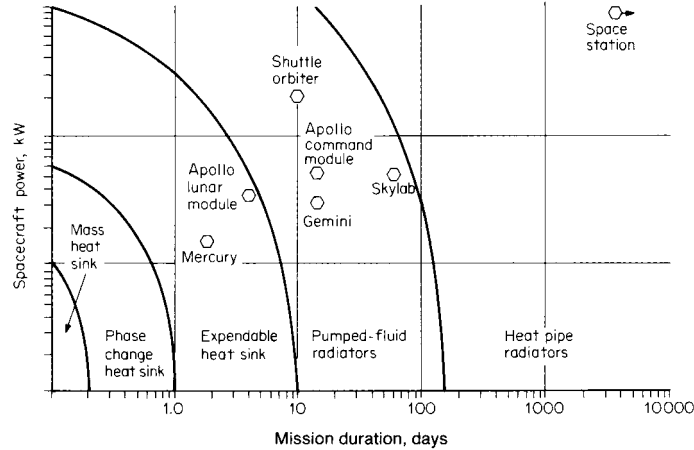


Fig. 11.6.31 Range of application of various heat-rejection methods.

managed and the duration of the mission. Figure 11.6.31 graphically depicts the areas of applicability for various types of heat-rejection devices as a function of these parameters.

Small heat-rejection requirements can sometimes be met by direct heat sinking to the structure (or a fluid reservoir). Often, passive heat sinks need to be supplemented with fusible heat sinks (to take advantage of the latent heat of fusion) or evaporative heat sinks (to take advantage of the latent heat of evaporation). Of the three types of heat sinks, the evaporative heat sink is the only one which has been used as the primary vehicle heat-rejection device in the manned spaceflight program to date. Both the Mercury spacecraft and the lunar module utilized a water evaporative heat sink in this manner. However, the Apollo spacecraft and the shuttle have also used evaporative heat sinks and Skylab used a fusible heat sink as supplemental heat rejection devices.

Since space is the ultimate heat sink for any nonexpendable heat rejection, devices which allow the thermal energy which has been collected in spacecraft coolant circuits to be radiated to space become the mainstay of the thermal management system. These "radiators" take many forms. The simplest design involves routing the cooling circuits to the external skin of the spacecraft so that the thermal energy can be radiated to deep space. Because of spacecraft configuration restrictions, only partial use can be made of the external skin of the spacecraft, and the amount of thermal energy which can be rejected by this technique is thereby limited. Although the Gemini and Apollo spacecraft success-

fully used integral skin radiators, the unique characteristics of the outer surface of the orbiter required a different technique be adopted for its radiator design. Accordingly, the radiators were designed to be deployed from inside of the payload bay doors. This not only provides good exposure to space, but also, in the case of the forward panels, allows two-sided exposure of the panels, thereby doubling the active radiating area.

Heat rejected Q_{rej} , according to the Stefan-Boltzmann law, is given by the following equation:

$$Q_{rej} = \epsilon \gamma AT^4$$

where $\gamma = \text{constant}, 0.174 \times 10^{-8} \text{ Btu}/(\text{h} \cdot \text{ft}^2 \cdot \text{R}^4)$; $\epsilon = \text{emittance property of surface (termed emissivity)}$, $A = \text{area available for radiation}$; and $T = \text{radiating temperature}$. From this equation it is obvious that a radiator with both sides exposed will reject twice as much heat to space as one of the same dimensions which is integral with the skin of the vehicle. A space radiator can absorb as well as reject thermal energy. The net heat rejected Q_{net} from a radiator is given by the following equation:

$$Q_{net} = Q_{rej} - \sum_N^{A=1} Q_{abs}$$

The energy absorbed by the radiator, Q_{abs} , can come from various sources (see Fig. 11.6.32).

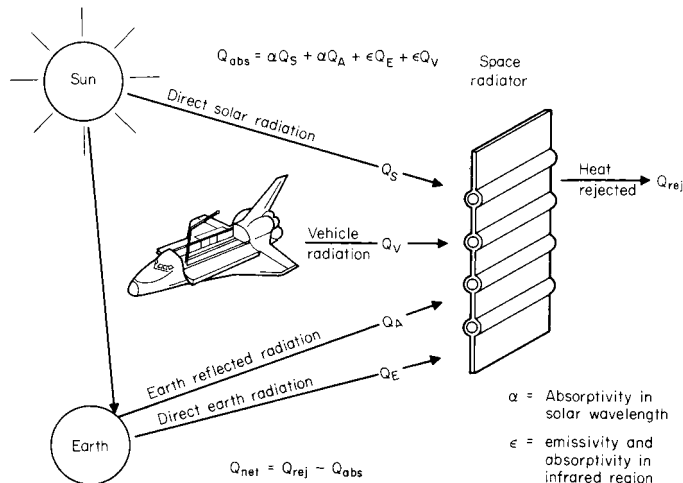


Fig. 11.6.32 Space radiator energy balance.

$\alpha = \text{Absorptivity in solar wavelength}$
 $\epsilon = \text{emissivity and absorptivity in infrared region}$

11-124 ASTRONAUTICS

The most common heat sources for an earth-orbiting spacecraft are direct solar impingement, reflected solar energy from the earth (i.e., albedo), direct radiation from the earth, radiation from other parts of the spacecraft, and radiation from other spacecraft in the immediate vicinity. These energy sources are absorbed on the radiator surface in direct proportion to the absorptance characteristic of the surface, termed absorptivity. Emissivity and absorptivity are unique to each surface material but are variables directly linked to the temperature of the source of the radiation (i.e., wavelength of the radiation). Therefore, since absorptivity and emissivity are characteristics of the surface, the careful selection of a surface coating can significantly enhance the effectiveness of the radiator. The coating should have a high emissivity in the wavelength of the rejected energy from the radiator (for good radiation efficiency) and a low absorptivity in the wavelength of the impinging radiation (for minimal absorbed energy). Since generally the earth and the surrounding spacecraft are producing thermal energy of essentially the same wavelength as the radiator, it is necessary to restrict the view of the radiating surface to these objects since absorptivity and emissivity of a surface are equal for the same wavelength energy. Thus, radiators which can be located so that they are not obstructed from viewing deep space by elements of the spacecraft or other spacecraft in the vicinity will be much more effective in rejecting waste heat. The sun, however, emits thermal energy of a dramatically different wavelength and, therefore, coatings can be selected which absorb less than 10 percent of the solar energy while radiating nearly 90 percent of the energy at the emitting temperature of the radiator.

For applications which require large radiating surface areas as compared to the vehicle's size, integral skin radiators offer insufficient area and thus space radiators which use deployment schemes must be considered. However, as radiators become larger the mechanisms become very complicated. To circumvent the mechanical problems of deployment, a new radiator concept has been developed which allows in-orbit construction. This concept utilizes a single-tube heat pipe as the primary element (see Fig. 11.6.33).

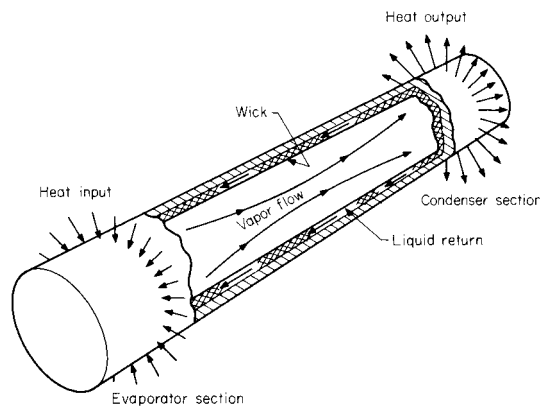


Fig. 11.6.33 Basic heat-pipe operation.

There are two distinct advantages of heat pipe radiators. The first is that assembly of large surface areas in-orbit can be effected without breaking into the thermal control circuit. This is practical since the heat pipe radiator element is completely self-contained. The second advantage is that in-orbit damage from accidental collision or meteoroid puncture affects only that portion of the radiator actually damaged and does not drain the entire radiating surface of fluid as it would the radia-

tors which have been used on spacecraft to date. Because of this advantage, future missions which require either of the three types of radiators (i.e., integral skin, deployable, or space constructible) will utilize the heat pipe concept to transport the thermal energy to the exposed radiating surface.

The design of space radiators can take many forms, but the basic concept is an exposed surface made of a conducting material with regularly spaced fluid tubes to distribute the heat over the surface (see Fig. 11.6.34).

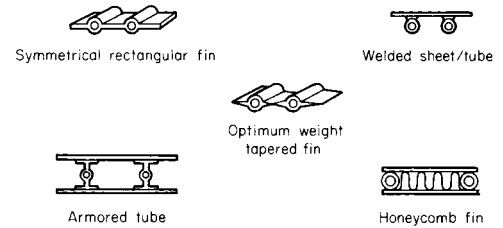


Fig. 11.6.34 Typical radiator tube/fin configurations.

The selection of the material and configuration of the radiating surface (i.e., honeycomb, box structure, thin sheet, etc.) determine its thermal conductance. This conductance, when coupled with tube spacing and the internal heat transfer characteristics within the tube and fluid system, determines the temperature gradient on the radiating surface

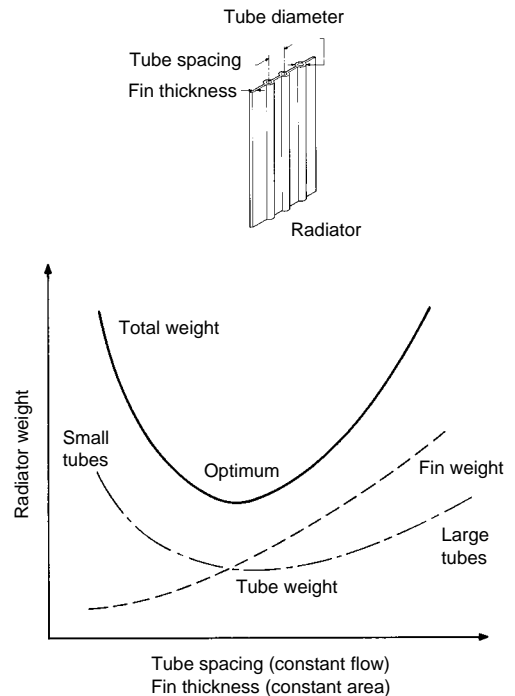


Fig. 11.6.35 Radiator configuration optimization.

between adjacent tubes. This so-called "fin effectiveness" represents a loss in radiating potential for any particular radiator design; therefore, these parameters should be selected carefully to optimize the radiator design within the constraints of each application. Figure 11.6.35 demonstrates the effect of the configuration parameters of the radiator on panel weight.

DOCKING OF TWO FREE-FLYING SPACECRAFT

by Siamak Ghofranian and Matthew S. Schmidt

Rockwell Aerospace

REFERENCES: Ghofranian, Schmidt, Briscoe, and Shliesing, "Space Shuttle Docking to MIR, Mission-1"; Ghofranian, Schmidt, Briscoe, and Shliesing, "Simulation of Shuttle/MIR Docking"; Ghofranian, Schmidt, Lin, Khalessi, and Razi, "Probabilistic Analysis of Docking Mechanism Induced Loads for MIR/Shuttle Mission"; *35th Structures, Structural Dynamics, and Materials Conf. AIAA/ASME/ASCE/AHS/ASC*. Haug, "Computer Aided Kinematics and Dynamics of Mechanical Systems," vol 1: "Basic Methods," Allyn and Bacon. Greenwood, "Principles of Dynamics," Prentice-Hall.

The information in this section covers the mechanics of docking two free-flying unconstrained vehicles in space. Different methods of mating are addressed with the emphasis applied to docking. The content does not encompass all facets of the procedure, but it does bring forth the physics of the operation which make the process an engineering challenge.

Types of Mating

The understanding of mating is a precursor to preliminary design. Different techniques of mating free-flying bodies are often discussed when planning the rendezvous of two vehicles in space. The mating of two structures can be performed in three ways: docking, berthing or a combination of both. **Docking** relies on the transfer of vehicle momentum to provide the means to force the docking ports into alignment. If a significant amount of momentum is required for capture, jet firings can be used to introduce the impulse into the system as needed. **Berthing** relies on a secondary system, such as a robotic arm to enforce the docking ports into alignment. The active vehicle grapples the other with a robot manipulator and guides the structural interfaces together. If manipulator usage is attempted, specific design factors need to be considered: arm configuration, gearbox stiffness, linkage flexibility, and controllability.

Mating of two structures in space is by every means considered a multibody dynamic event. Docking involves a significant level of momentum transfer, while berthing involves relatively little. The dynamics result from the deliberate impact of the two vehicles. As docking occurs the system responds with rigid-body motion and mechanical motion of the docking device. Depending on the relative states between the vehicles and the mode in which the maneuver is attempted, the response of the system and the physics vary considerably.

For discussion purposes the two docking vehicles can be considered as a target vehicle (passive) and a docking vehicle (active). The passive vehicle maintains attitude control as the active vehicle is navigated along an approach corridor. The active vehicle holds an attitude control mode with translational control authority. As the corridor narrows, sighting aids, range, and range-rate feedback on both vehicles are used to guide the docking ports into contact.

As the vehicles approach, a closing velocity exists. From a design standpoint the operation of a docking system involves various mechanism operational phases: mechanism deployment, interface contact and capture, attenuation of relative motion, mechanism retraction, and structural lockup. The **deployment phase** is where the mechanism is driven from its stowed position to its ready-to-dock position. Vehicle interface contact and capture are initiated when the docking ports of each vehicle are maneuvered into contact. Ideally, a positive closing velocity should be maintained from initial contact through capture. Once an opening velocity develops, the probability of a failed capture

increases. As the vehicles interact the mechanism interfaces are indexed into alignment as the system responds to the impact loads. The compliance of the system occurs in two forms: mechanism movement and rigid body vehicle motion.

When the docking interfaces interact, the system responds in six degrees of freedom and the docking system is stroked as the mechanism absorbs the relative misalignments. Once the interfaces are fully aligned, capture latches lock the opposing interfaces together, and the vehicles are "soft-docked." After capture, residual energy in the system allows relative motion between the structures to continue. Depending on the location of the docking system relative to the vehicle center of masses, the motion may dissipate due to the inherent hysteresis in the docking system; otherwise, separate energy-dissipation devices may be necessary. After attenuation the vehicles are likely to be misaligned due to the new relative equilibrium position of the spacecraft. Separate procedures or devices can be used to bring the structural interfaces into alignment.

The **retraction process** is where the active mechanism is driven back to its stowed position. Once they are fully retracted, the structural interfaces are latched at hard interfaces, and the vehicles are "hard-docked."

The mass of each vehicle is an essential part of the docking system design. The momentum of the docking vehicle is the medium which provides the force required by the docking mechanism to comply with the relative misalignments between the vehicles at the docking interface. The operation can be complicated if a vehicle center of mass is offset from the longitudinal axis of the docking system. As a result, the vehicle effective mass at the docking interface is reduced. Furthermore, the center of mass offset induces relative rotation after contact which complicates the capture and attenuation process. Ideally two vehicles should dock such that the velocity vector and longitudinal axis of the docking system have minimum offset from the center of mass. The relative rotation of the vehicles after contact is known as *jackknifing*.

The docking mechanism center-of-mass offset and the vehicle size significantly influence the design of the docking interfaces, attenuation components, docking aids, piloting procedures, and capture-assist methods. The relative vehicle misalignments and rates at the moment the docking interfaces first come into contact (initial conditions) should be known in order to size the mechanism attenuation components, to establish piloting procedures and training criteria, and to study the mechanics of the system before, during, and after docking.

The initial conditions result from vehicle as-built tolerances, thermal and dynamic distortions, variation in piloting performance, and control system tolerances. The misalignments are composed of lateral misalignments in the plane of the docking interface and angular misalignments about three axes. The rates are composed of translational velocities along three axes and angular velocities about three axes.

The mass and motion of the system are the basic ingredients for providing the energy necessary to join the interfaces. Ideally the interfaces should capture before an opening velocity develops between the docking interfaces. Adequate momentum at the docking port is required to actuate the mechanism. The impulse introduced to the system during the impact must be less than that required to reduce the relative interface velocity to zero. If the relative interface velocity goes to zero before capture, the vehicles will separate. For low closing velocities, a small axial impulse due to initial contact can reduce the relative interface velocity to zero and cause a "no capture" condition.

A drive system along the longitudinal axis of the docking mechanism or reaction control jets increases the probability of capture. It extends the docking system toward the target vehicle once initial contact is made and thus improves capture performance for a docking vehicle with a low closing velocity. However, a drawback of a drive system is that the reaction has the tendency to push the vehicles apart. The action of jet thrusting has the opposite effect; it tends to push the vehicles together. If the momentum required to provide a low possibility of no capture becomes operationally prohibitive, thrusting can be used as a substitute and applied as necessary.

11-126 PIPELINE TRANSMISSION

As energy introduced into the system increases, whether in the form of vehicle momentum or jets pulsing, a tradeoff exists between acceptable internal vehicle loads, allowable component stroke limits, vehicle jackknifing, and piloting capability.

Vehicle Mass and Inertia Effects

Concentrated spherical masses colliding in two dimensions can be used to describe the dynamic effects of an impact. The same class of examples are consistently used in beginning physics textbooks to describe the macroscopic concepts of impulse, momentum, and energy. The same theory should be applied to understand the requirements of mating two vehicles and perform conceptual and preliminary design studies. A single-degree-of-freedom mechanical equivalent exhibiting simple harmonic motion is a useful example for understanding the mechanics.

Consider two spacecraft in a two-dimensional plane on a planned course of docking without any misalignments and with some closing velocity. If only the docking-axis degree of freedom is considered, the effective mass of each body, M_1 and M_2 , can be computed from

$$M_1 \text{ (or } M_2) = M - (ML)^2/(I + ML^2)$$

where M is the vehicle mass, I is the vehicle mass moment of inertia about the center of mass, and L is the mass center offset from the docking axis. In this case the process of capture and attenuation can be thought of as a perfectly plastic impact of two bodies. The masses dock and stick together. After impact the two bodies continue their trajectory with some final velocity. The combined effective mass of the two bodies represented as a single degree of freedom can be computed from $M_{\text{eff}} = M_1 M_2 / (M_1 + M_2)$. Since momentum is conserved during a perfectly plastic impact, kinetic energy loss during docking can be computed from $\frac{1}{2} M_{\text{eff}} v^2$, where v is the capture velocity. Since at capture we know the effective mass of the system and the capture velocity, the

unknown parameter becomes the work required to bring the system to rest.

Design Parameters

The energy loss during docking is equal to the work done, $F \times d$, by the mechanism-attenuation components. If a hysteresis brake is used to bring the system to rest, then a trade can be performed on the force-distance relationship by using

$$\frac{1}{2} M_{\text{eff}} v^2 = Fd$$

where F represents the force necessary to bring the system to rest over distance d . Using the hysteresis brake as a starting point provides the average about which other devices would oscillate. For an underdamped spring/damper attenuation system, the relative motion and maximum force can be computed from

$$x = v/\omega_d \times e^{-\zeta\omega} \sin \omega_d t \quad \text{and} \quad F = Kx + C dx/dt$$

respectively. In this representation,

$$\omega_d = \omega(1 - \zeta^2)^{1/2} \quad \text{and} \quad \omega^2 = K/M_{\text{eff}}$$

where ζ represents the damping factor and K and C represent the attenuation component characteristics. As can be seen, minimal knowledge of the basic system characteristics can be used to design the type and arrangement of the attenuation components. During the design of the attenuation components the following components may prove useful: preloaded centering springs, staged springs, ON/OFF dampers, and variable-level hysteresis brakes. The material in this section is only a first look at understanding the design of a docking system. As more detail is developed, the effects of relative vehicle motion, interface contact dynamics, mechanism performance, and vehicle flexibility need to be simulated, which goes beyond the scope of this section. For a comprehensive background, the reader should refer to the cited references.

11.7 PIPELINE TRANSMISSION

by G. David Bounds

REFERENCES: AGA publication "Gas Facts." Huntington, "Natural Gas and Gasoline," McGraw-Hill. Leeston, Crichton, Jacobs, "The Dynamic Natural Gas Industry," University of Oklahoma Press. Lester, Hydraulics for Pipeliners, *Oil-dom*. Bell, "Petroleum Transportation Handbook," McGraw-Hill. Bureau of Mines, "Mineral Yearbook," Vol. II, Fuels. "The Transportation of Solids in Steel Pipelines," Colorado School of Mines Research Foundation, Inc. Echterhoff, "Pipeline Economics Revisited," PCGA, 1981. *Petroleum Supply Monthly*, Department of Energy, Energy Information Administration, March 1993–February 1994. "US Interstate Pipelines Begin 1993 on Upbeat," *Oil and Gas Journal*, Nov. 22, 1993.

NATURAL GAS

General According to AGA Estimates for 1991, approximately 65 percent of the U.S. natural-gas reserves occur in seven states (Texas, New Mexico, Oklahoma, Louisiana, Wyoming, Alaska, and Kansas) and only about 40 percent of the total natural gas produced there is consumed within those states. Within these seven states alone, estimated production in 1991 exceeded 16.6 trillion ft³ (472.6 billion m³). Total exports, interstate and international, from these states in 1991 were estimated at approximately 13.1 trillion ft³ (371.8 billion m³), while imports were approximately 4.5 trillion ft³ (127.4 billion m³). Offshore production is becoming increasingly significant. In 1991, approximately 18 percent of the total proven U.S. natural-gas reserves were located offshore.

Implementation of FERC Order 636 has had a significant impact on natural-gas transmission pipelines. Pipeline companies which built and operated gathering systems as needed to support contractual obligations

are now restricted from including costs for these activities with the costs of buying, transporting, and selling gas, due to the mandate that gathering be provided as a separate service. The swing in market demand has magnified the need for storage facilities in both gathering and market areas to provide the flexibility required to operate efficiently in an open-access market. Open-access marketing has replaced bundled sales services to meet the instantaneous needs of buyers at competitive prices. When open-access marketing was first tried in the early 1980s, competitive bidding resulted in curtailment of gas flow to approximately 18 trillion ft³ per year through a national pipeline grid that had moved 24 trillion ft³ per year in the 1970s. Hubs are now being established to provide access to natural gas capacity release so that pipeline capacity may be more effectively utilized than ever before. Electronic bulletin boards (EBBs) are being refined to operate on an ever-expanding information superhighway to provide open access to gas supplies and markets.

The need to transport natural gas from the producing regions to consuming areas throughout the country has generated a burgeoning network of transmission pipelines. In 1950, there were 314,000 mi (505,000 km) of gas pipelines in this country. By 1991, with natural gas supplying 24 percent of the nation's energy requirements, this mileage had increased to 1,225,000 mi (1,972,000 km), an increase of 390 percent in 40 years. Between the years of 1984 and 1986, the total length of gas transmission pipeline in the United States declined by 2,500 mi (4,000 km). The significant drop in demand for pipeline steel pushed many domestic pipe mills into insolvency. Other pipe mills specialized in production of a single type of longitudinal seam, such as seamless

(SMLS), double-submerged arc weld (DSAW), or electric resistance weld (ERW) pipe. Domestic pipeline installation rebounded in 1987, with the installation of approximately 2,800 mi (4,500 km) of large-diameter steel pipeline.

Modern gas pipelines consist of all diameters from 2 in to 42 in in all grades of specified minimum yield strengths (SMYS) from 35,000 to 70,000 lb/in². The type of longitudinal seams available are SMLS in sizes ranging from 2 in to 20 in, ERW in sizes ranging from 2 in to 24 in, and DSAW in sizes ranging from 16 in to 42 in. Higher yield strengths are usually more cost-effective in sizes larger than 10 in.

Although the trend has been toward the use of larger pipe diameters and pipe steel of greater tensile strength, the economics of pipe production and coating and the ease of handling, including transportation as well as installation, has led to greater utilization of 36-in-diameter (0.91-m) pipe with a specified minimum yield strength of 65,000 lb/in² (4,570 kg/cm²). In 1992, 36-in-diameter pipe accounted for approximately 36 percent of the total steel used in construction of large transmission pipelines. Although significant mileage of 42-in-diameter (1.07-m) pipeline has been placed in gas service, no new 42-in-diameter pipeline construction was recorded by the American Gas Association (AGA) in 1992.

Main line valves are usually ball or gate and are of the full-opening variety to allow for the passage of cleaning pigs and inspection tools. Ball, gate, and plug valves are installed on piping other than main line piping.

Pipe bends are usually made on site by a contractor; however, on short-distance pipelines, or in cases where a large degree of bend is required, shop-fabricated bends are produced by induction heating.

Repairs to a pipeline segment according to current regulations of the Department of Transportation (DOT) are to either replace the segment, or use welded steel sleeves. A new method currently being tested by both the DOT and industry is a polymer composite reinforcement wrap (Clock Spring) which is wrapped around the repair area. For this type of repair, welding is not required.

The rapidly growing network of large diameter pipelines, along with increasing pressure capabilities, has brought forth a considerable rise in prime mover and compressor requirements. Natural-gas pipelines in the United States have experienced an increase from about 6 million installed hp (4.5 million kW) in 1960 to 14 million hp (10.6 million kW) by the end of 1991, an increase of 233 percent in 30 years. Natural-gas engines, natural-gas turbines, and electric motors are most generally employed as prime movers on gas pipelines. The gas engines generally drive reciprocating compressors; gas turbines and electric-motor drivers are usually connected to centrifugal compressors. The industry trend is toward the use of larger, centrifugal compressor units because of the inherent economic advantages. Prime movers in general use have increased in size from the early 1950s to the early 1990s as follows: gas engines from 2,500 to 13,500 hp (1,865 to 10,070 kW), gas turbines from 1,000 to 50,000 hp (745 to 37,310 kW), and electric-motor drivers from 2,500 to 20,000 hp (1,865 to 14,920 kW). Modified aircraft-type jet engines are also employed as prime movers driving centrifugal compressors and range from 800 to 50,000 hp (600 to 37,310 kW).

Much progress has been made in automated operations of all types of pipelines. Valves, measuring and regulating stations, and other facilities are operated remotely or automatically. Factory-packaged compressor-station assemblies, most of which are highly automated, are now commonplace. Whole compressor stations with thousands of horsepower are operated unattended by the use of coded dispatching systems handled by high-speed communications.

Automatic supervision and operation of pipeline systems are becoming almost commonplace in today's climate of microprocessor-based remote terminal units (RTUs). These ultra-high-speed data-gathering systems can be used to gather operational data, do calculations, provide proportional integral derivative (PID) process control, and undertake other auxiliary functions. Data may be communicated to a central dispatch office for real-time control. A system of several hundred locations may be scanned and reported out in a few seconds.

Natural gas measurement stations usually consist of pressure control

valves, gas measurement, by either AGA dimensioned orifice(s) or by turbine meters, and flow control valves. Overpressure protection may also be required. If a large temperature drop is anticipated across any of the pressure-reducing valves, then a radiant heater or indirect-fired heater may be required. A rough estimate of temperature drop is 7°F per 100 lb/in² of pressure drop. Electronic flow measurement has become commonplace, meeting the requirements of current regulations. Micro-processors calculate, remotely monitor, and control flow in real time using the latest calculation methods of the AGA and American Petroleum Institute (API) reports. The quality of the gas is also measured by one of several means. For small-volume stations a continuous gas sampler accumulates a small volume for laboratory testing. Medium volume stations will use a sampler and/or a gravitometer, while large-volume stations will use a gas chromatograph.

Flow From the thermodynamic energy balance equations for the flow of compressible fluids (Sec. 4), the general flow formula is derived and expressed in *BuMines Monograph 6* (1935) as

$$Q = K \frac{T_0}{P_0} \left[\frac{(P_1^2 - P_2^2)d^5}{GT_f L_f} \right]^{1/2} \quad (11.7.1)$$

where Q is the rate of flow, ft³/day; T_0 is the temperature base, °R; P_0 is the pressure base, psia; P_1 is the initial gas pressure, psia; P_2 is the final gas pressure, psia; d is the internal pipe diameter, in; G is the specific gravity of the gas, which is dimensionless (for air, $G = 1.0$); T_f is the gas flowing temperature, °R; and L_f is the length of the pipeline, mi. The general flow equation for constant-volume (steady-state), isothermal, horizontal flow of natural gas is given by *U.S. BuMines Monograph 9* (1956) as

$$Q = 38.7744 \frac{T_b}{P_b} \left[\frac{(P_1^2 - P_2^2)D^5}{fZGTL} \right]^{0.5} \quad (11.7.2)$$

where Q = rate of flow, ft³/day; T_b = temperature base, °R; P_b = pressure base, psia; P_1 = inlet pressure, psia; P_2 = outlet pressure, psia; D = internal pipe diameter, in; f = friction factor, dimensionless; Z = average gas compressibility, dimensionless; G = gas gravity (for air, $G = 1.00$); T = average flowing temperature, °R; L = length of pipe, mi. Monograph 9 also gives a good discussion of friction factors and elevation corrections.

Other flow equations may be derived from the general equation by substitution of the proper expression for the friction factor. This applies to the Panhandle A equation which has the form

$$Q = 435.87 \left(\frac{T_b}{P_b} \right)^{1.0788} \left(\frac{P_1^2 - P_2^2}{G^{0.8539} TL} \right)^{0.5394} D^{2.6182} E \quad (11.7.3)$$

where E = pipeline flow efficiency, a dimensionless decimal fraction (design values of 0.88 to 0.96 are common). In the Panhandle A equation, the compressibility is included in the pipeline efficiency, and the other symbols are as previously defined. This formula may be solved graphically as described by C. W. Marvin, *Oil and Gas Journal*, Sept. 20, 1954.

An AGA paper, *Steady Flow in Gas Pipelines* (1965), gives a good general review of constant-volume gas flow equations, both with and without elevation corrections. Equations and test data are included for both the partially turbulent (Reynolds number dependent) flow regime and the fully turbulent flow regime using effective internal pipe roughness. In this reference the drag factor is introduced to account for pressure losses for fittings such as bends and valves and is applied in the partially turbulent flow regime.

When the volume of gas flowing varies with time and position (transient or unsteady-state flow), the simultaneous momentum and mass balance equations are usually solved by use of numerical methods and with the aid of computers. An AGA computer program, **Pipetran**, is available for this purpose, as are several related texts on transient flow. A paper entitled *Gas Transportation System Modeling* appears in the *1972 AGA Operating Proceedings*. Gas flowing in a pipeline undergoes a number of transient, or unsteady-state, flow conditions caused by such things as prime movers starting and stopping, valves opening and closing,

11-128 PIPELINE TRANSMISSION

ing, and flows either into or out of the pipeline. DOS-based computer programs, such as **TransFlow** (Gregg Engineering) and **GASUS** (Stoner & Associates) and others, allow the engineer to model simple as well as complex pipeline situations. These programs can be used to test proposed system expansions such as loops or additional compressor stations, to perform capacity studies, and to evaluate the effects of the transients mentioned above.

Compression The theoretical horsepower requirements for a station compressing natural gas may be calculated by polytropic compression formulas (see Sec. 4). The change of state that takes place in almost all reciprocating compressors is close to polytropic. Heat of compression is taken away by the jacket cooling and by radiation, and a small amount of heat is added by piston-ring friction. Compression by centrifugal compressors is even closer to polytropic (see Sec. 14).

For general design, the horsepower requirements for a station compressing natural gas with reciprocating compressors can be calculated as follows:

$$\text{Reciprocating station horsepower} = \text{hp} Z_s \frac{T_s}{520} \quad (11.7.4)$$

The value for hp can be taken from Fig. 11.7.1, typical manufacturer's curve; T_s is suction temperature, °R; and Z_s can be taken from Fig. 11.7.2.

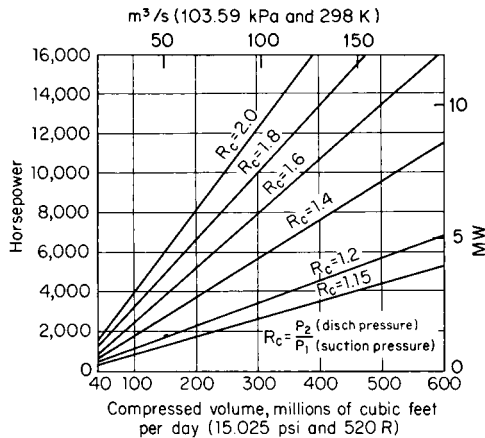


Fig. 11.7.1 Reciprocating-compressor horsepower (MW) graph. $R_c = P_2/P_1 =$ discharge pressure, lb/in² abs ÷ suction pressure, lb/in² abs.

Similarly, the horsepower requirements for a station compressing natural gas with centrifugal compressors can be calculated as follows:

$$\text{Centrifugal station horsepower} = \frac{\text{hp} Z_s}{E_c} \frac{T_s}{520} \quad (11.7.5)$$

The value for hp can be taken from Fig. 11.7.3, typical centrifugal compressor horsepower curve; E_c is the centrifugal-compressor shaft efficiency. (Design shaft efficiencies of 80 to 85 percent are common.)

Compression ratios across a single machine normally do not exceed 3.0 because of outlet temperature limitations. For greater ratios, compressors can be arranged in series operation with an interstage gas cooler placed between the individual units. Multiple units can also be placed in parallel operation in order to increase flexibility and provide for routine maintenance.

Design The pipe and fittings for gas transmission lines are manufactured in accordance with the specifications of the API, ANSI, ASTM, and MSS (see also Sec. 8). Interstate pipelines are installed and operated in conformance with regulations of the U.S. Department of Transportation (DOT). The ANSI B31.8 Code and the *Gas Measure-*

ment Committee Report 3 of the AGA provide supplemental design guidelines. The equation for pipeline design pressure, as dictated by the DOT in Part 192 of Title 49, Code of Federal Regulations, is

$$P = \frac{2St}{D} FET \quad (11.7.6)$$

where P = design pressure, psig; S = specified minimum yield strength, lb/in²; t = nominal wall thickness, in; D = nominal outside

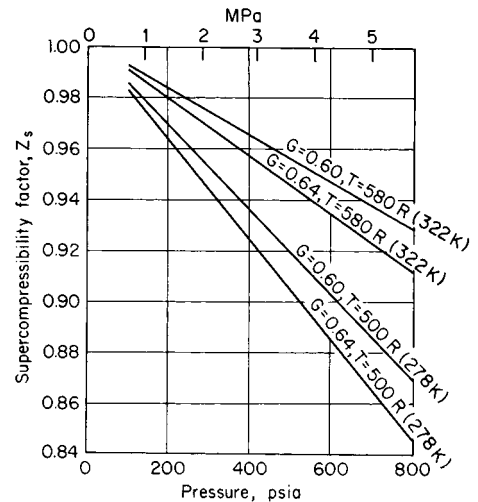


Fig. 11.7.2 Supercompressibility factor Z for natural gas. (Natural gas, 1 percent N_2 .)

diameter, in; F = design factor based on population density in the area through which the line passes, dimensionless; E = longitudinal joint factor, dimensionless; and T = temperature derating factor (applies above 250°F only), dimensionless. For offshore lines and cross-country pipelines in areas where the population density is very low, the factor F is 0.72. For seamless, double-submerged arc weld or electric resistance weld pipe with an E value of 1.00 and an operating temperature below 250°F in these low-population density areas, the equation can be written

$$P = 1.44St/D \quad (11.7.7)$$

The selection of the diameter, steel strength, and wall thickness of a line and the determination of the optimum station spacing and sizing are

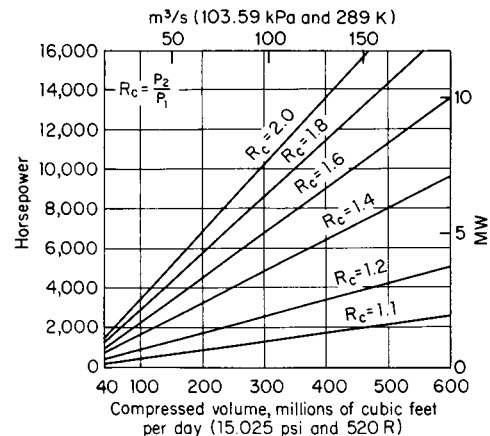


Fig. 11.7.3 Centrifugal-compressor horsepower (MW) graph. $R_c = P_2/P_1 =$ discharge pressure, lb/in² abs ÷ suction pressure, lb/in² abs.

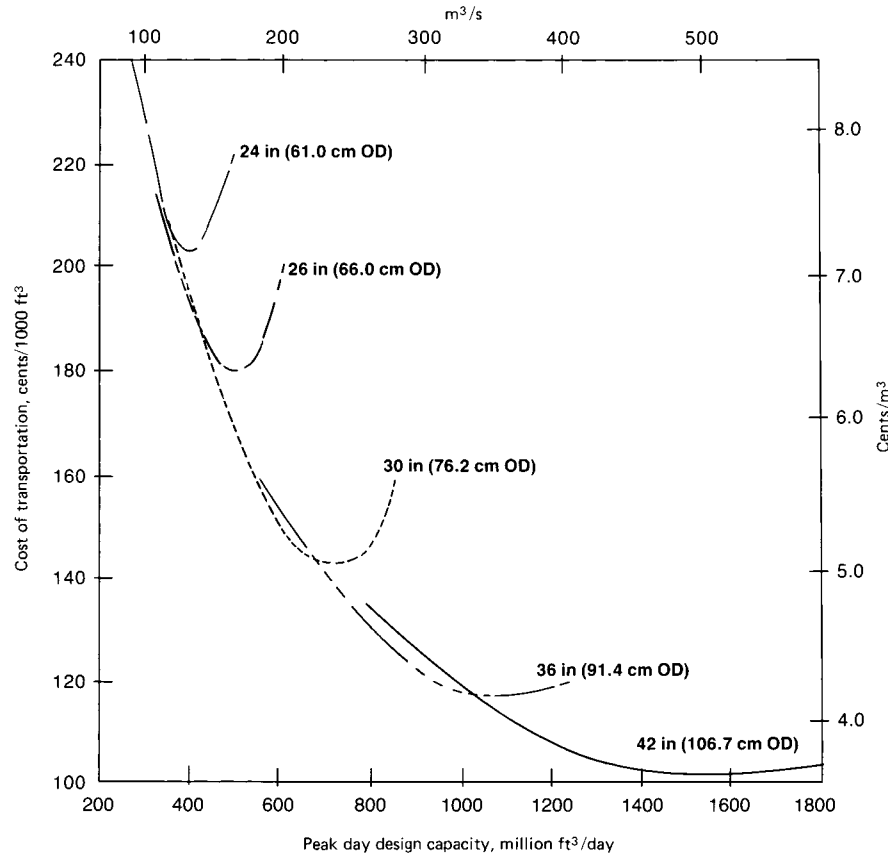


Fig. 11.7.4 Schematic relationship of cost of transportation versus design capacity for a given length of line with various pipeline diameters at equal design pressures.

based on transportation economics. Figures 11.7.4 through 11.7.6 show schematically methods of analysis commonly used to relate design factors to the cost of transportation. A perspective of various elements of the cost of transportation for a long-distance, large-diameter, fully developed pipeline system is presented in Fig. 11.7.7.

The cost of installed pipelines varies greatly with the location, the type of terrain, the design pressure, the total length to be constructed, and many other factors. In general, figures from \$23,000 to \$38,000 per inch (per 2.54 cm) of OD represent the range of approximate costs per mile (per 1.61 km) of installed pipeline. Offshore pipeline installed costs vary with such items as length, water depth, bottom conditions, pipeline crossings, depth of bury, and many other factors. These costs range from \$38,000 to \$54,000 per inch (per 2.54 cm) of OD per mile (per 1.61 km) for a typical offshore pipeline. Compressor-station installed costs vary widely with the amount and type of horsepower to be installed and with the location, the type of construction, and weather conditions. The installed costs of gas-turbine stations range from \$900 to \$1,600 per installed hp (\$1,206 to \$2,145 per kW); gas-engine stations, from \$1,000 to \$1,800 per hp (\$1,340 to \$2,413 per kW); and electric-motor stations, from \$600 to \$1,500 per hp (\$800 to \$2,000 per kW).

After a pipeline system is constructed and fully utilized, expansion of delivery capacity can be accomplished by adding pipeline loops (connecting segments of line parallel to the original line), by adding additional horsepower at compressor stations, or by a combination of these two methods.

CRUDE OIL AND OIL PRODUCTS

General Approximately 91 percent of the U.S. proven liquid hydrocarbon reserves are situated in the seven states of Alaska, California, Louisiana, New Mexico, Oklahoma, Texas, and Wyoming or in the marine areas off their coasts. Offshore production is becoming increasingly significant. The refinement of multiphase pumping systems has enhanced crude oil recovery from formerly marginal offshore fields. In 1991, approximately 11 percent of the total proven crude oil reserves were located in federal waters offshore of California, Louisiana, and Texas. The major markets in which petroleum products are consumed are remote from the proven reserves. About one-half of all petroleum consumed in the United States is imported and must be moved from ports to the centers of consumption. Eighty-nine percent of all movements of petroleum and petroleum products is made by pipelines. The interstate pipelines alone transport over 11.4 billion bbl (1.82 billion m³) of petroleum a year. There are about 163,000 mi (262,300 km) of operating interstate liquid-petroleum trunk lines in the United States.

Centrifugal pumps have been used extensively. Generally, these units are multistaged, installed in series or parallel, depending on the application. Many operators install smaller multiple units instead of larger single units to improve operating efficiency and flexibility.

Reciprocating pumps are installed in parallel; i.e., a common suction and a common discharge header are utilized by all pumps. There are instances where rotary, gear, and vane-type pumps have been employed to fulfill specific requirements.

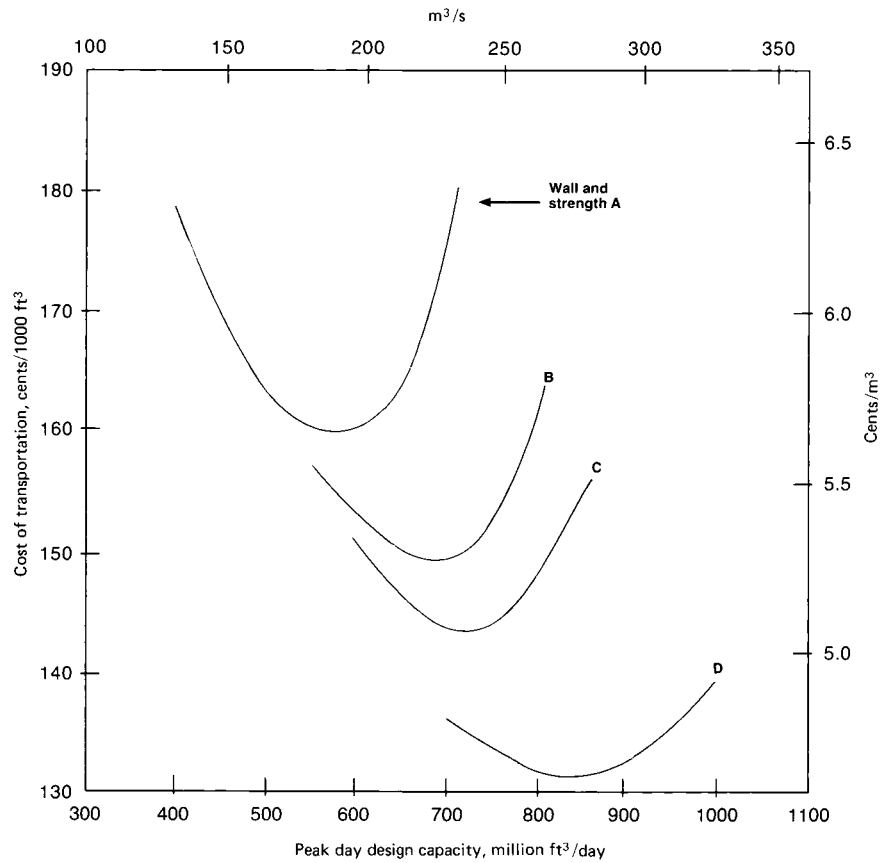


Fig. 11.7.5 Schematic relationship of cost of transportation versus pipeline steel strength and wall thickness.
 A = 30 in × 0.312 in, WT × 52,000 lb/in² min. yield (779-lb/in² operating pressure).
 B = 30 in × 0.344 in, WT × 56,000 lb/in² min. yield (923-lb/in² operating pressure).
 C = 30 in × 0.350 in, WT × 60,000 lb/in² min. yield (1,008-lb/in² operating pressure).
 D = 30 in × 0.385 in, WT × 65,000 lb/in² min. yield (1,200-lb/in² operating pressure).

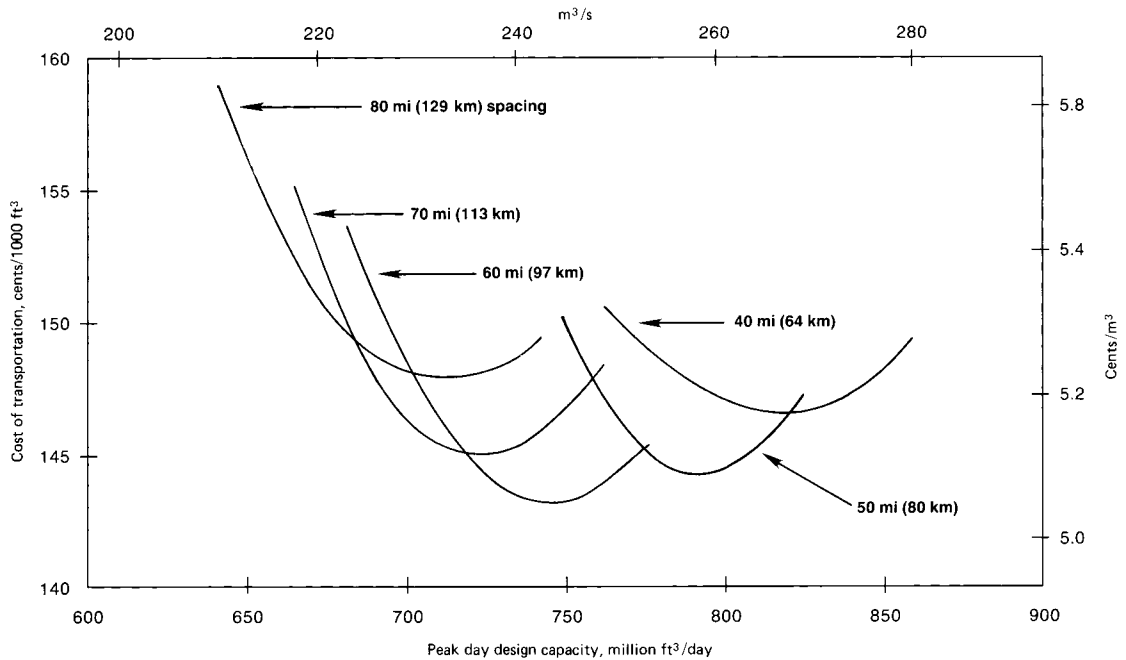


Fig. 11.7.6 Schematic relationship of cost of transportation versus design capacity for a given pipeline diameter and length, with various spacings of compressor stations.

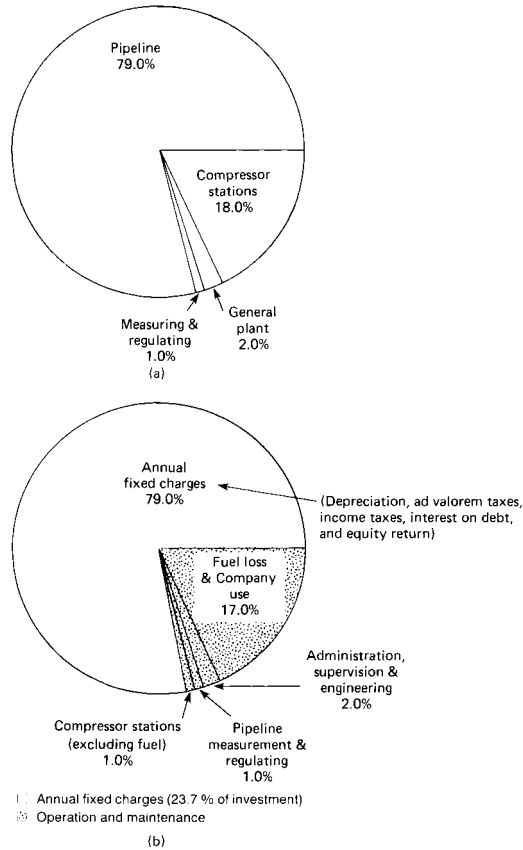


Fig. 11.7.7 Analysis of (a) investment and (b) cost of transportation.

Electrically driven centrifugal pumps are now widely employed for the liquid pipeline industry because they are environmentally friendly and because of their compactness, low initial costs, and ease of control. Centrifugal pumps driven by gas-turbine engines have also come into routine use.

Positive-displacement and turbine meters are in general use on products systems (see Sec. 16). Totalizers for multimeter installations and remote transmission of readings are an industry standard. Greater application of meters with crude-oil gathering facilities is being made as automatic-custody units are installed.

Flow The Darcy formula,

$$h_f = fLV^2/D2g \quad (11.7.8)$$

where h_f = friction loss, ft; f = friction factor (empirical values), dimensionless; L = length of pipe, ft; D = ID, ft; V = velocity flow, ft/s; and $g = 32.2 \text{ ft/s}^2$, is in general use by engineers making crude-oil pipeline calculations. The Darcy formula, when stated in a form utilizing conventional pipeline units, is

$$P = 34.87fB^2S/d^5 \quad (11.7.9)$$

where P = friction press drop, lb/(in² · mi); f = friction factor (empirical values), dimensionless; B = flow rate, bbl/h (42 gal/bbl); S = specific gravity of the oil, dimensionless; d = ID, in.

The Williams and Hazen formula, which has wide acceptance for product pipeline calculations, can be stated in a form employing conventional pipeline terms as follows:

$$P = \frac{2340B^{1.852}S}{C^{1.852}d^{4.870}} \quad (11.7.10)$$

Table 11.7.1

Pump-station installed hp, total	Cost per installed hp (1hp = 0.746 kW)
250–500	\$760–800
500–750	\$560–600
750–1,000	\$440–480
1,000–2,000	\$310–350
Above 2,000	\$275

where P = friction press drop, lb/in² per 1,000 ft of pipe length; B = flow rate, bbl/h; S = specific gravity of the oil product; C = friction factor, dimensionless; and d = ID, in. The friction factor C includes the effect of viscosity and differs with each product (C for gasoline is 150; for no. 2 furnace oil, 130; for kerosene, 134).

The brake horsepower for pumping oil is $RS h/3960E$ or $BP/2450E$, where R = flow rate, gal/min; S = specific gravity of the oil; h = pump head, ft; E = pump efficiency, decimal fraction; B = flow rate, bbl/h; and P = pump differential pressure, lb/in².

Design The pipe and fittings for oil transmission lines are manufactured in accordance with specifications of the API and are fabricated, installed, and operated in the United States in conformance with Federal Regulations, DOT, Part 195 (see also Sec. 8). Many factors influence the working pressure of an oil line, and the ANSI B31.4 code for pressure piping is used as a guide in these matters. A study of the hydraulic gradient, land profile, and static-head conditions is made in conjunction with the selection of the main-line pipe (Sec. 3).

Determining the pipe size and station spacing to transport a given oil or oil product at a specified rate of flow and to provide the lowest cost of transportation is a complex matter. Usually the basic approach is to prepare (1) a series of pipeline cost estimates covering a range of pipe diameters and wall thicknesses and (2) a series of station cost estimates for evaluation of the effect of station spacing. By applying capital charges to the system cost estimates and estimating the system operating costs, a series of transportation-cost curves similar to those in Fig. 11.7.8 can be drawn.

Estimates of \$20,000 to \$40,000 per in (per 2.54 cm) of OD represent the cost per mile (1.61 km) of installed trunk pipeline. The tabulation of pump-station investment costs for automated electric-motor, centrifugal-type installations presented in Table 11.7.1 can be used for preliminary evaluations.

Careful design and good operating practice must be followed to minimize contamination due to interface mixing in oil-product pipelines. When the throughput capacity of an oil line becomes fully utilized, additional capacity can be obtained by installing a parallel pipeline or a partial-loop line. A partial loop is a parallel line which runs for only part of the distance between stations. In the case of product lines, careful attention must be paid to the design of the facilities where the loop line is tied into the original pipeline to prevent commingling of products.

SOLIDS

General Solids may be transported by pipeline by a number of different methods. In *capsule pipelining*, dry solids are placed in a circular capsule which is then pumped down the pipeline. This method can have economic and other advantages in many cases, especially where water is scarce, because the water is never contaminated and can be returned easily in a closed loop.

Another method being developed for the transport of coal is by *coal logs*. Pulverized coal is mixed with a binder (usually petroleum-based) to form a solid log, designed to resist water absorption, that can be transported down the pipeline intact. No dewatering is required with this method of coal transportation and because the binder is combustible it enhances burning.

The most prevalent method of transporting solids by pipeline is by slurry. A slurry is formed by mixing the solid in pulverized form with a true liquid, usually water, to a consistency which can be pumped down the pipeline as a liquid. Nonvolatile gases, such as carbon dioxide, may

11-132 PIPELINE TRANSMISSION

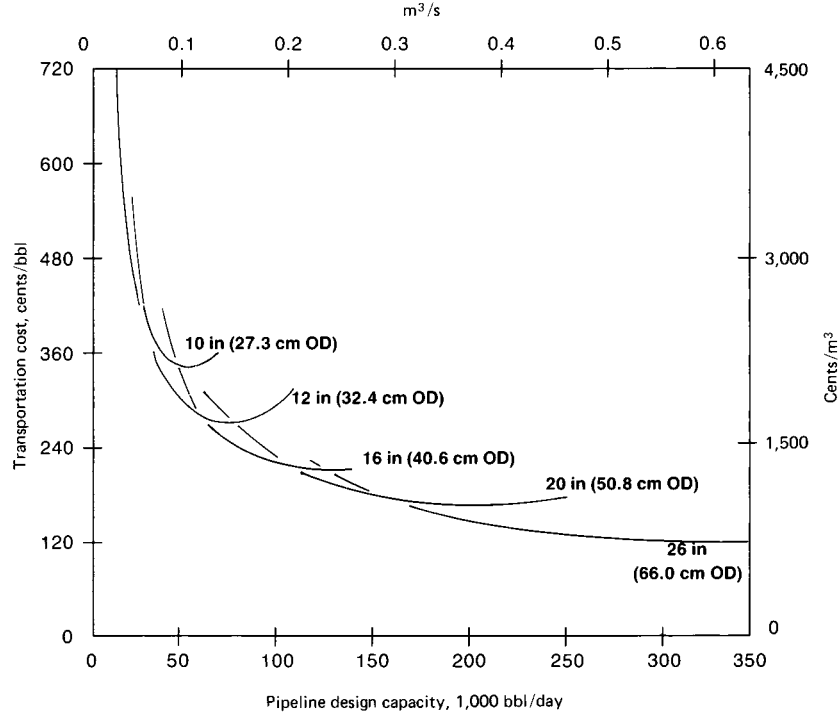


Fig. 11.7.8 Schematic relationship of pipeline capacity to cost of transportation.

also be used as the carrying fluid. In some instances, the carrying fluid may also be marketed after separation from the solid.

Slurry Transport Some of the solids being transported in slurry form considerable distances by pipeline are coal, coal refuse, gilsonite, phosphate rock, tin ore, nickel ore, copper ore, gold ore, kaolin, lime-

stone, clay, borax, sand, and gravel. Solids pipelines differ from pipelines for oil, gas, and other true fluids in that the product to be transported must be designed and prepared for pipeline transportation. After much research in the field of slurry hydrotransportation, methods for predicting the energy requirements for pipeline systems have vastly

Table 11.7.2 Summary of Selected Slurry Pipelines

Location	Length,* mi	Diameter,† in	Capacity,‡ millions of tons/year	Concentration, % by weight
Coal slurry				
Black Mesa, Arizona	273	18	4.8	45–50
Consolidation, Ohio	108	10	1.3	50
Belovo–Novosibirsk, Russia	155	20	3.0	60
Limestone slurry				
Rugby, England	57	10	1.7	50–60
Calaveras, California	17	7	1.5	70
Gladstone, Australia	18	8	1.8	62–64
Trinidad	6	8	0.6	60
Copper concentrate slurry				
Bougainville, New Guinea	17	6	1.0	56–70
KBI, Turkey	38	5	1.0	45
Pinto Valley, Arizona	11	4	0.4	55–65
China	7	5	0.6	60
Iron concentrate slurry				
Savage River, Tasmania	53	9	2.3	55–60
Samarco, Brazil	245	20	12.0	60–70
Kudremukh, India	44	18	7.5	60–70
La Perla–Hercules, Mexico	53/183	8/14	4.5	60–68
Phosphate concentrate slurry				
Valep, Brazil	74	9	2.0	60–65
Chevron Resources, U.S.A.	95	10	2.9	53–60
Goiásfertil, Brazil	9	6	0.9	62–65
Kaolin clay slurry				
Huber, U.S.A.	21	6	0.7	40
Cornwall, England	25	10	2.9	55

* 1 mi = 1.61 km.

† 1 in = 25.4 mm.

‡ 1 ton = 907 kg.

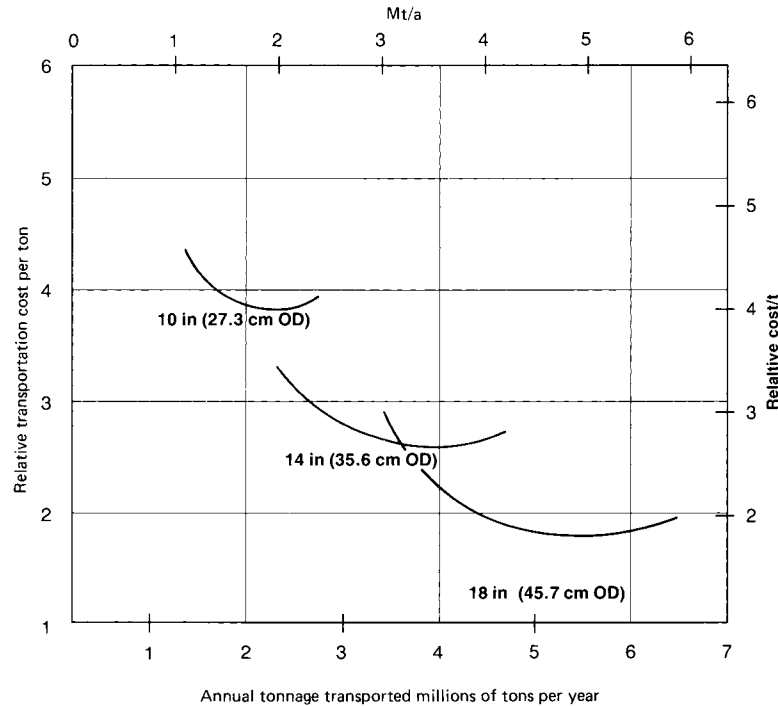


Fig. 11.7.9 System relative transportation cost for various main-line pipe sizes.

improved and slurries are transported today at much higher concentrations than 10 years ago. In the early 1980s, slurry designs ranging from 45 to 58 percent concentration, by weight, were common. Today, ultra-fine coal-water mixtures with concentrations, by weight, ranging up to 75 percent, or more, are used. Dispersants and chemical additives, such as **Carbogel** and **Densecoal** are used to reduce drag and facilitate pumping. These additives significantly reduce the operating costs of slurry pipelines. Additional savings are realized by direct burning of these high-concentration coal-water mixtures through a nozzle, since dewatering is not required.

Current trends in the construction of solids pipelines and those proposed for construction indicate that future transportation of minerals and other commodities will bear more consideration. Some of the commercially successful slurry pipelines throughout the world are listed in Table 11.7.2.

Advances in slurry rheology studies and technology related to homogeneous and heterogeneous slurry transport have made the potential of slurry pipelining unlimited. Immediate advantages for slurry pipelines exist where the solids to be transported are remotely located; however, each potential slurry transport project possesses some other advantages. Materials must satisfy the following conditions to be transported by long-distance pipelines: (1) the largest particle size must be limited to that which can readily pass through commercially available pumps, pipes, and other equipment; (2) solids must mix and separate easily from the carrying fluids or be consumable in the slurry state; (3) material degradation must be negligible or beneficial to pipelining and utilization; (4) material must not react with the carrying fluid or become contaminated in the pipeline; (5) the solids-liquid mixture must not be excessively corrosive to pipe, pumps, and equipment; (6) solids must not be so abrasive as to cause excessive wear at carrying velocities.

Coal Slurry Uncleaned coal can be transported by pipeline, but a more stable and economic long-distance pipeline operation can be achieved with clean coal. The use of clean coal allows a variety of supply sources; produces a slurry with a lower, more uniform friction-head loss; reduces the pipe-wall wear; and increases the system capacity. Cleaning pipeline coal costs considerably less than cleaning coals

for other forms of transportation since drying can be eliminated after the cleaning operation.

Coal-slurry preparation normally consists of a wet grinding process for reducing clean coal to the proper particle size and size-range distribution. The final slurry-water concentration can be adjusted before it enters the pipeline with quality control of the slurry holding tanks. The cost of slurry preparation is only slightly affected by changes in concentration or size consist. The normal slurry-preparation-plant practice is to hold the concentration within 1 percent of design to provide a slurry with a uniform pressure drop. Continued research has made it possible to predict accurately the anticipated pressure drop in a pipeline by using a laboratory and computer correlation.

Optimum characteristics for a slurry are (1) maximum concentration, (2) low rate of settling, and (3) minimum friction-head loss. Variables which can be manipulated to control and optimize slurry design are particle shape, size distribution, concentration, and ash content. Established computer techniques are used to evaluate these variables.

Design Because of the many slurry variations, there is no single formula available by which the friction-head loss can be readily determined for all slurry applications. A general approach is described by Wasp, Thompson, and Snoek (*The Era of Slurry Pipelines, Chemtech*, Sept. 1971, pp. 552-562), and by Wasp, Kenny, and Gandhi in their book, "Solid-Liquid Flow Slurry Pipeline Transportation," giving calculation methods which have been developed for predicting slurry pressure drops. The described methods are quite accurate and can be used for preliminary design. Additional calculation procedures and methods for specifying slurry size consist (solid size-range distribution) and velocity have been developed by continuing research and may be found in the following books: Shook and Roco, "Slurry Flow Principles and Practice," Butterworth Heinemann, 1991, and Wilson, Addie, and Clift, "Slurry Transport Using Centrifugal Pumps," Elsevier, 1992. Slurry hydraulics should be verified with bench-scale tests and compared with commercial operating data reference points or pilot-plant operations before constructing a full-scale long-distance pipeline.

Slurry velocities are generally limited to a minimum critical velocity to prevent solids from settling to the bottom of the pipe and a maximum velocity to prevent excessive friction-head loss and pipe-wall wear.

11-134 CONTAINERIZATION

These velocity limitations and the throughput volume determine the diameter of the mainline pipe. The relationship of volume and velocity to the pipe diameter is expressed as $ID = 0.6392 \sqrt{(\text{gal}/\text{min})/V}$, where the ID is in inches, gal/min is the volume rate of slurry flow (gallons per minute), and V is flow velocity, ft/s.

Pipe-wall thickness in inches is computed by the modified Barlow formula as $[(PD/2SF) + t_c]/t_m$, where P = maximum pressure, lb/in²; D = pipe OD, in; S = minimum yield strength of the pipe, lb/in²; F = safety factor; t_m = pipe mill tolerance, usually 0.875; and t_c = internal erosion/corrosion allowances, in, for the life of the system. The internal metal loss results from the erosion of corrosion products from the pipe wall and thus can be limited with chemical inhibitors and velocity control. This metal loss occurs in all pipeline steels and according to Cowper, Thompson, et al., *Processing Steps: Keys to Successful Slurry-Pipeline Systems*, *Chem. Eng.*, Feb. 7, 1972, pp. 58–67, must be evaluated on a case-by-case basis. A minimum pipe wall of 0.250 in (0.635 cm) is often used to provide mechanical strength for large lines even where pressures and wear permit the use of a thinner wall. Coal pipelines employ a graduated wall thickness to meet the demands of the hydraulic gradient, which saves pipe costs.

Pump-station hydraulic horsepower is calculated as $(P_d - P_s)(Q)/1,716$ where $(P_d - P_s)$ = pressure rise across the station lb/in²,

Q = maximum flow rate through the station in gallons per minute, and 1,716 is a constant, gal/(ft·in²). Stations usually employ positive-displacement reciprocating pumps of the type used for oil-field mud pumps, as they attain high pressures with low slurry velocities. This allows fewer stations and lower overall costs than with centrifugal pumps. Stations are located where the friction-head loss and the effects of terrain have reduced the pressure head to 100 ft (30.48 m). Centrifugal pump usage is advantageous in low-pressure, high-velocity applications such as coarse coal transportation for short distances.

The annual tonnage throughput for any diameter line can be varied within the velocity limits or by intermittent operation near the low velocity limit. The optimum main-line size for high-load-factor systems is found by comparing the relative cost of transportation for a series of pipe sizes, as in Fig. 11.7.9.

When a main-line size is selected, the cost of transportation for that line size at various rates of throughput is weighed against the projected system growth and compared with other line sizes to determine the size which gives the best overall system economics. Coal pipelines cannot be expanded by line looping because of the velocity limitations. Some expansion can be attained by oversizing the line and operating it intermittently near the minimum velocity in the earlier years of life.

11.8 CONTAINERIZATION (Staff Contribution)

REFERENCE: Muller, "Intermodal Freight Transportation," 2d ed., Eno Foundation for Transportation.

Shipping of freight has always suffered from pilferage and other losses associated with the handling of cargo and its repeated exposure to weather conditions and to human access. In addition, the extremely labor-intensive loading and unloading practices of the past became more and more expensive. In the late 1920s and early 1930s the forerunners of present-day container service were offered. They varied from containers on trucks to services in which railroad cars were loaded onto rubber-tired trailers and delivered to the customer's door with no intermediate handling of the cargo. Starting in 1956, containerization as we know it today came into being.

The immense savings in shipping costs resulted in the rapid growth of containerization throughout the world in the 1960s and 1970s and in international standardization. The time savings obtainable through the use of containers is particularly noticeable in maritime service. It is estimated that a container-handling ship can achieve a 4:1 sea-to-port time ratio compared to 1:1 for a conventional break-bulk ship.

CONTAINER SPECIFICATIONS

There are many standards which apply to containers, among which are ISO, ANSI, the International Container Bureau (BIC), and the American Bureau of Shipping (ABS).

Types Ninety percent of containers are dry, nonrefrigerated units with double doors on one end. Other types include refrigerated and/or insulated units, ventilated units, tank containers, and frames with folding ends or corner posts for carrying large items such as automobiles.

Condensation can be a problem inside a closed container. While a good unit can protect against outside elements, it cannot protect against condensation inside the container unless special steps are taken. Condensation typically arises from the moisture in the product being shipped; temperature changes during the trip; or moisture from dunnage, packing, or the container itself.

Construction materials usually consist of a steel, aluminum, or fiberglass outer cover on an internal steel frame. Containers are designed to

be stacked up to six units high. Since containers are designed with oceangoing shipment in mind where the container, and those stacked on top of it, will be rising and falling with the movement of the ship, the additional acceleration forces have to be taken into account. This is usually done by rating the maximum stacking load using a g force of 1.8.

Figure 11.8.1 shows a typical 20-ft container. At each of the eight corners there are special fittings which facilitate the lifting, stacking, interconnecting, and tying down of units. These fittings have specially shaped slots and holes which enable standard crane and sling hooks and clevises to be used as well as special hooks and twist-locks.

Sizes The most widely used containers are 20 ft (6.1 m) or 40 ft (12.2 m) long by 8 ft (2.5 m) wide by 8 ft (2.5 m) high. The usual height of 102 in (2.6 m) includes an 8-in-deep (200-mm) underframe. This frame often has two, or sometimes four, transverse slots for forklift forks. Standard lengths are: 20, 35, 40, 45, and 48 ft (6.1, 10.7, 12.2, 13.7, and 14.6 m).

Typical specifications for a 20-ft (6.1-m) container are: maximum gross weight of 52,910 lb (24,000 kg), tare of 5,070 lb (2,300 kg), payload of 47,840 lb (21,700 kg), cubic capacity of 1,171 ft³ (33.2 m³), and allowable stacked weight for a g force of 1.8 of 423,280 lb (192,000 kg).

Typical specifications for a 40-ft (12.2-m) container are: maximum gross weight of 67,200 lb (30,480 kg), tare of 8,223 lb (3,730 kg), payload of 58,977 lb (26,750 kg), allowable stacked weight for a g force of 1.8 of 304,170 lb (182,880 kg), cubic capacity of 2,300 ft³ (65 m³). Thus a 40-ft (12.2-m) container has roughly the same volume as a 40-ft (12.2-m) highway semitrailer. A typical 40-ft (12.2-m) dry-cargo container with an aluminum outer skin weighs about 6,000 lb (2,720 kg).

Specifications for a typical 40-ft (12.2-m) refrigerated container are: maximum gross weight of 67,200 lb (30,480 kg), tare of 8,770 lb (3,980 kg), payload of 58,430 lb (26,500 kg), allowable stacked weight for a g force of 1.8 of 423,307 lb (192,000 kg), cubic capacity of 2,076 ft³ (58.8 m³). The refrigeration system specifications are: minimum inside temperature of 0°F (−18°C), maximum outside temperature of 100°F (38°C). The refrigeration system is powered through

cables connected to the loading site, or to a generator mounted in the bed of the container chassis or trailer.

Some companies have a sufficiently large volume of shipping to have containers differing from these specifications. For example, the refrigerated containers used to ship Chiquita bananas are 43 ft (13.1 m) long. Their specifications are: maximum gross weight of 67,200 lb (30,480 kg), tare of 8,270 lb (3,750 kg), payload of 58,930 lb (26,730 kg), allowable stacked weight for a g force of 1.8 is 335,980 lb (152,400 kg), and a cubic capacity of 2,324 ft³ (65.8 m³). The height of the floor above the bottom of the underframe is 11 in (280 mm). The refrigeration rating is 16,721 Btu/h (4,214 kcal/h). Electric power supplied is three-phase at 460 V, 60 Hz (or 380 V, 50 Hz). The overall heat-transfer rate is 7,965 Btu/h (2,007 kcal/h).

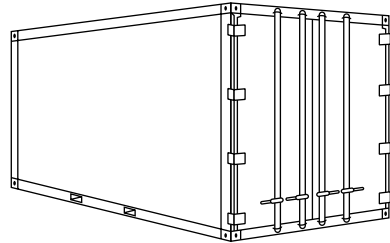


Fig. 11.8.1 Typical 20-ft container.

ROAD WEIGHT LIMITS

The gross weight of a typical 40-ft (12.2-m) dry-cargo container is about 67,000 lb (30,000 kg). The special-purpose semitrailer for carrying containers on the highway is called a **container chassis** and weighs about 10,000 lb (4,500 kg). The towing tractor weighs about 16,000 lb (7,256 kg). Many U.S. highways do not allow such heavy loads. Typical allowable axle loads are 12,000 lb (5,442 kg) on the front wheels, 34,000 lb (15,420 kg) on the tractor rear wheels, and 34,000 lb (15,420 kg) on the chassis wheels. So if the container is to be forwarded by truck in the United States, the load must be limited to 54,000 lb (24,500 kg) and, on many secondary roads, even less. Similar constraints exist elsewhere in the world as well. As with any closed shipping space, depending on the density of the material being shipped, the weight or the volume may be the controlling factor.

CONTAINER FLEETS

As of 1988 about half of the world's containers were owned by container-leasing companies. Most of the remainder were owned by carri-

ers. About four percent were owned by shippers. Container shipment figures and fleet sizes are usually give in TEUs (twenty-foot equivalent units). A TEU is the equivalent of a 20-ft (6.1-m) by 8-ft (2.5-m) by 8-ft (2.5-m) unit.

Containers are easy to make. As a result the competition among manufacturers is intense. The low-cost manufacturers are in Japan, Taiwan, the Peoples Republic of China, and South Korea. Prices as low as \$2,000 for a 20-ft (6.1-m) container were current in 1984.

CONTAINER TERMINALS

A typical marine container terminal may have 50 acres (20 hectares) of yard space. It can load and unload 150 to 200 ships a year, and in so doing handle 60,000 to 80,000 containers. Under such circumstances the requirements for record keeping and fast, efficient handling are very severe. Specialized container-handling cranes and carriers have been developed to facilitate safe, fast, damage-free handling.

Handling Equipment By its design and purpose, the container is intended to go from shipper to receiver without any access to the contents. The container with its load may, however, travel by truck trailer from the shipper to the railroad, by rail to a marine terminal, by ship across the ocean, and again by rail and by truck trailer to the receiver. While the container is on the truck trailer, rail car, or ship, little or no handling needs to be done. When a container changes from one mode of transportation to another, at intermodal or transfer points, the container requires handling.

The general transfer tasks of **container-handling machinery** are: ship to/from rail, ship to/from truck, and rail to/from truck. Since a ship may have a capacity of up to 4,400 20-ft containers, extensive yard storage space has to be available. A 50-car double-stacked railroad train can handle up to 200 containers. Container-handling equipment varies from a simple crane with some slings or a large forklift truck at low-volume sites to special-purpose gantry and boom cranes and straddle carriers at high-volume sites.

Terminal designs come in two basic types: decked and wheeled systems. With a **wheeled** system, the containers are stored on their highway trailers. They are transferred to/from the loading crane by terminal tractors, which are also called *yardhorses*. In a **decked** system, the containers are removed from their highway trailers, rail cars, or ships and stacked in rows on the paved yard surface. When the containers are to be loaded, they are picked up at the stacked location, if possible by straddle carriers or mobile cranes, and loaded onto outgoing highway trailers, railcars, or ships. When the full area of the container storage yard is not accessible to the cranes, containers may be loaded onto yard trailers and transported from their stack location to the cranes. An equivalent procedure is also used for incoming containers where they must be transferred by yard trailer from the cranes to their yard storage location.